There and Back Again: A Protein's Tale
Uncovering the Quality Control Factors Mediating Peripheral Myelin Protein 22 Trafficking

By

Justin Tyler Marinko

Dissertation

Submitted to the Faculty of the

Graduate School of Vanderbilt University

in partial fulfillments of the requirements

for the degree of

DOCTOR OF PHILOSOPHY

in

Biochemistry

December 12, 2020

Nashville, TN

Approved:

Charles Sanders, PhD

Bruce Carter, PhD

Lauren Jackson, PhD

Lars Plate, PhD

Kevin Schey, PhD

“The only limit to your impact is your imagination and commitment”

-Tony Robbins

“I would have written a shorter letter, but I did not have the time”

-Blaise Pascal

To my parents, who supported me when no one else would.

Acknowledgments

First and foremost, I would like to acknowledge my advisor Dr. Chuck Sanders. Dr. Sanders believed in me and gave me the chance to work in his lab when I was still a green 1st year graduate student. He has nurtured and aided in my development ever since. Even though I have never conducted a full NMR experiment on my own and have bucked the trend of a traditional Sanders Lab trainee by doing mostly cell biology, Dr. Sanders has stood by me and helped me grow as both a scientist and person. While Dr. Sanders allowed me to be independent, coming up with my own experiments and project ideas, he was always there to talk when I was confused about data or the next step to take in my project. Dr. Sanders has been the perfect mentor and there is no chance I would be writing this dissertation without his guidance. Even when he falls asleep sometimes in late afternoon group meetings, Dr. Sanders always perks up at the end and ask the most poignant questions to get your research on the right track. It was as if he could absorb the meeting via diffusion simply by being there. Dr. Sanders has been a great mentor and I cannot envision graduate school without his guidance. Thank you, Chuck, for all that you've done getting me to this point.

I would also like to acknowledge all of the members of the Sanders and Mega Lab, past and present, who put up with me on a day-to-day basis. Those that know me know I can be quite chatty and I thank everyone who has indulged me in a conversation over the years. Specifically, I want to acknowledge Dr. Jon Schlebach who really started this PMP22 project and taught me a lot my first summer in the lab. Additionally, Arina Hadziselimovic, our lab manager. Arina taught me incredible amounts of molecular biology and had to put up with my incessant requests for reagents. Without Arina the Sanders lab would cease to function. I must also acknowledge my collaborators: Dr. Mel Ohi, Dr. Anne Kensworthy, Dr. Bruce Carter, Dr. Lars Plate, and Madison Wright. All of my collaborators have taught me new and incredible techniques that were applied throughout this dissertation. These collaborators also served as advisors allowing me to grow as a scientist.

I would also like to acknowledge my friends, both those I've known for years prior to graduate school, and the countless number I've made at Vanderbilt and in Nashville. There are far too many friends to name specifically, and I would most assuredly forget some people, but to everyone who has been a friend to me over these past five years I thank you for your support. However, I specifically need to acknowledge Chris Hofmann, Eric Figueroa, Michaela Fooksa, and Lydia Roseman as these friends also had the unfortunate pleasure of

living with me for some period over the past five years. Thank you for putting up with my crazy and absurd personality.

I also would like to acknowledge my funding sources which have paid the bills over the past five years and allowed me to live this lavish life I've become accustomed to. I was supported by National Institutes of Health Fellowship F31 NS113494 and National Institutes of Health Training Grant T32 NS00749. I was also funded by a Russell Hamilton Dissertation Enhancement grant from the Graduated Leadership Initiative. Additionally, I was supported by National Institutes of Health Grants R01 NS095989 (awarded to Dr. Sanders).

And last, but most certainly not least, I want to acknowledge my family. To Kobe, who has been a best friend over the years and with whom I share an almost identical personality. And to my parents, Lee and Erik. You both have blessed me with and nurtured my scientific curiosity and have always supported me in my endeavors. You have both sacrificed, working extra jobs, and taking the time to help me with homework growing up, to give me the education that I needed in order to achieve this accomplishment. You have both always served as an inspiration to me and I hope to one day be half the people that you both are. You set lofty standards because you want me to achieve my potential. Thank you for all that you have and that you continue to do to support me. I love you, and I feel incredibly proud to have you both as my parents. You inspire me every day.

Table of Contents

LIST OF FIGURES:

Chapter I. Membrane Protein Folding and Quality Control

Chapter I was adapted with permission from one of my previously published articles. (*2*)

1. Introduction. Linking Biophysical Studies with Membrane Protein Folding in the Cell

By definition, integral membrane proteins (MPs) are components of lipid bilayers, and cannot be extracted into solution without first dissolving the bilayer. Given that these molecules are embedded in the bilayer, their conformational state is influenced by an array of weak, competing interactions between the protein and other components of the bilayer. Such complex solvation shapes the conformational energetics of MPs in a manner that is distinct from water-soluble proteins. This divergence is highlighted by the existence of a specialized ensemble of quality control proteins that are specifically devoted to facilitating MP folding and to managing their misfolding in the cell. These quality control proteins constitute an important component of the web of molecular chaperones and other proteins that stabilize the cellular proteome—the so-called "proteostasis network." Efforts to rationalize how the conformational equilibria associated with the folding and misfolding of MPs influence their interactions with quality control machinery and the proteostasis network are still in their infancy, but are relevant to understanding and treating many diseases.

Our understanding of the structure and conformational energetics of MPs lags behind that of water-soluble proteins. The first experimentally determined structure of a MP was generated in 1985 (the photosynthetic reaction center), which was nearly thirty years after completion of the first high resolution structure of a water soluble protein (myoglobin, 1958).(*3, 4*) In that same time frame the first studies demonstrating the reversible folding of polytopic membrane proteins were reported.(*5-8*) The first *quantitative* studies of the folding energetics of polytopic MPs were not published till the mid-1990s,(*9, 10*) long after Anfinsen's classic early 1960's work demonstrating the reversibility of ribonuclease unfolding.(*11, 12*). The first detailed studies of the structure-stability relationships for a MP were published in 1992.(*13-15*) Nevertheless, after a slow start, physicochemical studies of MP folding have rapidly advanced in recent years, revealing much mechanistic insights into the folding of purified MPs in model membranes. With reverence, I refer the reader to some of the excellent previous reviews of MP folding involving isolated proteins, most of which

include coverage of topics that I do not endeavor to re-review in this introductory chapter—in particular the structural basis for MP stability.(*16-33*)

An emerging frontier in studies of MP folding is integration of studies of MP folding using purified proteins with studies of the folding of MPs in the context of living cells. There has been a wealth of parallel progress in recent years in these disciplines, which now have much to offer each other. Additional impetus for bridge-building is provided by recent advances in human genomics, which have highlighted numerous relationships between defects in MP folding and human disease that may be addressable using emerging chemical tools. Here, I endeavor to review results from studies of purified MPs that are of particular importance for understanding how MPs fold in the context of living cells. I also examine recent progress in the myriad of studies devoted to identifying the key molecular players for managing MP folding and misfolding *in vivo*. In particular, I focus on the chaperones and other proteins that comprise the folding quality control system of the endoplasmic reticulum (ER), which serves as the primary site of MP assembly in eukaryotic cells. Finally, I examine how MP misfolding under physiological conditions, specifically of peripheral myelin protein 22 (PMP22) contributes to the debilitating peripheral neuropathy Charcot-Marie-Tooth (CMT) disease. It is hoped that this introductory chapter will stimulate cross-talk between traditionally disparate areas of study, resulting in synergy that results in true “bench to bedside” progress that both illuminates the detailed chemical basis for key life processes and also is of great benefit to humankind.

2. Intrinsic Differences between Membrane Proteins and Water-Soluble Proteins

2.1. The Membrane Environment and the Native Structures of Membrane Proteins

Natively folded MPs adopt conformational states that are partly, or in some cases nearly completely, embedded within the membrane. With a handful of important exceptions (such as the cyclooxygenases and caveolins),(*34-36*) the vast majority of mammalian MPs have at least one segment that spans the bilayer. These transmembrane (TM) segments typically consist of an alpha-helix with a hydrophobic stretch of 18-28 amino acids flanked by polar residues.(*37-39*) Beta barrel MPs based on anti-parallel transmembrane beta sheets are found in mitochondrial and prokaryotic outer membranes. For both classes of MPs, polar side chains near the edge of TM domains interact with lipid head groups and water molecules in a manner that helps stabilize their native topological orientation in the membrane.(*40, 41*) Energetic barriers associated with

the translocation of these and other polar groups across the membrane is likely to prohibit many topological rearrangements.(*42*) With some notable exceptions (see **Section 3.7**), it seems likely that few helical MPs are capable of efficient spontaneous insertion across the bilayer. This energetic constraint restricts the number of topological orientations that are kinetically accessible to integral MPs.(*43*) In most cases, the native topology (or something close to it) must be established co-translationally with the assistance of the Sec translocon protein complex (see **Section 4.1**) or related membrane-integrative system such as Tim/Tom mitochondrial membrane translocases. The Sec translocon effectively circumvents the insertion barrier by providing hydrophobic segments access to the membrane core through a lateral opening within its transbilayer pore.(*44*) This represents one of enabling strategies developed by nature to allow polypeptides to fold to a functional state within lipid bilayers on biologically relevant time scales.

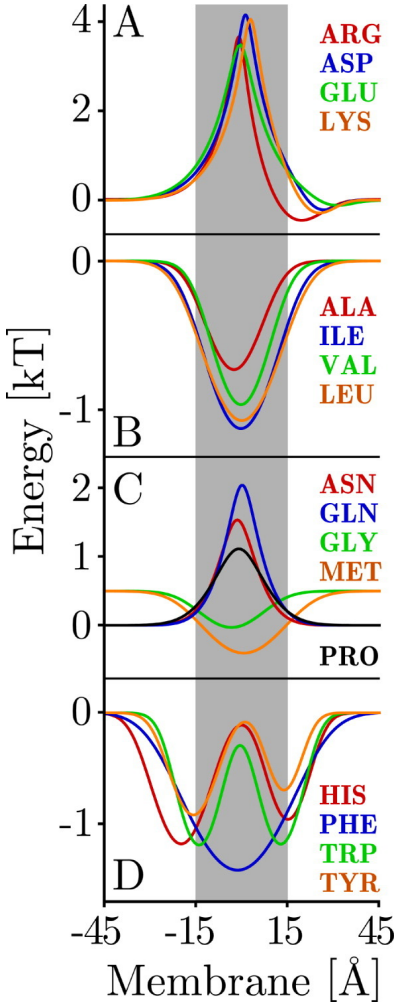

Figure 1. Depth-Dependent Statistical Distributions of Amino Acids within Transmembrane Domains.

Experimental depth dependent compositional biases within transmembrane domains were used to train a probabilistic potential energy function for each A) charged, B) hydrophobic, C) polar and D) aromatic amino acid. Lower energies correspond to higher probabilities of finding the corresponding residue at a given depth. An X-coordinate of 0 Å corresponds to the center of the membrane normal.

After MP translation, the physicochemical properties of the lipid bilayer enforce constraints on the conformational equilibria of integral MPs. For instance, the hydrophobic nature of the membrane core imposes a steep energetic penalty associated with the solvation of unpaired hydrogen bond donors and acceptors.(*16, 17*) This essentially forces the backbone of TM segments to adopt regular secondary structure within the bilayer so that the hydrogen bonding potential of the backbone amide protons and carbonyl oxygens are satisfied by intramolecular interactions. This requirement is satisfied both for MPs with α-helical transmembrane segments and those that form transmembrane beta barrels. As a result of these energetic constraints, the central portions of naturally evolved transmembrane segments are enriched in the hydrophobic amino acids, and polar residues are typically rare within the

membrane core (**Fig. 1**). This sequence bias is particularly pronounced on the lipid-exposed surface of the TM domain.(*45, 46*) Nevertheless, it should be noted that between backbone carbonyl oxygens, amide hydrogens, and the occasional polar side chain, TM segments are actually quite rich in hydrogen bonding groups. The abundance of polar groups within protein molecules provides ample opportunities to form intramolecular hydrogen bonds in a manner that provides some structural plasticity.(*47, 48*) Furthermore, though the membrane core is hydrophobic, the dynamics and imperfect packing of lipid acyl chains allows water to penetrate the bilayer to a surprisingly high degree.(*49, 50*) Bound water molecules are often observed in the TM domains of MP crystal structures.(*51*) Biophysical experiments such as pulse radiolysis and FT-IR spectroscopy have also provided confirmation that water molecules are often associated with TM domains under native-like conditions.(*52*) The presence of water within the bilayer helps explain a number of anomalous structural features that have been observed within the TM domains of some MPs. For example, aquaporins and some other membrane proteins have “re-entrant” strands of residues that extend into one face of the membrane and return to the same face without spanning the bilayer. The residues in these extended membrane-buried segments appear to have unsatisfied backbone hydrogen bonding potentials and possibly interact with water molecules.(*53-55*) There are also TM helices in polytopic membrane proteins that are surprisingly polar.(*56, 57*) Access of water to the membrane may also help to explain the observation that the kinetic barriers associated with rearrangement of membrane-buried hydrogen bonds in flexible MPs can be surprisingly low.(*48*) Even without buried water, TM helices are often kinked in due to proline residues and/or native tertiary contacts.(*48, 58, 59*) Some MPs also feature helices bearing a pi bulge or that are broken by a short strand.(*54, 60*) Certain MPs also feature sizable gaps (fenestrations) within their TM domains connecting the membrane phase to polar cavities within the protein core.(*61-63*) Together, these observations suggest the surprising conformational diversity of MPs may arise partly from the appreciable hydration of proteins within membranes. As the pace of MP structure determination continues to accelerate, we will likely continue to find even more exciting twists and turns that underlie their biochemical functions.

MPs are often sensitive to the physical properties of their bilayer solvent. Most lipids are roughly cylindrical in shape and are arranged with their long axes orthogonal to the plane of the membrane, which allows them to neatly pack into a two-dimensional sheets. However, in part due to the abundance of unsaturated fatty acids in mesophilic organisms, there is typically a gradient of lateral pressure extending from

the bilayer interface into the highly dynamic bilayer core, where the fluidity can approach that of liquid hydrocarbons.(*64*) The lateral pressure exerted by lipid acyl chains has a direct impact on the conformational equilibria of MPs.(*65-68*) Moreover, lateral pressure can be tuned by membrane curvature, which is another factor that influences the conformational energetics of MPs.(*69*) Highly curved membranes are sometimes enriched in lipid packing defects, which can lower the energetic barriers associated with the insertion of proteins across the membrane.(*70, 71*) Membrane curvature is, of course, critical for many biological processes.(*72, 73*) Surface binding proteins such as caveolins, protein containing amphipathic helices, and proteins containing BAR domains can dynamically control membrane curvature. This manipulation of curvature is required for many cellular processes such as vesicle budding, transport, and fusion.(*74-76*) Lateral pressure may also influence the orientation of TM domains. In some cases, TM helices are tilted relative to the bilayer normal, which may occur as a result of a mismatch between the length of the TM domain and the thickness of the membrane (hydrophobic mismatch, **Fig. 2**).(*77, 78*) In other cases, it appears that the span of TM segments is asymmetrically adjustable.(*79*) Thus, thickness represents an additional membrane property that may tune the conformational states of integral MPs (**Fig. 2**).

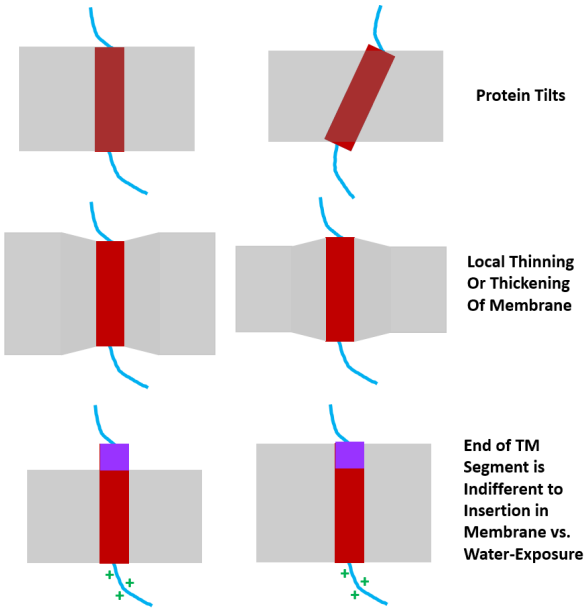

Figure 2. Adaptation of Transmembrane Domains to Variations in Bilayer Thickness.

Cartoons depict ways TM domains adapt to changes in bilayer. A thinning of the membrane may cause TM domains to tilt with respect to the membrane (top). Alternatively, the bilayer may be locally distorted in order to facilitate the solvation of a lengthy TM domain (middle). Thickening of the bilayer may also result in the extension of TM helices out of the bilayer when sites located at the end of the helix have similar preferences for aqueous exposure or membrane burial (bottom).

Native membranes have protein-to-lipid mass ratios (P/L) ranging from 0.25 to 5.(*80*) MPs occupy 20% of the surface area of red blood cells,(*81*) which have a P/L of 1.3. Under non-physiological conditions in which the concentration of MPs within the bilayer is typically much lower, membrane thickness is largely determined by lipid composition. Saturated acyl chains produce thicker bilayers whereas unsaturated chains dynamically splay outward in a manner that allows the two leaflets to pack more closely together. In contrast, the rigid, flat surface of cholesterol stabilizes extended

conformational states of adjacent phospholipid acyl chains in a manner that typically increases membrane thickness and lipid conformational order.(*82*) There is also evidence to suggest that, in the context of protein-rich environments of cellular membranes, the properties of the MPs themselves influence membrane thickness, which varies from organelle to organelle.(*83*) In some cases, proteins satisfy the energetic strain associated with hydrophobic mismatch of transmembrane segments by altering the packing of their annular lipids in order to change the thickness of the local bilayer (hydrophobic matching, see **Fig. 2**).(*84*) Other MPs may form oligomers to reduce the solvent-accessible surface area of mismatched TM domains.(*85, 86*) In many cases, the formation of transmembrane oligomers helps to optimize van der Waals interactions through interhelical packing,(*87, 88*) and can reduce unfavorable clashes between polar side chains and acyl chains within the membrane core.(*89*) It has been suggested that 60% of all single span plasma membrane proteins form homodimers.(*90*) Together, the physical constraints imposed by the bilayer significantly restrict the conformational space that is accessible to integral MPs. Indeed, Bowie and co-workers have argued that the total number of possible folds that are accessible to MPs is limited relative to soluble proteins.(*91*)

A distinctive trait of plasma, endosome, and lysosome membranes relative to those of the nucleus, mitochondria, endoplasmic reticulum and Golgi, is the presence of higher concentrations of both cholesterol and sphingolipids in the former (Figure 3).(*80, 92-94*) Cholesterol has an ordering effect on the chains of neighboring lipids even when the bilayer remains in the disordered phase.(*95, 96*) One of the ways that sphingolipids differ from glycerolipids is that the sphingosine backbone includes a potential hydrogen bond-donating moiety that may lead to enhanced lipid-lipid and interfacial water-lipid interactions.(*97, 98*) Whether the presence of high levels of cholesterol and sphingolipids in membranes alter the energetics of

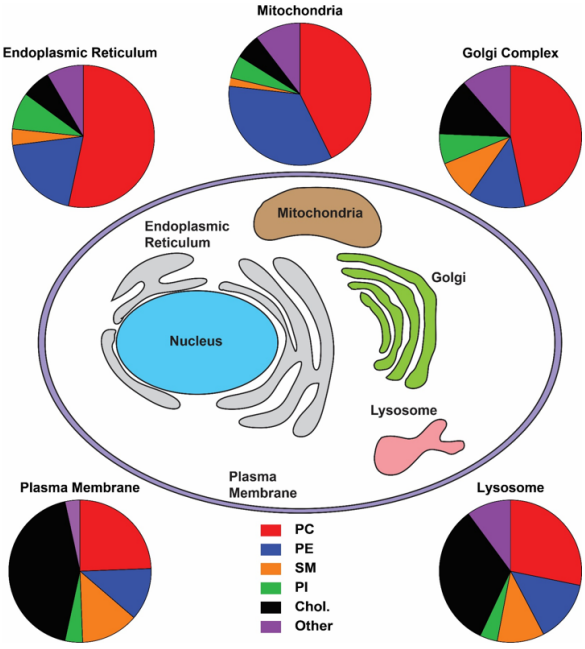

Figure 3. Lipid compositions of membrane from various organelles in mammalian cells.

The lipid composition of membranes from rat liver cells (derived from multiple sources) are shown. Abbreviations: PC: phosphatidylcholine, PE: phosphatidylethanolamine, SM: sphingomyelin, PI: phosphatidylinositol, Chol: cholesterol..

membrane protein folding and stability is largely unexplored, but seems likely. In this regard, an interesting preliminary observations is that high levels of cholesterol in the membrane tend to promote alignment of otherwise tilted transmembrane helices with the bilayer normal.(*99*). It has also been reported that plasma MPs tend to have longer TM segments than resident MPs of the Golgi and endoplasmic reticulum.(*39*)

The original fluid mosaic model(*100*) continues to serve as a point of reference for our understanding of the organization and dynamics of biological membranes. Nevertheless, the simplistic assumptions of this model have been subject to a variety of clarifications, revisions, and updates over the years.(*101-103*) The controversy associated with “lipid rafts” is of particular note with respect to MP folding.

It has long been appreciated that bilayers are capable of forming a liquid-ordered phase (L_o) at certain temperatures and lipid compositions (especially those rich in cholesterol and sphingolipids). Lipids within L_o phase membranes exhibit conformational and diffusional order that is somewhere between those within dynamic liquid-disordered (L_d, also referred to as the fluid, liquid crystalline, or L_α phase) and highly ordered gel phase membranes.(*104-106*) Various cholesterol and sphingolipid-rich membranes such as those of myelin, caveolae, and the apical surfaces of some epithelial cells have characteristics akin to L_o phase membranes.(*107-110*) Like synthetic L_o membranes, these natural membranes are also resistant to detergent solubilization.(*111-113*) These considerations have contributed to the hypothesis that the plasma membranes of higher organisms contain phase-separated “lipid rafts” that exhibit L_o-like phase behavior.(*104, 114-117*)

Macroscopic L_d and L_o phases are capable of coexisting within a single lipid vesicle in a manner that can be visualized by confocal fluorescence microscopy.(*118, 119*) However, until very recently(*120*) there was little evidence to suggest that the intact membranes of living cells were capable of undergoing robust phase separation. For this reason, the very existence of lipid rafts and their potential biological relevance have proven controversial.(*121, 122*)

The existence of lipid rafts is typically debated in the context of eukaryotic plasma membranes. Direct observation of coexisting phases in the plasma membranes of living cells has proven extremely challenging. However, macroscopic phase separation does occur upon lowering the temperature (to well below physiological temperature) in giant plasma membrane-derived vesicles” (GPMVs) that have been blebbed from eukaryotic plasma membranes.(*115, 119, 122*) Many different membrane proteins, especially those that are palmitoylated, appear to preferentially partition into the L_o phase under these conditions.(*123-126*) Others are

enriched at the interface of the L_o and L_d phases.(*127-130*) However, the manner in which these observations pertain to the behavior of intact bilayers under physiological conditions remains the subject of active investigation.

There is considerable evidence to suggest that small (<50 nm) ordered domains are capable of transiently forming in the context of otherwise disordered plasma membranes. Over the past 15 years, a classic series of studies from the Keller, Veatch, and Baird labs have offered a satisfying explanation for the dynamic co-existence of less-ordered and more-ordered phases within plasma membranes.(*131-134*) This explanation is based on appreciation of the fact that the phase diagrams of multicomponent systems (in this case for membrane bilayers) sometimes have compositions for which there is a critical temperature, T_c.(*135*) Critical points, which are a general feature of multidimensional phase diagrams, occur at the limit of the two-phase region in which the L_o and L_d phases coexist. At a critical point, the compositions and populations of both phases are equal and lipids randomly fluctuate between phases in a manner mediated by thermal energy (k_BT). Below T_c (at fixed membrane composition) the membrane demixes into two stable macroscopic phases. Above T_c, the phases appear to mix into a single phase. Nevertheless, ensembles of lipids are still capable of transiently sampling ordered phases above T_c through “critical fluctuations.” As the temperature is increased above T_c, the size of these fluctuations (their “correlation length”) decreases. The shapes of these transient ordered domains are irregular as a result of the reduced line tension between phases. Notably, the physical basis for this framework can be modeled reasonably well using a two dimensional Ising model, which provides a mechanistic framework that can be used to rationalize membrane organization.(*136*)

Remarkably, studies of GPMVs from mammalian plasma membranes exhibit critical behavior at reduced temperatures, with T_c values on the order of 10-20° below 37°C.(*131, 133, 134*) This phenomenon has been documented in GPMVs derived from multiple cell types through a series of painstaking and rigorous observations.(*131-134*) These collective observations suggest that small portions (<50 nm) of the plasma membrane are likely to transiently sample ordered phases at physiological temperature. These phases likely have only slight differences in composition and order than the co-mingled disordered phase. This framework offers a very satisfying resolution to the “lipid raft” controversy by providing a generalized physical explanation for the extensive number of nuanced biochemical and biophysical observations suggesting biological membranes do not behave as ideal liquid phase assemblies. Plasma membrane do contain more-highly

disordered domains in co-existence with more fluid microdomains. However, not only are these domains transient—mere fluctuations!—but the differences in the lipid compositions and order between the less and more highly ordered domains are likely to be quite modest.(*137*) Indeed, imaging mass spectrometry studies have documented that cholesterol is distributed uniformly across intact mammalian plasma membranes,(*138, 139*) though sphingomyelin appears to form small clusters.(*140, 141*)

The biological implications of critical behavior within biological membranes is just beginning to be explored. For example, critical behavior provides a quantitative framework that accounts for the manner in which certain receptors undergo spatial clustering and oligomerization.(*136*) It is interesting to ponder how the dynamic jostling of MPs between percolating more- and less-ordered phases in the plasma membrane might alter MP stability and the energetics of oligomerization. This is clearly an avenue for future exploration. At the same time, we note that appreciation of critical behavior in biological membrane will ultimately need to be melded with what is understood about of how cytoskeletal attachment points, lipid asymmetry, and abundant membrane proteins alter membrane-based phenomena, including MP folding and stability.

2.2. Tolerance versus Adaptation to Varying Membrane Environment

Longstanding interest in how lipids interact with MPs has heightened in recent years as advances in both computational and experimental structural biology (especially mass spectrometry) have provided new details on the nature of these interactions.(*142, 143*) Moreover, biochemical and biophysical studies have revealed some of the ways by which MP function is regulated by lipids that act as allosteric ligands.(*144-148*) For instance, phosphatidylinositol-4,5-diphosphate (PIP2) and polyunsaturated fatty acids (PUFAs) regulate the function of many different MPs through specific binding interactions.(*149, 150*) The functions of MPs can also be tuned by variations in bulk lipid composition.(*151, 152*)

Stoichiometric complexes between certain proteins and lipids have been found to promote the stability and organization of native MP complexes.(*153-157*) The formation of correct membrane topology and folding of certain proteins sometimes requires specific protein-lipid interactions.(*158-161*) MP folding and stability also depends on both bulk membrane composition and the physical properties of the bilayer.(*65, 162-166*) Disruption of lipid-MP interactions is likely responsible for some diseases.(*167*)

In addition to *adapting* to the chemical and physical properties of the membrane environment, native MP conformations must, to some extent, also have evolved to *tolerate* variations in membrane lipid composition.(*168, 169*) Eukaryotic MPs must remain folded and functional in the face of fairly dramatic changes in lipid composition that occur as proteins are shuttled from the ER to the Golgi and beyond. Each of these organelles has its own distinctive lipid composition (**Fig. 3**),(*93, 94*) which likely plays a role in the tuning of the structure and function of resident MPs. It has been empirically shown that the subset of MPs that reside within these organelles exhibit distinct distributions of TM domain lengths, which implies these proteins may have been tailored to fold and function within distinct membranes.(*39*) Nevertheless, there are several lines of evidence to suggest their native structures typically persist across divergent membranes. For instance, the lipids of archaebacteria have exotic structures compared to eubacteria and eukaryotes,(*170*) yet the native structures MPs from archaea appear to be similar to those of the homologous proteins from eubacteria and eukaryotes (**Fig. 4**).(*168, 171*) Furthermore, certain lipid biosynthetic have been completely knocked out in *E. coli* in a manner that dramatically alters membrane lipid composition and yet results in only limited influence on cellular viability.(*172, 173*) This implies that most of the proteins that reside within these reformatted membranes retain function. Indeed, it has been shown that there is no single type of phospholipid that *E. coli* cannot survive without.(*173, 174*) Given this apparent tolerance, it is perhaps unsurprising that a great many MPs retain their native fold within the artificial environment of

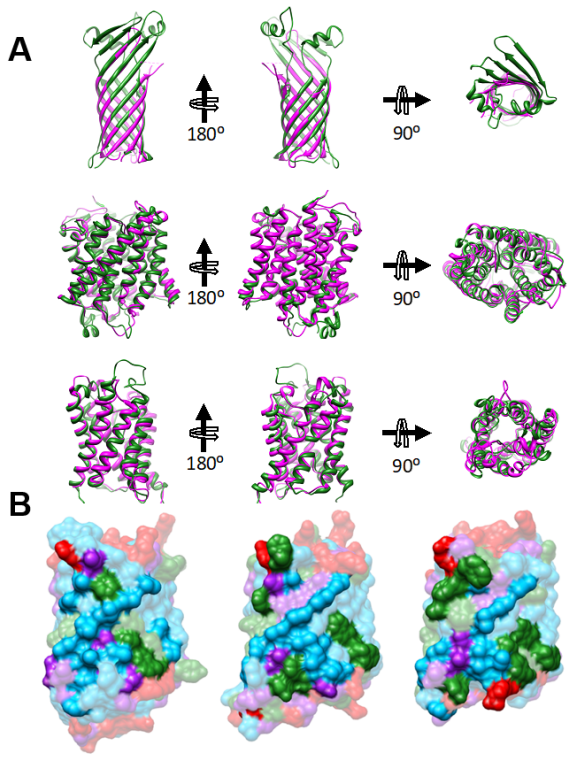

Figure 4. Comparison of MP structures from the disparate domains of life. (A) Superpositions of structures of thermophilic archaeal MPs on those of mesophilic counterparts reveal high similarity.

Superposition of porins TtoA from Thermus thermophilus (green, PDB ID: 3DZM) and OmpA from *E. coli* (magenta, PDB ID: 1QJP). (Middle Panel) Superposition of ammonium transporters Amt-1 from the archaeal hyperthermophile *A. fulgidus* (green, PDB ID: 2B2H) and AmtB from *E. coli* (magenta, PDB ID: 1U77). (Bottom Panel) Superposition of aquaporin from *A. fulgidus* (green, PDB ID: 3NE2) with AqpZ from E. coli (magenta, PDB ID: 1RC2). View onto the membrane surface is from the periplasm/extracellular space. **(**B) The lipid-contact faces of aquaporins from three domains of life exhibit common features. Shown are aquaporins from a hyperthermophilic archaebacterium, *A. fulgidus* (PDB ID: 3NE2, left), *E. coli* (PDB ID: 1RC2, center), and *O. airies* (sheep) (PDB ID: 3M9I, right). Residues are colored as follows; red: polar residues; blue: large hydrophobic; green: aromatic/His; purple: small (Gly, Ala, Ser, Cys).

detergent micelles, which have very different physical chemical properties than *bona fide* membranes. Indeed, some MPs continue to fold and function even when solubilized by amphipathic polymers, which shield the hydrophobic portions of the molecule from water.(*33, 175, 176*)

Altogether, the growing body of data regarding how MPs interact with bilayers and specific lipids indicates that MPs have evolved in concert with the membranes in which they reside to satisfy the imperative of being able to robustly fold and function even in membranes of varying compositions, while in many cases also being appropriately regulated by specific lipid binding and varying membrane properties. When considering this dichotomy from the perspective of MP folding, it should not be surprising that there are examples where specific lipid interactions are required for folding.(*158-161*)

3. Kinetics and Thermodynamics of Membrane Protein Folding

3.1. Conformational Stability and the Physiologically Relevant Unfolded States of Integral Membrane Proteins.

Proteins sample a continuum of conformational states regardless of whether they reside in water or in a lipid bilayer. The relative abundance of molecules that adopt a given conformational state is primarily dictated by the kinetic and/or thermodynamic barriers that separate this state from competing conformations.(*177*) The magnitude of these energetic barriers is largely determined by the primary structure of the protein, how the molecule is solvated, and the abundance of cofactors that bind and stabilize certain conformations. Only a small subset of compactly folded, energetically accessible conformational states are capable of mediating protein function. Thus, the fraction of protein that is functional may largely depend on the free energy difference between the native ensemble and the lowest

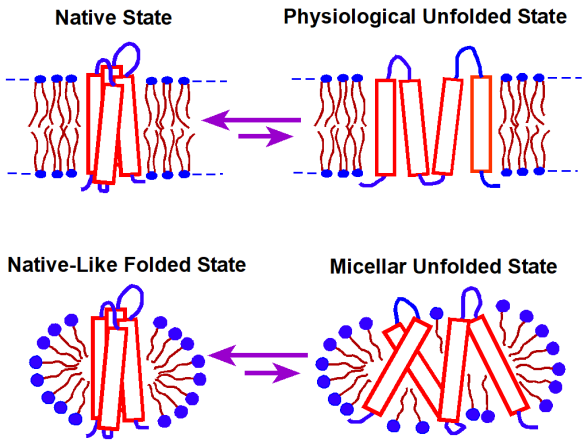

Figure 5. Folding equilibrium for a MP in lipid bilayers versus in detergent micelles.

The native conformation is often the most favorable conformational state for MPs in bilayers and micelles. However, the structural properties of the accessible denatured states, the energies between folded and unfolded states, and the magnitude of the energetic barriers that separate them from the native state may differ in bilayers and in micelles.

energy non-functional conformational state(s) that are populated under native conditions, which we will refer to hereafter as the *physiological unfolded state* (**Fig. 5**). The physiological unfolded states are likely akin to transient partially unfolded states of water-soluble proteins that lack ordered structure in one or more subdomains.(*178, 179*) However, far less is known about the physiological unfolded states of helical integral MPs, or how they exchange with the native state. This uncertainty constitutes a central caveat to ongoing discussions of MP folding and stability. Nevertheless, some educated guesses about the properties of the physiological unfolded states of α-helical MPs can be made in light of the physicochemical properties of these proteins and of the membrane itself. First, given their sheer hydrophobicity, polytopic α-helical MPs are likely to remain confined within the membrane throughout most of their lifespan, regardless of their conformational state. Given the low dielectric constant within this environment,(*16, 42*) hydrophobic TM segments are likely to retain their helical secondary structure, even under conditions in which the native tertiary structure is lost. Thus, the physiological unfolded states likely constitute bundles of weakly interacting helices within the membrane; an ensemble of structures akin to the first stage of the classic 2-stage model for MP folding originally suggested by Popot & Engelman.(*16*)

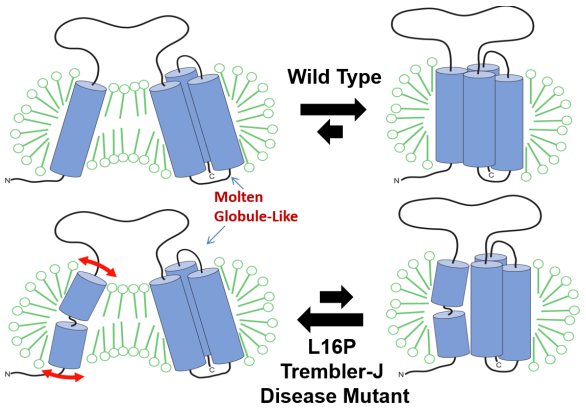

Figure 6. Folding equilibrium for WT and L16P mutant PMP22.

This is was determined using NMR and other methods under conditions where PMP22 is solubilized in tetradecylphosphocholine micelles at 25 °C. The L16P mutation site is located in the first TM helix with the proline substitution resulting in the flexible hinge illustrated in the lower left panel. We suggest that the "partially unfolded state" depicted on the left may actually be similar to the true physiological unfolded state. Further unfolding is restrained by the short loops connect TM2 to TM3 and TM3 to TM4.

Though technical barriers have largely prevented characterization of physiologically relevant unfolded states in their native environment, a handful of studies have provided clues about the properties of non-native states that are energetically accessible *in vitro*.(*5, 180-184*) Here, I will focus on two recent examples. Solution nuclear magnetic resonance (NMR) studies of peripheral myelin protein 22 (PMP22) in micelles have revealed that the folded form of this protein is in equilibrium with a conformational state in which the N-terminal TM segment is fully dissociated from the other 3 TM segments, the latter of which interact in a molten globule-like manner (**Fig. 6**).(*184*) Furthermore, this conformational state is promoted by the pathogenic L16P mutation within its first TM domain. In a second

example, NMR studies of the KCNQ1 voltage sensor domain have also revealed that mutations known to promote cellular mistrafficking of the full length channel also perturb how the TM helices interact within LMPG micelles.(*185*) None of the 47 mutations examined in that study caused the protein to dissociate from the micelle or to transition to a random coil state. However, the NMR spectra of mutant forms of KCNQ1 that were seen to be trafficking-defective in cells exhibited peak broadening that is consistent with molten globular structure, a well-known folding intermediate state for many water-soluble proteins (see Section 5.4.1).(*185, 186*) The extent to which these conformational transitions in detergent micelles relate to physiological unfolded states is not yet well-established. Nevertheless, the observed effects of these destabilizing mutations *in vitro* are intriguing. In the following, I summarize current knowledge regarding the conformational equilibria of integral MPs, with how folding/unfolding transitions relate to the molecular basis of MP misfolding and disease.

3.2. Native Membrane Protein Structures are Thermodynamically Stable

Christian Anfinsen's landmark investigations into the folding of RNase A established that the native conformations of water-soluble proteins tend to reside within free energy minima.(*11, 12*) Like all conformational transitions, it stands to reason that MP folding should also serve to reduce the free energy of the system. However, MPs must navigate their conformational energy landscapes within a much more complex solvent, which is likely to alter the kinetic barriers to folding. For this reason, early investigations of MP folding were mindful of the possibility that the functional structures of integral MPs could be kinetically accessible yet thermodynamically unstable. Pioneering investigations of the α-helical MP bacteriorhodopsin (bR) demonstrated the native fold could be regenerated from the SDS-denatured state upon addition of cholate and/or soy bean lipids.(*5*) This key observation echoed Anfinsen's finding that the primary structure contains all of the information needed for the protein to achieve its functional structure under native-like conditions. This conclusion was also supported by subsequent observations that natively folded bR could be regenerated from denatured proteolytic bR fragments.(*8*) Since these investigations there have been numerous studies of MP folding in mixed micelles, bicelles, and synthetic lipid bilayers(*187, 188*) showing that a wide array of β-barrel and α-helical MPs are capable of reclaiming their native structures regardless of whether the proteins are first denatured using organic solvent,(*189*) chaotropes,(*166, 190-194*) anionic detergents,(*10, 48, 195-197*) steric trapping,(*198, 199*) or mechanical force.(*200-202*) Thus, there is now ample evidence to suggest the native

conformations of integral MPs are thermodynamically stable relative to an array of non-native denatured states including the “physiological unfolded state” described in Section 3.1 and **Fig. 5**. It is also clear that some denatured integral MPs can find their way back to the native conformation on experimentally accessible time scales. Nevertheless, even when a MP reaches its thermodynamically-favored functional conformation, it is not always clear that such folded states are at equilibrium with physiological unfolded states, as is discussed further below.

Experimental investigations of water-soluble proteins most often utilize concentrated urea or guanidinium to induce global unfolding. Although certain proteins retain residual structure under these conditions,(*203*) the denatured ensemble of most water soluble proteins is dominated by random coil structure. This lack of well-defined intramolecular interactions provides a useful reference state in investigations of the contributions of intramolecular interactions to conformational stability. However, many α-helical MPs cannot generally be unfolded in this manner,(*204*) and even those that exhibit sensitivity to urea typically retain helical secondary structure within a diverse array of commonly employed membranes and membrane mimetics (**Fig. 7**).(*166, 192-194*) In contrast, β-barrel MPs globally unfold and partition into the aqueous phase in concentrated urea solutions,(*190*) a transition that can be rendered fully reversible. Under controlled conditions,(*191*) dilution of the protein/denaturant solution in the presence of lipid vesicles results in the spontaneous transfer of denatured β-barrel proteins into the bilayer in a manner that is reversibly coupled to folding. The energetics of these folding transitions are highly sensitive to the experimental conditions (especially the properties of the lipid bilayer) and vary considerably among members of the β-barrel family.(*25, 26, 188, 190, 205*) Nevertheless, in many

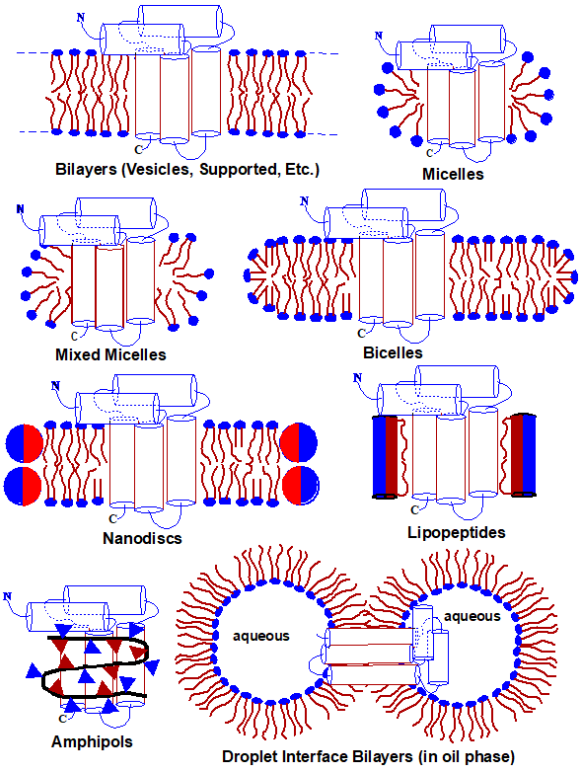

Figure 7. Classes of model membrane used in studies of purified MPs.

Not illustrated here are “lipodisqs”, which resemble nanodiscs except that a synthetic amphipathic polymer is used to stabilize the edge of the bilayered disc instead of an amphipathic protein.

cases β-barrel folding appears to be extremely favorable under ambient conditions. Indeed, the strong driving force associated with this reaction appears to provide some of the energy needed for the sorting of proteins destined for the outer membrane in the periplasm.(*206*) Ongoing studies of the mechanisms by which molecular chaperones assist in the folding and assembly of β-barrels offer the potential to provide additional insights into the energetics of bacterial proteostasis systems.(*207, 208*) Beyond the biological relevance of these measurements, the nature of this transition has also provided unique opportunities to evaluate the transfer free energies of amino acid side chains from the aqueous phase into the lipid bilayer.(*191, 209-211*) Together these special properties of β-barrels have made them an extremely useful system for investigating MP insertion and folding.

In contrast to β-barrels, α-helical MPs typically cannot be driven from membranes into the aqueous phase without excessive aggregation (with exceptions described in Section 3.7). In the cell, most α-helical MPs are co-translationally inserted into the membrane in a manner that obviates the need for them to transiently reside in the aqueous phase. Furthermore, the removal of helical proteins from the membrane under physiological conditions requires hydrolysis of hundreds of ATP molecules(*212*) and is typically coupled to proteolysis or to the formation of ordered aggregates known as aggresomes.(*213*) Thus, α-helical MPs are unlikely to sample fully hydrated states under physiological conditions. Accordingly, it is likely that the physiological folding trajectories within the membrane primarily involve transitions between non-native helical intermediate states. Experimental efforts to assess the conformational stability of these proteins have most often employed anionic detergents (typically SDS) to induce denaturation in the context of mixed micelle solvents.(*5, 7, 10*) Helical MPs typically retain secondary structure but lose their native tertiary structure in the SDS-denatured state.(*10, 214, 215*) When the concentration of denaturant is expressed in terms of detergent mole fraction,(*10*) equilibrium unfolding transitions typically exhibit the markings of a cooperative two-state unfolding reaction.(*10, 196, 197, 216-218*) In the context of these conformational transitions, mutagenesis studies have revealed that, despite vast differences in solvation, the stabilization afforded by native hydrogen bonds and packing interactions are on par with those in the context of water-soluble proteins.(*48, 205, 219*) The interpretation of these measurements is certainly complicated by the presence of residual structure in the denatured state. The loss of native contacts upon denaturation is likely coupled to the formation of a spectrum of weaker non-native interactions in the denatured ensemble. Nevertheless, this likely parallels the

physiological reaction coordinate in which the native conformation must compete with a spectrum of alternative arrangements of weakly interacting helices in the physiological unfolded state. Overall, these observations suggest that the *effective* strength of native interactions are likely to be considerably lower than would expected based on the dielectric constant within the bilayer.(*16, 42*) In addition to the presence of modest levels of water in the membrane core, the protein itself offers hydrogen bonding groups that are capable of competing with native interactions.(*47*) A better understanding of the structural properties of the physiological unfolded state within biological membranes is needed in order to clarify the true stability of the native fold relative to physiological unfolded states.

3.3. Native Membrane Protein Structures can be Kinetically Stable

Cells are non-equilibrium systems, and kinetic control of chemical reactions is a mechanistic pillar of biomolecular regulation. With regard to protein folding and assembly in the cell, many chaperone-assisted folding and degradation networks appear to be under kinetic control.(*220-223*) Thus, in some cases slow unfolding (kinetic stability) may be an essential property of long-lived MPs. Pioneering investigations into the relaxation kinetics of bR in mixed micelles provided some of the first evidence suggesting that some natively folded MPs may exhibit extreme kinetic stability. An extrapolation of the observed unfolding rate constant at high mole fraction of the denaturing detergent SDS (X_{SDS}) was interpreted to suggest the half-life of bR unfolding is on the order of thousands of years in lipid bicelles.(*215*) Though the unfolding of bR is undoubtedly slow, this estimation required a lengthy extrapolation from a condition in which the protein resides within an SDS-rich mixed micelle to a condition in which the protein resides within a DMPC-rich, SDS-free bicelle. The general extrapolation method has been criticized.(*196,197*) Despite this caveat, a number of subsequent observations have suggested that at least some MPs may unfold slowly. Bowie and co-workers showed that the half-life for dissociation of the subunits of diacylglycerol kinase in beta-octylglucoside micelles (considered mildly destabilizing relative to more ideal model membranes) is on the order of two weeks.(*224*) A recent investigation of the *E. coli* intramembrane protease GlpG revealed that unfolding requires weeks in lipid bicelles as monitored by steric trapping,(*212*) a timespan in reasonable agreement with its extrapolated rate constants for SDS-mediated denaturation.(*196*) Indeed, the application of magnetic tweezers to GlpG also revealed the native state resides within a steep energy well.(*225*) It remains unclear whether high kinetic

stability is a common property of integral MPs or whether this is a special property of these particular proteins, each of which also exhibits considerable thermodynamic stability.(*10, 196, 198, 199*) DsbB exhibits modest thermodynamic stability and folds and unfolds relatively rapidly.(*226, 227*) Nevertheless, the metastable human protein PMP22, which is only marginally stable in DPC micelles, requires hours for relaxation under this condition.(*197*) The notion that some helical MPs fold into thermodynamically preferred native states that are then effectively kinetically trapped potentially has wide-ranging implications for MP folding in the cell. Considerations regarding the kinetics of conformational exchange may also be a relevant factor in efforts to develop small molecules that correct the folding and stability of disease-linked MPs, as is discussed further below.

Could kinetic entrapment of the native state of some MPs be biochemically tunable? Interestingly, it has been demonstrated that the binding of retinal to bacteriorhodopsin, the apoform of bR, appears to decrease its rate of unfolding by over ten orders of magnitude.(*228*) The physical basis for this effect suggests the binding of small molecules may potentially play a general role in the tuning of the kinetic and/ or thermodynamic stability of integral MPs.(*229-234*) Because small molecules tend to selectively bind to natively folded proteins, binding should universally decrease the rate of unfolding and increase thermodynamic stability in a manner related to the binding affinity and ligand concentration, provided ligand dissociation occurs prior to formation of the transition state for unfolding (**Fig. 8**). Indeed, many G protein-coupled receptors (GPCRs) are known to bind agonists and antagonists with nanomolar to picomolar affinity, resulting in increased protein stability.(*235, 236*) Specific interactions of lipids with proteins also appears to frequently enhance the stability of MP oligomers.(*153*) Thus, it is quite plausible that MPs rely on specific lipid and/or physiological small molecule interactions to tune their relaxation kinetics in a manner that alters their cellular trafficking and turnover. In many cases, the extent to which drug binding influences the unfolding kinetics of MPs may also be relevant to their mechanism of drug action. It is also noteworthy that, in some cases,

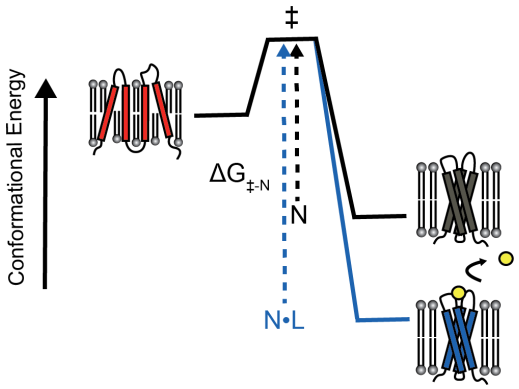

Figure 8. Effect of Ligand Binding on the Kinetic Stability of Integral Membrane Proteins.

If the native binding pocket is disrupted prior to the rate limiting step for unfolding, then excess ligand will selectively stabilize the native conformation (N) relative to the transition state for unfolding (‡) and the denatured state (red). In this case, the rate of unfolding and the fraction of unfolded protein at equilibrium will be decreased in the presence of ligand.

metabolite binding to certain MPs appear to *destabilize* the folded state, leading to regulated degradation.(*230, 237, 238*) Additional investigations into the linkage between ligand binding, kinetic stability, and the cellular proteostasis of integral MPs are needed.

3.4. Membrane Protein Folding Kinetics

Anfinsen's formative experiments provided a framework for understanding how proteins select their functional structures from a vast sea of competing non-native conformations. Nevertheless, Cyrus Leventhal subsequently noted that this thermodynamic perspective did not provide an obvious explanation for the fact that proteins navigate this immense conformational space within remarkably short time scales.(*239*) Considerable efforts spanning decades sought to elucidate the nature of the kinetic intermediates involved in the rapid folding of water-soluble proteins. These investigations revealed considerable heterogeneity in the pathways by which proteins achieve their native secondary, tertiary, and quaternary structures. Many proteins appear to fold through a discreet set of structurally defined intermediates,(*240, 241*) while others appear to fold through an array of parallel pathways.(*242*) Despite this mechanistic heterogeneity, the fact that certain structural intermediates seem to form more readily than others suggests that proteins solve this kinetic dilemma through a biased search: the formation of early intermediate structures (or a folding core) dramatically reduces the accessible search space for subsequent transitions. Though considerably less is known about MP folding kinetics, it is clear that even the physiological unfolded state of MPs tends to retain secondary structure within the bilayer in a manner that should severely constrict their conformational search. Accordingly, the topological and secondary structural constraints imposed by the bilayer may vastly simplify the MP folding problem.(*243*) Nevertheless, technical challenges have plagued efforts both to measure the rate of protein folding within the membrane and to elucidate the factors that influence the kinetics of this process. It is therefore unclear whether the kinetic mechanisms that govern MP folding reactions parallel those of soluble proteins.

Pioneering investigations into MP folding kinetics focused on the folding of SDS-denatured bR in bicelles (see **Fig. 7**). Spectroscopic investigations of this process revealed that, much like the folding of soluble proteins, the folding of bR occurs through a series of transient structural intermediates.(*9*) Observations of this process using multiple spectroscopic tools suggested early intermediates involve the formation of tertiary

contacts while the binding of the retinal ligand and the extension of the native helices occur later.(*9, 244, 245*) Nevertheless, these investigations were insufficient to reveal the nature of the structural transitions that limit the rate of folding. Efforts to probe the structural properties of the transition state for BR folding under conditions in which folding occurs through a single phase were initially probed using phi-value analysis.(*246*). Phi-value analysis is applied to proteins in the form of a mutagenic approach to identify native tertiary contacts that are formed within the transition state.(*247*) However, interpretation of the BR measurements was complicated by the fact that variations in the concentrations of lipids and detergents obscured the influence of mutations on the rate of BR folding under these conditions.(*248*) Under more controlled conditions, a subsequent analysis of an array of bR mutants distributed throughout its three dimensional structure failed to identify any native tertiary contacts that appreciably limit the rate of folding.(*249*) The apparent absence of a folding core is interesting considering that the kinetics of water-soluble protein folding is typically rate-limited by the formation of sequence-distant tertiary contacts.(*250*) Based on these results, it was proposed that bR folding is rate-limited by a topological search, in which pre-formed TM helices sample an array of interhelical contacts.(*249*) This interpretation was supported by the recent findings that bR folding can be accelerated by simply reducing the size of the bicelle, which is likely to reduce the degrees of freedom in the denatured ensemble.(*251*) Thus, it appears the energetic barrier to bR folding is rooted in conformational entropy, at least in bicelles. These investigations paint a picture of the conformational energy landscape of bR that resembles the hypothetical champagne glass-shaped landscape originally described by Dill & Chan (**Fig. 9**);(*177*) the protein must explore a variety of near-isoenergetic orientations of pre-formed helices before eventually stumbling upon the native topology. Nevertheless, given the artificial nature of the

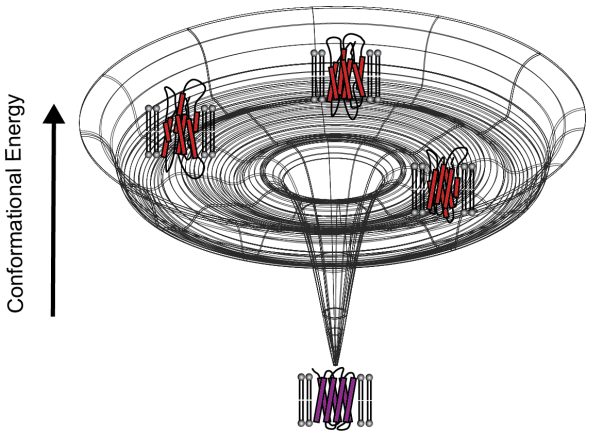

Figure 9. Hypothetical Morphology of the Conformational Energy Landscape for bR in DMPC/ CHAPSO/ SDS Bicelles.

This cartoon depicts a hypothetical energy landscape that describe the conformational energetics of bR in bicelles. The upper rim of the conformational energy landscape represents the random coil state, which is unlikely to be sampled within membranous environments. Instead, the TM segments are likely to persist in an ensemble of helical bundles within the denatured state, which is represented by the secondary basin of the energy landscape. To find the native conformation, helical TM segments must explore various topological configuration until the native topology is achieved and folding can proceed downhill. It is emphasized that for many membrane proteins, the folding funnel will be much more complicated than as proposed here for the well-characterized case of BR.

micellar/bicellar solvent used for these studies, it is uncertain whether these findings can be fully extrapolated to the mechanism of bR folding within natural membranes, much less to other polytopic MPs.

Phi-value analysis has been employed to evaluate the nature of the transition state of two other α-helical MPs to date. An analysis of the kinetic effects of 12 alanine mutants enabled phi-value analysis of the *E. coli* disulfide bond reducing protein B (DsbB),(*252*) an α-helical MP that folds by way of a single observable kinetic intermediate in mixed micelles. The results of this analysis revealed that two residues near the edge of a TM domain appear to be involved in the rate limiting step for the formation of the intermediate, and that native contacts appear to propagate from this region within the intermediate state.(*252*) Similarly, an exhaustive kinetic analysis of 69 GlpG variants also identified two residues near the cytosolic edges of two neighboring N-terminal helices that appear to form native contacts in the transition state.(*196*) In contrast with the findings for bR folding, the folding of these two proteins appears to be rate-limited by the formation of native contacts near the edges of specific TM domains. Though these results are potentially suggestive of mechanistic differences between bR, DsbB, and GlpG, caution must be exercised when comparing these studies. It is possible that differences in the mixed micelle/ bicelle components may alter the denatured state ensemble in a manner that fundamentally distorts their folding trajectories. Nevertheless, these findings highlight the potential for mechanistic diversity in the folding kinetics of helical MPs. Moving forward, it may be particularly interesting to consider how folding pathways may vary for helical MPs containing stable soluble domains, which often appear to have evolved from soluble proteins(*253*). Can the rapid folding of a soluble domain seed folding within the membrane, or vice versa? Additional studies are needed to explore how folding pathways may be navigated under such circumstances.

Unlike α-helical MPs, investigations of the folding kinetics of β-barrels are less muddled by the potential influence of residual structure in the denatured state (although see(*183*)). Furthermore, investigations of the folding kinetics of β-barrels can be carried out using true lipid bilayers, which is a distinct advantage relative to kinetic investigations of α-helical MPs. Nevertheless, the kinetic mechanism(s) that modulate the folding of β-barrels *in vitro* still appear to be exquisitely complex. Initial studies of outer membrane protein (OMP) folding kinetics from aqueous solution to the folded form in lipid vesicles were conducted by Jahnig and co-workers,(*71, 207, 208, 254, 255*) and subsequently continued in an extensive study by Kleinschmidt and Tamm.(*188, 256-259*) Many of the kinetic constraints of these reactions have been characterized, including the

general magnitude of the activation energies associated with rate-limiting transitions. However, the interpretation of β-barrel folding kinetics is complicated by the fact that structural transitions coincide with the transfer of the protein from the aqueous phase to the membrane interface and eventually from the interface to the membrane core. Indeed, the rate limiting transitions for β-barrel folding are sensitive to the lipid to protein ratio, to the composition of the lipid head groups and chain lengths, and to the lateral pressure of the bilayer.(*260*) Nevertheless, phi-value analysis of the β-barrel protein PagP revealed that the rate-limiting step for folding likely involves the formation of numerous native-like interactions between side chains that are coupled with the transfer of the protein from the interface to the membrane core.(*261*) This transition state presumably also involves protein-lipid contacts that distort the bilayer, as the rate of OMP folding is accelerated under conditions that introduce lipid packing defects.(*262*) A recent comprehensive investigation of the folding kinetics of OmpA revealed that the folding of this protein occurs with no fewer than five intermediate states, some of which are off-pathway, even under the most optimal conditions.(*263*) Given the vast array of intermediates that accumulate *in vitro* along with the fact that the folding of purified β-barrels is rate-limited by its transfer into the bilayer under certain experimental conditions, it is perhaps unsurprising that outer MP biogenesis in cells relies on the activity of BamA,(*264*) a chaperone that catalyzes the insertion of β-barrels into the membrane.(*265*) The reader is also referred to elegant studies of the interactions of unfolded OmpA with the periplasmic chaperone Skp, which helps the nascent porin reach the other membrane without aggregating or prematurely forming tertiary structure.(*208, 266*)

3.5. Helical Membrane Protein Folding within Lipid Bilayers

Kinetic and thermodynamic investigations of folding and unfolding in micelles, bicelles, and synthetic membranes have yielded considerable insights into the conformational energetics of integral MPs. However, given the drawbacks of these artificial solvents, there is still much to be learned about the conformational equilibria of MPs in their native environments. This is especially true for α-helical MPs, for which biophysical studies in lipid bilayers are few and far between. Nevertheless, several recent breakthroughs have paved the way for the next generation of folding studies.(*200*) For instance, a recent report from the Booth lab demonstrated that *E. coli* LeuT, a structural homolog of neurotransmitter sodium symporters, can be reversibly unfolded by urea in the context of a variety of synthetic liposomes, provided that sub-micellar concentrations of

β-octylglucoside are included to facilitate the equilibration of urea across the bilayer.(*166*) Under these conditions, urea induces a partial loss of secondary structure and a complete loss of function,(*166*) as would be anticipated for a physiological unfolded state. Unlike the OMPs, urea does not lead to dissociation of LeuT from the bilayer to the aqueous phase. Instead, the results show that the structural properties of its denatured state and the free energy of unfolding can be tuned by lipid head groups and by the lateral pressure within the bilayer.(*166*) The native conformation is modestly favored (2.5 - 3.8 kcal/ mol) over the corresponding denatured ensembles in the vesicles of varying composition.(*166*) This suggests subtle differences in the bilayer can tune the properties of the unfolded state to re-shape the relevant features of the conformational energy landscape—a key consideration for eukaryotic MPs that must traffic through a range of different membranes within the secretory pathway.(*174*) The Booth lab has demonstrated that several transporter proteins are susceptible to denaturation by urea,(*166, 192, 193*) which may open the door for comparative studies on a range of other transporters using this approach. Thus, the unique properties of these proteins may provide an opportunity to explore a range of hypotheses regarding the nature of α-helical MP folding within the bilayer.

An additional class of next-generation experiments have sought to do away with chemical denaturants entirely. The development of steric trapping approaches, which couple the energetics of biotin-streptavidin binding to the occlusion of intra or inter-molecular contacts,(*267*) has been employed to probe the partial unfolding of helical MPs and the dissociation of helical oligomers within micelles, bicelles, and membranes (see more detailed reviews(*23, 268*)). This approach offers several key advantages, including the fact that the denatured or dissociated state remains embedded within the membrane environment. Initial applications to measure the strength of glycophorin A dimers demonstrated the power of this technique, as dimerization was found to be stronger in synthetic membranes than in micelles.(*269*) Strikingly, subsequent investigation found that natural lipid compositions significantly weaken this dimerization.(*270*)

Application of steric trapping to the unfolding of GlpG, which contains six TM domains, has provided evidence that this protein unfolds through a series of sub-global unfolding transitions.(*199*) These results were recently echoed by single molecule studies in which GlpG was mechanically unfolded within a lipid bicelle.(*271*) This denaturant-free approach probes the dissociation of TM helices within lipid bicelles as the N- and C-termini are pulled apart laterally using magnetic tweezers (**Fig. 10**). A recent application of this approach

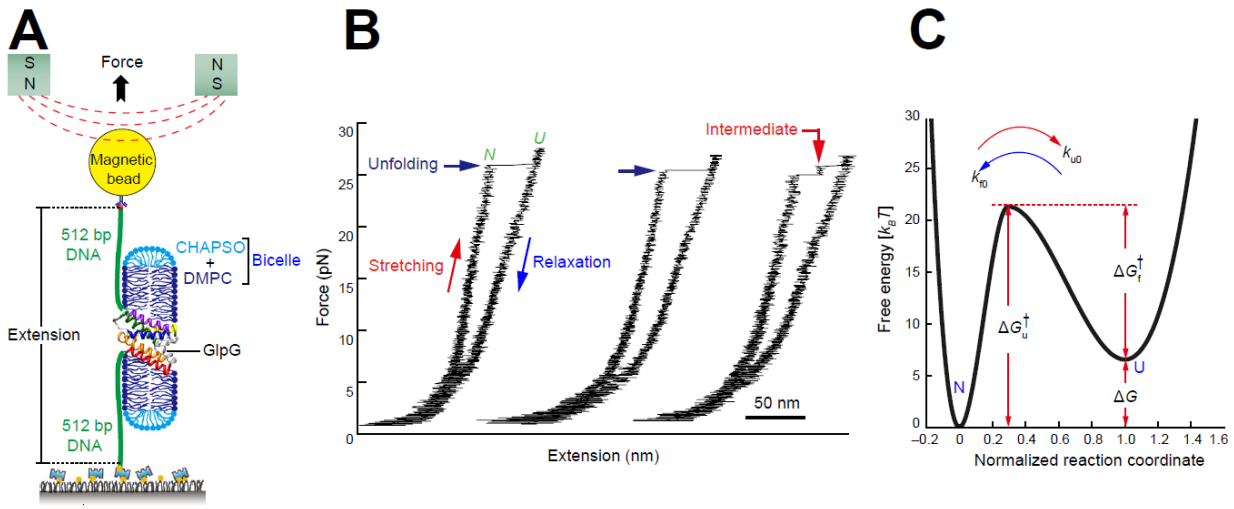

Figure 10. Single-molecule forced unfolding of a MP, GlpG.

(A) Schematic of the single-molecule magnetic tweezers experiment for studying the unfolding and refolding of GlpG in a bicelle. The protein termini have been conjugated with DNA, with the end of one DNA molecule being surface anchored and the other end being attached to a bead that can be pulled away from the surface to force unfolding of the protein in the plane of the bicelle bilayer. **(B)** Representative force-extension curves for repeated GlpG unfolding and refolding transitions. **(C)** The energy landscape for folding/unfolding of GlpG in bicelles. k_{f0} and k_{u0}: kinetic rates for folding and unfolding at zero force. ΔG: unfolding free energy. ΔGu† and ΔGf†: kinetic energy barriers for unfolding and folding, respectively.

to the ClC chloride transporter revealed that the intact subdomains of this protein are capable of separating prior to force-mediated sub-global unfolding within the bilayer.(*201*) Interestingly, each of these magnetic tweezer studies has provided compelling evidence that both the native and partially unfolded forms of these proteins are kinetically stable; a clear indication that excursions between the native and partially unfolded forms occur on a time scale of minutes to hours. The apparent spectrum of partially unfolded forms that are accessible by these techniques as well as the marginal free energy differences that separate them is reminiscent of the transient partially unfolded forms of soluble proteins that are observable by hydrogen/ deuterium exchange.(*178*) Indeed, it has long been postulated that TM helices and/ or helical bundles may behave as domain-like structural units.(*16, 42, 272*) Thus, this interpretation of the conformational energy landscape seems quite plausible in light of recent observations.

Next-generation approaches to study the conformational transitions within lipid bicelles and synthetic liposomes will play a critical role in ongoing efforts to rationalize the conformational energy landscapes of integral MPs. However, additional steps will be needed to bridge the current gap between MP biophysics and the gritty reality of biological membranes. In this regard, advances in quantitative microscopy have provided new insights into the manner in which MPs move and interact within eukaryotic plasma membranes. Recent

theoretical and methodological advances from the Hristova lab have yielded a quantitative fluorescence resonance energy transfer (FRET) approach for the determination of equilibrium constants for MP dimerization within the plasma membranes of live cells.(*201, 273, 274*) Emerging applications of this technique have revealed that, in contrast with established views, several receptor tyrosine kinases including fibroblast grown factor (FGF) and vascular endothelial growth factor 2 (VEGFR-2) form dimers and auto-phosphorylate in the absence of activating ligands.(*275*) Recent advances in fluorescence cross-correlation spectroscopy have also provided an additional route to measure equilibrium dissociation constants, as well as the lateral diffusion coefficients for monomers and oligomers within the plasma membrane of live mammalian cells.(*276, 277*) Advanced applications of super-resolution microscopy have also provided a fascinating glimpse into how critical fluctuations of membrane phases(*134*) drive the sorting and activation of B cell receptors within the plasma membrane.(*136*) These and other emerging advances in microscopy and single particle tracking show great promise for future efforts to understand how MPs exist within their native cellular environment.

3.6. Misfolding of Purified Membrane Proteins

Misfolding is very often the unwanted companion of scientists seeking to reconstitute purified MPs into model membranes. Misfolding of nascent MPs also routinely occurs under physiological conditions, which is part of the reason that cells have an elaborate system for detecting, correcting, and sometimes degrading misfolded MPs (see Section 4). MP misfolding in the cell often results in a pathogenic loss of MP function or the formation of toxic aggregates. Nevertheless, despite considerable biomedical relevance, there have been relatively few structural studies of MP misfolding *in vitro*. The most extensively developed of these studies involved *E. coli* diacylglycerol kinase (DAGK),(*278*) a 122 residue homotrimer in which each subunit contains three TM helices.(*279, 280*)

Pioneering studies in the Bowie lab quantified the thermodynamic stability of DAGK in mixed micelles.(*10*) Wild type (WT) DAGK exhibits considerable thermodynamic stability under these conditions. Moreover, the Bowie lab found that DAGK seems to be structurally and catalytically tolerant of mutations.(*281, 282*) This paved the way to a long term study by the Sanders lab of a library of 120 single-cysteine DAGK mutants generated starting with a catalytically native-like quadruple mutant form of DAGK in which both native Cys residues were mutated to Ala (C46A, C13A) and that also contained W117R and S118T mutations. It was

soon discovered that, unlike the WT protein, many variants within this single-Cys library are highly prone to misfolding *in vitro*.(*283*) These variants therefore afforded an opportunity to systematically explore MP misfolding.

Exploration of DAGK misfolding benefited from two additional properties of this small yet complex membrane enzyme.(*194*) First, in the presence of concentrated urea or guanidinium, it is possible to solubilize DAGK in the absence of any detergent or lipid. In concentrated urea under acidic conditions, DAGK retains some secondary structure but loses its quaternary and tertiary structure. However, at low pH in concentrated guanidinium the protein is almost completely unfolded. Secondly, dilution of small aliquots from these DAGK/denaturant solutions into neutral pH detergent/lipid mixed micelles or into solutions containing synthetic liposomes results in the spontaneous insertion and folding of DAGK to its functional state (**Fig. 11**). However, this coupled insertion and folding reaction is typically inefficient. Non-productive folding does not typically result in classical aggregation under these conditions.(*194*) Careful kinetic studies by Lorch and Booth revealed considerable complexity in the kinetics of these folding transitions.(*284*)

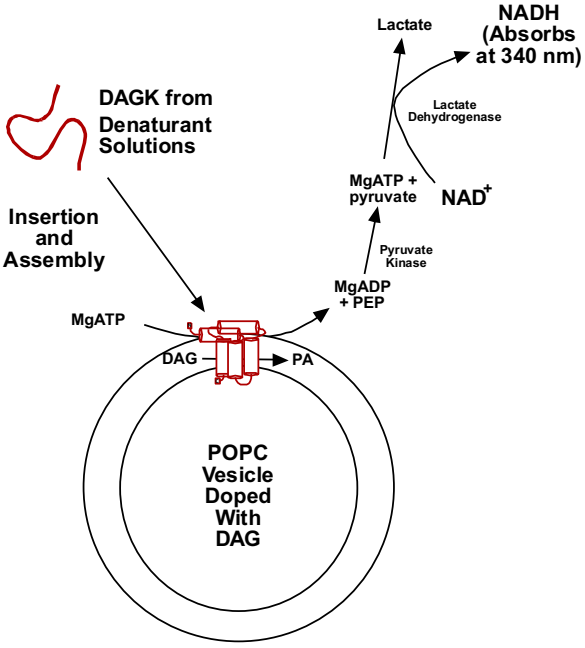

Figure 11. Assay to measure the efficiency of spontaneous insertion, folding, and trimerization of DAGK into pre-formed lipid vesicles following a many-fold dilution of a small aliquot of the pure enzyme in lipid and detergent-free urea or guanidinium solutions.

Successful folding of the protein is accompanied by the appearance of enzyme activity that is monitored through a spectrophotometrically-detected coupled assay system. The degree of misfolding is assessed based on comparing the final observed enzyme activity with the activity expected for 100% folding efficiency. Abbreviations: DAG, diacylglycerol; PEP, phosphenolpyruvate, NAD^+ and NADH, oxidized and reduced forms of nicotinamidedinucleotide.

The rates and efficiency of DAGK folding were typically greater when folding was initiated from detergent solutions (rather than denaturants) into vesicles, an observation that likely reflects both the preservation of structural elements in micelles and also the potential impact of sub-micellar detergent concentrations on the properties of the bilayer.(*194*) Moreover, the enzyme retained an ability to assemble into its functional state when urea solutions were diluted into buffer prior to the addition of mixed micelles.(*285*)

Initial WT studies were followed by studies of the folding and insertion of the single-Cys and other mutant forms of DAGK. For a panel of ~30 mutants, it was observed that the rate and efficiency of folding into vesicles is strongly correlated with protein stability as determined by resistance both to SDS-induced unfolding and irreversible heat inactivation.(*285, 286*) There were, however, interesting outliers. For example, the Y16C mutation does not destabilize DAGK and yet this mutant was severely folding-deficient.(*287*) Y16C likely affects the kinetics of a key step in the DAGK insertion and folding pathway without affecting protein stability.

Altogether, the results of the folding and misfolding of DAGK led to two potentially important observations that may extend to MP folding in physiological and possibly even disease conditions. First, the strong correlation between folding efficiency and protein stability led to the hypothesis that, when considering a panel of mutant forms of the same MP, the key determinant of the relative folding efficiencies for these mutants in cells is the relative thermodynamic stability of each mutant.(*286, 288*) As will be described later in this chapter, this hypothesis has now been tested for two disease-linked mutant forms of human proteins in cells and has, so far, held up well.(*185, 289*) Secondly, while the "misfolding is linked to instability" correlation is strong, it is not absolute, as revealed by the Y16C DAGK mutant, which appears to adversely alter the folding transition state but not the stability. Though they are likely to be rare, mutations that destabilize the folding transition state are likely to be represented among the large number of human mutations that promote human disease. Successful therapeutic approaches to stabilize the transition state may be very different from those required to address destabilized mutant forms of the very same protein.

Whether MP misfolding transitions are commonly related to formation of amyloid-like assemblies remains unclear, though there is good reason to believe these phenomena may sometimes be connected. DAGK was not found to form amyloids or even classical aggregates *in vitro*,(*194*) However, Vendruscolo and colleagues recently demonstrated that lactose permease is capable of forming fibrils with many characteristics of classical amyloid fibrils under certain conditions.(*290*) This observation provides additional support for the notion that nearly any protein can form an amyloid,(*291*) though in this case the physiological relevance is unclear.

The conversion of a membrane protein to amyloids does appear to play a direct role in the molecular basis of at least one human disease. Mature lung surfactant protein-C (SP-C) has 35 residues and, in its healthy physiological form, has a single transmembrane α-helix.(*292*) However, this same segment, which is

rich in valine, also has a strong propensity to form beta structures, leading to formation of amyloid structures. For this reason, nature has endowed nascent SP-C with a BRICHOS prodomain that suppresses amyloid formation, ensuring healthy SP-C function. However, any one of roughly 50 known mutations in pro-SP-C is sufficient to disrupt the protective function of the BRICHOS domain, resulting in amyloid formation that causes interstitial lung disease (ILD).(*292*)

Another likely physiological connection between membranes and amyloid formation is for the amyloid-β polypeptide, which is a proteolytic fragment of the transmembrane C99 domain of the amyloid precursor protein and represents the primary component of the amyloid plaques found in Alzheimer's patients. While amyloid-β is somewhat soluble, under some conditions it is known to spontaneously insert into membranes in a manner that promotes its homomeric assembly into pores.(*293-297*) Moreover, even short of insertion to adopt a transbilayer structure, amyloid-β retains considerable affinity for membranes, a fact that impacts formation of amyloid-β oligomers and amyloid fibrils.(*298-308*) The same is true for a variety of other membrane-active peptides that form amyloid fibrils, such as the α-synuclein protein involved in Parkinson's(*309, 310*) and the islet amyloid polypeptide that may contribute to some forms of diabetes.(*311-313*) The interactions of amyloid-forming proteins and amyloid assemblies with membranes is highly likely to be important in the etiology and pathology of disorders such as Alzheimer's and Parkinson's, although definitively establishing the pathophysiological relevance of phenomena observed in studies of isolated molecules (or even in model cell lines) to neurodegenerative disease in a living human being remains a daunting task.

The human prion protein (PrP), which is the root cause of several related neurodegenerative disorders, exists in both a membrane-anchored glycosylphosphatidylinositol (GPI) modified form and a form that contains a single TM helix. Interestingly, the TM form of PrP can exist in both possible distinct topologies (review in(*314*)). The conversion of "healthy" PrP to the toxic and infectious PrP^{sc} form of that seeds the formation of toxic aggregates appears to occur at the membrane.(*315*) This process may also be linked to the formation of amyloid-like PrP fibrils.(*316*) Whether these phenomena are etiologically related to the dread prion disorders is not yet established.

4. Folding of Membrane Proteins in Eukaryotic Cells

4.1. Membrane Integration at or near the Translocon

The vast majority of MPs are integrated into cell membrane with the assistance of dedicated cellular machinery. The most common pathway involves the action of the heterotrimeric translocon complex known as Sec61 in eukaryotes or SecYEG in bacteria and archaea, which acts in concert with the ribosome to thread the nascent chain into the membrane. However, there are subsets of MPs that rely on other assembly pathways. For example, certain inner MPs in Gram negative bacteria utilize an insertase known as YidC,(*317*) whereas the OMPs in Gram negatives are dependent on a mechanistically distinct membrane integrase known as BamA.(*264*) Posttranslational membrane integration of some bacterial proteins can also be achieved through the actions of the SecA ATPase.(*318*) Eukaryotic tail anchored proteins find their way into the membrane by way of the guided entry of tail-anchored protein (GET) pathway, including the membrane-bound GET1/GET2 complex.(*319-321*) Furthermore, the recently-characterized endoplasmic reticulum membrane protein complex (EMC) appears to actively facilitate the integration of range of MPs, perhaps often in concert with the Sec61 complex.(*322-324*) Other organelles, such as mitochondria, have their own systems. Given the central importance of MP biosynthesis and assembly in life processes, it is unsurprising that nature has developed multiple mechanisms to both facilitate membrane integration and to suppress and manage misfolding during

and after MP translation. For the purposes of this chapter, we will focus on the structure, mechanism, and activity of the Sec61 translocon complex and its associated chaperones and other folding accessory proteins

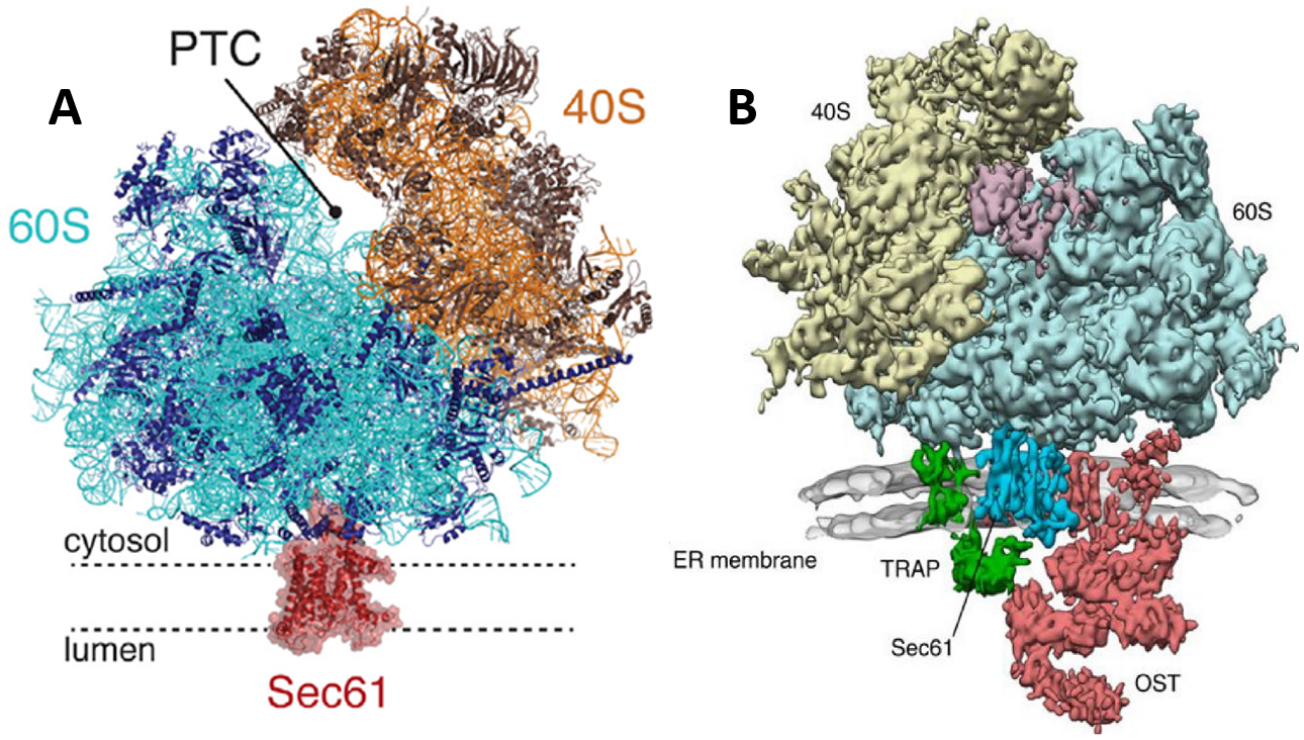

Figure 12. Structure of the Ribosome-Translocon Complex.

(A) A 3.4 Å resolution model of a mammalian ribosome (blue and brown) bound to the Sec61 complex (red) determined by single particle Cryo-EM is shown. The absence of tRNA in the peptidyl transfer center (PTC) indicates this complex represents the inactive conformation of the complex. Subtle structural rearrangements have been observed within the active complex (not shown). Panel adapted with permission from[359]. Copyright 2014, Cell Press. **(B)** Sec61 Translocon and Complex With the Ribosome, TRAP, and the Oligosaccharyl Transferase. Segmented densities for the 40S (yellow) and 60S (light blue) ribosomal subunits, translation elongation factors (magenta), Sec61 (blue), TRAP (green), and OST (red) from a sub-tomogram average of the ER membrane associated translocon complex filtered to 9.0 Å resolution.

4.1.1. Structure and Function of the Translocon

MPs across all kingdoms of life are produced and integrated into the membrane through the concerted actions of the ribosome and the Sec61/YEG complex. Structural models derived from crystallographic and cryo-EM data have provided a wealth of insight into the structure and function of this complex (**Fig. 12**). The core functional unit of the translocon is a heterotrimeric complex consisting of Sec α, β, and γ subunits in the ER membrane of eukaryotes or SecY, E, and G in the plasma membrane of bacterial and archaeal cells.(*325, 326*) In most cases, stalled ribosomes carrying the transcripts of secreted proteins or of integral MPs are delivered

to this heterotrimeric complex by the signal recognition particle (SRP) and its receptor. Upon delivery, the ribosome associates with the translocon through its universal ribosomal adaptor site located within the cytosolic loops connecting TM segments 6/7 and TM segments 8/9 of Secα/Y.(*325, 327-330*) Once associated with the translocon, the ribosome resumes translation of the client protein and the nascent polypeptide chain is guided into the protein-conducting channel (PCC) by the C-terminal helix of Sec α/Y.(*331*) The PCC is contained within the Sec α/Y subunit, which contains ten TM helices that form two pseudo-symmetric lobes composed of TM segments 1-5 and 6-10.(*331*) The interface between these lobes creates a polar, hourglass-shaped cavity that is filled with water.(*332, 333*) The cytosolic and luminal chambers are separated by a 5-6 Å pore created by a ring of hydrophobic residues, which forms a seal around the nascent chain and minimizes the exchange of ions and small molecules between the cytosol and ER lumen during translation.(*325, 332, 333*) In the inactive state, ion leakage through the PCC is also prevented by the association of a plug domain (TM2a) with the luminal/extracellular face of Sec α/Y.(*329, 332, 334, 335*) Association of the translating ribosome with the translocon causes a subtle conformational change that guides the nascent chain through the gasket into the ER lumen and displaces the plug.(*330*) During translation, the separation of TM segments 2b/3 and 7/8b creates a lateral gate that allows the nascent chain to transiently sample the membrane environment.(*44, 327-331, 333, 336*) Upon entry of a hydrophobic segment of the nascent chain into the PCC, a rigid body rotation of several TM helices within the N-terminal lobe of Sec α/Y opens the lateral gate in a manner that facilitates entry of the nascent chain into the bilayer.(*330, 337*) This movement of hydrophobic segments through the lateral gate and into the membrane (topogenesis) establishes the orientation of TM helices with respect to the membrane (topology). It is widely assumed that nascent TM helices typically move from the PCC to the membrane. However, given the energetic and geometric constraints involved in topogenesis, it has also been argued that many nascent TM domains may initially partition into the membrane interface prior to topological isomerization.(*338*) Considering the relatively weak energetic drivers involved in these reactions and the passive nature of these molecular machines, it seems likely that nascent membrane proteins may find more than one way into the membrane.

Though a single monomeric Sec61/YEG complex is sufficient to mediate topogenesis, it should be noted that several ribosome-translocon complexes may occupy a single mRNA transcript at the ER membrane.(*326, 339*) Formation of these polysomes presumably increases the local concentration of nascent

MPs in a manner that may help nascent MPs to form native oligomeric assemblies. Indeed, this aspect of topogenesis appears to bias the oligomerization state of AcrB in the inner membrane of *E. coli*.(*340*) A minimal complex composed of Sec α/Y and Sec γ/E is sufficient to mediate basal translocation.(*341*) Nevertheless, native translocons are associated with a wide variety of accessory subunits that serve to tune the activity of the translocon and to carry out processing of the nascent chain in order to better suit the needs of divergent client proteins.

Fig. 12B depicts the manner in which some of these chaperones associated with the ribosome-translocon complex. The ~200 kDa hetero-octameric complex known as the oligosaccharyltransferase complex (OST)(*342*) is found in nearly half of all native translocons,(*343, 344*) and catalyzes the glycosylation of asparagine side chains of N-X-S/T motifs (where X is any amino acid except Pro), which is one of the most common protein modifications in eukaryotes. Indeed, N-linked glycosylation in known to play a key role in the folding and trafficking of a wide array of MP substrates.(*345*) N-glycosylation can take place either co-translationally or post-translationally.(*346*) In many cases, maturation of the nascent chain also requires proteolytic removal of signal peptides, which are often found in MPs containing luminal/ extracellular domains upstream of their TM domains. Removal of signal peptides is mediated by signal peptidases, which are a family of intramembrane proteases.(*347*)

Proper folding of translocon substrates may also hinge upon interactions of the nascent chain with certain intramembrane chaperones within the translocon complex. For instance, the translocating chain-associated membrane protein (TRAM) is an abundant integral membrane glycoprotein that associates with the translocon and improves the translocation of certain substrates.(*348*) Though its precise mechanism of action is unclear, TRAM appears to mediate the handoff of polar TM domains from the translocon into the lipid bilayer in a manner that depends upon the sequence context of the client protein.(*44, 349*) Similarly, the heterotetrameric translocon-associated protein (TRAP) complex(*350*) appears to enhance the translocation of certain substrates bearing ambiguous topogenic signals.(*351, 352*) The EMC also associates with some emerging MPs co-translationally, especially those enriched with charged residues, to facilitate proper membrane integration, to protect clients from premature degradation, and to enable interactions with chaperones.(*323*) Correct orientation of proteins with semi-polar signal peptides also appears to depend on the highly abundant Sec62 subunit,(*353*) which also mediates the posttranslational translocation of certain client

proteins.(*354*) Sec62 is associated with another Hsp40 homolog at the translocon known as Sec63, the J-domain of which facilitates BiP-mediated ratcheting of nascent polypeptides into the ER lumen.(*355*) Thus, some of these subunits serve to connect the translocon to other components of the cellular proteostasis network.(*356*)

It should be recognized that many of the accessory subunits alluded to above are present at sub-stoichiometric concentrations within the ER membrane, which renders native translocon complexes functionally heterogeneous.(*343, 357*) This polydispersity is clearly physiologically relevant, as mutations that alter the relative abundance and association of OST are linked to congenital glycosylation diseases.(*358*) Furthermore, this observation implies that the co-translational folding of integral MPs cannot be mediated by a single set of core chaperones. Rather, the chaperones available to the nascent chain are likely to be determined by the organization of its ribosome-translocon complex. Ongoing investigation into the structure and function of these subunits and other relevant chaperones will undoubtedly provide key insights into the manner in which these dynamic assemblies facilitate the production and processing of the membrane proteome.

4.1.2. Energetics of Translocon-Mediated Membrane Integration

Though the structure of the translocon complex is intricate, topogenesis itself is thought to be driven by the minimalist principles associated with the partitioning of the nascent polypeptide chain between the PCC and the membrane.(*44, 359*) Because the PCC is hydrated(*332*) and the membrane core is hydrophobic, the energetics associated with lateral partitioning of the nascent chain between the translocon and the membrane mirrors the transfer free energies of polypeptides between oil and water,(*359, 360*) with subtle deviations potentially arising from certain kinetic constraints.(*361*) An analysis of the contribution of non-native amino acids to the energetics of translocon-mediated membrane integration revealed that transfer free energy scales with hydrophobic surface area of the nascent chain.(*362*) However, biological membranes are not a uniform solvent, and the relative abundance of bulk water and other polar chemical groups varies as a function of membrane depth.(*363, 364*) Due to this transverse heterogeneity, the transfer free energy of amino acid side chains from the translocon into the bilayer (or from the aqueous phase to the bilayer)(*191, 209*) also exhibit an appreciable dependence upon their depth within the membrane.(*365, 366*) Native bilayers are also asymmetric with respect to the electrostatic properties of the inner and outer leaflets, as lipids with anionic head groups are

enriched within the cytosolic leaflet. The net-negative charge of the cytosolic membrane interface facilitates the formation of electrostatic interactions between lipid head groups and cationic amino acid side chains in a manner that biases the orientation of TM domains with respect to the membrane.(*367*) This energetic bias apparently plays a key role in the stabilization of the native topology, as cationic side chains are highly enriched near the cytosolic edge of TM domains.(*40, 368*) The generality of this "positive-inside rule" in combination with current estimates for the energetics of translocon-mediated membrane integration can be used to predict MP topology from sequence with considerable accuracy.(*366, 369*)

The energetics of topogenesis are sufficient to guide the cotranslational membrane integration of thousands of chemically diverse substrate proteins in the absence of their native structures. This is remarkable considering that the magnitude of the forces driving membrane integration of the nascent chain are relatively modest. Furthermore, many client proteins bear TM domains that are enriched with polar residues, which are critical for function.(*17, 370*) An analysis of the sequences of known MPs using an experimentally trained energetic algorithm revealed that ~25% of TM domains within polytopic MPs are likely too polar to spontaneously partition into the membrane in the absence of additional stabilizing interactions.(*371*) Polar TM segments like these introduce frustration into the nascent chain, which can promote the formation of aberrant topomers.(*372, 373*) The formation of these non-native topologies during biosynthesis is perhaps inevitable for certain client proteins considering the tertiary contacts that stabilize the native topology may be inaccessible during translation. Proper membrane integration of some topologically frustrated segments may hinge on the formation of interhelical contacts with neighboring TM domains.(*368, 374*) Strong topological preferences in neighboring TM domains can also drive polar segments into the membrane.(*362*) For instance, the topology of the nascent form of aquaporin 1 features only four of six TM domains within the membrane, and the membrane integration of the remaining two TM domains is accomplished through a posttranslational inversion of its third TM domain.(*245, 375*) Protein-lipid interactions also appear capable of inverting the entire N-terminal domain of *E. coli* lactose permease.(*376*) However, there are few examples of proteins that undergo such an extreme topological re-arrangement, and it seems that many MPs are likely to remain trapped within the global topology established by the translocon.(*43*) Nevertheless, a comparison of crystal structures and energetic predictions suggests that, in many cases, the segments selected by the translocon may only partially overlap with native TM helices.(*377*) Thus, posttranslational folding reactions may often involve mild to moderate adjustments to

the nascent topology. These sorts of topological isomerizations are likely constrained by the polarity and size of soluble loops, which influence the magnitude of the kinetic barriers involved in their movement across the bilayer.(*378, 379*)

The persistence of nascent MPs within non-native topologies may potentially contribute to cellular misfolding, as aberrant topomers are rapidly degraded in the cell.(*380*) Indeed, it has been estimated that 10-15% of mutations associated with diseases of MP misfolding enhance formation of aberrant topomers,(*289, 381*) which suggests that the fidelity of topogenesis is tied to the efficiency of MP folding. Proteins exhibiting gross topological defects are likely to remain kinetically trapped in non-native topologies. Additional investigations into the connection between cotranslational folding and membrane proteostasis are needed.

4.2. Formation of Tertiary and Quaternary Structure in the Endoplasmic Reticulum

MP folding in the cell is assisted not only by the translocon and related MP complexes, but also by a series of other "quality control" proteins that assess the conformational state of the client MP. These processes ultimately facilitate correct folding in a manner that is coupled to the subsequent trafficking of the protein through the secretory pathway. These proteins also target misfolded MPs for terminal degradation. Quality control systems vary considerably between organisms, tissues, cells, and organelles. For the purposes of this chapter, I will focus on the quality control system of the *mammalian* endoplasmic reticulum. However, it must be noted that a good deal of what we know about ER quality control stems from studies of quality control in yeast, as is represented by a vast literature (c.f.(*382*)). A diagram summarizing the central ER-based pathways for MP folding, misfolding, and degradation is given in **Fig. 13**.

4.2.1. Endoplasmic Reticulum Quality Control

MPs begin to fold into their proper tertiary structure in a manner that is concurrent with their co-translational membrane integration. While MP folding QC begins even at the ribosome,(*383*) this process is mainly surveilled and managed by the ER quality control (ERQC) network.(*384-393*) (*18, 387*) Beyond the translocon, ERQC can be further broken down into three overlapping sub-systems: the coterie of proteins involved in facilitating ER-associated folding (ERAF), those involved in recognizing properly folded proteins and targeting them for export to the Golgi or other destinations, and those involved in recognizing and targeting misfolded

proteins for degradation in a pathway known as ER associated degradation (ERAD). In the following sections, I will discuss these systems. We note that the ERQC network also works in collaboration with the ER-based unfolded protein response (UPR), a system that produces a transcription response to stress associated with the burden of protein production and folding in the lumen and membrane of the ER.(*386, 388, 394*) This linkage between ERQC and the UPR is critical to the function of the overall cellular proteostasis network and for biogenesis of the ~35% of all cellular proteins that reside in or pass through the secretory pathway.

The extent to which MP folding occurs at or near the translocon versus after clearage from the translocon likely varies among client proteins. Nevertheless, there are two observations that suggest many MPs may complete folding only long after dissociation from the translocon complex. First, while it has long

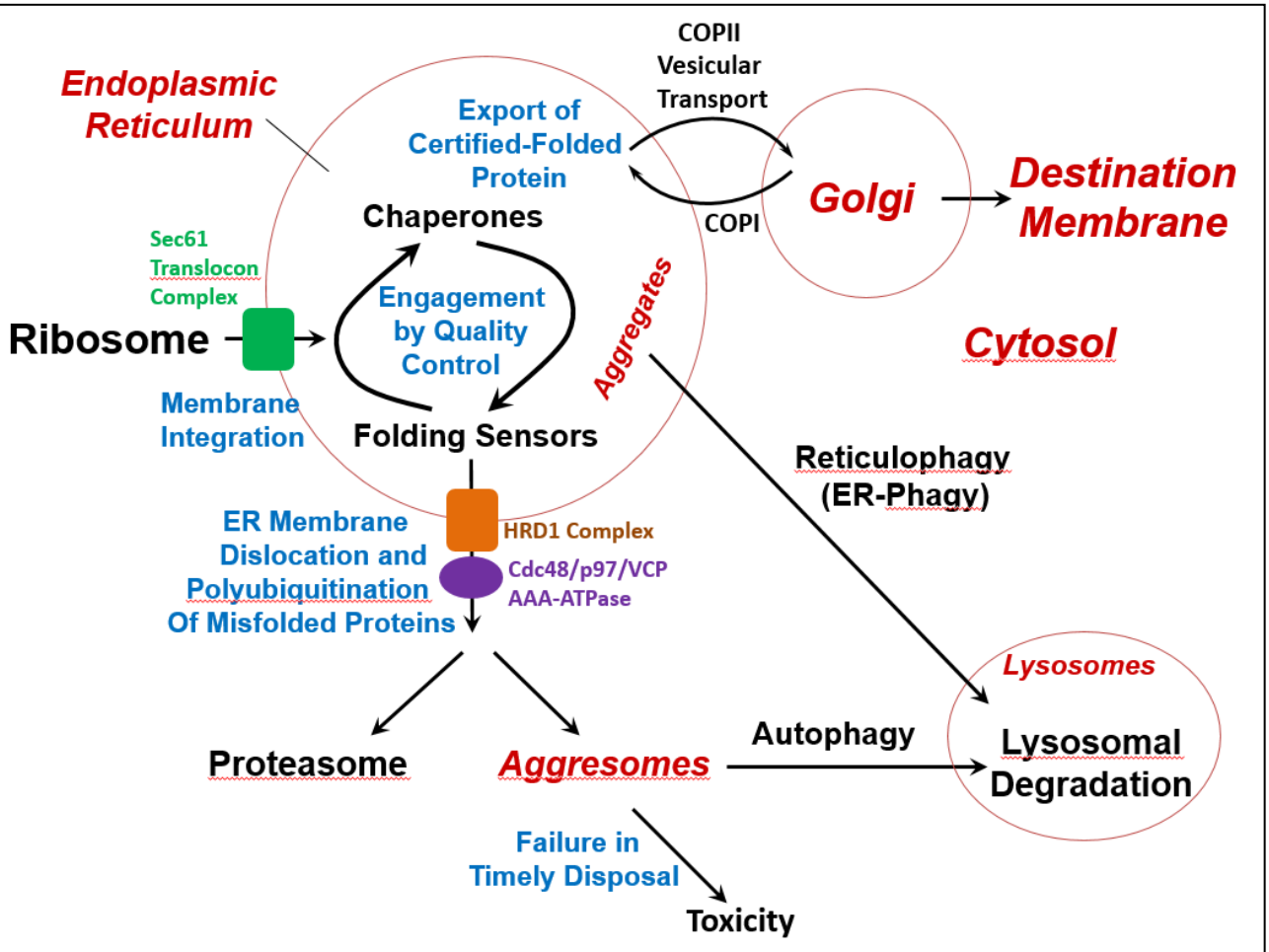

Figure 13. Overview of MP folding in the early secretory pathway of mammalian cells

This figure encompasses ERAD, ERAF, and ERES, plus some components of the broader proteostatic network.

been recognized that there are spatially distinct domains of the ER—the translocon-rich "rough ER" and the translocon-depleted "smooth ER"—studies over the past decade have revealed that the architecture of the ER

is actually much more complex. The ER now appears to extend throughout the cell, making direct contacts with other organelles thorough “membrane contact sites”.(*395*) Different domains of the ER feature biased protein compositions, which are likely associated with distinct ER region-specific functions.(*225*) This observation implies that certain aspects of MP folding may be facilitated and managed in spatially distal domains of the ER. Consistent with this notion is the fact that MPs can spend considerable time in the ER prior to export to the Golgi—much longer than the time required for completion of translation and membrane integration. For instance, mature cystic fibrosis transmembrane regulator (CFTR) begins to appear at the plasma membrane on the order of 1-2 hours after the initiation of translation, while degradation of misfolded CFTR occurs with a half-life of 45 minutes.(*396-398*) Similarly, the half-life of biosynthesis and trafficking of the epithelial ENaC channel is roughly an hour, with half-lives for the degradation of misfolded protein on the order of 15-20 minutes.(*399, 400*) Nascent PMP22 associates with the ER-resident lectin chaperone calnexin with a half-life of 11 minutes, indicating nascent PMP22 molecules that engage within this chaperone spend at least minutes in the ER before trafficking on to the Golgi. By comparison, the folding-defective L16P disease mutant of PMP22 forms a complex with calnexin that exhibits a half-life of over an hour.(*401*) These rough kinetic estimates highlight the fact that most MPs require considerable time to clear ERQC. Further studies and advances in technology are needed to better understand how kinetic control of MP trafficking influences MP biogenesis.

4.2.2 The Calnexin Cycle as a Central Component of Endoplasmic Reticulum Quality Control for Membrane Protein Folding

An estimated 70% of proteins inserted into the ER are co-translationally N-glycosylated on their luminal domain by the addition of one or more units of a 14-sugar complex oligosaccharide (“core N-glycan”).(*402, 403*) In mammals, this glycoform is composed of three glucoses, nine mannoses and three N-acetylglucosamines arranged in a tree-like structure (shown in **Fig. 14A**). Core N-glycan biosynthesis is initiated on the cytosolic face of the ER membrane and completed on the luminal side via sequential additions of uridine diphosphate-linked monosaccharides to a membrane-anchored dolichol phosphate scaffold.(*404, 405*) OST catalyzes the luminal addition of this oligosaccharide *en bloc* to asparagine residues of N-X-S/T sequence motifs of nascent proteins.(*387, 404, 405*) In order to catalyze N-glycosylation, OST requires local structural flexibility at the glycosylation site.(*404*) N-glycosylation can be disrupted by tunicamycin, a compound often used to induce ER

stress, and that inhibits the enzyme GlcNAc-1-phosphotransferase responsible for catalyzing the initial addition of N-acetylglucosamine to dolichol phosphate.(*406*) N-glycans increase the hydrophilicity of the polypeptide chain and may potentially facilitate arrangement of the ER-luminal segments/domains in a way that could stabilize and/or alter the tertiary structure of the membrane domain. The steric properties of these glycans can also help prevent proteolytic cleavage and decrease the propensity for protein aggregation. Beyond the physical effects of these modifications on the folding process, N-glycans also serve as “folding barcodes” for components of the ERQC to track the trajectory of the nascent protein through the lectin chaperone pathway (**Fig. 14B**).(*404, 405, 407*) Modification of the core oligosaccharide through the addition or removal of sugars is coupled to the folding of the nascent protein and its binding to ERQC proteins.

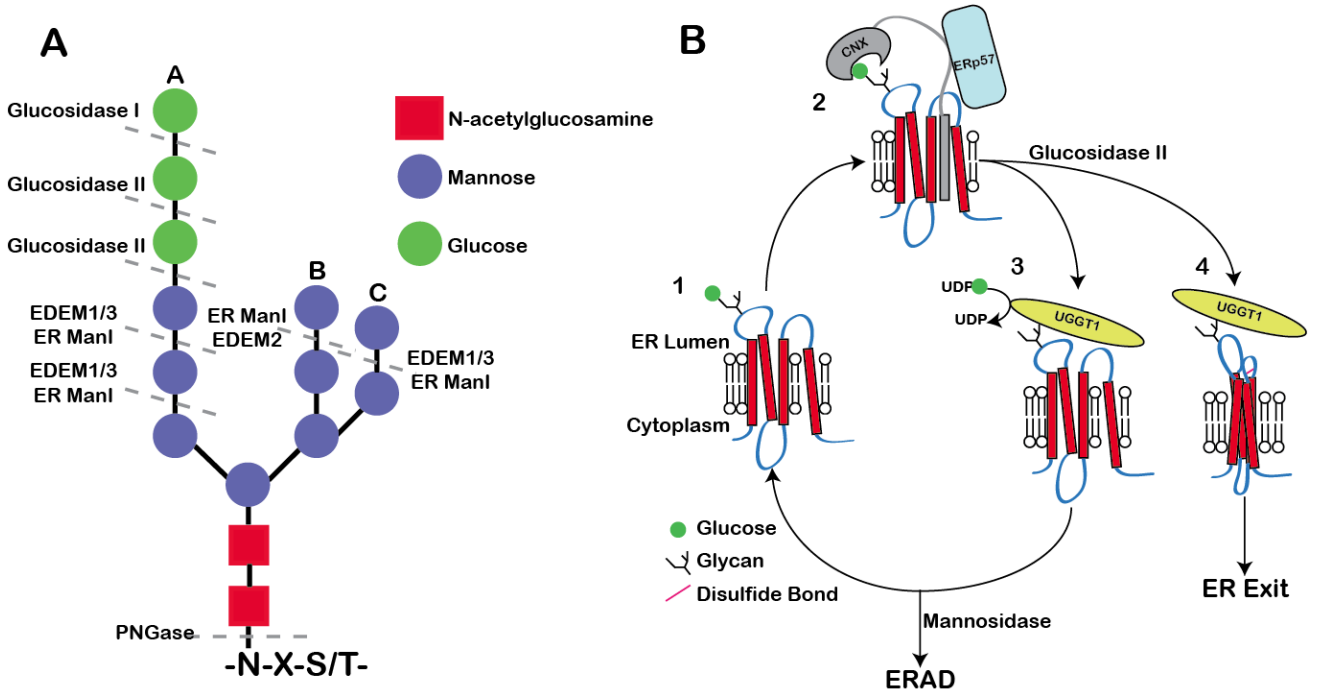

Figure 14. N-Linked Glycan and the Calnexin Cycle.

As proteins are translocated into the ER membrane they are tagged with a 14-sugar moiety at N-X-S/T (where X is any amino acid but P) sequence motifs as shown in (**A**). This post-translational modification serves a multitude of functions for the protein including increasing hydrophilicity, preventing aggregation, influencing tertiary contacts, and serving as a folding 'barcode'. Through sequential cleavage of monosaccharides (grey dotted lines), the folding polypeptide can be engaged with different lectin chaperones involved in either ERAF or ERAD. The enzymes responsible for cleaving various glyosidic linkages are shown. The predominant folding pathway for glycosylated proteins is shown in (**B**). Monoglucosylated proteins (**1**) are engaged by the membrane-anchored lectin chaperone calnexin (**2,** grey). Calnexin provides the protein with an isolated environment to fold, recruits essential co-chaperones such as the disulfide isomerase ERp57 (cyan), and may also facilitate the proper tertiary packing of a MP by associating with exposed hydrophilic residues in the plane of the membrane. Association is transient; glucosidase II cleaves the terminal glucose residue on the glycan chain freeing the client polypeptide from engagement with calnexin. Proteins that have yet to attain their proper tertiary structure (**3**), are sensed by UGGT1 (orange) and re-glucosylated, allowing reentry into the calnexin cycle (**1**). Proteins that have obtained their proper structure and post-translational modifications (particularly disulfide bonding) are sensed by UGGT1 and funneled towards the ER export machinery for ER exit (**4**). Polypeptides that fail to complete folding after consecutive cycles are eventually funneled out of the cycle and targeted for ERAD by the action of mannosidases.

Once transferred onto a nascent protein, the terminal glucose residue on the core N-glycan is cleaved by the membrane-anchored glucosidase I. This hydrolytic event enables the nascent glycoprotein protein to engage with the lectin chaperone malectin.(*387, 408*) Malectin displays an affinity for misfolded conformations of proteins, and its overexpression reduces the total protein trafficking out of the ER.(*409*) Malectin may serve as the initial sensor of the conformational state of nascent chains early in their lifetime, possibly targeting certain misfolded proteins for degradation. This function would reduce the burden on downstream chaperones by reducing the flux through later branches of ERAD. Malectin may also protect against aggregation and accumulation of misfolded proteins in the ER.(*410*) However, it is not yet clear whether malectin is involved in the surveillance of all nascent N-glycoproteins, or if it exhibits selectivity.

ER luminal glycosidase II, the next component of the lectin pathway, cleaves the outermost remaining glucose to yield a monoglucosylated N-linked glycan. Cleavage of this glucose residue promotes interactions with either the membrane-anchored lectin chaperone calnexin or its soluble paralog calreticulin (**Fig. 14B** step 2**)**.(*385-388, 405*) Because of its co-localization in the ER membrane, most nascent integral MPs preferentially interact with calnexin.(*408, 411*). Calnexin is a Ca^{2+} binding protein composed of a luminal N-terminal lectin domain (275 residues) followed by an extended proline-rich "P-domain" (ca. 135 residues), a single TM segment, and a highly acidic cytosolic domain (ca. 90 residues).(*408, 412*) Calnexin and its water soluble homolog, calreticulin, appear to be critical folding sensors of ERQC. Elegant biochemical studies have shown that calnexin interacts with misfolded, monoglycosylated glycoproteins with sub-micromolar affinities *in vitro*.(*405, 413*) Transient interactions of calnexin with partially folded proteins occur with a half-life on the order of minutes to hours depending on the substrate, with sequestration by calnexin potentially affording clients a protective environment during folding.(*405, 414*) Calnexin also recruits the accessory chaperones ER protein 57 (ERp57) and cyclophilin P (CycP) via interactions with its P domain, which catalyze the oxidation of free cysteines and cis/trans isomerization of proline residues, respectively.(*385, 387, 405, 408*) Interestingly, it has been shown that calnexin can selectively bind misfolded conformations of integral MPs, even in the absence of glycosylation.(*414-417*) For glycoproteins, it is possible that the glycosylation status of a protein may trigger initial binding or increase the affinity of a client for calnexin, but that its actual chaperone activity involves a different set of client-calnexin interactions involving their TM domains. For example, the lone TM segment of calnexin has been shown to be both necessary and sufficient to retain trafficking-defective mutants of the γ-aminobutyric acid (GABA) transporter in the ER, localizing it to concentric assemblies that can be visualized by EM (discussed further below).(*418*) Likewise, the recognition of the misfolding-prone L16P disease mutant form of PMP22 by calnexin appears to involve direct recognition by calnexin of folding defects in the PMP22 TM domain.(*401, 414, 419*) It has also been hypothesized that the TM domain of calnexin can recognize mis- or partially-assembled helices of polytopic MPs or unassembled oligomers by serving as a temporary stand-in for unpaired TM domains.(*418, 420*) Thus, the chaperone activity of calnexin is multifaceted and involves both glycosylation-dependent and independent modes.

Once released from calnexin/calreticulin, the terminal glucose residue on the N-glycan of a substrate protein is cleaved by glucosidase II, which lowers the affinity of the substrate for calnexin/calreticulin. At this

point, the client protein is engaged by another folding sensor, the UDP-glucose:glycoprotein glucosyltransferase-1 (UGGT1).(*386-388, 408, 421*) Proteins that have failed to mature fully at this point are recognized by UGGT1, which catalyzes the re-addition of a glucose residue from UDP-glucose to the N-glycan of the client protein (**Fig. 14B** step 3). This modification reactivates interactions of the client protein with calnexin and/ or calreticulin and continued ER retention.(*386-388, 408*) Only some proteins must be cycled back through the lectin chaperone pathway in this manner. Biochemical and cellular biological assays have shown UGGT1 exhibits a preference for incompletely folded substrates over either full folded or irreversibly misfolded proteins. (*422-424*) Thus, folded proteins appear to escape re-glucosylation of UGGT1, which allows them to proceed to engage the ER export machinery and escape the ER (see Fig. 14B step 4). Knocking out UGGT1 in mice results in embryonic lethality, suggesting that this pathway is essential in multicellular organisms. However, studies in mouse embryonic fibroblasts show that the maturation of most proteins is unaffected by the loss of UGGT1,(*425*) suggesting that only a subset of essential proteins need to associate with calnexin more than once to complete maturation.

How UGGT1 monitors the conformational state of integral MP substrates is unclear. UGGT1 is a soluble 170 kDa protein whose N-terminal region contains a hydrophobic pocket that could potentially detect misfolded polypeptides, with its C-terminal domain potentially catalyzing glucosylation.(*426*) Interestingly, UGGT1 accommodates a wide variety of substrates that vary considerably in terms of both size and shape. It should also be noted that this protein catalyzes glucosylation of N-glycans as far as 40 Å from misfolded domains.(*427, 428*) Recent structural studies of UGGT1 showed that there is a high degree of flexibility between the folding sensor region of the protein and the glucose transfer region.(*427, 428*) Introduction of interdomain disulfide bridges reduced this intrinsic flexibility and decreased enzymatic activity.(*429*) The interdomain flexibility of UGGT1 may facilitate protein substrate promiscuity and promote the ability of the enzyme to re-glucosylate N-glycans located at variable distances from the misfolding-recognition site. Based on our current knowledge of UGGT1, it seems likely to interact with misfolded substrates through improperly exposed hydrophobic residues within the ER lumen. It has also been suggested that that UGGT1 is able to recognize improper introduction of a polar residue into a TM site.(*430*)

Terminally misfolded or slowly folding proteins are eventually funneled out of the calnexin cycle through the action of mannosidases. Cleavage of the terminal mannose residue on the A chain of the N-glycan (**Fig.**

14A) inhibits glucose re-addition and targets the protein for degradation (see below). Multiple proteins with mannosidase activity are present in the ER, including ER alpha-1,2 mannosidase I (ER Man I) and ER degradation enhancing α-mannosidase protein (EDEM) isoforms 1, 2 and 3.(*386-388, 405, 408*) ER Man I inhibitors have been shown to selectively slow the degradation of misfolded proteins in the ER.(*387*) Thus, these enzymes appear to convert glycoproteins into targets for the ERAD pathway (discussed below). These observations have collectively led to the 'mannose timer' hypothesis for ERQC,(*386, 405, 431*) which is that nascent glycoproteins only have a certain amount of time to fold and exit the ER before they are eventually cleaved and targeted to ERAD by a catalytically sluggish mannosidase. This logic may explain why degradation of nascent proteins is typically slow, even under conditions of proteotoxic stress.(*432*) Slow folding kinetics may well constitute a key determinant of the fraction of nascent proteins that face cleavage following mannosidase action. Various aspects of the activity of these mannosidases have yet to be characterized in detail, though there is some evidence that they have the capacity to directly recognize conformational defects (see Section 4.3.1).(*433*)

4.2.3. Other Mechanisms of Endoplasmic Reticulum Quality Control

Not all ERQC is dependent on protein glycosylation, and there is mounting evidence to suggest non-glycosylated proteins can also interact with ERQC proteins that were previously believed to serve in a glycosylation-dependent manner.(*416, 417, 434*) Additionally, some components of the ERQC pathway may play a role in both glycan-dependent and glycan-independent pathways. For instance, the ER-localized heat shock protein 70 (Hsp70) family member "binding immunoglobin protein" (BiP) is involved in ERAF and ERAD of both glycosylated and non-glycosylated MPs.(*388, 435*) This chaperone is found in the ER lumen where it plays a role in the recognition of misfolded MPs. BiP contains both an ATPase domain and a substrate-binding domain.(*436*) The substrate binding domain contains a hydrophobic binding pocket that recognizes exposed hydrophobic residues. When bound to ATP, BiP exists in an open state. Upon substrate binding, BiP hydrolyzes ATP and 'clamps' down on its substrate. Nucleotide exchange factors (NEFs) Sil1 and Drp170 catalyze the exchange of ADP for ATP and facilitate the release of the client protein.(*437*) BiP also associates with a variety co-chaperones including DNAJ/Hsp40 family (ERdJ1-7) proteins that facilitate oxidative folding, rearrangement of disulfide bonds, and disulfide bond reduction.(*438*) Since BiP is soluble, it presumably

interacts with misfolded MPs through recognition of exposed hydrophobic patches in luminal domains or through interactions with mis-incorporated membrane domains that become exposed to the aqueous lumen.

BiP clients and those for the calnexin cycle are not mutually exclusive; proteins may 'ping-pong' between both pathways during maturation.(*405, 435*) The location of the N-glycan within the primary structure of the nascent chain may also influence its trajectory through ERQC. N-glycans within the first ~50 residues of a protein usually target it to the calnexin cycle in a manner that bypasses BiP.(*439*) Indeed, BiP binding to misfolded substrates is increased when calnexin is knocked down or out.(*440, 441*) Thus, it appears that nascent MP substrates may kinetically partition between the BiP and calnexin pathways in a manner that is dictated by their intrinsic conformational properties.

Another important chaperone involved in ERQC is the Hsp90 family member, glucose-regulated protein 94 (GRP94). GRP94 is involved in both ERAF and in targeting proteins to ERAD, and is the only known Hsp90 member within the ER lumen.(*442*) The ATPase activity of GRP94 is essential for its chaperoning activity *in vivo.* However, the exact mechanism of action for GRP94 has yet to be elucidated.(*443*) Unlike BiP, GRP94 appears to interact with a more limited number of substrates, including the Toll-like receptors, integrins, and members of the low density lipoprotein receptor (LDLR) family.(*444-446*) Cytosolic Hsp90s typically bind substrates after Hsp70, and it appears likely that GRP94 engages substrates released by BiP.(*444*) GRP94 also interacts with OS-9, which is a component of the ERAD pathway. Nevertheless, how GRP94 facilitates the degradation of misfolded proteins is unclear.(*447*) Much work is still needed to elucidate the role(s) of GRP94 in both the ERAF and ERAD pathways.

Protein disulfide isomerases (PDIs) also plays important roles in ERQC.(*387, 435, 448*) PDIs are the primary oxidants of cysteine thiols in the ER, and can break (reduce), form (oxidize), or rearrange (isomerize) disulfide bonds depending on the oxidation state of its Cys-X-X-Cys active site.(*449*) PDIs serve as chaperones that recognize exposed hydrophobic patches in misfolded proteins.(*448*) Of particular importance is the ERdj5 protein, which has the dual function of being both a PDI and a J-domain co-chaperone.(*450*) Recent solution state NMR studies have mapped the PDI substrate binding site using unfolded ribonuclease A as substrate, and also using substrate peptides mastoparan and somatostatin.(*451*) These studies showed that PDIs specifically recognize misfolded proteins with exposed hydrophobic patches in a manner that

circumvents the kinetic barriers associated with the isomerization of disulfide bonds. This activity helps overcome kinetic entrapment of intermediate folding states.

The compartmentalization afforded by the ER membrane is also essential for these quality control reactions. The segregation of proteins into ER sub-compartments appears to help guide immature, mature, and misfolded proteins through the cell.(*225*) Certain proteins appear to cycle between the bulk ER and so-called quality control vesicles (QCVs) that are enriched for ER Man I.(*452*) This spatial segregation presumably protects nascent glycoproteins against premature mannose trimming by ER Man I. Misfolded proteins also appear to localize within sub-compartments known as ER quality control compartments. ERAD machinery that recognize misfolded proteins, such as OS-9, and HMG-CoA reductase degradation protein 1 (Hrd1, discussed below), are enriched within this compartment. Additional quality control proteins and ERAD machinery including calnexin, calreticulin, EDEM1, and Derlin-1, are also found within this compartment in the presence of proteotoxic stress.(*452, 453*) Finally, mature proteins appear to accumulate near ER exit sites, which stem from smooth ER membranes.(*454*) These exit sites are enriched with ER to Golgi transport machinery, as further discussed below.

Calnexin appears to play a critical role in the sorting of substrate proteins between different ER sub-compartments. As noted above, the TM region of calnexin sequesters misfolded GABA receptors in distinct regions of the ER.(*418*) In yeast, it has been shown that a model misfolded integral MP Ste6p localizes to distinct vesicular ER quality control compartments adjacent to the bulk ER.(*455, 456*) These compartments are composed of proliferated, tubular, ER membranes that are absent in cells not expressing the misfolded variant of Ste6p and their presence was shown not to affect the trafficking of other proteins. Compartmentalization of misfolded proteins is likely to be advantageous because it restricts their diffusion and concentrates them in a manner that potentially increases the efficiency of degradation.(*456*) Additionally, the sequestration of misfolded proteins likely minimizes their aberrant interactions with healthy proteins.

Finally, many MPs, such as the CFTR, have large soluble domain facing the cytosol. The folding of these domains is mediated by some of the same chaperones (Hsp70s and Hsp90s) and accessory proteins that interact with water soluble cytosolic proteins (c.f.(*457*)). The folding of proteins such as CFTR involves the coordinated action of both ER-resident and cytosolic chaperones and folding sensors.

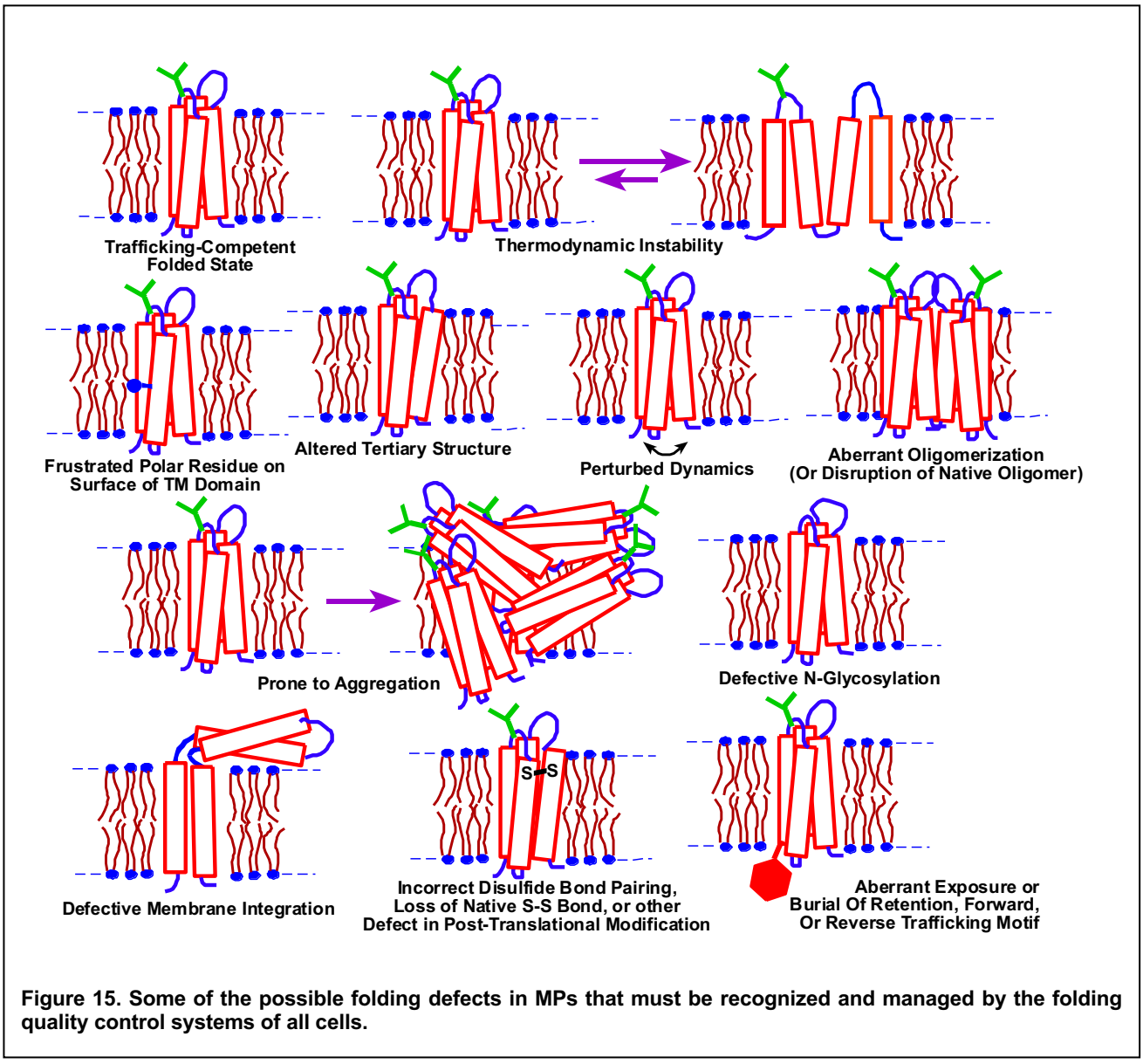

Figure 15. Some of the possible folding defects in MPs that must be recognized and managed by the folding quality control systems of all cells.

4.2.4. Recognition of Misfolded Membrane Proteins and the Logic of Endoplasmic Reticulum Quality Control

Fig. 15 diagrams some of the tertiary and quaternary defects in MPs that could potentially occur within the ER membrane. MP folding quality control systems must have mechanisms for the specific recognition of these defects.(*458*) This is a tall order; native protein structures vary considerably with respect to their shapes, sizes, and conformational dynamics. What are the structural features that the folding sensors of ERQC proteins recognize and how specific are these interactions? For soluble proteins or aqueous domains of MPs within the

ER lumen, ERQC seems most often to recognize exposed hydrophobic segments.(*385-388, 448*) UGGT1 and BiP utilize this mechanism this mechanism, for example.(*436, 459*)

How misassembly of TM domains is recognized is poorly understood, but likely involves their intrinsic structural properties.(*460, 461*) The aberrant partial or total exposure of a TM segment within the ER lumen or cytosol may represent a structural cue indicating misfolding or instability of these proteins (**Fig. 16A**).(*400, 462*) As noted earlier, many polytopic integral MPs (and single pass integral MPs that function as dimers or higher order oligomers) have TM segments that are only marginally hydrophobic.(*18, 463*) Solvation of these helices within the membrane may be contingent on the formation of proper tertiary or quaternary contacts. Single amino acid mutations within these domains could potentially disrupt native helical packing interactions. These helices or helical hairpins could then "slip" into the ER lumen (or cytosol), thereby exposing hydrophobic patches for recognition by BiP or other folding sensor/chaperones, as has been demonstrated for the Na^+/K^+ ATPase.(*245, 464, 465*) The Na^+/K^+ ATPase is comprised of 10 TM α subunit and a single TM β subunit, which heterooligomerize to form the functional transporter. In the absence of the β subunit, the C terminal TM helices fail to properly integrate into the membrane, and the TM7/8 hairpin becomes exposed to the cytosol (**Fig. 16A**).(*464*) Exposure of hydrophobic residues apparently results in the recognition of this domain by cytosolic sensors, leading to increased degradation of the protein within the cell. The single pass TM α subunit of the αβ T cell receptor (αβTCR) provides a second example of this phenomenon.(*462*) In the absence of the β subunit, the α subunit of TCR slips completely out of the membrane and into the ER lumen where it is recognized by BiP and targeted for degradation. If the β subunit is present, or if the α subunit is rendered more hydrophobic via addition of Leu residues, the α subunit instead remains embedded within the ER membrane and can eventually traffic to the plasma membrane.(*462*) Thus, the marginal hydrophobicity of some TM helices seems actually to be exploited by ERQC as a means for monitoring the folding and assembly of certain MP complexes.

A second mechanism by which ERQC may monitor the folding and oligomerization status of TM domains is through the exposure of hydrophilic residues in the hydrophobic membrane core (**Fig. 16B**). Many polytopic integral MPs contain hydrophilic amino acid residues in the membrane that, although energetically unfavorable, are important for formation of tertiary or quaternary structure and/or functional dynamics.(*18, 463*) Misassembled proteins may expose these residues within the hydrophobic membrane phase, where they may readily form lateral interactions with ERQC MPs. For instance, the TM segments of the E3 ubiquitin ligase Hrd1, a key player in ERAD (discussed below), appear to specifically recognize some misfolded polytopic MPs with exposed polar residues in the hydrophobic interior of the membrane.(*466, 467*) The presence of a variety of hydrophilic residues within the TM domains of Hrd1 may endow this protein a high degree of substrate promiscuity. Calnexin may also recognize some misfolded MPs through this mechanism. The hydroxyl groups of Tyr^{487} and Thr^{490} within the lone TM domain of calnexin may mediate recognition of exposed hydrophilic sites; they appear to be involved in the QC of GABA receptors and other misfolded, non-glycosylated MPs.(*418, 441*)

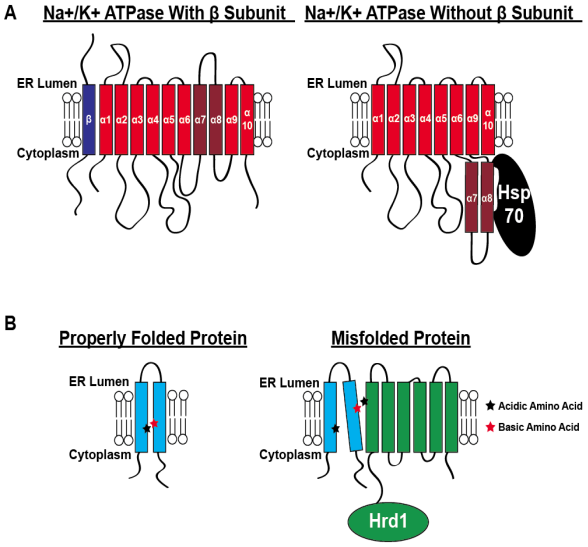

Figure 16. Examples of Mechanisms for ERQC Detection of a Misfolded Integral MP.

In (**A),** the 10 TM α subunit (red) of the Na^+, K^+ ATPase is able to properly integrate into the ER membrane in the presence of the single-pass TM β subunit (blue). In the absence of the β subunit, TM helices 7 and 8 fail to properly integrate into the ER membrane and sidle into the cytoplasm where they can be recognized by the Hsp70 chaperone (black), leading to targeting for degradation. In (**B)**, a hypothetical dual pass TM protein (cyan) requires a salt-bridge (acidic and basic amino acids shown with stars) in the plane of the membrane in order to maintain its proper fold. If the protein is misfolded or unstable, it can expose these hydrophilic amino acids in the plane of the membrane. Hrd1 (green), contains a number of hydrophilic amino acids in the plane of the membrane that may aid in recognizing aberrantly-exposed polar residues in MPs, resulting in ERAD targeting.

A third mechanism by which components of ERQC can recognize unstable or misfolded MPs may involve the recognition of “dangling strands” within polytopic MPs, or TM domains that fail to associate with their neighboring TM domains. The recognition of unstable PMP22 variants by calnexin may be based on this principle. Cell biology results have suggested that calnexin recognizes certain unstable mutants of PMP22 via a mechanism that involves recognition of the first of four TM helices present in PMP22.(*414, 468*) Structural studies later showed that this helix transiently dissociates from TM helices 2-4 (see **Fig. 6**).(*184*) Together,

these observations raise the intriguing possibility that calnexin and other ERQC proteins may recognize dangling TM helices in polytopic proteins. Yet, it remains unclear *how* the single TM helix of calnexin accomplishes this feat of molecular recognition.

ERQC also appears to have the capacity to recognize and dispose via ERAD of aggregated membrane proteins in the ER.(*469, 470*) The protein(s) responsible for this recognition event are not yet known.

Finally, some MPs have short amino acid motifs referred to a that are structurally buried and thereby masked from recognition by components of ERQC in folded proteins, but are exposed for recognition by folding sensors upon unfolding or misfolding. Exposure of these motifs lead to their ER retention and/or degradation.(*471-474*) Motifs that lead to degradation are often referred to as “degrons”.

As indicated above and recently reviewed elsewhere,(*460*) emerging clues are suggestive of the structural “symptoms” of MP misfolding as well as the manner in which they may be recognized. It seems particularly interesting that ERQC appears to have a include a number of mechanisms for detecting thermodynamically unstable and/or slow folding MPs, as well as misfolded conformations and aggregates. There is still much to learn about this fascinating topic—we know just enough to whet our appetite for discovery of additional classes of defects, folding sensor, and recognition mechanisms.

4.2.5. Endoplasmic Reticulum-to-Golgi Export System

Transport of mature proteins from the ER to the Golgi complex is the productive outcome of ERQC. Transport is a highly selective process mediated by coat protein complex II (COPII) transport vesicles.(*475*) Selectivity is maintained by two distinct, yet complimentary mechanisms: selective loading of mature cargo into transport vesicles and sequestration of incompletely folded proteins away from transport vesicles. Export occurs at specific exit sites in the smooth ER, which are enriched for proteins involved in COPII mediated trafficking.(*476*) The selective loading of cargo into transport vesicles is mediated by Sec24 in conjunction with specific cargo receptors in COPII vesicles.(*475, 477*) Sec24 binds to export signals exposed on the cytosolic side of the ER membrane present on cargo proteins or on cargo receptors. Along with its heterodimeric partner Sec23, Sec24 recruits the remaining proteins necessary for COPII vesicular transport from the ER to the Golgi.(*477*) Eukaryotic organisms express four separate isoforms of Sec24 (A-D) and each isoform contains up to four non-overlapping cargo recognition sites that accommodate the diverse cargo proteins that transit

through this pathway.(*478*) Properly folded and/or oligomerized MPs sometimes present export signals that promote direct interactions with Sec24. However, not all proteins bound for ER exit contain these signals; cargo can also be selected for COPII trafficking via specific TM cargo receptors.(*475, 477*) These receptors specifically bind mature proteins either within the membrane core or on the luminal face of the ER membrane, whereas Sec24 proteins tend to bind their recognition sequences on the cytosolic face of the membrane. Some of these receptors, such as ERGIC53, VIP36, and VIPL, are lectins that recognize the glycosylation state of the cargo protein in order to differentiate between mature and immature states.(*479*) Other receptors such as Erv14, Erv26, and iRhoms interact with TM regions of cargo proteins and direct them into transport vesicles.(*480-482*) Our understanding of how these receptors specifically recognize integral MP cargo is in its infancy.

In order to prevent the forward trafficking of immature proteins, immature or misfolded proteins are selectively excluded from transport vesicles. The resident ER chaperones BiP, calnexin, and PDI, which interact with immature or misfolded proteins, are depleted from ER exit sites.(*386, 475*) By sequestering these chaperones away from exit sites, the probability of exporting immature proteins to the Golgi is reduced. Upon inhibition of certain chaperone interactions involved in this concentrative export pathway, misfolded MP variants that are normally retained within the ER sometimes manage to leak through the export system.(*483*) This suggests that compartmentalization of misfolded proteins away from ER exit sites by ER chaperones helps retain these proteins in the ER.

It is worth considering whether the sequestration of MPs from the ER export machinery may be promoted by the biophysical properties of the membrane itself. The hydrophobicity of TM domains appears to influence their access to export sites.(*484-486*) Although not definitively proven, it has been suggested that ER exit sites have a different lipid composition than the bulk ER.(*484*) This may reflect an enrichment of these sites with lipids that are synthesized within the ER (such as sterols and ceramide) primarily for export to downstream organelle membranes (Golgi and plasma membranes).(*93, 487*) This idea is supported by the observation that the depletion of cholesterol from the ER inhibits COPII transport.(*488, 489*) Mature (well-folded) polytopic MPs may preferentially partition into these cholesterol-rich ER exit site membrane domains.(*484*)

4.2.6. Quality Control beyond the Endoplasmic Reticulum

Cellular sorting mechanisms are not 100% efficient. Furthermore, MPs presumably continue to sample non-native conformations well after they are exported from the ER provided their unfolding rates are not glacial. To prevent issues arising from misfolded molecules in the late secretory pathway and beyond, the cell has developed a number of QC mechanisms for service beyond the ER. For instance, the Rer1 and ERp44 proteins specifically recognize immature proteins in the Golgi and facilitate their retrograde trafficking to the ER.(*419, 490, 491*) Rer1 is a TM protein that has been shown to specifically recognize misfolded integral MPs, most likely through contacts with hydrophilic residues in its transmembrane domain.(*419, 490*) Rer1 contains an ER retention KDEL motif, which allows it to be recognized by the KDEL (ERD2) receptor, and to associate with COPI vesicles as cargo for return to the ER. ERp44 is a soluble member of the PDI family that contains only a single cysteine residue within its active site, rendering it nonfunctional as an isomerase.(*491, 492*) In the neutral environment of the ER, the substrate binding site of ERp44 is occupied by its own C-terminal tail. However, within the more acidic environment of the Golgi lumen, this C-terminus is displaced and its single reduced cysteine residue is exposed in order to facilitate mixed disulfide bond formation with immature proteins. This conformational change also exposes a KDEL motif, which enables ERp44 and its substrate to traffic back to the ER as cargo in COPI vesicles. Once in the ER, conventional PDIs can remove the substrate from ERp44, which allows the chaperone to return to the Golgi.(*491, 492*) Some immature proteins have been shown to transport out of the ER in complex with BiP.(*493, 494*) These Golgi retrieval mechanisms appear to function as an additional layer of quality control beyond the ER. There is now much evidence that even the plasma membrane has its own quality control system to monitor the structural integrity of MPs, triggering degradation of those deemed defective.(*495, 496*)

4.3. The Degradative ERAD Branch of Endoplasmic Reticulum Quality Control

Proteins that are unable to pass QC in a timely manner are removed from the ER and degraded via the ERAD pathway (**Fig. 13**). ERAD involves four coupled steps: substrate selection, substrate retrotranslocation from the ER to the cytosol, substrate ubiquitination, and substrate degradation via the 26S proteasome (**Fig. 17**).(*225, 461, 497-499*) Most of these steps are accomplished by a multi-protein complex centered around RING finger-containing membrane-embedded E3 ubiquitin ligases (E3s).(*500, 501*) Failure to degrade misfolded MPs may

induce ER stress, which typically leads to activation of an additional wing of the proteostasis network, the UPR.(*502*) Among many other effects, the activation of the UPR leads to the upregulation of a series of chaperones that help to buffer protein misfolding within the ER lumen.(*503*) In extreme cases the failure of ERAD and consequent accumulation of misfolded protein can lead to a UPR-triggered apoptotic responses, which in some cases can contribute to human disease. This *trans*-acting effect of misfolded proteins may constitute a form of “toxic gain of function”. While ERAD is also responsible for degradation of water-soluble proteins that misfold in the ER lumen, I will here focus on MPs. Examples of MPs that appear to sometimes elude ERAD upon misfolding, and for which a loss of function is compounded by toxic gain of function include the proteolipid protein (Pelizaeus-Merzbacher disease), PMP22 (Charcot-Marie-Tooth disease, CMTD), and rhodopsin (retinitis pigmentosa).(*389, 504, 505*) Here, I will briefly explain some of the known pathways and proteins involved in ERAD, as well as how the cell overcomes the energy barriers involved in the removal of integral MPs from the ER membrane.

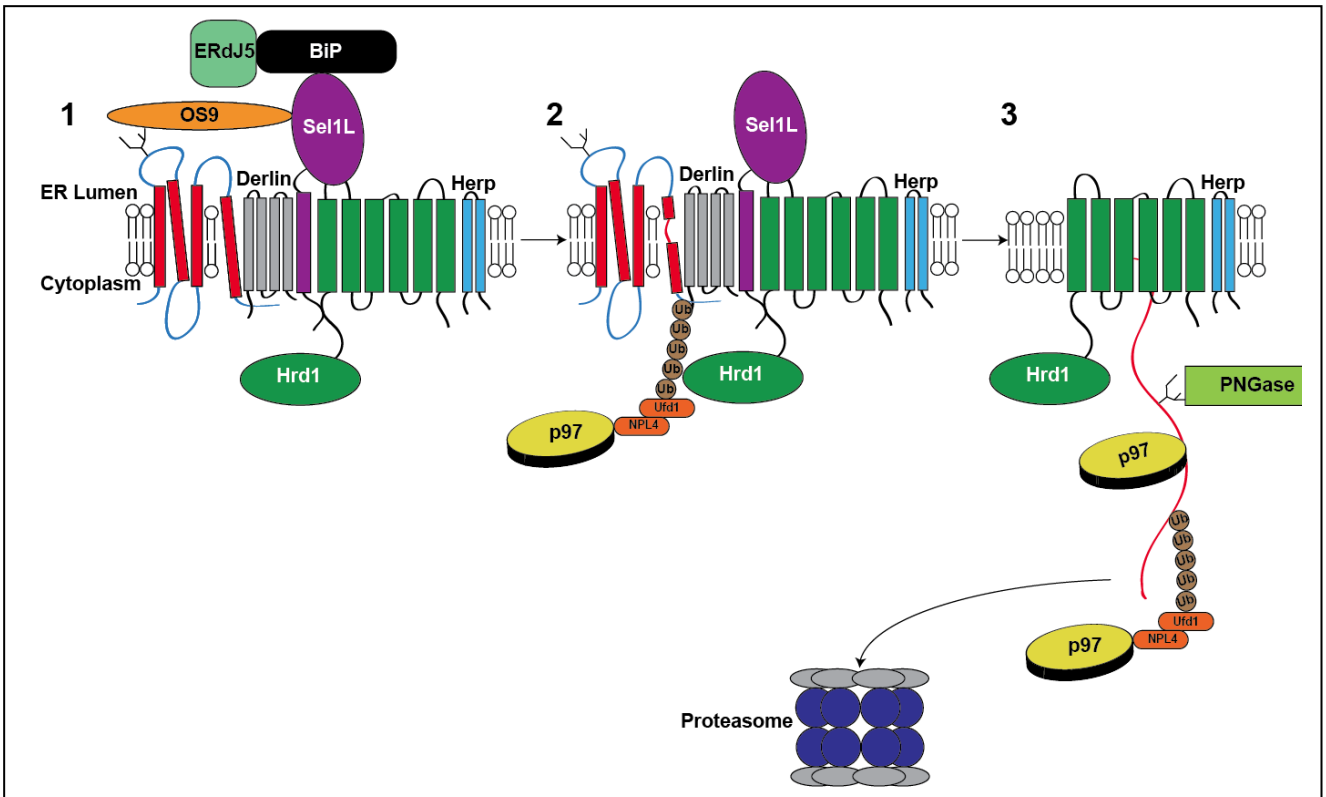

Figure 17. ERAD of a representative integral MP

In **step 1**, a misfolded protein (red) is recognized either through its N-glycan by the ER lectin chaperone OS9 (orange) or in the plane of the membrane by proteins such as the derlins (grey) or Hrd1 (green). Sel1L (purple) nucleates an ERAD complex in the ER membrane and also recruits ER luminal factors such as BiP and its PDI cochaperone ERdJ5 (teal). Herp (cyan) localizes the E3 ubiquitin ligase Hrd1 to ERAD sites. In **step 2**, the derlins may function to lower the energetic barrier for substrate retrotranslocation by partially unwinding helices in the plane of the membrane. The cytoplasmic region of Hrd1 catalyzes the addition of ubiquitin (brown) to lysine residues on the ERAD substrate. Ufd1 and NPL4 (dark orange) associate with the AAA ATPase p97 (yellow) and recognize the ubiquitinated ERAD substrate. **In step 3**, the ERAD substrate is retrotranslocated into the cytoplasm potentially through a pore formed by Hrd1. PNGase (light green) then removes the N-linked glycan from the ERAD substrate. The substrate is pulled out of the membrane via the energy provided by p97 ATPase activity which also functions as a retrochaperone to maintain the solubility of the ERAD substrate in the cytoplasm. The ERAD substrate is eventually degraded via the 26S proteasome (grey and navy).

4.3.1. Pathways and Proteins of ERAD

Many of the pioneering studies on the biochemical mechanisms of ERAD utilized yeast as a model organism. Although the main principles are conserved from yeast to mammals, the mammalian system is far more complicated. For example, the degradation of all ERAD substrates is mediated by only two E3s in yeast, Hrd1p and Doa10, in combination with a number of shared ERAD factors.(*390, 497, 506*) Hrd1p is utilized to degrade proteins with conformational defects within the membrane or luminal domains, while Doa10 seems to mainly degrade proteins with defects within cytosolic domains. By comparison, greater than 30 E3s localize to the ER membrane in mammals, where they have been hypothesized and sometimes confirmed to play a role in ERAD.(*507, 508*) These E3s exhibit a broad range of substrate specificities—some are non-specific while others appear to specialize in the degradation of a single substrate. Additionally, distinct combinations of

ERAD factors are required for the degradation of certain client proteins.(*509*) Beautiful work integrating proteomics, functional genomics, and gene expression data has elucidated the organization of many of these ERAD complexes in mammals.(*500, 501*) For the sake of brevity, here I focus on the most studied ERAD complex found in mammals, centered around Hrd1 and some of its more prominent auxiliary factors. Hrd1 has been implicated in the degradation of numerous integral MPs.(*235, 419, 500, 506*)

As described in Section 4.2.2, glycosylated ERAD substrates are removed from the calnexin cycle and targeted for ERAD through the trimming of mannose residues by ERManI and the EDEMs.(*404, 405, 434, 448*) Moreover, substrates containing anywhere from five to seven mannose residues interact with the OS9 or XTP3B lectins through a mannose-6 phosphate receptor homology (MRH) domain, which uses a double Trp motif to recognize the sugar on the ERAD substrate (**Fig. 17** step 1).(*506, 510, 511*) Surprisingly, this pathway does not appear to exclusively handle glycosylated proteins. Overexpression of EDEM1 (with or without its carbohydrate recognition domain) increases the degradation of both glycosylated and non-glycosylated MPs.(*434*) OS9 and XTP3B may also interact with substrates through exposed hydrophobic residues, either directly or indirectly, through interactions with BiP or GRP94.(*447, 506, 510, 511*) OS9 and XTP3B then link substrates to the membrane-anchored scaffolding protein Sel1L, most likely though interactions with ER lumen-exposed N-linked glycans on Sel1L.(*447*) Sel1L also scaffolds essential reductases such as ERFAD and BiP-associated ERdj5 on the luminal side of the ER membrane in order to reduce disulfide bond prior to removal of the substrate from the ER membrane.(*500*) Additionally, Sel1L nucleates a complex with integral membrane ERAD components including but not limited to Herp, VIMP, Derlin1, Derlin2, Derlin3, and Hrd1 (**Fig. 17** step 1).(*497, 500, 501*) This complex in turn recruits the cytosolic VCP/p97/Cdc48 AAA+ ATPase (hereafter referred to as p97) as well as necessary cofactors required to drive substrate retrotranslocation.(*497, 500, 501*)

ERAD factors located in the ER membrane and in the cytosol serve distinct functions. Herp, which is upregulated during ER stress, has been shown to localize Hrd1 to sites at the ER membrane where ERAD occurs.(*512*) The highly tunable expression of Herp affords the cell granular control over the ERAD process. VIMP has been implicated in both substrate and p97 recruitment to the ERAD complex, although its interaction with p97 may be functionally redundant considering that Hrd1 and the Derlin proteins also contain cytosolic p97-binding motifs.(*301, 500, 513*) The function of the Derlin family of proteins remains somewhat enigmatic. The Derlins are a family of inactive rhomboid pseudoproteases proposed to carry out a variety of functions

including ERAD substrate recognition, retrotranslocation of misfolded proteins (passage across the ER membrane into the cytosol), or destabilization of TM helices (**Fig. 17** step 2).(*497, 500, 514, 515*) This latter function will be expanded on in the next section. Hrd1 is a polytopic protein with a cytosolic ubiquitin E3 RING finger ubiquitin ligase that ubiquitinates ERAD substrates on their cytosolic face.(*498, 501, 506*)

Hrd1 has also been hypothesized to serve as the major retrotranslocation channel of responsible for the extrusion of misfolded ubiquitinated MPs from the ER membrane (**Fig. 17** step 3). Reconstitution of Hrd1 in liposomes containing a membrane-anchored ERAD substrate is sufficient to catalyze retrotranslocation of the substrate in the presence of cytosolic ATP and requisite components for ubiquitination.(*333*) However, it is unclear from these experiments if the substrate was fully extracted from the membrane in the absence of p97. In any case, Hrd1 autoubiquitination was enough to initiate substrate retrotranslocation. *In vitro* analysis of the retrotranslocation of HMG-CoA reductase showed this process to be dependent on Hrd1 but not on other proposed retrotranslocation channels (Sec61 and Derlins).(*466*) Interestingly, a recent cryo-EM structure of the dimeric form of yeast Hrd1 revealed an aqueous cavity bridging the ER lumen to the cytosol.(*516*) This structure also features a 'lateral seal' that could potentially accommodate entry of an integral MP substrate into the channel. This feature is reminiscent of the lateral gate of the Sec61 translocon (see Section 4.1.1), which facilitates cotranslational membrane integration of nascent proteins. Once a client protein is exposed to the cytosol, Hrd1 ubiquitinates lysine residues using its RING finger domain and expands these ubiquitin chains to enhance the affinity of the substrate protein for the proteasome.(*235, 390, 461, 497, 498, 507*)

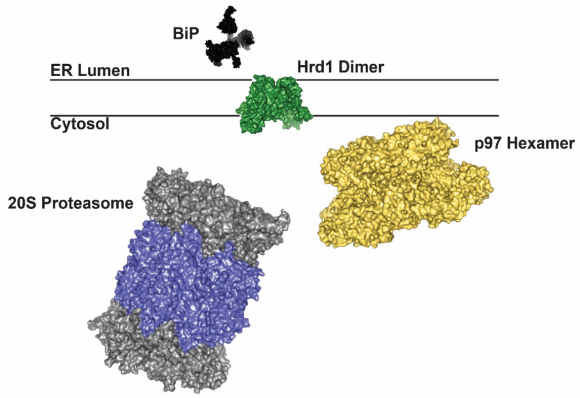

Figure 18. To-scale surface representation the structures of some of the key players involved in ERAD.

Human BiP (black; PDB: 5E84), Hrd1 from *S. cerevisiae* (green; PDB: 5V6P), human p97 (yellow; PDB: 5FTJ), and the human 20S proteasome (α subunits in grey, β subunits in navy; PDB: 5LE5).

The cytosolic components of the ERAD complex, which include the p97 AAA+ ATPase and the glycolytic enzyme PNGase, function to prepare the ERAD substrates for proteasomal degradation and to deliver the substrate to the 26S proteasome (**Fig. 17** steps 2 and 3). p97 binds to ubiquitinated substrates on the cytosolic side of the ER membrane via its cofactors Ufd1 and Npl4.(*517*) It then removes the substrate from

the membrane by using ATP hydrolysis to generate (discussed further below).(*518*) Once substrates are removed from the ER membrane, PNGase removes all N-linked glycans from the substrate to prepare it for proteolytic digestion.(*461*) It was recently demonstrated that the yeast homolog of p97, Cdc48, also helps to maintain the solubility of dislocated integral MPs prior to proteasomal degradation.(*515*) Additionally, Hsp104 has been shown to associate with ubiquitinated, and retrotranslocated substrates in complex with the p97 homologue in yeast.(*469*) Thus, p97 and Hsp104 appear to function together as 'retrochaperones' in order to prevent the cytosolic aggregation of hydrophobic substrates before delivering them to the 26S proteasome for degradation. Once an ERAD substrate is delivered to the proteasome, it's ubiquitin linkages are cleaved prior to protein degradation. The proteasome appears to be tightly coupled to p97.(*519*) **Fig. 18** provides a space filling representations of key components of the later ERAD pathway, offering a perspective of scale.

4.3.2. Energetics of Membrane Protein Retrotranslocation

The removal of misfolded integral MPs from the membrane comes at a steep energetic cost. The free energy difference between native, membrane-integrated bacteriorhodopsin and a hydrated, unfolded state of the protein was estimated at 230 ± 40 kcal mol^{-1} by atomic force microscopy; an average free energy change of about 1.3 kcal mol^{-1} per residue!(*202*) Although this may be an extreme case given the high stability of bacteriorhodopsin, it nevertheless serves as a useful benchmark for the magnitude of the energetic barriers the cell must overcome in order to dislocate hydrophobic proteins from the membrane. One of the machines that accomplishes this task is the *E. coli* protease FtsH, which forms a TM hexamer with the proteolytic/ATPase sites located in the cytosol. Elegant studies of the degradation of the helical multispan rhomboid GlpG by purified FtsH in the lab of Heedeok Hong revealed that FtsH acts by accelerating the unfolding rate of GlpG by a factor of at least 800, a process that is coupled to complete degradation and solubilization of the rhomboid fragments. (*212*) The half-life for FtsH-mediated degradation of a single rhomboid molecule is on the order of 25 minutes, with the combined unfolding-degradation-translocation process being driven by consumption of 380-550 ATP molecules.(*212*) In eukaryotes, p97 is also able to couple ATP hydrolysis to mechanical force by way of a series of conformational changes. Each p97 forms a water soluble homohexameric complex, with each subunit containing an N-terminal domain and two conserved AAA domains that, together, form stacked rings.(*520, 521*) The p97 oligomer contains six ATP binding sites and physiological ATPase activity.(*521, 522*)

The specific mechanisms by which p97 bridges its ubiquitinated substrates with the other components of the retrotranslocation complex in order to pull it through Hrd1 is not certain, but has been hypothesized to involve ATP-mediated molecular “ratcheting”.(*517, 521*)

Certain aspects of the structure and function of the Derlin proteins may also shed light on how the energetic barriers to retrotranslocation can be overcome. The Derlins are a family of inactive pseudorhomboid proteases that lack the catalytic Ser-His dyad.(*500, 515*) Rhomboid proteases are believed to bind their substrates in the plane of the membrane to partially (and passively) unfold the TM helices of substrate proteins in order to expose the scissile bond for proteolysis. Since the non-catalytic pseudorhomboids retain the essential active site architecture, they may also be able to bind proteins in the plane of the membrane and partially unwind the TM helix (**Fig. 17** step 2). Such unwinding would lower the energy required for retrotranslocation since the per-residue free energy cost of disrupting H-bonds within the membrane is on the order of ~4 kcal mol^{-1}.(*18, 523*) The unique structure of the rhomboid proteins has also been proposed to reduce the thickness of the membrane bilayer, reducing the permeability barrier and potentially altering hydration within the membrane in a manner that facilitates the breaking of native hydrogen bonds.(*404*) It was recently shown that the pseudorhomboid domain of a yeast homologue of the Derlin proteins, Dfm1, was required for retrotranslocation of multiple integral MP substrates.(*515*) The association of ERAD substrates with Derlin proteins may therefore constitute a required precursor for retrotranslocation of integral MPs that helps to lower the energetic cost of removing them from the membrane.

Another mechanism by which cells lower the energetic cost of retrotranslocation is through intramembrane proteolysis. Cleavage of MP substrates by presenilin, the catalytic subunit of the γ-secretase complex, or by rhomboid proteases constitute two classic examples. γ-Secretase cleaves a wide variety of single-span MPs within the TM domain, which results in the formation of new polar termini and reduced summed hydrophobicity that promotes release of the remnants of the TM domain from the membrane along with any associated soluble domains. Prominent γ-secretase substrates include the 99 residue amyloid precursor protein C-terminal domain (C99, the immediate precursor of the amyloid-beta polypeptides), the Notch receptor, and receptor tyrosine kinases such as the ErbB epidermal growth factor receptors. The ER-resident rhomboid-like protein 4 protease (RHBDL4) also mediates the turnover of certain MP substrates.(*524*) However, RHBDL4, which is upregulated in response to ER stress, cleaves both single pass and polytopic

MPs.(*524, 525*) Although RHBDL4 has yet to be linked to the turnover of any endogenous ERAD substrates, proteolytic processing by this protein could very well be involved in the dissociation of misfolded MPs from the membrane.

4.3.3. Aggresomes and Autophagy

The balance between chaperone-mediated folding and degradation are typically kept in check through various lines of cellular regulation. However, the accumulation of misfolded MPs under stress conditions sometimes exceeds the capacity of the proteasomal degradation pathway. Under these conditions, the accumulation of protein aggregates can trigger disposal through orthogonal degradation pathways. As the proteasome becomes saturated, cytosolic aggregates of ERAD substrates are actively side-tracked to perinuclear foci known as aggresomes (**Fig. 13**).(*526, 527*) This process is believed to protect cells by sequestering cytotoxic aggregates and promoting their clearance through macroautophagy. A number of disease-linked MPs are known to form aggresomes, including CFTR,(*213*) PMP22,(*528-531*) rhodopsin,(*532, 533*) caveolin-1,(*534*) SIMPLE,(*535*) ABCG2,(*536*) and presenilin.(*537*) However, the manner in which the cell senses proteotoxic stress, adapts, and re-routs the flux of misfolded proteins remains unclear. The nature of the intermediate states that bridge retrotanslocation from the ER membrane to aggresome deposition is also not known.

Water-soluble proteins can also be transported into aggresomes via pathways that likely overlap with those of MPs.(*538*) Indeed, a wide variety of proteostatic stressors can promote the accumulation of soluble protein aggregates that are also picked up by common components of the proteostasis network.(*539, 540*) In some cases, aggresome formation seems to arise from specific unstable domains or signal sequences. For example, an ankyrin repeat domain within synphilin-1 is sufficient to direct it to aggresomes, though replacement of this domain with an aggregation-prone segment of the huntingtin protein is also capable targeting the protein to the aggresome network.(*541*) Alternatively, ERAD substrates can be differentially directed to these pathways by specific ubiquitin linkages. For instance, K63-linked polyubiquitination (attachment of ubiquitin to substrate and subsequent polyubiquitination via ubiquitin's K63 residue, K63U) appears to target certain clients for degradation through the aggresomal/lysosomal pathway, whereas K48-linked polyubiquitination targets misfolded proteins for proteasomal degradation.(*542*) Furthermore, the specificity of these pathways appears to be linked to certain pathologies. For example, the E3 ligases parkin

and TRAF6 are involved in catalyzing K63U modifications, with mutations in parkin constituting a common cause of familial Parkinson disease.(*543, 544*) Knockdown of the deubiquitinating enzyme ataxin reduces the extent to which destabilized CFTR and superoxide dismutase variants are packaged into aggresomes; the consequences of which include programmed cell death.(*545, 546*) Similarly, knockdown of PLIC1, a ubiquitin-like protein that binds to the ubiquitin-interacting motif of ataxin 3, also inhibits aggresome formation.(*547*)

The downstream recruitment of client proteins to perinuclear aggresomes requires a network of adaptor and motor proteins that come in diverse shapes and sizes. The cargo receptors p62 and NBR1 bind to ubiquitinated proteins in a manner that promotes the stabilization of these aggregates.(*538*) Other adapters, such as histone deacetylase (HDAC6) recognizes K63U-modified proteins in a manner that connects them to dynein motors. These motor proteins then engage in retrograde transport along the microtubule network in order to deliver protein aggregates to the aggresome, which are then bundled into vimentin cages at the microtubule organizing center.(*548*) It should also be noted that the activity of HDAC6 is also modulated both by phosphorylation and through protein-protein interactions with various cargo receptors, chaperones, and E3 ligases.(*549*) Finally, aggresome formation can be mediated by the Bcl-2-associated athanogene 3 (BAG3) co-chaperone in response to the upregulation of Hsp70. This is mediated through formation of a ternary complex containing the molecular adaptor 14-3-3 and dynein.(*550, 551*) Taken together, the complexity of these aggresomal pathways provides an example of the multi-faceted regulation of the proteostasis network. Aggresome formation is rendered tunable through gene expression, protein-protein interactions, and post-translational modifications.

Though protein aggregates are typically associated with toxicity, we emphasize that aggresomes are generally considered to be protective storage compartments for sequestering misfolded proteins until they can be safely disposed of via autophagy. Indeed, certain adaptors and cargo receptors found near aggresomes appear to seed the formation of autophagosomes that eventually fuse with lysosome to promote their degradation.(*552, 553*) Aging and/ or mutations that compromise autophagy result in a failure to clear aggresomes, which potentially may promote disease states.(*538, 554*)

In a related vein, it should be appreciated that misfolded proteins sometimes aggregate within the ER. Such aggregates and the associated local membrane can be targeted for autophagy and lysosomal degradation via a pathway sometimes referred to as ER-phagy or reticulophagy (see **Fig. 13**).(*555-558*)

5. Membrane Protein Misfolding in Human Disease

5.1 The Sometimes Delicate Balance between Folding and Misfolding

While some proteins appear remarkably tolerant to single amino acid mutations,(*559, 560*) there is much evidence that the folding of nascent proteins in the cell, including some MPs, is often strikingly inefficient.(*389, 561-568*) For example, the *in vivo* efficiency for the folding and maturation of human wild type PMP22, as inferred from its steady-state glycosylation and cellular trafficking, has been reported by multiple groups to be only ca. 20%, which apparently is sufficient to generate the population of functional PMP22 required to maintain healthy PMS myelin in humans.(*289, 569, 570*) Inefficient folding, which typically leads to significant levels of misfolding and/or degradation, implies that the energetic barriers involved in folding and misfolding pathways are often similar in magnitude. As we have previously treated in more detail,(*288*) this implies that mutations that disrupt only a single hydrogen bond, ion pair, or hydrophobic interaction may significantly reduce the yield of folded protein. In these cases, pathology can arise when the level of the functional protein drops below the threshold required for normal health and/or when the accumulation of misfolded proteins becomes toxic. This often-delicate balance between folding and misfolding of wild type MPs possibly helps to explain why a diverse spectrum of mutations distributed throughout the three dimensional structure of a misfolding-prone protein are all capable of causing the same human disease phenotype.(*288, 562*)

5.2. Contributions of Pathogenic Mutations in Integral Membrane Proteins to Disease Etiology

Mutations that promote MP misfolding are known to cause or contribute to a wide variety of human diseases. While our focus will be destabilized MP variants, it should be noted that the propensity of wild-type proteins to misfold is also relevant to certain pathologies. For instance, the proteotoxic stress arising from the overexpression of WT PMP22 upon gene duplication is responsible for the most common (type 1A) form of CMTD. The misfolding of WT proteins may also exacerbate proteotoxicity arising from post-translational modifications(*571*) or environmental stressors that include fever, oxidative stress, or defects in QC stemming from gene variations affecting components of the proteostasis network.(*572-574*) In this regard, it is important to recognize the implications of the extensive connectivity of the proteostasis network. Sometimes the *cumulative* load of misfolded proteins may represent the root source of pathophysiology rather than the defects in a single protein.(*575*) For hereditary diseases or those caused by a germline mutation, the deleterious

effects of the mutation may have consequences in whichever tissues affected protein is expressed. Alternatively, diseases can also arise from somatic mutations that occur spontaneously within a single cell.(*576*) Somatic mutations in oncogenes can cause a single cell to proliferate into a tumor.(*577*) It has long been hypothesized that sporadic mutations may also trigger prion disorders in which mutant PrP from a single cell adopts the toxic scrapie conformation that can seed the toxic conversions of WT protein from surrounding cells into its infectious conformation.(*578, 579*) It has also been suggested that the progression of the sporadic form of Alzheimer's disease may also involve the propagation of toxic oligomer folds in the brain.(*580*) Small amounts of misfolded proteins resulting from sporadic mutations could also conceivably trigger toxic autoimmune responses.

Diseases that arise from mutations in a single gene (monogenic) and that follow a Mendelian pattern of inheritance represent the best-characterized examples of diseases of MP misfolding. For many disorders, it only takes one mutation in one protein to cause disease. However, for a given inherited disorder, there may be an entire panel of proteins in which a single mutation is sufficient for causation. For example, mutations impacting the expression level or amino acid sequence of PMP22 are by far the most common cause of CMTD. Nevertheless, the same clinical pathophysiology can also arise from mutations in any one of more than 40 other proteins, many of which are likely to carry out functions on pathways linked to PMP22 function.(*581*) However, mechanistic insights garnered from investigations of inherited disorders are likely to be relevant both to sporadic disorders and to complex disorders that arise from a combination of genetic and non-genetic risk factors. In the case of complex disorders involving the interplay and additivity of multiple disease-predisposing risk factors, MP misfolding may represent one piece of a larger puzzle.

How common are diseases arising from the pathogenic consequences of MP misfolding? A search of the UNIPROT database(*582*) for all disease-linked human proteins returned ca. 4,000 hits (not counting splice-variants), which accounts for ~20% of the proteome. This number is perhaps unsurprising given that ca. 20% of yeast proteins are essential for viability.(*583*) Of the 4,000 disease-linked human proteins in UNIPROT, about 1,100 have at least one TM segment. Given that MPs constitute ~25% of the proteome, this seems reasonable. How many of these 1,100 disease-linked MPs undergo misfolding as the primary disease-promoting defect? We suggest that there are four lines of evidence to suggest that misfolding is the most common disease mechanism. (1) Many disease-linked MPs are mistrafficked within the cell.(*389, 584, 585*)

While misfolding is not the only phenomenon that can cause mistrafficking, it seem likely to be the most common cause in light of what we know about the intimate linkage between folding and trafficking along ER-to-plasma membrane pathway. (2) The pathogenic defects in most disease-linked MPs can typically be promoted by a wide variety of substitutions that typically do not cluster within a functional site or domain.(*561*) For example, **Fig. 19** shows both the sites of known diabetes insipidus mutations in the human vasopressin V2 receptor, as well as a list of the specific disease-causing mutations.(*586*) This scatter of disease sites throughout the sequence suggests the pathogenic effect often does not directly perturb an active site or a protein-protein binding interface, as was also found to be the case for retinitis pigmentosa mutations in rhodopsin, a related class A GPCR of known 3D structure.(*288*) Instead, this distribution indicates that most mutations are likely to either disrupt the cooperative interactions between TM helices that stabilize the native fold or destabilize interaction of the protein with the membrane phase. Indeed, it is known that the vast majority of disease mutations in the V2R cause mis-trafficking of the receptor, consistent with these classes of defects.(*587-592*) (3) Pathogenic mutations in MPs are biased toward non-conservative mutations that are likely to perturb tightly packed native conformations or TM domain-membrane interactions. Of 96 sites in V2R for which there are known disease mutations, 80 of them are located in TM helices.(*586*) Moreover, mutations that introduce charged residues, proline, or glycine for native aliphatic residues within TM domains are quite common among pathogenic mutations within MPs.(*593*) (4) Rigorous experimental investigations of the effects of pathogenic mutations in disease-linked MPs have revealed that a majority of the tested disease mutations reduce the conformational stability of the protein in a way that appears to be directly linked to their cellular mistrafficking (c.f.(*185, 289*)). Similar observations have previously been made for water soluble proteins that are linked to inherited disorders.(*594-598*) Taken together, the available data suggest the pathogenic misfolding of MPs is of central importance to a wide variety of diseases.(*599*) Thus, investigations into the nature of these conformational defects are needed to provide basic insight into the many ways that mutations disrupt the folding of disease-linked MPs.

5.3. The Most Common Defect of Disease-Linked MPs Appears to be Destabilization of Native Structure

From studies of both model and disease-linked MPs, it seems to be the case that the most common defect leading to misfolding is rooted in thermodynamics: destabilization of the native state.(*285, 286, 389, 563, 564*) It should also, of course, be emphasized that some disease mutations operate via mechanisms that are

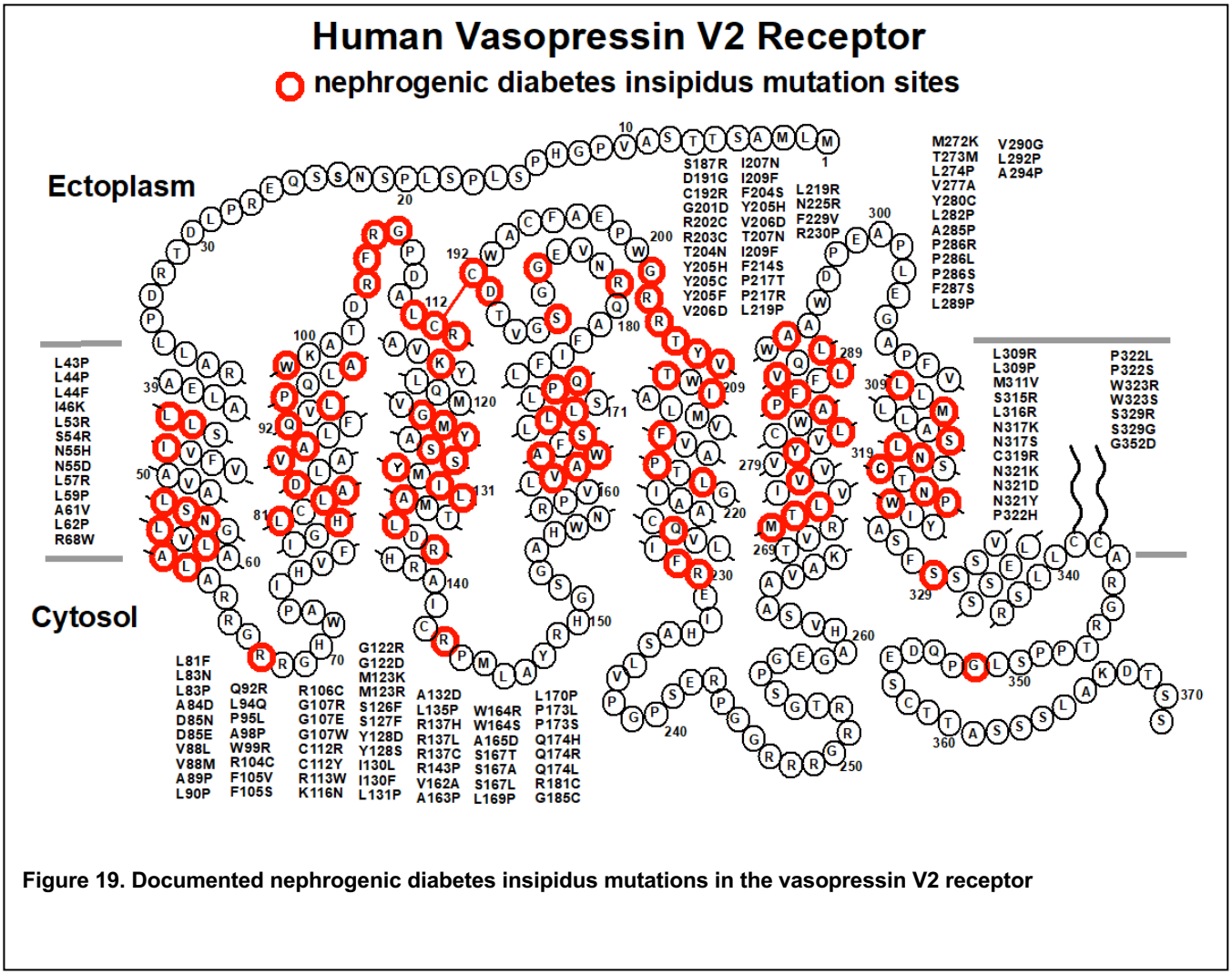

Figure 19. Documented nephrogenic diabetes insipidus mutations in the vasopressin V2 receptor

unrelated to misfolding. For example, while studies of LQTS mutations in KCNQ1 revealed that destabilizing mutations that lead to misfolding are by far the most common single class of disease mutations, there are less common disease mutants that cause loss of channel function without altering folding and/or trafficking.(*185*)

The notion that many mutations promote disease through a reduction in protein stability may be good news from a therapeutic standpoint for two reasons. First, it implies that a single drug that acts by stabilizing protein structure could potentially be used to treat most patients carrying any one of a series of destabilizing mutations in the target protein. Secondly, the fact that energetic perturbations associated with the disease

mutant forms are modest suggest that drugs need not be “super-stabilizers”, a modest enhancement in stability conferred by drug binding may often be all that is needed to restore native-like folding efficiency.

5.4 Peripheral Myelin Protein 22 and Charcot-Marie-Tooth Disease

We now arrive at the specific subject of my dissertation research: PMP22 and its role in CMTD. Mutations affecting the *PMP22* gene are the leading cause of the debilitating peripheral neuropathy CMTD as well as the related dysmyelinating disorders Djerine-Sottas syndrome (DSS, severe) and hereditary neuropathy with liability to pressure palsies (HNPP, mild).(*404, 600, 601*) Patients with CMTD suffer from clinical symptoms ranging in severity (depending on the causative mutation), including impaired tendon reflexes, progressive weakness and atrophy of the distal musculature, abnormalities of the peripheral nerve and its adjacent myelin sheath, and—in the most severe cases—blindness, auditory loss, and confinement to a wheelchair.(*404, 602, 603*) Disease symptoms are thought to be the consequence of abnormal myelin production and assembly by the myelin-producing Schwann cells of the peripheral nervous system. PMP22 is one of the most abundant proteins in compact myelin, where it is believed to play a structural role.(*168*) However, PMP22 is also likely involved a number of other processes within Schwann cells including cellular proliferation, differentiation, and cell death.(*168, 404, 601, 604*)

PMP22 is a tetraspan integral MP, and was the first multispan eukaryotic MP for which thermodynamic stability of folding was measured.(*605*) Spectroscopic studies revealed that the conformational stability of WT PMP22 is strikingly modest in detergent micelles: the native conformation is favored over the denatured ensemble by only 1.5 ±0.1 kcal mol^{-1} in the presences of stabilizing osmolytes. Such marginal stability perhaps accounts for why most of the nascent protein is rapidly degraded within the ER following biosynthesis; only ~20% of the nascent protein manages to fully mature and traffic to the plasma membrane.(*569, 570*) The rest is either degraded by the proteasome or deposited into aggresomes.(*404, 419*)

The most common (type 1A) form of CMTD (CMT1A) arises from a heterozygous duplication of the chromosome 17p.11-2.12, which results in trisomy (three copies) of WT *PMP22*. CMT1A is a common inherited disordered (1:5,000 people).(*404, 600, 601*) The exact mechanism underlying the pathogenicity associated with expression of third copy of *PMP22* is not yet clearly established. However, it has been hypothesized that the elevated expression in conjunction with the instability of the PMP22 protein imposes a

heavy burden on ERQC, causing proteotoxic stress and the formation of aggresomes.(*529, 605*) While aggresomes are not toxic if they are properly engaged by the autophagy pathway, the activity of the autophagy pathway is believe to decline with age,(*606*) which could lead to chronic accumulation of PMP22 aggresomes.(*529, 607*) This may account for the fact that CMT1A patients only exhibit disease symptoms later in life even though they are born with the causitive mutations. This model for the etiology of CMT1A, if correct, provides an example of a disease related to MP misfolding that is caused by a combination of both toxicity of the misfolded protein and loss of native function.

More rare forms of Charcot-Marie-Tooth disease (recently dubbed CMT1E(*600*)) as well as the related DSS and HNPP are caused by heterozygous expression of WT PMP22 in combination with missense variants of PMP22, over 35 of which have been identified to date. Experimental correlations between conformational stability, trafficking efficiency, and disease severity have been demonstrated for a cross-section of these variants.(*289*) The thermodynamic stability of these variants appears to be directly correlated with the efficiency of cellular trafficking: the efficiency of protein folding scales with trafficking to the plasma membrane (**Fig. 20**). The degree of PMP22 destabilization also correlates linearly with patient nerve conduction velocities, which serve as quantitative clinical readouts of disease severity (**Fig. 20**).(*289*) Mutations causing the mild HNPP phenotype were the least destabilizing, while mutations causing the severe DSS were the most destabilizing. These results point to the thermodynamic stability of PMP22 as being the prime determinant of the maturation and trafficking of PMP22 in the cell. ERQC evidently recognizes some conformational trait of misfolded PMP22 in the ER that scales with the stability of the native tertiary structure. **Fig. 20** shows the structural locations of the PMP22 mutants whose stabilities were probed, revealing that most of the severe mutations are for sites located in the interior of the TM domain, where side chains interact mostly with other TM sites rather than with the lipid phase.(*608*)

Interestingly, a heterozygous deletion in the chromosome bearing the *PMP22* gene also causes a mild disease phenotype (HNPP).(*404*) Disease in these patients arises from the lack of a second allele and the resulting deficiency of WT PMP22 expression. This mild disease phenotype is actually less severe that those arising from the heterozygous expression of missense variants (CMT1A and DSS patients).(*601*) There are two possible explanations that may contribute to this difference. First, a toxic gain-of-function due to formation of mutant PMP22 aggregates may exacerbate the partial loss of PMP22 expression in heterozygotes

expressing a single mutant variant in combination with WT. Secondly, certain mutant forms of PMP22 expressed in heterozygotes are capable of forming non-productive oligomers with the WT protein.(*609*) Recognition of these non-native oligomers by ERQC may cause a dominant negative effect leading to the degradation of the WT protein, which may further reduce the abundance of the WT protein.

Exactly how the misfolding of PMP22 is managed by ERQC is not yet well understood, but there are some clues. BiP, calreticulin, and ERp57 do not appear to be important for the maturation of PMP22.(*401, 468*) However, there is evidence that calnexin may serve as both a PMP22 chaperone and folding sensor.(*401, 414, 419, 468*) As noted earlier, calnexin binds WT PMP22 under cellular conditions with a half-life of about 11 minutes, an interaction that depends on the presence of PMP22's single N-linked glycan. However, calnexin sequesters the severely misfolded L16P PMP22 mutant ("Trembler-J") with a half-life of more than an hour. This interaction appears to specifically involve TM1, which includes the mutated residue. Interestingly, binding of calnexin to L16P PMP22 also appears to occur in a manner that is independent of the glycosylation state of the mutant protein.(*414*) NMR structural studies have shown that this mutant samples a conformational state in which TM1 is dissociated from the other three TM helices, a conformational state that may be detected by calnexin (**Fig. 6**).(*184*) However, it cannot be ruled out that calnexin may instead recognize the swiveling kink introduced into TM1 helix by the L16P mutation. It is interesting to note that *cnx -/-* calnexin knockout mice are viable but display abnormalities in their peripheral nerves, potentially highlighting the role that calnexin plays in managing folding and misfolding of PMP22 and perhaps other myelin MPs.(*610*) It is also noteworthy that misfolded PMP22 variants that escape the ER are retrieved from the Golgi complex and returned to the ER through the action of the Rer1 protein,(*419*) while inducible cytosolic Hsp70 may be involved in shepherding misfolded PMP22 molecules through the lysosomal degradation pathway.(*611*)

In my dissertation research I have studies a wide variety of features of PMP22. I have examined its functional role in promoting myelination (Chapter 2), its ability to partition into ordered membrane phases and alter the biophysical properties of these membranes (Chapter 3), the relationship between PMP22 expression levels and trafficking efficiency (Chapter 4), and how folded and misfolded PMP22 is differentiated by the ERQC (Chapter 5). I have spent countless hours thinking about this protein and its involvement in CMTD and I hope that the results of these hours will be useful in developing a treatment for this debilitating neuropathy. Furthermore, I hope that my work on membrane protein folding in general will be of use to the scientific community at large. I hope that this thesis serves as an accurate representation of my scientific accomplishments at Vanderbilt University.

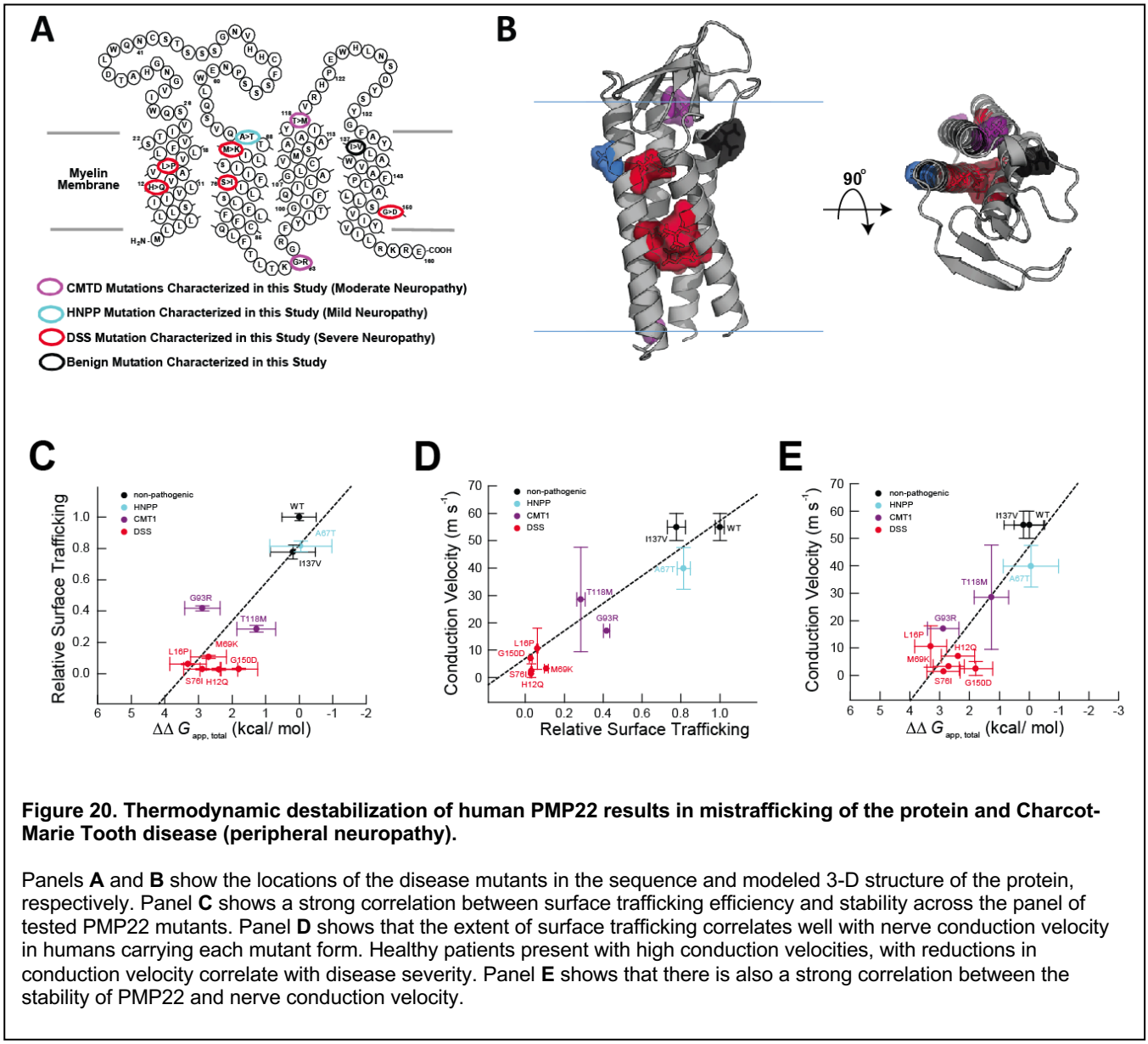

Figure 20. Thermodynamic destabilization of human PMP22 results in mistrafficking of the protein and Charcot-Marie Tooth disease (peripheral neuropathy).

Panels **A** and **B** show the locations of the disease mutants in the sequence and modeled 3-D structure of the protein, respectively. Panel **C** shows a strong correlation between surface trafficking efficiency and stability across the panel of tested PMP22 mutants. Panel **D** shows that the extent of surface trafficking correlates well with nerve conduction velocity in humans carrying each mutant form. Healthy patients present with high conduction velocities, with reductions in conduction velocity correlate with disease severity. Panel **E** shows that there is also a strong correlation between the stability of PMP22 and nerve conduction velocity.

7. Future Directions

Progress in our understanding of the kinetics and thermodynamics of MP folding *in vitro* has progressed immensely during the past three decades. These advances are underscored by impressive *de novo* design efforts that have yielded membrane peptides and MPs with fundamentally new structures and/ or functions.(*612-618*) Methods are now in place for enhancing the stability of MPs(*619, 620*) and totally new ways of studying MP folding continue to be devised. Moreover, the interactions of client MPs with chaperone networks are beginning to be explored with quantitative, experimentally constrained systems modeling.(*222*) However, many gaps remain in our understanding of how the conformational properties of MPs relate to their behavior within the cell. For example, in the past decade, spectacular advances in crystallography and cryo-EM have given rise to a structural revolution in GPCR biochemistry and pharmacology. Nevertheless, quantitative investigations of the folding/unfolding kinetics and thermodynamic stability of GPCRs have, to date, proven elusive. Moreover, current computational platforms are still incapable of predicting the effects of mutations on the conformational equilibrium of MPs.(*621*) Based on our collective observations, we posit that the next such revolution is unlikely to arise solely from an understanding MPs in isolation, but rather from insights into the manner in which their conformational equilibria is navigated in the context of the cellular milieu.

It is imperative that emerging insight into the conformational stability of MPs is ultimately connected to a broader understanding of cellular processes. Recent progress provides considerable room for optimism. For example, the physical mechanisms associated with the Sec61-mediated cotranslational folding of nascent MPs have been outlined in considerable detail. However, the recent discovery that the EMC complex appears to work closely with Sec61 to initiate integral of MPs into the ER membrane(*324*) suggests that there are stunning discoveries still to be made, even for systems that appeared to be reasonably well understood. Along the same lines the energetics of cotranslational folding has yet to be connected with the structural properties of the nascent ensemble or the outcomes of cellular QC. The super-structural organization of the endoplasmic reticulum throughout the cell is now appreciated to be much more complex and sophisticated than long realized, with different domains of this organelle serving as focal points for different sub-systems of ERQC. Our current understanding of this superstructure and the spatial distributions of the component of ERQC is fuzzy, at best. While the pertinent biochemical activities of many central components of ERAD, such as the Hrd1 retrotranslocon, have been biochemically characterized, additional work is needed to rationalize how these

activities interface with specific conformational states of client proteins. There are still numerous proteins that are believed to be ERQC factors, but otherwise have unknown functions. The anticipated wave of experiments in these areas will likely yield major discoveries that merge structural biochemistry and biophysical chemistry with a broader understanding of cellular systems.

It is also essential to consolidate and establish new linkages between MP folding and misfolding in the cell and the molecular basis of disease. In many cases, recent observations have revealed the sources of the smoke—clear disease linkages for numerous membrane proteins, lists of mutations, and so forth—but have yet to elucidate the mechanistic basis of the fire. Beyond their emerging impact in the clinic, small molecule pharmacological chaperones represent a tremendous tool for biochemical and biophysical investigations of MP misfolding in the cell. Ongoing HTS efforts to identify new stabilizing molecules in conjunction with mechanistic studies of their effects are likely to provide new insights into the many ways in which MP misfolding can be curtailed in the cell. Such advances are also likely to help streamline next-generation drug discovery platforms.

Future investigations of these topics must find new ways to reckon with and to utilize the emerging wave of genomic sequencing data. Indeed, the opportunities for molecular scientists to contribute to personalized (or “precision”) medical diagnostics and decision-making are numerous.(*622*) The tools and perspectives of biochemistry and biophysics are needed to interpret the effects of rare variants in disease-linked MPs. Such information may prove critical for the use of genomic information in the clinic, especially for cases in which different pathogenic mechanisms can arise from a spectrum of mutations within a single protein.(*185*) Such advances may provide novel ways to optimally match certain medications to specific patient genotypes. Deciphering the complexity within individual genomes will require next-generation tools to enable rapid, low cost, and reliable experimental or predictive methods for these purposes. It is increasingly clear that misfolding is the most common consequence of pathogenic mutations in MPs. However, novel methods to parse the spectrum of molecular defects associated with these mutations are sorely needed.

8. Dissertation Aims

Charcot-Marie-Tooth disease (CMT) and closely related Dejerine-Sottas syndrome (DSS) and hereditary neuropathy with liability to pressure palsies (HNPP) are the most common neurodegenerative disorders of the peripheral nervous system (PNS), afflicting 1:2500 individuals (collectively referred to as CMTD). Mutations in *peripheral myelin protein 22* (*PMP22*) including gene duplication, gene deletion, and various missense mutations

are the most frequently observed genetic mutations in patients suffering from CMTD. These mutations cause fluctuations in the amount of mature PMP22 at the plasma membrane (PM) of Schwann cells, which is believed to play a role in the observed myelin abnormalities of CMTD. There are currently no treatments for CMTD beyond symptom management. PMP22 folds in the context of the endoplasmic reticulum (ER) quality control (QC) network which also mediates forward trafficking or retention and degradation processes. The proteins responsible for directing PMP22 trafficking out of the ER and toward the PM and those responsible for retaining PMP22 in the ER and targeting it for degradation are currently unknown. At the PM, PMP22 is localized to cholesterol-rich membrane domains that are closely linked to the actin cytoskeleton and performs an unknown function in compact myelin. Proper trafficking to the myelin compartment for another membrane protein of the PNS, P_0, requires association with these cholesterol-rich membrane domains. Furthermore, mutations in *PMP22* cause a decrease in cholesterol levels at the PM and a disruption in the linkage of the cytoskeleton to the PM, impairing the adhesion and migration capacity of Schwann cells, which may explain the myelin abnormalities observed in CMTD patients. This suggests that PMP22 association with cholesterol-rich membrane domains is important for Schwann cell function and potentially PMP22 trafficking. Despite the importance of both PMP22 trafficking to the PM and its association with cholesterol-rich membrane domains, *we currently do not understand the mechanism by which cells accomplish these feats*. Understanding how PMP22 traffics out of the ER and the role that membrane domain association plays in this process may elucidate novel therapeutic strategies to treat patients who suffer from these neuropathies.

The overall goal of this project is to understand, at a molecular level, how PMP22 traffics out of the ER towards the PM, its function at the PM, and how trafficking and function is affected by different CMTD mutations. The results from this work will uncover novel, patient-specific, strategies for developing therapeutics for CMTD.

In Chapter III, I used electron microscopy to characterize the ability of PMP22 to modulate lipid ultrastructure. PMP22 recombinantly expressed and reconstituted into synthetic lipid vesicles was found to modify the lipid ultrastructure of these lipid vesicles. Namely, PMP22 was sufficient to induce the wrapping of these vesicles into myelin-like assemblies (MLAs). MLA formation was dependent on protein identity and lipid composition. Negative-stain, single particle Cryo-electron microscopy and tomography was used to characterize these lipid assemblies.

In Chapters V and VI, I will describe features of PMP22 including expression levels, post-translational modification and protein interactions that modify its trafficking. A novel flow cytometry based assay was used to monitor the trafficking of a number of different PMP22 disease mutants. The conformational stability of different PMP22 mutants as well as protein glycosylation was be tested for their contributions to PMP22 maturation and ER QC interactions. Co-IP assays were used to monitor the differing interactions between members of the ER QC and different PMP22 mutants to understand how changes in the interaction network affect PMP22 cell surface expression. In a collaboration with Dr. Lars Plate, co- IP and mass spectrometry based proteomics was used identify novel PMP22 interacting proteins in Schwann cells.

In Chapter IV, I will describe the factors that cause PMP22 to associate with cholesterol-rich membrane domains and assess the effects of this association on PMP22 trafficking. Giant plasma membrane derived vesicles (GPMVs) were made from PMP22 expressing HeLa and Schwann cells and the propensity of PMP22 to partition into cholesterol-rich environments was quantitated using confocal microscopy. Mutational analysis was used to elucidate what factors cause PMP22 to preferentially partition into this environment; I specifically examined the roles of PMP22 palmitoylation, cholesterol binding motifs, and transmembrane hydrophobicity. I also explored the correlation between PMP22 trafficking and membrane domain association. Results from this aim can be used to inform efforts to develop novel therapeutics to treat patients who suffer from CMTD.

The proposed research identified a function of PMP22 *in vitro,* uncovered novel protein interactions, post-translational modifications, and sequence motifs that affect PMP22 trafficking and membrane domain partitioning. This research provides valuable new information for scientists attempting to discover ways to treat patients who suffer from CMTD.

Chapter II. Techniques and Methods

1. Introduction

The biochemical and biophysical techniques used during my thesis work to address my proposed hypotheses are outlined below. Classical techniques such as western blotting, molecular cloning, and cell culturing were omitted from this dissertation for the sake of brevity but can be found in the respected publications in which they were used.

2. Expression, Purification, and Reconstitution on PMP22 into Synthetic Vesicles

PMP22 was expressed in one-shot BL21 Star (*DE3*) *E. coli* as a fusion protein construct consisting of an N-terminal 76-amino acid segment of the lambda repressor (which serves to drive the protein into inclusion bodies) followed by a His_{10}-tag, a seven amino-acid linker, a thrombin cleavage site, an 11 amino-acid strep-tag and, finally, the human-PMP22 sequence. The fusion protein was solubilized from inclusion bodies using the zwitterionic detergent Empigen BB and purified using Ni(II)-NTA Superflow resin (0.5 ml/1g of original cell pellet) packed into a gravity column. While bound to the Ni-NTA resin, the detergent was exchanged for *n*-decylmaltoside (DM), a mild, uncharged detergent, by repetitive, pulsed washing of the column (20 column volumes in one half column volume pulses) with 0.5% DM in 25 mM sodium phosphate buffer, pH 7.2. The fusion construct was cleaved by incubation with Recothrom® Thrombin overnight. This cleavage reaction was followed by a second purification over Ni-NTA resin. Cleaved PMP22 (no His tag) has a modest affinity for divalent metal cations, including Ni(II). Cleaved PMP22 was eluted from the Ni(II) resin in a stepwise fashion using 10-30 mM imidazole in a 50 mM Tris pH 8.0 buffer. The uncleaved PMP22 and the His_{10}-tag containing fusion cleavage product remain bound to the resin at these imidazole concentrations. Protein purity was assessed via SDS-PAGE and the pure fractions were pooled (*1*). In some cases, PMP22 was purified using a method in which the 2nd Ni-NTA column used to purify the cleaved protein was replaced by an ion exchange chromatography column eluted with a salt gradient.

Cleaved and purified PMP22 in DM micelles and a pH 8.0 buffer that containing approximately 20 mM imidazole, 50 mM Tris, and 0.5 mM dithiothreitol (DTT) was concentrated to 1.0 mg/ml as determined by A_{280}

using a molecular weight of 19.2 kDa and an extinction coefficient of 44,900 $M^{-1}cm^{-1}$ prior to reconstitution into vesicles.

1.0 mg/ml WT PMP22 and the various PMP22 mutants used in these studies were equilibrated with mixed micelles containing 53 mM DM plus 5.3 mM POPC and 1.3 mM ESM in water at the lipid-to-protein mass ratios described in the results section. Each PMP22-mixed micelle solution was pipetted into dialysis buttons, which were covered by hydrated dialysis membrane with a molecular weight cutoff of 20 kDa that had been pretreated by boiling in 1 mM EDTA for 5 minutes to remove metal ions. Buttons were dialyzed for 10 days at room temperature against a buffer containing 10 mM Tris pH 8.0, 150 mM NaCl, and 0.5 mM fresh DTT, which was changed daily. Protein-free vesicle controls were prepared by mixing mixed micelles and PMP22 elution buffer together at the same volume-to-volume ratio as the experimental conditions and dialyzed in the same buffer. Alternatively, multilamellar vesicle controls were prepared by mixing dry lipids with water and agitating.

For confirmation that PMP22 had been reconstituted into lipid vesicles we performed a lipid flotation assay. After dialysis, a 750 µL sample was prepared of 20 µg PMP22 reconstituted into liposomes and dialysis buffer containing 50% (w/v) sucrose. This sample was placed at the bottom of a 5 mL polypropylene ultracentrifuge tube. A 750 µL sample of 20 µg PMP22 in DM micelles and dialysis buffer containing 50% sucrose was placed in another ultracentrifuge tube as a control. 3.38 mL of dialysis buffer containing 40% sucrose was layered on top of the liposome or micelle layer followed by 750 µL of dialysis buffer containing no sucrose. This created a stepwise sucrose gradient. All layers in the micelle sample contained 0.05% DM so as to not dilute the DM below the critical micelle concentration. Samples were then centrifuged at 160,000 x g at 4^{o}C for 16 hours using a Beckman L90K Ultracentrifuge equipped with a SW 55 Ti rotor. After ultracentrifugation, samples were collected from the sucrose gradient in 500 µL fractions from the top down using a glass Hamilton syringe; the fractions were analyzed by SDS-PAGE followed by silver staining.

3. Electron Microscopy of PMP22 in Lipid Vesicles

For negative stain EM grids, 2 µL of reconstituted PMP22-lipid assemblies were adsorbed to a glow discharged 200-mesh copper grid covered with carbon-coated collodion film. Grids were washed in two drops of water and stained with two drops of uranyl formate (0.75%). Samples were imaged using an FEI Morgagni

equipped with a 1K x 1K CCD camera. Measurements to determine the “interperiod distance” were carried out using Advanced Microscopy Techniques (AMT) software. Approximately 200 measurements were made to determine the “interperiod distance” for multiple MLAs from different images. Images for presentation were contrast-adjusted in Photoshop and a high-pass filter was applied to enhance contrast between layers. No imaging adjustments were made to images prior to any type of quantification.

For cryo-EM, 3 µL of PMP22/lipid assemblies were pipetted directly onto glow-discharged Quantifoil R2/2 Holey Carbon (200 Mesh Copper) grids and plunged into liquid ethane using a Vitrobot set to 60% humidity at 22 °C. Vitrobot settings included a blot time of 3.5 seconds, an offset of -1, and a drain time of 1 second. Images were collected using a Tecnai F20 electron microscope equipped with a field emission gun at an acceleration voltage of 200 kV under low-dose conditions at a magnification of 68,661x (2.18 Å/pixel) using a defocus value of -2.0-4.0 µm. Images were recorded on a 4k × 4k Gatan CCD camera.

For cryo-electron tomography, prior to plunge-freezing, 10 nm colloidal gold particles were added as fiduciary markers so that tilted images could be aligned. To add gold particles, 1.5 µL of sample were pipetted directly onto a grid as described above, and 1.5 µL of 10 nm colloidal gold was then pipetted directly onto the same grid prior to plunge freezing. Tilt series (-65° to +65°) were acquired in two degree increments on the F30 Polara using SerialEM and a 4K x 4K Ultrascan CCD Camera at a magnification of 35,654x using a defocus value of 5.0-8.0 µm. The total electron dose for each tilt-series was approximately 100 $e^-/Å^2$. Tomograms were assembled and segmented using the IMOD software package. Images were aligned computationally using the coarse alignment, followed by alignment using a fiducial model generated in eTomo. Briefly, fiducials were picked by hand and automatically tracked through the coarsely aligned tilt series images using the built-in tool. Manual adjustment of individual fiducials was performed on each tilt image, and fiducials that could not be reliably traced throughout the model were removed. From the fiducial model, fine alignment of the images in the tilt series was performed in an iterative fashion. After the aligned stack was generated, backprojection methods were used to build a final tomogram. To reduce the data size, the final tomogram volume was trimmed to the section of the tomogram containing the MLA of interest. Models were generated using 3dmod. All model objects were created as open contours, except for the central vesicle, to allow for confident tracing of sections of bilayer density and to prevent the “closing” of vesicles where there was uncertainty regarding the presence of density.

4. GPMV Preparation, Imaging, and Quantification

~24 hours prior to transfection, cultured mammalian cells were plated so as to be 40-50% confluent at the time of transfection. Cells were transfected using FuGene Transfection Reagent with a FuGene:DNA ratio of 3:1 in OptiMEM. 6 cm^2 plates were transfected with 1.5 µg DNA. The transfection medium was removed from cells ~12-15 hours post-transfection and cells were washed with DPBS and fresh culture media was added to each plate. 36 hours after transfection, the medium was removed from cells and cells were washed three times with inactive GPMV buffer (10 mM HEPES, 150 mM NaCl, 2 mM $CaCl_2$ pH 7.4). Cells were consistently 70-80% confluent at the time of GPMV prep. Active GPMV buffer (GPMV buffer plus 2 mM DTT and 25 mM formaldehyde) was then added to the plates, and cells were incubated at 37° C with gentle shaking (70 RPM) for 90 minutes. DiIC12 or NBD-PE was then added to the plates from a stock solution of 0.5 mg/mL in EtOH to a final concentration of 0.5 µg/mL and cells were gently rocked at room temperature for 15 minutes. The GPMV-containing supernatant was then decanted into 1.5 mL Eppendorf tubes, and an anti-myc AF647 mAb was added to the solution (1:750 uL dilution) and gently agitated in the dark at room temperature for at least 3 hours. GPMVs were then allowed to settle in the dark to the bottom of the tube at 4°C for 2-24 hours (we observed no difference in GPMV quality whether we imaged immediately or at 24-hour post GPMV prep). 30 minutes prior to imaging, 270 µL of GPMV solution was pipetted from the bottom of the Eppendorf tube and sandwiched between 2 coverslips coated with 0.1% BSA and separated by a 0.5 mm thick silicone isolator.

GPMVs were imaged using a Zeiss LSM 510 confocal microscope using a 1.2 NA Zeiss Plan-Neofluor 40X objective. The confocal pinhole was set to 150 nm for all experiments. The fluorophores were excited using the 488 nm line of a 40 mW argon laser (NBD-PE, mEGFP, and AF-488), the 543 nm line of a HeNe laser (DiIC-12, propidium iodide), or the 633 nm line of a HeNe laser (AF-647). Images were collected at a 1X digital zoom for the case of miscibility temperature measurements and at 8-10X digital zoom for quantifying phase partitioning with a 512x512 pixel resolution. The stage was cooled using a Linkan Peltier Cooling system.

For quantification, GPMVs were labeled with either a disordered membrane phase marker (DiIC-12) or an ordered membrane phase marker (NBD-PE). PMP22-containing GPMVs were then labeled with anti-myc AF647-labeled antibodies. To determine the phase partitioning of PMP22, GPMVs were imaged in the green or red (NBD-PE or DiIC-12 respectively) and far-red channels, sequentially. To determine the phase partitioning

of tg-LAT, GPMVs were imaged in the green and red channels sequentially. Line scans across a single GPMV were performed in all channels using the ImageJ software to determine the fluorescent intensity at every pixel. The position of the line was set so that it intersected with both an ordered and disordered region of the GPMV using the DiIC12 or NBD-PE channels as the references. This same line was used to measure the intensity in the protein (PMP22 or tgLAT) channel. The line scans were smoothened using a moving average (10 pixels) in Microsoft Excel. Ordered phase domain partitioning, $P_{ordered}$ was then calculated as

$$P_{ordered} = \frac{I_{ordered}}{I_{ordered} + I_{disordered}}$$

where $I_{ordered}$ and $I_{disordered}$ are the fluorescence intensity of the protein channels in the ordered and disordered phases, respectively. Three independent lines were chosen for each GPMV and the mean $P_{ordered}$ was calculated and reported for individual GPMVs.

For measurements of miscibility temperature, 5x5 tile scans of GPMV samples were imaged at 1X digital zoom at temperatures ranging from 12.5° C to 32.5°C. Images were then randomized and GPMVs were blindly and manually classified as being either phase-separated or containing a single uniform phase. The fraction of vesicles that were phase separated at each temperature was then calculated. Plotting %-phase separated versus temperature yielded a curve that was fit to a sigmoidal function and the miscibility temperature (T_{Misc}) was defined as the temperature at which 50% of GPMVs were phase separated. Three independent biological experiments were performed and >100 GPMVs were imaged and classified for each temperature of each repeat. Classifications were performed blindly to the temperature at which the images were collected.

To calculate GPMV ordered domain size, images of GPMVs derived from cells transfected either with an empty or N41Q PMP22 pCDNA3.1 vector were collected in a high throughput manner on an ImageXpress Micro XL (Molecular Devices) using a 40X objective. MATLAB (MathWorks) was used to calculate the radius of each GPMV in pixels, and the percentage of GPMVs in the ordered phase using the DiIC12 dye to mark the disordered phase. The radius was converted from pixel to μm using the conversion factor of 0.34 μm:1 pixel for the 40X objective. The circumference of each GPMV was then calculated using the equation:

circumference=2π*radius, and ordered domain size was calculated by multiplying the fraction of each GPMV that was in the ordered phase by its circumference.

5. Quantification of PMP22 Palmitoylation

~24 hours after cells were transfected, cells were incubated overnight in media containing 100 μM 17-ODYA and a 1% final concentration of DMSO (or just DMSO for no 17-ODYA control). Cells were then incubated for 90 minutes with or without 2 mM DTT. Following incubation, cells were lysed for 1 hour at 4°C in 150 μL lysis buffer (50 mM Tris, 150 mM NaCl, 0.3% CHAPS, 0.1% SDS, pH 7.4). Lysates were cleared via centrifugation for 15 mins at 14,000xg. Protein concentrations were determined via Bradford assay and 75 μg total protein was added to 10 μL of anti-myc conjugated magnetic beads for each lysate. Volumes for each lysate were brought up to 150 μL total in lysis buffer and beads and lysates were incubated with end-over-end rotation at 4°C overnight. The following day, beads were washed three times with lysis buffer and bound proteins were eluted with 25 μL of elution buffer (50 mM HEPES, 150 mM NaCl, 2% SDS pH 7.0) and transferred to fresh tubes. The following was added to the eluents: biotin azide to a final concentration of 20 μM, TCEP to a final concentration of 1 μM, 20 μM TBTA, and 2 μM $CuSO_4$. Reactions were mixed at room temperature with end-over-end rotation for 2 hours before being quenched via the addition of EDTA to a final concentration of 1 mM. Samples were then split in two and analyzed via western blotting for PMP22 (1:8000 dilution of c-myc antibody) and biotin (1:1000 dilution of biotin antibody).

6. Flow Cytometry Trafficking Assay

Cells were plated ~24 hours prior to transfection so as to be ~ 50% confluent at the time of tranasfection. 6 cm^2 plates were transfected using the calcium phosphate technique with 1.5 μg DNA per plate. After ~18 hours the transfection media was then removed and the cells were allowed to grow in DMEM containing 10% FBS, penicillin, and streptomycin for an additional 24 hours. Transfected cells were trypsinized and prepared for FACS analysis using the Fix & Perm kit in accordance with the manufacturer's instructions. Briefly, half of the cells from a confluent 6 cm culture dish (ca. 1.6×10^6 cells) were suspended in 100 μL of culture media, and a PE-labeled monoclonal anti-myc antibody (clone 9E10) was added to the solution to a final concentration of 0.75 μg/mL to immunostain PMP22 on the surface of the cell. The cells were then incubated in the dark at

room temperature for 30 min. 100 µL of the fixation solution was then added to the media, and the cells were incubated for 15 min in the dark at room temperature. The cells were then rinsed and pelleted by centrifugation twice with 3 mL of PBS containing 5% FBS and 0.1% NaN3 (rinse solution). The cells were then suspended in 100 µL of the permeabilization solution, and an Alexa Fluor 647-labeled monoclonal anti-myc antibody (clone 9E10) was added to the solution to a final concentration of 0.75 µg/mL to label intracellular PMP22. After a 30 min incubation in the dark at room temperature, the cells were again rinsed and pelleted by centrifugation twice using rinse solution then resuspended in 300 µL of the rinse solution prior to FACS analysis.

Immunostained cells were analyzed with a FACS Canto II flow cytometer. Single cells were selected based their light scattering area and width profiles. 2500 transfected cells expressing PMP22 were analyzed from each sample by gating on GFP-positive cells (excited with a 488 nm laser, detected with 515–545 nm emission filter). The single-cell PE intensity (surface PMP22, excited with a 488 nm laser, detected with 564–606 nm emission filter) and Alexa Fluor 647 intensity (internal PMP22, excited with a 633 nm laser, detected with 650–670 nm emission filter) signals were corrected for nonspecific binding by subtracting the average intensities of untransfected, GFP-negative cells within each sample. To correct for the difference in the fluorescence intensity of the two antibodies, cells expressing WT PMP22 were stained with either the PE-labeled antibody or the Alexa Fluor 647-labeled antibody prior to FACS analysis, and the ratio of the average intensities of these cells was used to normalize the two signals. Single-cell trafficking efficiency values were then calculated from the ratio of the corrected PE signal of a given cell over the sum of its corrected Alexa Fluor 647 and PE signals. Average trafficking efficiency values calculated in this fashion were found to be similar to those determined by a comparison of the population-averaged intensities of intact (surface PMP22) and permeabilized (total PMP22) cells stained with the same concentration of the same fluorescently labeled antibody. Single-cell fluorescence intensity values below the background intensity were assigned an intensity of 0. Results were analyzed and visualized using FlowJo X software.

From titrations of both intact and permeable cells expressing WT PMP22 with fluorescently labeled antibodies, we found the average fluorescence intensity to be linearly dependent upon the antibody concentration. This confirms that fluorescence intensity values fall within the linear range of the detectors. Moreover, this ensures that the observed trafficking efficiency values are independent of the chosen antibody concentration. Compensation for spillover of the fluorescence signals between the channels utilized for the

analysis as well as the gates for the selection of single cells, GFP-positive cells, and GFP-negative cells was initially set manually but was kept consistent for the collection of all data sets obtained thereafter.

7. Co-Immunoprecipitation and Proteomic Analysis

~36 hours post-transfection, confluent 10 cm^2 plates were harvested via scraping in ice-cold PBS and pelleted via centrifugation. Cells were then lysed in lysis buffer (40 mM HEPES, 100 mM NaCl, 2 mM EDTA, 0.3% CHAPS, 10% glycerol, 1 mM PMSF, 1x HALT protease inhibitor, pH 7.8) for 20 minutes at 4°C with gentle rotation. Insoluble fractions were then removed via centrifugation and protein concentration determined via Bradford assay. 150 μg of total protein lysate was then mixed with 15 μL of anti-myc magnetic beads (Pierce) preequilibrated with lysis buffer and the volume brought up to 500 μL with TBS (25 mM Tris, 100 mM NaCl, pH 7.8). The mixture was then mixed with end-over-end rotation at 4°C for 90 minutes. Beads were then washed with 3x 250 μL volumes of TBS plus 0.25% Tween-20. Samples were then eluted with 2x 50 μL washes of elution buffer (50 mM Tris, 300 mM NaCl, 4% SDS, 2mM TCEP, 1 mM EDTA, pH 7.8) with beads vortexed and allowed to equilibrate with elution buffer for 15 min at 37°C for each wash.

Following elution, proteins were precipitated using chloroform/methanol extraction and protein pellets were allowed to air dry for 60 minutes at room temperature. Protein pellets were then resuspended in 50 μL 0.1% RapiGest SF. Disulfide bonds were reduced with 1 mM TCEP and free sulfhydryl groups acetylated with 1 mM iodoacetamide and samples were incubated for 30 minutes at room temperature in the dark. Samples were then digested with 0.5 ug trypsin overnight at 37°C under 700 rpm shaking. Samples were then labeled using 6-plex tandem mass tags (TMT; Thermo Scientific) according to the manufacturers protocol. TMT-labeled samples were then mixed and acidified with formic acid to a pH <2. Volume of the samples was then reduced to 1/6th the initial volume on a speed-vac and then adjusted back to the original volume with Buffer A (H_2O, 5% acetonitrile, 0.1% formic acid).

MudPIT microcolumns were prepared as previously described(*623*). Peptide samples were directly loaded onto the columns using a high-pressure chamber. Samples were then washed for 30 minutes with buffer A. LC-MS/MS analysis was performed using a Q-Exactive HF (Thermo Fisher) or Exploris480 (Thermo Fisher) mass spectrometer equipped with an Ultimate3000 RSLCnano system (Thermo Fisher). MudPIT experiments were performed with 10uL sequential injections of 0, 10, 30, 60, 545 and 100% buffer C (500mM

ammonium acetate in buffer A), followed by a final injection of 90% buffer C with 10% buffer B (99.9% acetonitrile, 0.1% formic acid v/v) and each step followed by a 130 minute gradient from 5% to 80% B with a flow rate of either 300 or 500nL/minute on a 20cm fused silica microcapillary column (ID 100 um) ending with a laser-pulled tip filled with Aqua C18, 3um, 100 Å resin (Phenomenex). Electrospray ionization (ESI) was performed directly from the analytical column by applying a voltage of 2.0 or 2.2kV with an inlet capillary temperature of 275°C. Using the Q-Exactive HF, data-dependent acquisition of mass spectra was carried out by performing a full scan from 300-1800 m/z with a resolution of 60,000. The top 15 peaks for each full scan were fragmented by HCD using normalized collision energy of 35 or 38, 0.7 m/z isolation window, 120 ms maximum injection time, at a resolution of 15,000 scanned from 100 to 1800 m/z and dynamic exclusion set to 60s. Using the Exploris480, data-dependent acquisition of mass spectra was carried out by performing a full scan from 400-1600m/z at a resolution of 120,000.

Top-speed data acquisition was used for acquiring MS/MS spectra using a cycle time of 3 seconds, with a normalized collision energy of 36, 0.4m/z isolation window, 120ms maximum injection time, at a resolution of 30000 with the first mass (m/z) starting at 110. Peptide identification and TMT-based protein quantification was carried out using Proteome Discoverer 2.3 or 2.4. MS/MS spectra were extracted from Thermo Xcalibur .raw file format and searched using SEQUEST against a Uniprot human proteome database (released 05/2014). The database was curated to remove redundant protein and splice-isoforms, and supplemented with common biological MS contaminants. Searches were carried out using a decoy database of reversed peptide sequences and the following parameters: 10ppm peptide precursor tolerance, 0.02 Da fragment mass tolerance, minimum peptide length of 6 amino acids, trypsin cleavage with a maximum of two missed cleavages, dynamic methionine modification of 15.995 Da (oxidation), static cysteine modification of 57.0215 Da (carbamidomethylation), and static N-terminal and lysine modifications of 229.1629 Da (TMT sixplex). SEQUEST search results were filtered using Percolator to minimize the peptide false discovery rate to 1% and a minimum of two peptides per protein identification. TMT reporter ion intensities were quantified using the Reporter Ion Quantification processing node in Proteome 575 Discoverer 2.3 or 2.4 and summed for peptides belonging to the same protein.

8. Generation of CRISPR KO Cell Lines

CRISPR technology was utilized to generate genetic KO cells as previously described(*624*). gRNAs were designed to target early exons of the CNX, Rer1, UGGT1, and LMAN1. gRNA oligomers (gRNA sequences shown in **Supplemental Table 2**) were annealed, phosphorylated, and ligated into digested pspCas9(BB)-2A-puro plasmid (plasmid no. 62988, Addgene, Cambridge, MA). HEK293 cells were suspended in 2 ml of DMEM supplemented with 10% FBS and plated in 6-well plates. The following day, 5 µg of each plasmid was combined with 10 µl Lipofectamine 2000 reagent (Invitrogen) in 1 ml Opti-MEM and incubated at room temperature for 30 min. Culture medium was replaced with the appropriate plasmid-lipofectamine solution, and cells were incubated at 37°C for 24 h. The medium was then replaced with fresh DMEM plus 10% FBS, and cells were allowed to recover for 24 h at 37°C prior to the addition of 0.75 µg/ml puromycin. Cells were incubated at 37°C for 48 h before replacing the medium. After recovering for ~1–2 weeks, cells were pelleted, resuspended in sorting buffer (PBS + 4% FBS), and strained to separate clumps of cells. Solutions were sorted by flow cytometry using a 5-laser BD LSRII with a 100 µm nozzle at the Vanderbilt Medical Center Flow Cytometry Core to isolate single cell cultures in 96-well plates for each cell line. Clones were incubated until they reached ~70% confluency and then passaged until enough cells could be harvested for KO validation via Western blotting.

Chapter III. PMP22 Alters Membrane Ultrastructure

Chapter III was adapted with permission from one of my previously published journal articles. (*625*)

1. Introduction

PMP22 has important but poorly understood roles in peripheral nervous system (PNS) myelin. Myelin provides the insulating sheath to axons that serves to facilitate rapid conduction of electric impulses (*626*). In the PNS, compact myelin is formed when membrane tongues extend from myelinating Schwann cells to spirally wrap around an adjacent axon. The appropriate structural organization of myelin membranes is critical for proper nerve conduction.

PNS compact myelin membranes are composed of specific lipid and protein components that are essential to its function (*626*). The lipid bilayers of compact myelin contain high concentrations of cholesterol and sphingolipids. Proteins found in PNS compact myelin include myelin protein zero (MPZ), PMP22, and myelin basic protein (MBP) (*627*). While the striking ultrastructure of myelin has been studied for many decades using various forms of imaging and scattering techniques (*628-631*), the molecular mechanism(s) responsible for the formation and maintenance of this complex membrane assembly are still being investigated.

PMP22 is a tetraspan helical integral membrane protein that is highly expressed (2-5% by weight of myelin proteins) in myelinating Schwann cells (*601*). Regulated expression and proper folding of PMP22 is essential for the development and maintenance of normal myelin in Schwann cells (*601, 632, 633*). A spectrum of heritable peripheral neuropathies is associated with aberrations in the *PMP22* gene. These disorders include the most common inherited peripheral neuropathy Charcot-Marie-Tooth disease type-1A (CMT1A) that occurs with trisomy of PMP22 (*634*) and results in overproduction of the protein. Hereditary neuropathy with liability to pressure palsies (HNPP), with a heterozygous deletion of *PMP22,* results in underexpression of the protein. CMT1E is caused by missense mutations of *PMP22* that alter the protein amino acid sequence. Collectively, these defects affect 1 out of 2500 individuals (*635-642*). Nerve biopsies from CMT1A patients show that the proliferative Schwann cells around axons resemble “onion bulbs” (*643*). Loss of one of the two *PMP22* alleles results in HNPP, in which PNS myelin has characteristic “sausage-shape swellings that appear to be caused

by abnormal membrane organization and/or myelin decompaction" (*644, 645*). Other disorders of widely varying severity are caused by dominant heterozygous *PMP22* missense mutations (CMT1E) including the "trembler-J" (*TrJ*) L16P mutation of PMP22, which leads to abnormal interactions between the myelin sheath and the axon, abnormally thin myelin, and aberrant myelin wrapping (*646*). The connection between disease phenotypes and abnormal copy number or missense mutations in *PMP22* highlights the importance of this membrane protein in myelin function.

Amino acid changes encoded by missense mutations disrupt the trafficking of PMP22 to the plasma membrane by increasing the propensity of the protein to misfold, resulting in targeting by the endoplasmic reticulum-associated degradation (ERAD) system for disposal (*1, 401, 531, 647-651*). However, degradation of misfolded PMP22 is likely not 100% efficient (*528, 530, 649, 652, 653*). Thus, the severity of the phenotypes caused by PMP22 point mutations are postulated to result from a combined loss of functional PMP22 at the plasma membrane and cellular stress induced by misfolded protein. Additionally, some PMP22 disease mutants do reach the plasma membrane (*1*), suggesting that these mutants could directly disrupt or alter PMP22 functions in myelin membranes. Importantly, all disease phenotypes resulting from PMP22 mutations lead to dysmyelination and axonal loss (*601, 635*).

Although PMP22 clearly plays an essential role in myelinating Schwann cells, the biochemical function(s) of PMP22 are not well characterized. In this chapter, I show that PMP22 reconstituted into model lipid bilayers causes the formation of protein-lipid superstructures that exhibit morphological similarities to compact myelin. These results reveal that PMP22 has an intrinsic capacity to promote the organization of membrane ultrastructure. This is the first biochemical evidence that isolated PMP22 can organize membranes and provides mechanistic insight into the function of PMP22 in PNS myelin.

2. Results

2.1 PMP22 forms myelin-like assemblies when reconstituted into lipid bilayers

In an attempt to determine the structure of PMP22, we began crystallization trials to generate two-dimensional (2D) crystals. PMP22 was reconstituted into vesicles composed of 1-palmitoyl-2-oleoyl-sn-glycero-3-phosphocholine:egg sphingomyelin (POPC:ESM; 4:1 molar ratio) at a lipid-to-protein ratio (LPR) of 1.0 (w:w) via dialysis to remove the detergent β-*n*-decylmaltoside (DM) present in the starting PMP22-containing

detergent/lipid mixed micelles (~4 mol% PMP22 relative to total moles of lipid). Although this procedure did not result in the formation of single layered 2D crystals, analysis by negative stain electron microscopy revealed there were easily-visualized lipid-protein assemblies that are distinctly multi-layered (**Fig. 21 A-C**). This indicates that the layer edges of these structures are exposed to bulk solvent, where they are accessible to stain. These assemblies appear to share several structural traits with PNS myelin (see Discussion), and are strikingly similar to intermediate assemblies observing the formation of myelin in calanoid copeopods, invertebrate planktonic crustaceans—see figures 4, 6, and 9 in Wilson and Hartline (*654*). We therefore refer to the PMP22-lipids superstructures as “myelin-like assemblies” (MLAs). MLAs were never observed in control reconstitutions carried out in the absence of PMP22 (**Fig. 21D and E**) or in reconstitutions using an unrelated tetraspan membrane protein, the voltage sensor domain of the human KCNQ1 potassium channel (Q1-VSD) (**Fig. 21F**). MLAs were not observed to form when a similar membrane reconstitution was applied to PMP22 using the lipids 1-pamitoyl-2-oleoylphosphatidylcholine (POPC), dipalmitoylphosphatidylcholine (DPPC), 6:1 POPC:1-pamitoyl-2-oleoylphophatidylglycerol (POPG), or 6:1 DPPC: dipalmitoylphosphatidylglycerol (DPPG). No MLAs were found in PMP22 reconstitutions using either total or polar brain lipids.

While MLAs were seen only in 4:1 POPC:ESM lipid reconstitutions that contained PMP22, other types of assemblies, including vesicles, clustered vesicles, and protein aggregation, were also observed in MLA-containing samples. To more carefully characterize the protein/lipid reconstitutions, we quantified the objects seen on the negative stain EM grids. These were classified as MLAs, disordered MLAs (MLA-like assemblies composed of disorganized and/or "frayed" layers), vesicles, clumped vesicles (vesicles so close together they could not be individually counted), and aggregates that may be composed of protein, lipids, or a combination of protein and lipids (**Fig. 21G**). In all reconstitution experiments carried out with PMP22 present, vesicles were always the most commonly observed objects, followed by MLAs. Several other less common morphological classes of assemblies including disordered MLAs, clumped vesicles, and aggregates were also sometimes observed. The vesicles formed in PMP22-lipid reconstitutions and lipid-only reconstitutions were of similar appearance and size in negative stain EM.

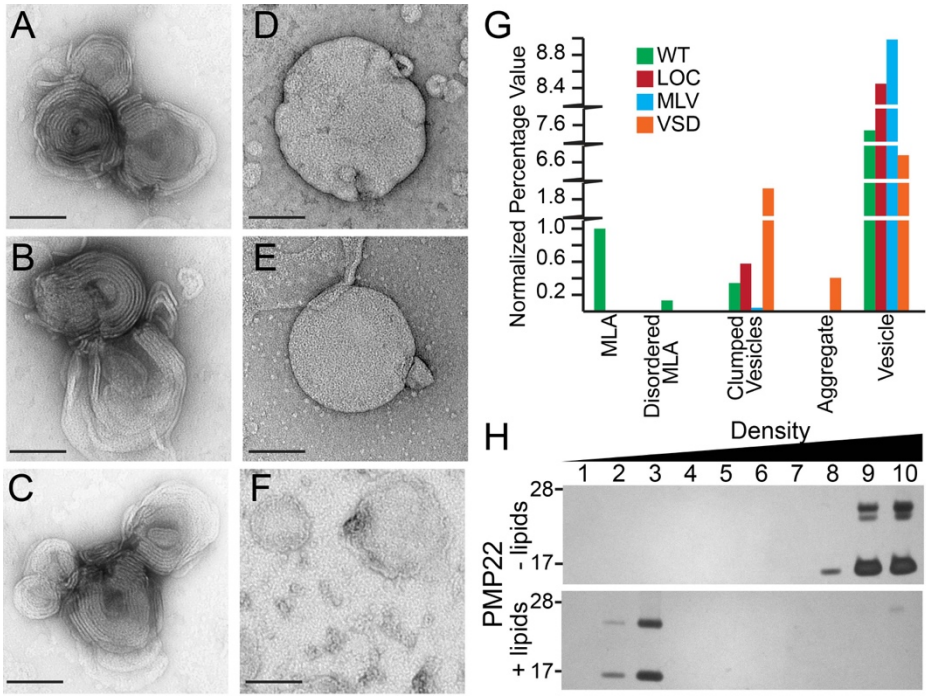

Figure 21. PMP22 forms ordered assemblies upon reconstitution into lipid vesicles.

(A-C) Examples of protein-lipid myelin-like assemblies (MLAs) created when PMP22 is reconstituted into 4:1 POPC:ESM vesicles via the dialysis method and visualized by negative stain EM; **(D)** Representative image of multilamellar vesicles (MLVs) prepared in the absence of protein via the dialysis method (LOC, lipid-only control); **(E)** MLVs prepared by spontaneous bilayer formation through hydration of lipids with water; **(F)** Control assemblies containing 4:1 POPC:ESM and the tetraspan voltage sensor domain (VSD) of KCNQ1 reconstituted via the dialysis method. Scale bar for all panels, 100 nm. **(G)** Quantification of the relative percentage of MLAs present in a series of negative stain EM images of WT PMP22, lipid-only control (LOC), multilamellar vesicles (MLVs), and the tetraspan VSD domain of KCNQ1. All individual object counts were converted to percentage of total counts for a particular sample and were normalized to the percentage of total counts represented by MLAs in the WT PMP22 control, which was set to 1.0. Green = WT, Red = LOC, Blue = MLV, Orange = VSD. **(H)** Sucrose gradient analysis of PMP22 reconstituted for 10 days without (-, top) or with (+, bottom) lipids. Fractions were collected from top (low density) to bottom (high density) and analyzed by SDS-PAGE with silver staining.

To ensure that PMP22 is found in the lipid assemblies we conducted a membrane flotation assay. PMP22 was subjected to the usual reconstitution method, both with 4:1 POPC:ESM and, in parallel, in the complete absence of lipids. The results mixtures were the loaded at the bottom of a step-wise sucrose

gradient, and centrifuged (**Fig. 21H**). PMP22 “reconstituted” without lipids remains pelleted in the high density sucrose fractions, most likely as aggregated protein, (**Fig. 21H,** top), while PMP22 reconstituted with lipids floats into the lower density sucrose fractions, indicating that PMP22 is both stable during the reconstitution assay and is incorporated in the membrane assemblies (**Fig. 21H,** bottom).

2.2 Cryo-electron microscopy (cryo-EM) of PMP22-containing MLAs

To confirm that MLAs are not an artifact of the negative staining protocol and to gain further insight into MLA ultrastructure, we vitrified PMP22 and control lipid reconstitutions and examined them using cryo-EM. Visualizing the protein-free lipid reconstitutions in vitrified ice showed that multilamellar vesicles (MLVs) were the predominant assemblies formed by these reconstitutions (**Figs. 22A and B**), while MLAs were never observed. However, when the product mixtures of PMP22-lipid reconstitutions were visualized by cryo-EM, we observed the presence of both MLAs and MLVs. The MLAs had similar architectures as observed in negative stain (**Figs. 22C and D**). These appear to be compressed vesicles that stack and wrap around each other. Analyzing three independent MLA preparations frozen in vitrified ice we measured an average interperiod line distance of 153 ± 7 Å. The average interperiod line distance for MLVs was 181 ± 7 Å. The average interperiod line distance of the MLAs is smaller than the repeat pattern of ~177-185 Å measured in neutron and X-ray diffraction studies of intact mammalian peripheral nerves which would be expected due to the presence of other membrane proteins *in vivo* myelin (*630, 655-657*); however, our measured repeat is similar to the 160–166 Å repeat pattern reported for mammalian central nervous system (CNS) compact myelin (*657*). Cryo-EM analysis thereby confirms that PMP22 can drive the formation of lipid-protein structures with complex architectures that are morphologically different from the nested MLVs seen in lipid-only reconstitutions.

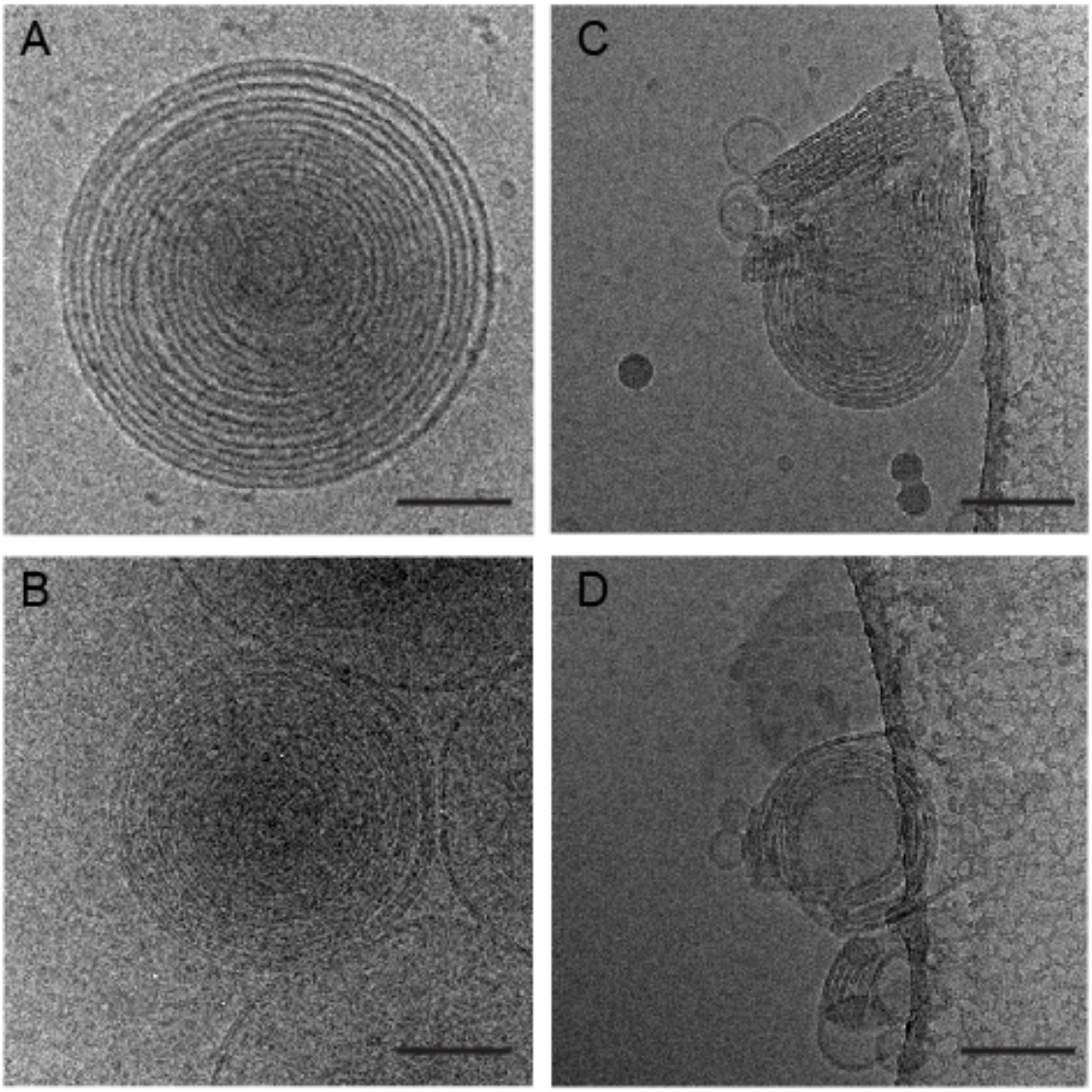

Figure 22. Differences between MLVs and MLAs are visible by cryo-EM

(A-B) Representative images of vitrified MLVs prepared in the absence of protein via the dialysis method **(A)** or by spontaneous bilayer formation through hydration of lipids-only with water **(B)**. **(C-D)** Examples of MLAs created when PMP22 is reconstituted into 4:1 POPC:ESM vesicles via the dialysis method and visualized using cryo-EM. Scale bar for all panels, 100 nm.

2.3 Tomography shows that MLAs are flattened, stacked, and wrapped vesicles

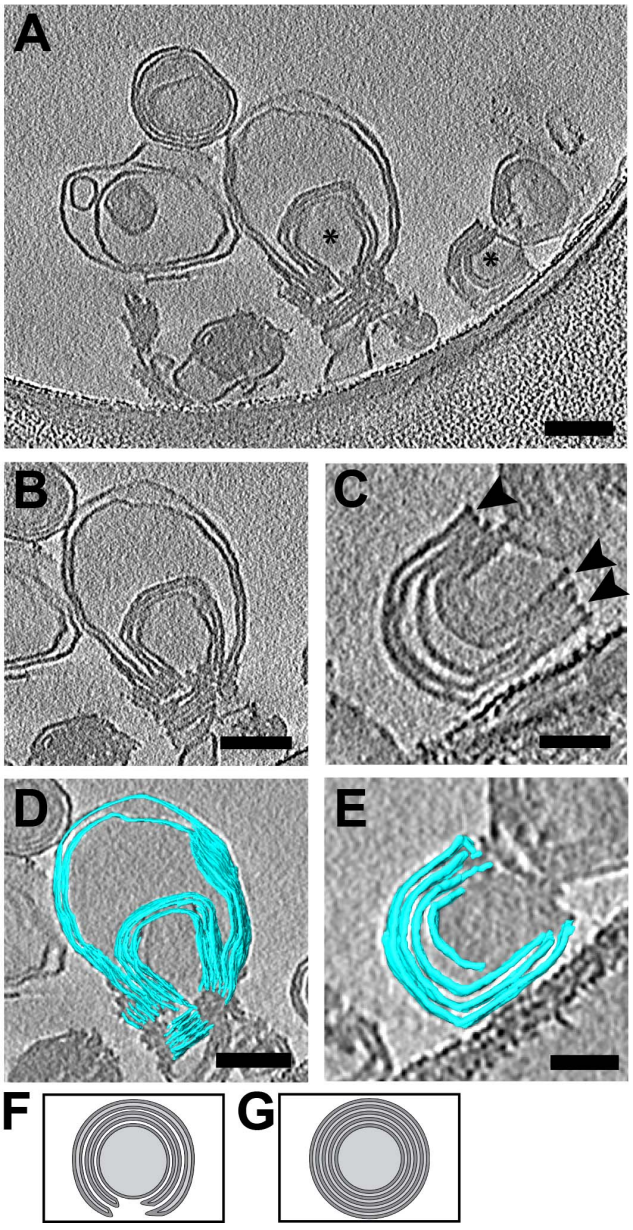

Figure 23. MLAs examined by cryo-ET.

(A) Representative tomographic slices (1.47 nm) of two MLAs. *, marks MLAs in image. **(B-C)** Two MLAs from A. Arrowheads indicate the ends of MLA. **(D-E)** Segmentation view of the corresponding MLA from B and C. Scale bars are 100 nm (A, B, and D) and 50 nm (C and E). **(F)** Model demonstrating the compressed, wrapped membranes of a MLA and **(G)** model demonstrating the nesting vesicles of MLVs.

While the negative-stain and cryo-electron microscopy experiments indicate that MLAs are distinct from multilamellar vesicles, a number of non-mutually exclusive morphological possibilities remain for how MLAs are organized. For example, MLAs could be a single, compressed spiraled vesicle similar to myelin, a series of compressed and wrapped single unilamellar vesicles, and/or spiraling sheets of lipid bilayers. To more closely examine the morphology of MLAs, we used cryo-electron tomography (cryo-ET). We generated tomograms (**Figs. 23 A-C**) of PMP22-induced MLAs that allowed for the construction of a 3D model by segmenting the density in each z-slice (**Figs. 23D and F**). These 3D reconstructions indicate that the examined MLAs are distinct from the architecture of MLVs and are composed of compressed, stacked, and wrapped unilamellar vesicles (**Fig. 23F**) and not nested vesicles (**Fig. 23G**). The 3D morphology of the MLAs, although not an exact recapitulation of the compressed and spiraling membranes found in Schwann cell-generated myelin, demonstrates that PMP22 can induce the flattening and wrapping of the vesicles into horseshoe shaped stacks. These results also confirm that MLAs closely resemble superstructures observed as intermediates in the process of myelin formation in calanoid copepods (*654*). The above results shown that PMP22 can directly alter membrane organization, *in vitro.*

2.4 Formation of MLAs depends on the ratio of PMP22 to lipids

The most common type of CMTD, CMT1A, is caused by the presence of a third wild type allele of PMP22 (*634*), resulting in a higher level of PMP22 than in healthy conditions. Nerve biopsies from CMT1A patients show that Schwann cells proliferate around axons without properly generating myelin, resembling "onion bulbs" (*643*). On the other hand, the presence of only a single *PMP22* allele results in a different phenotype, called HNPP, in which PNS myelin has abnormal thickening and swelling of the myelin sheath; the myelin defects observed in HNPP appear to be caused by increased lamellae due to abnormal membrane organization around the lateral segment of internode (*644, 645*). Taken together, these heritable conditions demonstrate that proper levels of PMP22 in Schwann cells are critical for proper myelin formation *in vivo* (*626, 632, 635, 658, 659*)

To determine whether MLA formation *in vitro* is also sensitive to PMP22 concentration, a series of PMP22 reconstitution assays were performed using a range of concentrations. LPRs ranged from 0.5 to 10 (w/w), spanning ~13 (8 mol% at LPR = 0.5) to ~256 (0.4 mol% at LPR = 10) lipid molecules per PMP22 in each reconstitution mixture. The highest percentage of MLAs, 17 ± 5%, were found at an LPR of 1.0, where there are ~26 lipid molecules per PMP22 (4 mol% protein) in the reconstitution assay (**Figs. 24C,D and G**). At the lowest LPR of 0.5, where there are only ~13 lipid molecules per PMP22 in the reconstitution mixture (*i.e.,* the highest concentration of PMP22), well-organized MLAs were difficult to find. Instead, the sample contained a significant increase in the number of *disordered* MLAs, where the lipid bilayers are not tightly adhered and

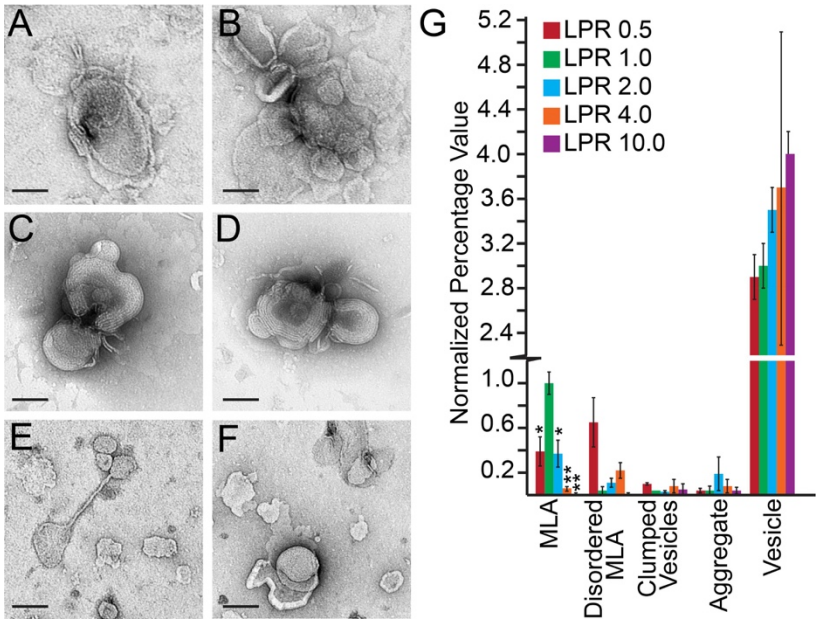

Figure 24. Altered PMP22 lipid-to-protein ratios disrupt MLA formation

Representative negative stain images of PMP22 reconstitution assays carried out at lipid-to-protein ratios (LPR (w/w)) of 0.5 **(A and B)**, 1.0 **(C and D)**, and 10.0 **(E and F)**. Scale bar for all panels, 100 nm. **(G)** Quantification of the relative percentage of MLAs present in a series of negative stain EM images of WT PMP22 reconstitutions at LPRs (w/w) of 0.5, 1.0. 2.0, 4.0, and 10.0. *All individual object counts were converted to percentage of total counts for a particular sample and were normalized to the percentage of counts represented by MLAs in the LPR 1.0 sample, which was set to 1.0. Red = LPR 0.5, Green = LPR 1.0, Blue = LPR 2.0, Orange = LPR 4.0, Purple = LPR 10.0. Error bars represent standard error of the mean (S.E.M.) between biological replicates. * = $p<0.05$, ** = $p<0.01$. Statistical significance is only indicated for MLAs.

have a more frayed appearance (**Figs. 24A, B, and G**). These results demonstrate that higher concentrations of PMP22 in the membrane (that is, lower LPRs) do not lead to the formation of more MLAs, but rather a higher incidence of disordered MLAs.

Successively lowering the amount of PMP22 in the reconstitutions from an LPR of 1.0 to higher LPRs led to progressively fewer MLAs. At an LPR of 2.0 (~51 lipid molecules per PMP22), we found a MLA prevalence of only 0.6 relative to reconstitutions at an LPR of 1.0. At an LPR of 4.0 (~102 lipid molecules per PMP22 in the reconstitution assay) the MLA prevalence was further reduced to 0.1 relative to reconstitutions done at an LPR of 1.0. At an LPR of 10, no MLAs were observed although a small number of disordered MLAs that do not contain tightly condensed layers were still seen in the images (**Figs. 24E-G**). These studies confirm that PMP22 is responsible for MLA formation. Too little PMP22 leads to fewer MLAs, while too much PMP22 in the reconstitution assay increases the formation of disordered MLAs. While the size and shape of the MLAs did not change as a function of the LPR, we did notice more clumped vesicles at LPRs of 0.5 and 4.0. This suggests that PMP22 found in vesicles that do not form MLAs may be able to participate in *trans*-homophilic interactions that can cause vesicles to stick together. These results confirm a role for PMP22 in MLA formation and are reminiscent of *in vivo* findings that the proper level of PMP22 is important for the correct initiation and formation of myelin (*632, 633, 659, 660*). However, it should be noted that the LPR of individual MLAs may deviate from the bulk LPR used in the reconstitution process.

2.5 Removal of cysteine residues does not abrogate MLA formation

To explore which regions of PMP22 are required for MLA formation, we performed structure-function studies. We first tested whether disulfide bond formation in PMP22 might be related to MLA formation. PMP22 contains four native cysteine residues. Two of these residues are found in the extracellular loop and, based on homology between PMP22 and claudin-15, are predicted to form an intramolecular disulfide cross-link (*608*). We simultaneously mutated all four cysteine residues creating a “Cys-less” PMP22 (C42S C53S C85A C109A PMP22) (**Figs. 25A and B**) and purified it alongside wild type (WT) PMP22. No significant differences were found between the ability of Cys-less and WT PMP22 to form MLAs (**Figs. 25A-C**). From these data we conclude that the formation of disulfide bonds are not required for MLA formation.

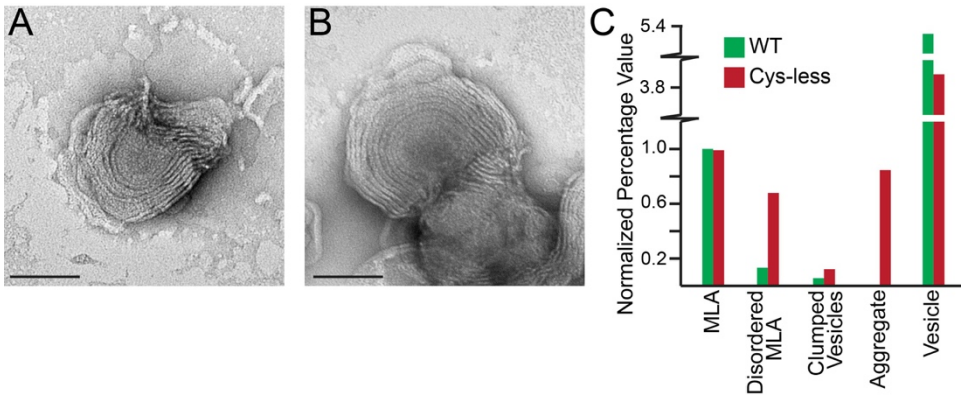

Figure 25. MLA formation is not dependent upon intermolecular disulfide linkage

(A and B) Representative negative stain images of MLAs formed in a reconstitution assay using a Cys-less PMP22 mutant (PMP22 C42S, C53S, C85A, C109A). Scale bar for both panels, 100 nm. **(C)** Quantification of the percentage of MLAs present in a series of negative stain EM images of WT and Cys-less PMP22 reconstitutions. *All individual object counts were converted to percentage of total counts for a particular sample and were normalized to the percentage of total counts represented by MLAs in the WT PMP22 control, which was set to 1.0. Green = WT control and Red = Cys-less PMP22.

2.6 PMP22 extracellular loops are important for MLA formation

A previous study using GST-fusion oligopeptides of PMP22 showed that its extracellular loops 1 and 2 (ECL1 and ECL2) could support both *trans*-homophilic interactions as well as *trans*-heterophilic interactions with myelin protein zero (MPZ) (*661*). To test the importance of ECL1 and ECL2 for MLA formation we expressed and purified GST-ECL1 and GST-ECL2 fusion proteins to use as a source of competitive binding in order to weaken any potential *trans*-homophilic loop interactions that form within the MLAs. We then also verified that GST alone did not reduce MLA formation by including GST at the same molar ratios in the PMP22-lipid reconstitution assay. When GST-ECL1 was included in PMP22 reconstitution assays at a 1:1 or a 4:1 molar ratio (GST-ECL1:PMP22), MLA formation was reduced by 50% and 40% respectively, compared to reconstitutions containing PMP22 alone (**Fig. 26A**). Addition of GST-ECL2 to the PMP22-lipid reconstitutions at a ratio of 1:1 (GST-ECL2:PMP22) reduced MLA formation by 60%, while a GST-ECL2 to PMP22 ratio of 4:1 led to a 98% reduction. Reconstitution of GST, GST-ECL1, and GST-ECL2 alone (*i.e.* without PMP22 present)

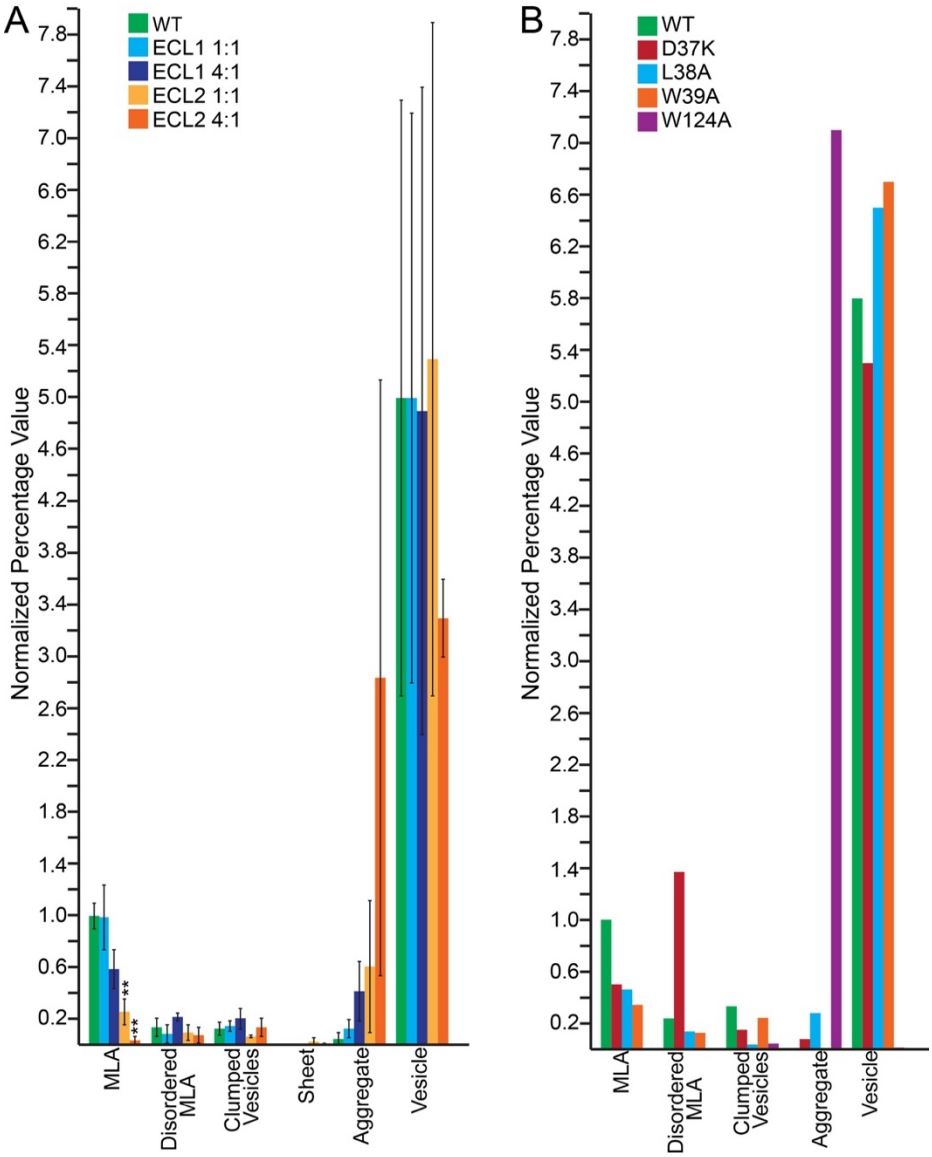

Figure 26. ECL1 and ECL2 are important for MLA formation

(A) Quantification of the relative percentage of MLAs present in a series of negative stain EM images of PMP22 reconstitutions of WT PMP22 only, WT PMP22 incubated with GST-ECL1, and WT PMP22 incubated with GST-ECL2. Green = WT control, Light Blue = GST-ECL1 + WT PMP22 (1:1 molar ratio), Dark Blue = GST-ECL1 + WT PMP22 (4:1 molar ratio), Light Orange = GST-ECL2 + WT PMP22 (1:1 molar ratio), Dark Orange = GST-ECL2 + WT PMP22 (4:1 molar ratio). Error bars represent S.E.M. between biological replicates. * = $p<0.05$, ** = $p<0.01$. Statistical significance is only indicated for MLAs. **(B)** Quantification of the relative percentage of MLAs present in a series of negative stain EM images of PMP22 reconstitutions of WT PMP22, ECL1 loop-mutants PMP22 D37K, L38A, or W39A, and ECL2 loop-mutant PMP22 W124A. Green = WT control, Red = D37K, Blue = L38A, Orange = W39A, and Purple = W124A. *For both panels: All individual object counts were converted to percentage of total counts for a particular sample and were normalized to the percentage of total counts represented by MLAs in the WT PMP22 control. All values were normalized to the percentage of WT control MLAs, which was set to 1.0.

did not lead to the formation of MLAs. The fact that high concentrations of both GST-ECL1 and GST-ECL2 reduced MLA formation suggests that both loops are important for the *in vitro* function of PMP22.

As another way to assess the roles of ECL1 and ECL2 in MLA formation, we prepared and purified PMP22 with mutations in either ECL1 or ECL2. PMP22 shares ~25% sequence identity with the claudins, including a claudin motif in ECL1 (*608*). In ECL1 individual residues from this motif were mutated (D37K, L38A, and W39A). Also, in ELC2 the highly conserved tryptophan residue (W124) was changed to alanine. The three PMP22 ECL1 mutants disrupted MLA formation relative to a PMP22 WT control by 50%, 50%, and 70%, respectively (**Fig. 26B**). However, the PMP22 W124A mutation in ECL2 was especially deleterious, completely disrupting MLA formation (**Fig. 26B**). These results confirm that PMP22's extracellular loops contribute to MLA formation, with ECL2 possibly having a more dominant role. However, it must be frankly acknowledged that these

experiments may not be the final word on the roles of ECL1 and ECL2 in MLA formation because they employed recombinant protein in which PMP22 was not natively N-glycosylated at Asn41 located in ECL1 (*662*). Nevertheless, the above results make it very clear that the extracellular loops of PMP22 play a critical role in MLA formation.

2.7 The L16P (Trembler-J) disease mutation of PMP22 disrupts MLA formation

The L16P "Trembler-J" (TrJ) mutation located in the first transmembrane domain (TM1) of PMP22 causes severe dysmyelinating neuropathy in both humans and mice (*601, 663, 664*). This mutation leads to abnormal differentiation of Schwann cells, which are arrested at the immature pre-myelination stage. As a consequence, interactions between the myelin sheath and the axon are disrupted, resulting in thin myelin. Additionally the excessive immature Schwann cells surrounding axons fail to form compact myelin (*646*). Biophysical studies have shown that the L16P mutation disrupts the structural organization of the TM1 domain, reducing the thermodynamic stability of PMP22 (*665*), with the majority of the mutant protein adopting a partially folded state (*608, 647, 665*). To test the effect of the L16P mutation on MLA formation, L16P PMP22 was purified and used in lipid reconstitution assays. Reconstitutions using this mutant yielded fewer MLAs compared to the WT control (**Fig. 27A**). The MLAs observed in the L16P PMP22 reconstitutions were composed of loosely-packed layered assemblies that appear more disorganized than the MLAs created by wild-type PMP22 (**Figs. 27B and C**).

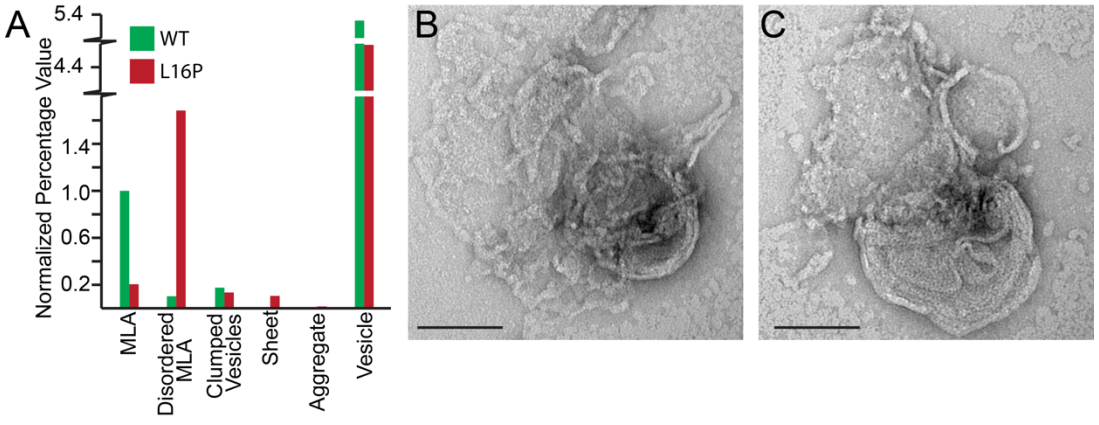

Figure 27. The L16P PMP22 (TremblerJ) mutation disrupts MLA formation.

(A) Quantification of the relative percentage of MLAs present in a series of negative stain EM images in both WT and L16P PMP22 reconstituted on the same day. *All individual object counts were converted to percentage of total counts for a particular sample and were normalized to the percentage of total counts represented by MLAs in the WT PMP22 control, which was set to 1.0. Green = WT control, Red = L16P. **(B and C)** Representative negative stain EM images of the disordered MLAs found in L16P PMP22 reconstitutions. Scale bar for both panels, 100 nm.

3. Discussion

3.1 Similarity of MLAs to PNS Myelin and Related Membrane Assemblies

PMP22 clearly has one or more essential roles in myelinating Schwann cells as reflected by its central role in common forms of Charcot-Marie-Tooth and related dysmyelinating disorders (*601, 635*). However, the biochemical functions of PMP22 are not understood. Using *in vitro* reconstitution assays, we showed that PMP22 drives the formation of complex lipid-protein superstructures composed of compressed and stacked membranes that wrap around a central vesicle. The formation of these structures is absolutely dependent on the presence of PMP22 and can be disrupted by varying PMP22 concentration, by introducing a disease mutation, by including GST-ECL1 or GST-ECL2 fusion peptides during membrane reconstitution, or by mutating residues in ECL1 and ECL2.

The organization of MLAs shares common traits with PNS myelin. Both MLAs and myelin include membrane compaction. For MLAs the vesicles are flattened, while for PNS myelin the bilayers that enclose the cytosol of a tongue-like membrane extension of a Schwann cell are drawn together to render the extension similar to double-layered tape. The flattened double bilayers of both MLAs and developing myelin are then multilayered—in the case of MLAs by stacking the flattened vesicles; in the case of myelin by spirally wrapping the flattened double bilayers around a cylindrical segment of an axon similar to wrapping tape around a spool. MLAs seem also to usually wrap around a central cylindrical vesicle, although the stacked and flattened vesicles wrap collectively and only a single time—no spiraling. While there remain clear differences between the supramolecular organization of MLAs and myelin, it is notable that the inclusion of a single myelin protein in reconstituted lipid bilayers is capable of altering the organization of resulting membrane assemblies so as to confer several traits that resemble key features of the organization of PNS myelin. There is a previous report showing that myelin basic protein (MBP) in aqueous DPC suspensions can alter the organization of detergent into regions of parallel arrays (*666*). Thus, it seems likely that multiple myelin proteins have important structural roles in establishing myelin architecture. However, since MBP is not a transmembrane protein, its potential effect on myelin membrane organization is likely via a distinct mechanism than PMP22. Considering the importance of myelin ultrastructure in nerve conductance, it is not surprising that cells have developed multiple robust and, perhaps independent, ways to ensure the proper organization of myelin membranes.

MLAs are even more strikingly similar to membrane assemblies thought to represent intermediate structures on the pathway to myelin development in certain marine copepods. Myelin in copepods can be regarded as an early evolutionary alternative form of vertebrate myelin and is generated directly by axons rather than by glial cells. As seen in figures 4, 6, and 9 of (*654*), developing copepod myelin includes assemblies that are composed of flattened vesicles/cisternae that are stacked and non-spirally wrapped that closely resemble MLAs. It is known that copepods (like all invertebrates (*667*)) lack myelin protein 0 (MPZ), the major adhesive protein of vertebrate PNS myelin (*668*). Whether myelin-forming copepods have a PMP22 homolog is not yet established, but seems feasible given that even *C. elegans* has a distant relative of PMP22 (*669*). Whether or not a PMP22 homolog is involved in copepod myelin formation, the fact that purified PMP22 can induce the formation of membrane assemblies that closely resemble a known intermediate structure in copepod myelin supports the likely mechanistic linkage between PMP22's ability to modify membrane structure and its roles in PNS myelin.

PMP22-containing MLAs also resemble assemblies termed "intracellular myelin-like figures" (IMLFs) that form in Schwann and HEK-293 cells upon expression of PMP22 (*401, 670*). IMLFs are comprised of multilayered "whorls" of spiraled membrane that form when overexpressed PMP22 fails to traffic to the cell surface and accumulates in the endoplasmic reticulum (ER). The similarity of MLAs and IMLFs further supports the notion that PMP22 has an intrinsic ability to both flatten membrane double layers and promote stacking of these layers.

3.2 Adhesive function of PMP22 in MLA formation and stabilization

Our results indicate that the extracellular ECL1 and ECL2 loops of PMP22 have an important role in MLA formation. This result is reminiscent of studies involving PMP22 expressed in HeLa cells that showed the protein can participate in *trans*-homophilic interactions to form an adhesive PMP22 bridge between cells (*661*) and that these interactions can be disrupted by adding ECL1 peptide as a GST fusion protein to the milieu surrounding the cells. Additional evidence for PMP22 playing a role in adhesion between lipid bilayers includes studies showing expression of PMP22 in certain epithelia, where it appears to be involved in forming and/or stabilizing membrane junctions (*671-674*). Both the present and past studies support a direct role for PMP22 in bilayer-bilayer adhesion.

While we have not yet directly observed the spatial distribution of PMP22 in MLAs, the properties of MLAs are consistent with stabilization of *trans*-homophilic interactions by the extracellular loops of PMP22, both inside the flattened vesicles and between the stacked outer leaflets of the flattened and stacked vesicles. *Trans*-homophilic interactions between PMP22 molecules on the outer surface of a cylindrical vesicle with the outermost leaflet of a stack of flattened vesicles is also likely responsible for the wrapping of the stacked multilayers around a central cylindrical vesicle in MLAs. It should be acknowledged that PMP22 likely assumes mixed topologies in MLAs, where half of the protein has its extracellular loops facing out of the vesicles and half with the loops inside. This is distinct from the environment within myelinating Schwann cells, where the loops are always extracellular and could only be involved in adhesion between juxtaposed outer leaflets of the spirialing Schwann cell-extended myelin double membrane.

3.3 Similarity of PMP22 function in MLA formation to other tetraspan proteins

Some other tetraspan proteins have the capacity to alter membrane architecture through *trans*-homophilic interactions. The proteolipid protein (PLP) is the major protein of the central nervous system myelin. When this tetraspan membrane protein was purified and reconstituted into lipid bilayers it led to formation of structures that the authors suggested represent layers of stacked and compressed vesicles (*675*), assemblies very similar to MLAs. Furthermore, the two extracellular loops of PLP have been proposed to participate in *trans*-homophilic interactions between adjacent membrane surfaces at the extracellular intraperiod line of CNS myelin (*676*). Analogous to PMP22, PLP is prone to mutation-induced misfolding that leads to a dysmyelinating disorder in the CNS, Pelizaeus-Merzbacher disease (*677*). Intriguingly, the average interperiod distance measured for MLAs in vitrified ice is 153 ± 7 Å. This is similar to the interperiod distance measured for mammalian CNS is160–166 Å, (*657*). Although it now seems clear that MPZ is the major adhesive protein of stable compact myelin under normal conditions (*633, 658, 678, 679*), it is still tempting to speculate that PMP22 may also play a structural role in PNS myelin that is to some degree resembles the central role of PLP in the structure of CNS myelin.

While the capacity of PMP22 to undergo *trans* homophilic adhesive interactions may not be critical to the stability of mature compact myelin, this does not preclude a possibly transient but important and role for such interactions in Schwann cell differentiation and myelin formation. It has long been known that PMP22

appears to play an important role in these processes (*601, 633, 635*). Additionally, the *trans* adhesive biochemical properties of PMP22 may also help to stabilize other (non-compact) domains or junctions within mature PNS myelin. Another family of tetraspan membrane proteins that alter membrane organization through *trans*-homophilic protein-protein interactions is the claudins, which are integral to the organization and stabilization of tight junctions (*680, 681*). Claudins facilitate adhesion by establishing *trans*-homophilic interactions between its extracellular loops to form paracellular barriers and channels between adjacent epithelial cells (*682, 683*). PMP22 shares ~25% sequence identity with the claudins including a claudin motif in ECL1, suggesting that they likely share similar folds (*608*). Indeed, PMP22 has been found to be a component of tight junctions in some epithelial cells (*673, 684*). PMP22 has also been shown to be important for the integrity of some of the specialize junctions that control permeability in PNS myelin (*674*).

Thus, a common theme between the tetraspan membrane proteins PLP, claudins, and PMP22 and the single span MPZ is that all of these proteins can form networks of *trans*-homophilic interactions across juxtaposed lipid bilayers that influence membrane ultrastructure. Given that the water soluble but membrane-interactive myelin basic protein has long been known to cause aggregation of vesicles and even of micelles (*666, 685, 686*), *trans* adhesive properties seem to intrinsic to multiple myelin proteins.

Possible additional (non-adhesive) roles for PMP2 in MLA formation

PMP22 may also promote MLA formation through additional mechanisms. For example, PMP22 could stabilize the high membrane curvature seen at the end of each pancaked vesicle, perhaps through *cis*-homophilic interactions, as has been suggested for ER membrane proteins that shape ER membrane organization (*687*). Additionally, it is possible that PMP22, if oligomerized within the same membrane, could promote membrane curvature through a protein-protein crowding mechanism (*688*). In order to generate a more detailed molecular understanding of PMP22's role in organizing membranes, additional studies are needed to examine whether PMP22 forms *cis*-homophilic interactions in membranes and to map the spatial distribution of PMP22 in MLAs.

4. Conclusions

In this work, we demonstrate that reconstitution of PMP22 into lipid bilayers results in the formation of MLA assemblies that share some similarity to myelin, albeit only to an extent. It was further demonstrated that MLA

formation depends on the level of PMP22 relative to lipid, is dependent upon both PMP22 ECL1 and ECL2 loops, and is disrupted by a misfolding-prone disease mutant form of PMP22. The intrinsic ability of PMP22 to alter the morphology of lipid bilayer assemblies supports the notion that PMP22 may play one or more a direct structural role in myelin organization, which includes contributing to adhesion across the extracellular space between apposed bilayers. Some of roles may well be transient, occurring during Schwan cell differentiation and myelin formation. Also, while it is clear that MPZ is the major adhesive protein in compact PNS myelin, we speculate that PMP22 likely plays niche roles in myelin adhesion and/or myelin junctions that complement the more generally prevalent role of MPZ. This likely helps explain why myelin compaction is not completely eliminated even when MPZ is completely knocked out (*689*). It should be added that MPZ and PMP22 located on the surface of apposed cell membranes have been proposed to form glycosylation-independent *trans* heterophilic complexes (*661, 690*), suggesting that the adhesive roles of these proteins may sometimes be directly cooperative.

While PMP22 is thought to play multiple roles in Schwann cell biology and myelin homeostasis, the capacity of PMP22 to promote MLA formation appears to provide a convenient biochemical assay for PMP22 function in organizing membrane ultrastructure. Moreover, because the capacity of PMP22 to promote MLA formation is critically dependent on the correct folding of this protein, MLA formation might even be exploited as the basis for an assay for use in high throughput screening of small molecules in a search for molecules that rescue misfolding-prone disease mutant forms of PMP22.

Chapter IV. Peripheral Myelin Protein 22 Preferentially Partitions into Ordered Phase Membrane Domains

Chapter IV was adapted with permission from one of my previously published journal articles.(*691*)

1. Introduction

Our current understanding of biological membranes has been shaped over the past 30 years by studies of membrane phase separation into ordered and disordered domains. Early on, these studies yielded the lipid raft hypothesis (*104, 114*) which was hotly debated in subsequent years.(*115, 117, 121, 692-694*) Based on a wealth of data it is now generally believed that phase separation does sometimes occur in sphingomyelin and cholesterol-rich membranes, such as in eukaryotic plasma membranes (PMs). While it is thought that phase-separated ordered membrane domains are often small in size, transient, and similar to the adjacent disordered phase in lipid composition(*115, 133, 695*), there also appear to be certain native membranes that are so cholesterol and sphingolipid-rich that their physical properties are, to a significant degree, akin to those of ideal liquid-ordered (Lo) phase model membranes.(*695-698*)

Early studies of membrane protein association with ordered membrane nanodomains were based largely on results involving the isolation of “detergent-resistant membranes”.(*699-702*) More recent biophysical studies conducted in intact phase-separated membranes have confirmed that a number of single-pass transmembrane proteins do indeed have a preference to partition into ordered phase domains relative to surrounding disordered bilayers. Particularly important in this regard are studies that have employed “giant plasma membrane vesicles” (GPMVs), which can be formed from a variety of mammalian cell types.(*697*) When GPMVs are isolated and then cooled, separation of microscopically-observable ordered and disordered membrane phases can occur, enabling quantitative studies of protein partitioning between the two phases.(*121, 123, 697, 703-705*) GPMVs therefore provide facile experimental access to conditions in which large and stable ordered phase domains co-exist with disordered membranes.(*703, 705, 706*) Groundbreaking studies of single span membrane proteins in this medium led to development of a convincing quantitative model describing the structural basis for why some proteins of this class preferentially partition into the ordered phase.(*125, 697, 704, 707-709*) Studies of the phase preferences of multispan membrane proteins remain at a

much earlier stage of development, with the exception of an important body of work for the perfringolysin O toxin (PFO), which auto inserts into membranes to form an oligomeric beta barrel in ordered phase domains.(*127, 710, 711*) Here, we present the first example of a helical multispan membrane protein that exhibits a pronounced preference for the ordered phase in GPMVs—the tetraspan peripheral myelin protein 22 (PMP22).

The human PMP22 is a 160-residue protein containing four transmembrane helices and intracellular N- and C-termini (**Fig. 32A**). PMP22 appears to play multiple roles in myelinating Schwann cells and peripheral myelin (*601, 625, 635, 712-714*) including cholesterol homeostasis.(*715*) This is especially important in Schwann cells given their specialized function as the factory for myelin production in the peripheral nervous system (PNS). Myelin membranes are unusually rich in both cholesterol and sphingolipids(*716, 717*) and are therefore highly ordered, as well suits their roles in providing electrical insulation and mechanical support to PNS axons. Mutations in the *pmp22* gene result in >70% of all cases of Charcot-Marie-Tooth disease (CMTD, prevalence: 1:2500) and related peripheral neuropathies.(*635, 640, 713*) These closely related disorders are characterized by defective myelin membranes that contain altered cholesterol levels relative to healthy myelin.(*718-720*)

The involvement of PMP22 in cholesterol trafficking as part of the process of myelin membrane formation suggests that this protein might have an intrinsic affinity for ordered membrane domains. Indeed, it has previously been reported that PMP22 is found in ordered membranes isolated from neurons following application of classical detergent-extraction methods.(*717, 721*) However, some of these early methods of membrane domain isolation, including that used to identify PMP22 as an ordered-domain associated protein, are thought to be artifact-prone.(*117, 694, 699-701*) Nevertheless, the likely role of PMP22 in Schwann cell cholesterol homeostasis combined with its residence in cholesterol and sphingolipid-rich myelin membranes suggest that the hypothesis that PMP22 may preferentially partition into ordered phase membranes has merit. This hypothesis is tested in this chapter.

2. Results

2.1 PMP22 preferentially partitions into ordered phase membrane domains of GPMVs

To examine the preference of PMP22 for the ordered versus the disordered phase in plasma membranes (PM), we expressed human PMP22 (**Fig. 28A**) in HeLa cells and then prepared GPMVs using established

protocols.(*705*) To render PMP22 easily immunodetectable, the c-myc tag was inserted into the second

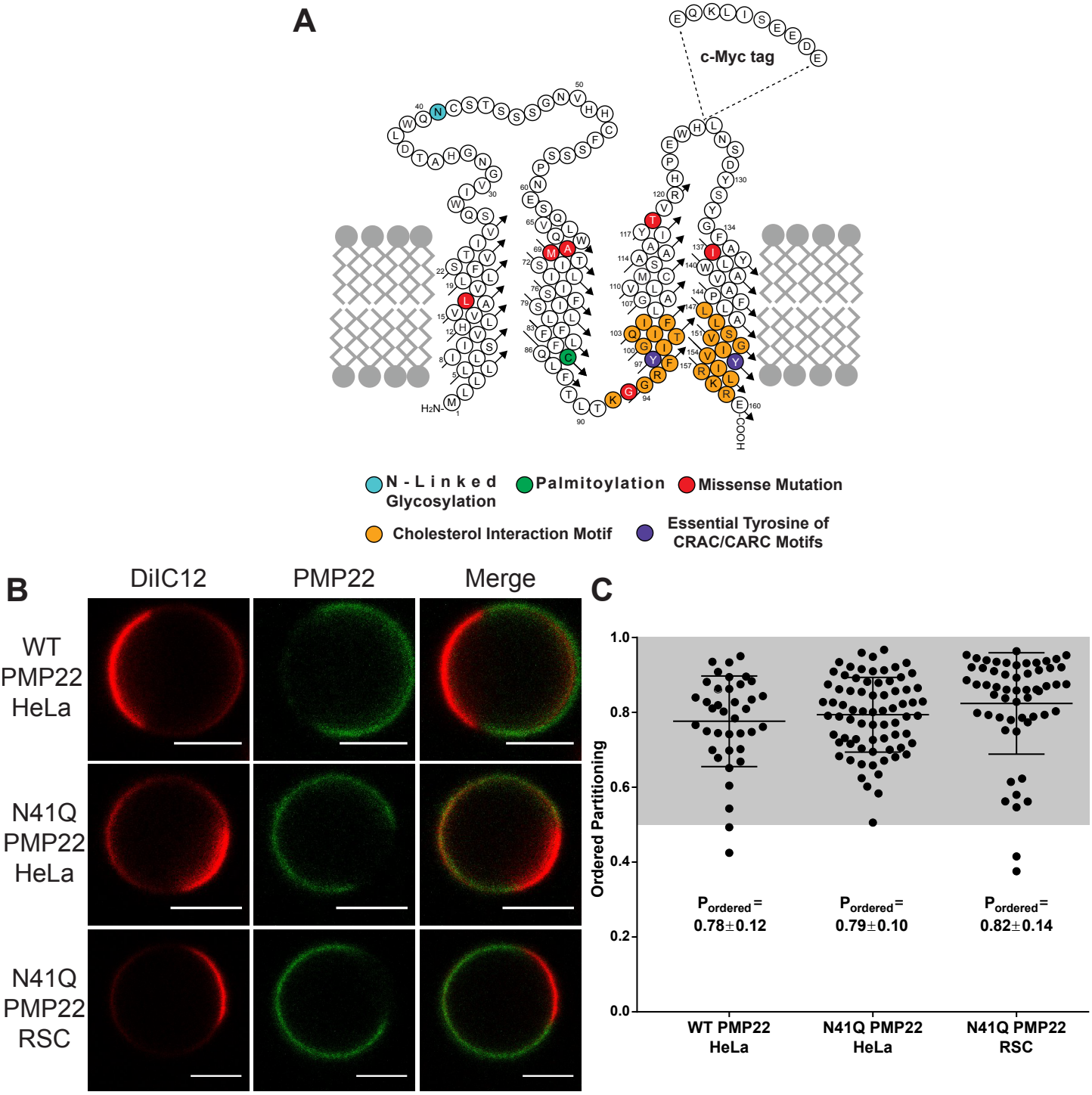

Figure 28. PMP22 partitions into ordered phase domains of GPMVs

(A) Cartoon topology map of PMP22 showing the locations of the myc-epitope tag, sites of post-translational modifications (cyan: glycosylation green: palmitoylation), cholesterol interaction motifs (orange) and their essential Tyr residues (purple), and the sites of the missense mutations examined in this study (L16P, A67T, M69K, G93R, I137V, and T118M; red). **(B)** Representative GPMVs containing WT or N41Q PMP22 derived either from HeLa cells or RSCs. Scale bar, 5 μm. The disordered phase marker is shown in red and PMP22 is shown in green. **(C)** Quantification of PMP22 partitioning coefficients from three independent biological experiments for each condition with >10 GPMVs collected per replicate. Each point represents an individual GPMV. Mean ± standard deviation (SD) is reported and plotted on graph.

extracellular loop, a modification that has no effect on PMP22 trafficking or function.(*1, 722*) PMP22 in GPMVs was visualized using confocal fluorescence microscopy using an anti-myc antibody conjugated to AlexaFluor 647 (AF647, green). Disordered phase domains within GPMVs were identified using the fluorescent carbocyanine lipid DiIC12 (red), which partitions preferentially into disordered membrane domains.(*706*) **Fig. 28B** shows representative PMP22-containing GPMVs. Within each phase PMP22 was uniformly distributed and showed no tendency to concentrate at the boundary between the ordered and disordered domains (**Fig. 28B**).

In our experiments we noticed an increase in the amount of PMP22-containing GPMVs when preparations were performed using cells overexpressing the N41Q N-glycosylation deficient variant of PMP22 (**Fig. 28A**, cyan) versus the wild type (WT) protein. Eliminating glycosylation of PMP22 does not affect its function or turnover.(*690, 723*) This observation is most likely due to an increased concentration of N41Q PMP22 at the PM compared to WT PMP22 (**Fig. 29**). Representative N41Q PMP22-containing GPMVs derived from both HeLa cells and primary rat Schwann cells (RSCs) are also shown in **Fig. 28B**. Both glycosylated and non-glycosylated PMP22 show a clear preference for ordered phase membrane domains, as evidenced by the lack of co-localization of the red DiIC12 and green AF647 channels. PMP22 shows a distinct preference for ordered membrane domains in GPMVs prepared from both HeLa cells and RSCs.

AF647 fluorescence intensity was quantified in ordered and disordered GPMV membrane domains to determine the relative concentration of PMP22 in each membrane phase. Following image quantitation, the ordered domain partitioning fraction ($P_{ordered}$) of PMP22 was calculated, where $P_{ordered}$ is: $([PMP22]_{ordered}/([PMP22]_{ordered} + [PMP22]_{disordered})$, and ranges from 0 to 1 with a value of 0.5 meaning the protein has equal affinity for both phases, while $P_{ordered} > 0.5$ means that the protein prefers the ordered phase, and $P_{ordered} < 0.5$ means that the protein prefers the disordered phase.(*708*)

GPMVs from HeLa cells showed clear phase separation at 20°C while those from RSCs exhibited phase separation at 15°C. Quantification of $P_{ordered}$ for WT and N41Q PMP22 in GPMVs derived from HeLa cells as well as for N41Q PMP22 in GPMVs derived from RSCs is shown in **Fig. 28C**. Data were acquired from three independent biological experiments for each condition and >10 GPMVs were analyzed per replicate. In HeLa GPMVs, WT PMP22 showed a $P_{ordered}$ of 0.78±0.12 (mean ± SD) and N41Q PMP22 showed a $P_{ordered}$ of 0.79±0.10. N41Q PMP22-containing RSC GPMVs displayed a $P_{ordered}$ of 0.82±0.14. As a control, we measured

the phase partitioning in both HeLa cells and RSC GPMVs of the well-studied mEGFP-labeled form of the single pass membrane protein, linker for activated T Cells (tgLAT; **Fig. 30**). The measured $P_{ordered}$ values of 0.54±0.11 and 0.55±0.07 for tgLAT in GPMVs derived from Hela and RSCs respectively are in line with those reported in the literature using the same GPMV preparation in rat basal leukemia cells.(*125, 704*) Additionally,

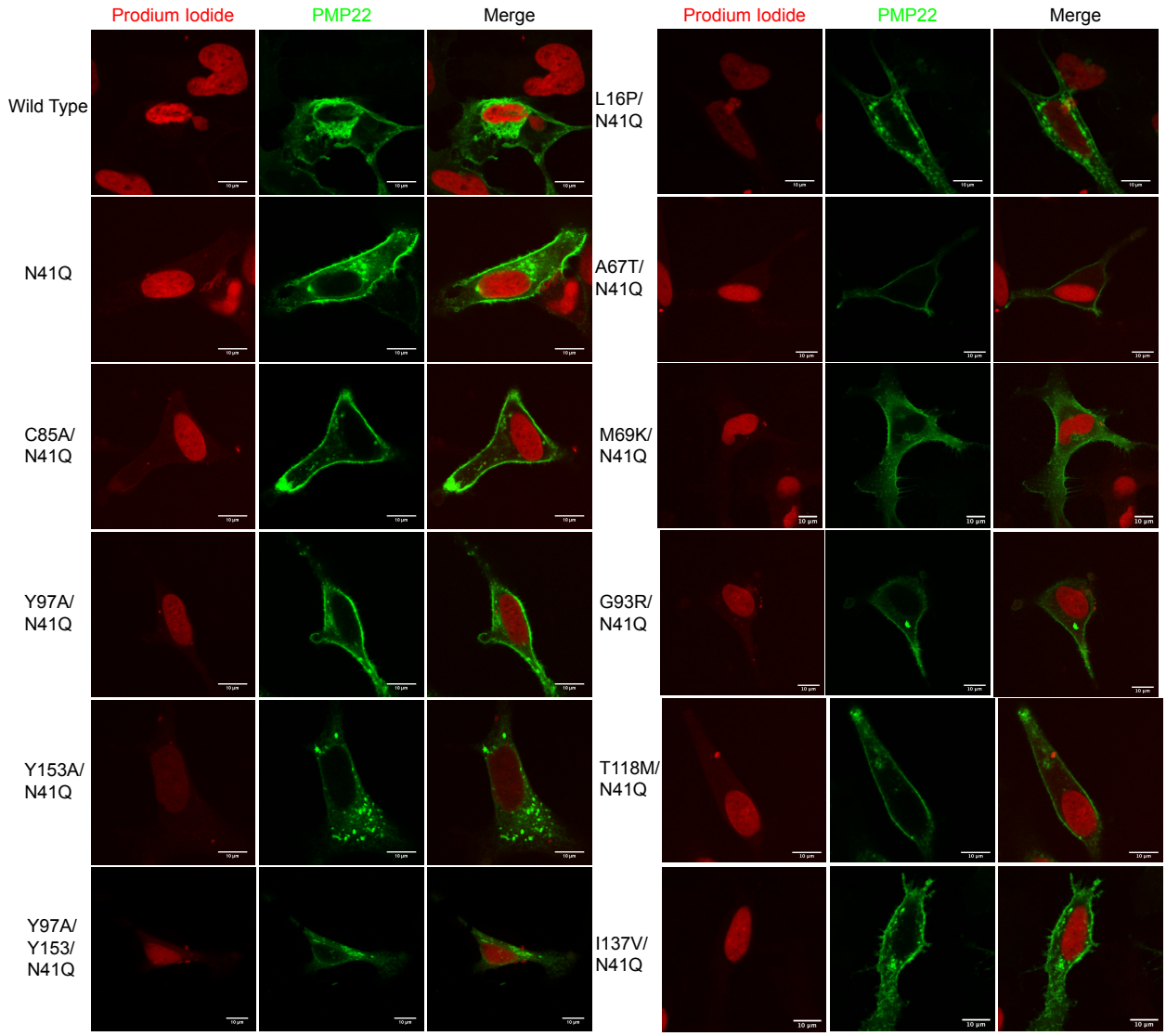

Figure 29. Localization of PMP22 variants in cells

Fixed and permeabilized cells were imaged via confocal microscopy using a 40x objective and an optical zoom of 3-4X. Propidium Iodide (PI, red) was used to identify the nuclei of cells and PMP22 was identified immunochemically via the myc epitope (green). Scale bar, 10 μm.

we measured $P_{ordered}$ for N41Q PMP22 in HeLa GPMVs using a different membrane phase marker, NBD-DSPE (**Fig. 31**), which identifies ordered membrane phase domains.(*706*) Using this marker, we calculated a $P_{ordered}$ of 0.82±0.06. To ensure that the antibody-induced dimerization of PMP22 was not impacting our partitioning results we measured PMP22 phase partitioning using an AF647-labeled antigen-binding fragment (Fab; **Fig.**

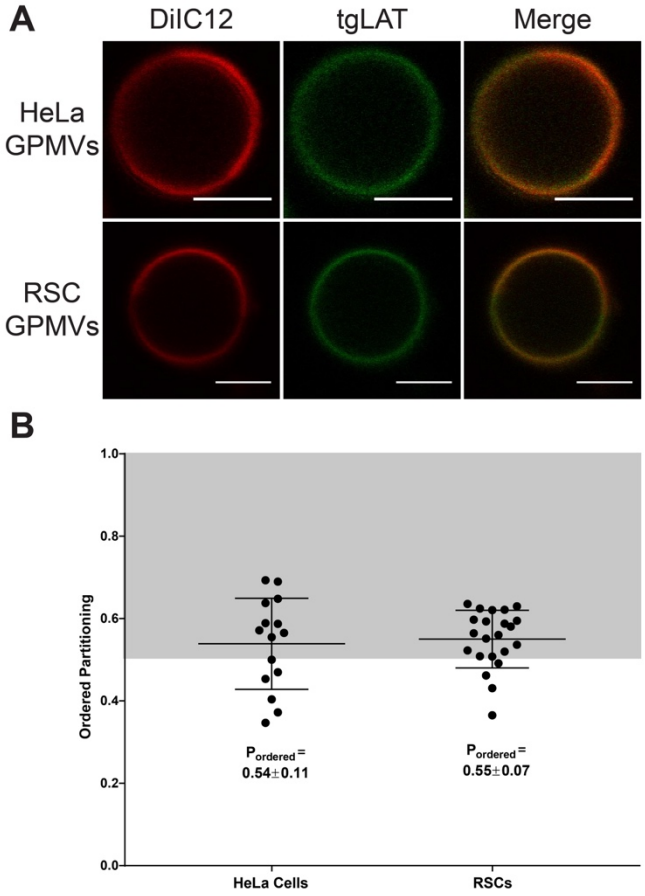

Figure 31. Phase preference for tgLAT in GPMVs derived from HeLa or RSCs

(A) Representative tgLAT-containing GPMVs derived from either HeLa or RSCs. Scale bar, 5 μm. **(B)** Quantification of $P_{ordered}$ for tgLAT from three independent biological experiments.

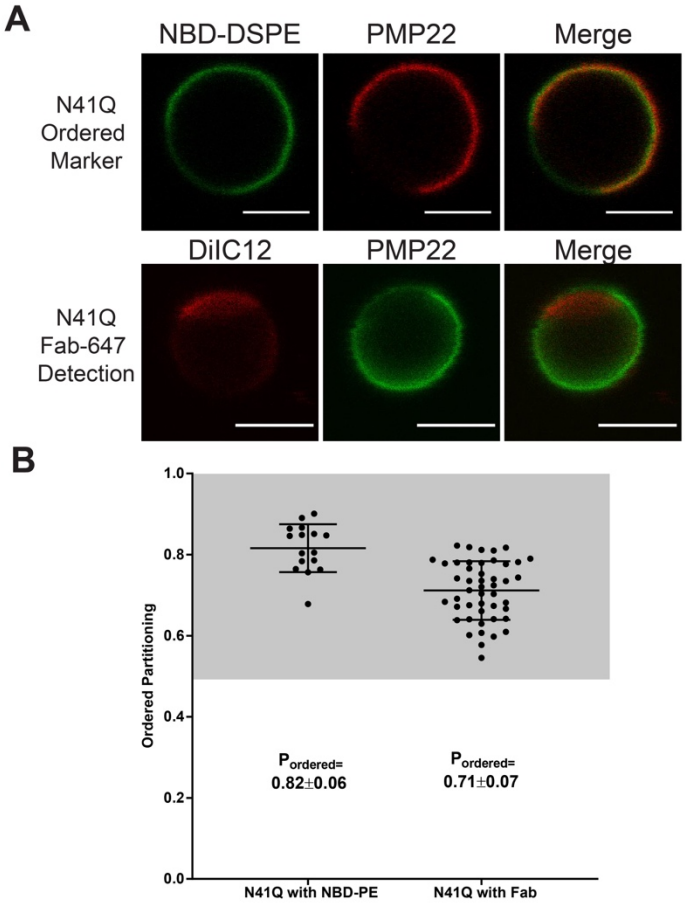

Figure 30. Phase preference with ordered phase marker or with antibody fragment

(A) Representative N41Q PMP22 (red) containing GPMVs stained with the ordered phase marker NBD-DSPE (green) and representative N41Q PMP22 (green) containing GPMV stained with DiIC12 (red) and PMP22 detected using AF647-Fab fragment targeted against the myc epitope. Scale bar, 5 μm. **(B)** Quantification of $P_{ordered}$ for N41Q PMP22 using the NBD-DSPE phase marker and N41Q PMP22 detected using the Fab fragment from three independent biological experiments.

31). While $P_{ordered}$ for PMP22 was slightly lower ($P_{ordered}$=0.71±0.07) when the Fab was used for detection, PMP22 still strongly preferred ordered membrane domains indicating that antibody-induced dimerization was not driving the observed phenomena. These results quantitatively demonstrate that PMP22 has a pronounced preference to partition into ordered membrane domains in GPMVs from both model mammalian cell lines and primary Schwann cells. Additionally, there were no significant differences in WT versus N41Q PMP22 phase partitioning indicating that this phase preference is not affected by N-linked glycosylation. In light of this result and because the level of surface expression for N41Q PMP22 made it easier to image, all subsequent experiments reported in this work utilized a N41Q PMP22 variant (in this chapter hereto referred to as “PMP22” for the sake of simplicity). Moreover, because HeLa-derived GPMVs

showed phase separation at a temperature closer to physiological levels and had higher transfection efficiencies compared to RSCs, all subsequent experiments utilized HeLa-derived GPMVs.

2.2 S-Palmitoylation of PMP22 is not a significant driver of its ordered phase preference

It was recently shown that PMP22 is palmitoylated at Cys85 (**Fig. 28A,** green).(*724*) In that study, this post-translational addition of a saturated fatty acid group on the cytosolic side of the protein was shown not to affect PMP22 processing/trafficking but was seen to be important for modulating epithelial cell shape and motility. For single pass transmembrane proteins, it has repeatedly been shown that palmitoylation plays a significant role in mediating membrane phase partitioning; one study estimated that this modification contributes ~0.5 kcal mol^{-1} free energy per chain in favor or ordered phase partitioning.(*125, 704*) The removal of palmitoylation from tgLAT disrupts the ordered phase preference of that protein and causes it to equally prefer both membrane phases.(*125*) We therefore tested to see if palmitoylation affects PMP22 partitioning into ordered membrane phases.

To eliminate the palmitoylation of PMP22 we mutated Cys85 to an Ala residue. This mutation did not affect the localization of PMP22 in HeLa cells (**Fig. 29**). We then measured the $P_{ordered}$ for C85A PMP22 in GPMVs. As seen in **Fig. 32A-B** palmitoylation did not dramatically affect the ordered phase preference of PMP22. We determined a $P_{ordered}$ for C85A PMP22 of 0.77±0.10. This value is almost identical to that reported for WT and N41Q PMP22 in **Fig. 28**. Because the standard method for GPMV preparation requires the use of the reducing agent dithiothreitol (DTT; 2 mM) we tested if PMP22 was still palmitoylated under these conditions. PMP22 transfected cells were incubated overnight with 100 mM of 17-octadecynoic acid (17-ODYA), a palmitic acid analogue containing an alkyne on the terminal carbon, which is known to be incorporated by thioesterases into palmitoylated proteins. Cells were then treated with or without 2 mM DTT for 90 min at 37°C, lysed, and PMP22 was immunoprecipitated. We then added a biotin handle to palmitoylated proteins using biotin azide and classical ‘click’ chemistry.(*724*) Palmitoylated PMP22 was identified via western blotting using an anti-biotin antibody (**Fig. 32C).** Palmitoylation was quantified as the intensity of the anti-biotin band over the anti c-myc band and normalized to the amount of palmitoylation found in N41Q PMP22 samples without DTT treatment (**Fig. 32D**). As seen in **Fig. 32C-D**, treatment of HeLa cells for 90 minutes with 2 mM DTT did not affect PMP22 palmitoylation. As expected, C85A PMP22 was not palmitoylated in these

experiments. These results show that S-palmitoylation of PMP22 is not a significant driver of ordered phase preference.

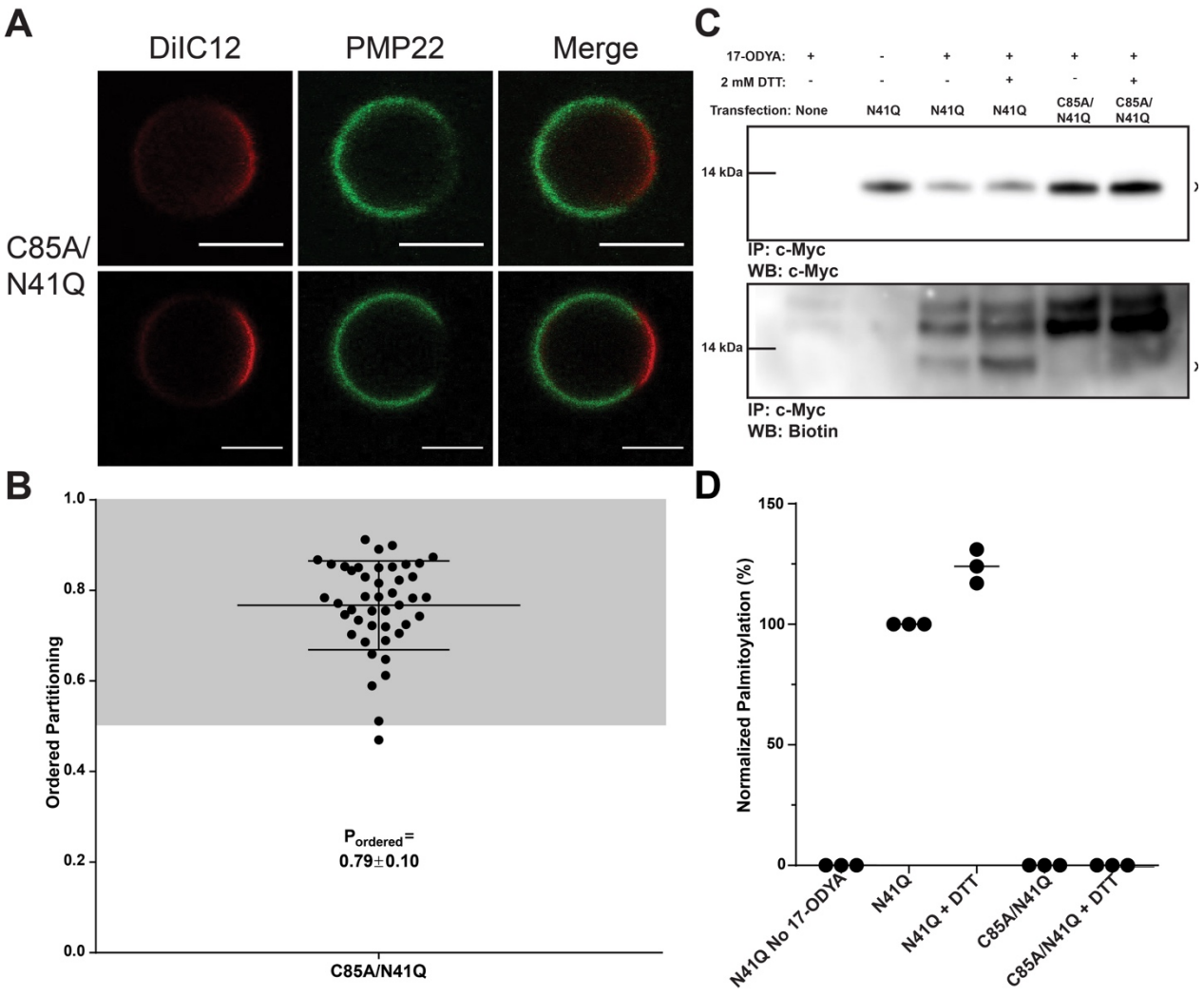

Figure 32. Palmitoylation is not required for PMP22 localization to the ordered phase

(A) Upper and lower triple images are representative examples of PMP22-containing GPMVs from C85A/N41Q PMP22-transfected HeLa cells. Scale bar, 5 μm. **(B)** Quantification of C85A PMP22 partitioning coefficients from three independent biological experiments with >10 GPMVs collected per replciate. Mean ± SD is reported and plotted on the graph. **(C)** Representative western blots of PMP22 and palmitoylated PMP22 from cells treated with or without 2 mM DTT. The top blot shows PMP22 immunopurified from cell lysates while the bottom blot shows palmitoylated protein from the immunopurified lysates which was identified via addition of a biotin handle to alkyne palmitate. **X** marks the PMP22 signal. **(D)** Quantification of the amount of palmitoylated PMP22 from three biological replicates. The amount of palmitoylated PMP22 from each sample is quantified by dividing the intensity from the biotin blot by the intensity of the myc blot and then normalized to the amount of palmitoylated PMP22 in the N41Q sample without DTT treatment.

2.3 Cholesterol binding motifs in PMP22 do not mediate its ordered phase preference

We next tested whether either or both of the predicted cholesterol binding sites in PMP22 play a role in its ordered phase preference. For the multispan beta barrel membrane protein perfringolysin O (PFO), it was

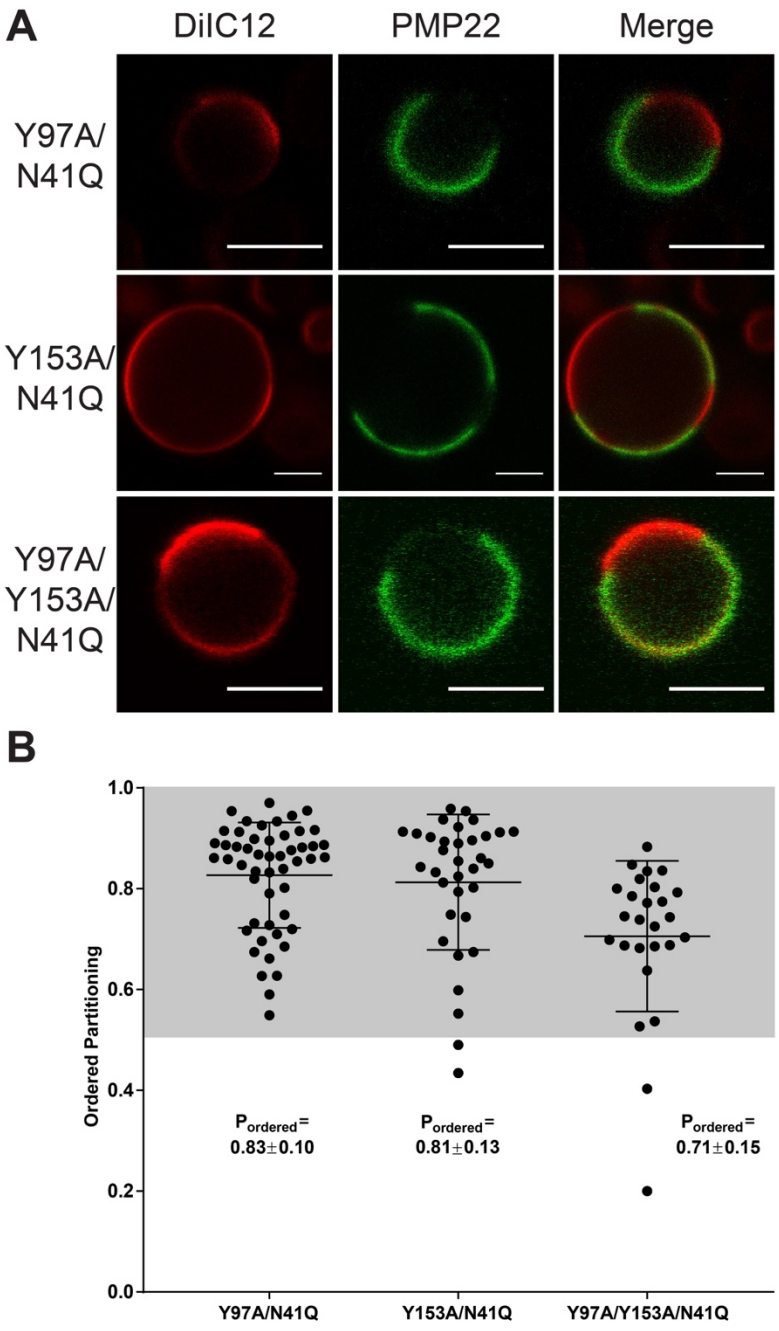

Figure 33. Cholesterol interaction motifs do not contribute to the ordered phase domain preference of PMP22

(A) Representative PMP22 containing GPMVs from Y97A/N41Q, Y153A/N41Q, and Y97A/Y153A/N41Q mutant forms of PMP22-transfected HeLa cells. Scale bar, 5 μm. **(B)** Quantification of PMP22 partitioning coefficients from three independent biological experiments with >10 GPMVs imaged per replicate. Mean ± SD is reported and plotted on the graph.

shown that protein-associated sterols could alter the phase partitioning properties of the protein in phase-separated synthetic lipid vesicles.(*710*) It has been shown that *pmp22 -/-* Schwann cells exhibit reduced plasma membrane levels and abnormal localization of cholesterol.(*714, 715*) These cells also show reduced migration, adhesion, and lamellipodia extension, all of which can be restored through external supplementation of cholesterol in the culture media. PMP22 contains both a classical cholesterol-recognition amino acid consensus (CRAC) motif in TM4 (L-X_{1-5}-Y-X_{1-5}-K) and an inverted CRAC (CARC) motif in TM3 (K-X_{1-4}-Y-X_{1-6}-I), as illustrated in orange in **Fig. 28A**. While these motifs are loosely defined and are not always indicative of direct cholesterol interaction(*725*), there is substantial experimental and computational evidence supporting the notion that these motifs are sometimes directly involved in binding cholesterol.(*726, 727*)

We mutated one or both of the essential Tyr residues in the CARC and CRAC motifs to Ala (Y97A, Y153A, and Y97A/Y153A mutants; **Fig. 28A,** purple). We then assessed the phase preference for each mutant in GPMVs. Mutation of Tyr97 had no effect on PM levels of PMP22 but mutation of Tyr153 or of both Tyr residues led to decreased PMP22 levels at the PM, suggesting lower expression and/or surface trafficking efficiency for these mutants (see **Fig.**

33). Nevertheless, the mutations did not significantly alter the ordered phase preference of PMP22 (**Fig. 33A-B)**. Y97A exhibited a $P_{ordered}$ of 0.83±0.10, Y153A exhibited a $P_{ordered}$ of 0.81±0.13, and the double mutant Y97A/Y153A yielded a $P_{ordered}$ of 0.71±0.15. $P_{ordered}$ for the double mutant was only slightly reduced. We interpret these results to indicate that the presence of CRAC and/or CARC motifs are not significant drivers of the preference of PMP22 for ordered phase domains.

2.4 Phase partitioning of disease mutant forms of PMP22

Since palmitoylation and cholesterol interaction motifs do not appear to play a major role in defining the phase preference of PMP22, we hypothesized that there is something intrinsic to the structure of the protein that drives its preferential association with the ordered phase. In order to test this hypothesis, we measured $P_{ordered}$ for a number of CMTD mutant forms of PMP22 **(Fig. 28A)**. These different mutants were previously observed to demonstrate a range of *in vitro* conformational stabilities, plasma membrane trafficking efficiencies in cultured cells, and disease severity as quantitated by nerve conduction velocities in CMTD patients with these PMP22 variants.(*1*)

We first examined PMP22 containing a disease mutation in TM1: the L16P variant (**Fig. 28A**, red), which is also known as the “Trembler-J” mutation because of its mouse phenotype.(*1, 635, 713*) Under WT/mutant heterozygous conditions L16P PMP22 causes severe demyelination in both human and mice. Moreover, previous biophysical studies of L16P PMP22 showed that the L16P mutation introduces a flexible hinge in the TM1 helix, destabilizing the fully folded form of the protein and causing it to adopt an unfolded or folding-intermediate state in which TM1 is disassociated from TM2-4, which remain bundled, but only as a molten-globule.(*1, 608, 665*) Folding stability measurements in detergent micelles revealed L16P PMP22 to be destabilized compared to WT PMP22 with a $\Delta\Delta G$ of 3.3±0.5.(*1*) While introduction of the L16P mutation resulted in significantly reduced cell surface expression compared to PMP22 (**Fig. 29**), we nevertheless were able to generate enough L16P PMP22-containing GPMVs to measure its phase preference—its $P_{ordered}$ was 0.32±0.17 (**Fig. 34**). The L16P mutation dramatically reverses the phase preference of PMP22 such that the protein now partitions preferentially into disordered membrane phase domains. This result led us to the hypothesize that the formation of stable tertiary structure in WT PMP22 is important for its preference to partition into ordered phase domains.

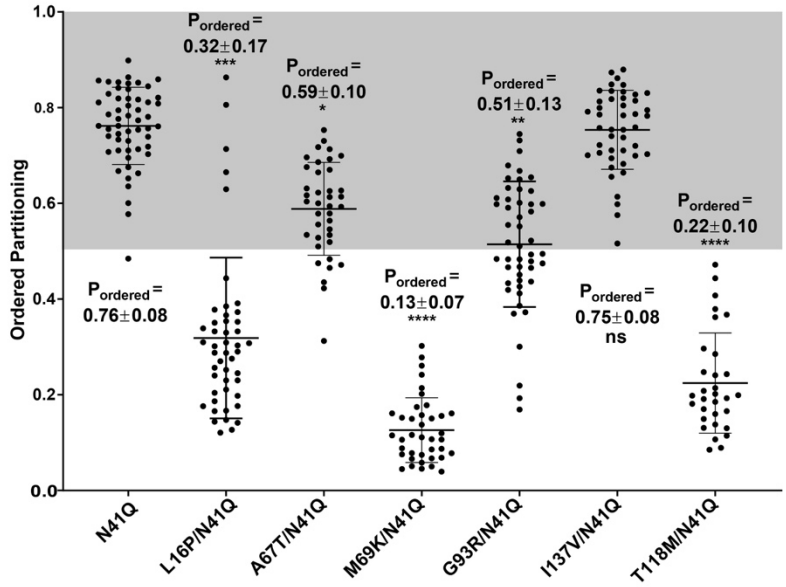

Figure 34. Phase partitioning of PMP22 missense mutation

Quantification of the PMP22 partitioning coefficients of N41Q along with various missense mutants from three biological experiments with >10 GPMVs collected per replicate. Mean ± SD is reported and plotted on the graph. The non-parametric Mann-Whitney U test was used for all statistical analysis. * p<0.05, **p<0.01, ***p<0.001, ****p<0.0001, ns=not significant; all statistics compare missense mutations to N41Q PMP22.

To test this hypothesis, we measured $P_{ordered}$ for five additional PMP22 disease variants known to display a range of stabilities. The first three, M69K, G93R, and T118M PMP22 (mutation sites located in TM2, the intracellular loop, and TM4, respectively; **Fig 28A**) are significantly destabilized compared to WT PMP22: M69K PMP22 exhibited a $\Delta\Delta G$ of 2.7±0.5, G93R PMP22 a $\Delta\Delta G$ of 2.9±0.5, and T118M a $\Delta\Delta G$ of 1.3±0.6.(*1*) The $P_{ordered}$ values for these variants showed a significantly reduced ordered phase preferences relative to WT PMP22 (**Fig 34**). M69K and T118M PMP22 were found to prefer disordered membrane phases with $P_{ordered}$ values of 0.13±0.07 and 0.22±0.10 respectively (**Fig. 34**). G93R PMP22 was found to have no preference for either phase of the membrane displaying a $P_{ordered}$ of 0.51±0.13 (**Fig. 34**). These results confirm that destabilized variants of PMP22 exhibit a reduced preference for ordered membrane phases.

We also examined the phase partitioning of two PMP22 variants that were only slightly destabilized, or not destabilized at all, compared to WT PMP22. In folding stability measurements, A67T and I137V PMP22 (located in TM2 and TM4 respectively; **Fig 28A**) displayed $\Delta\Delta G$ values of -0.1±0.9 and 0.2±0.7 respectively—very similar to WT. In GPMVs, both of these PMP22 variants showed marked preference for ordered phase domains (**Fig 34**). A67T PMP22 displayed a $P_{ordered}$ of 0.59±0.10, a value only modestly reduced compared to that for WT PMP22 (**Fig. 34**). The I137V variant exhibited a $P_{ordered}$ of 0.75±0.08 which is almost identical to the $P_{ordered}$ measured for WT PMP22 in paired experiments, 0.79±0.10 (**Fig. 34**). These results show that variants of PMP22 that retain conformational stability still prefer ordered membrane domains over disordered domains. Taken together, these results indicate linkage between conformational stability and/or tertiary packing of PMP22, and the preference of the protein for ordered membrane domains.

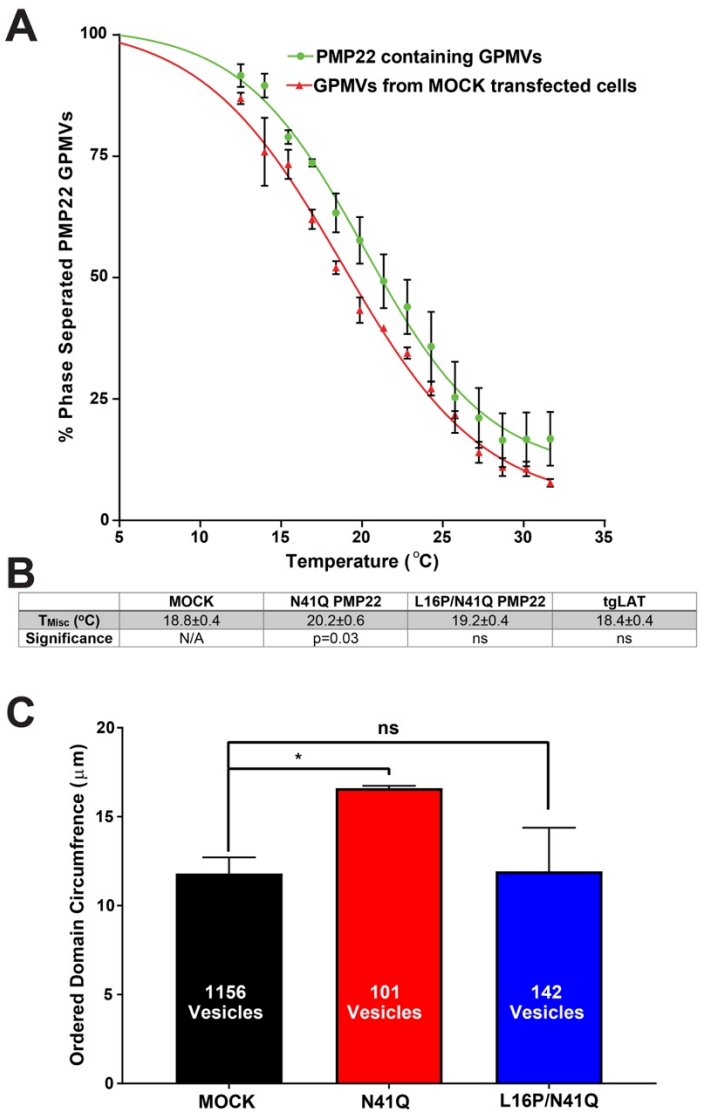

	MOCK	N41Q PMP22	L16P/N41Q PMP22	tgLAT
T_{Misc} (°C)	18.8±0.4	20.2±0.6	19.2±0.4	18.4±0.4
Significance	N/A	p=0.03	ns	ns

Figure 35. PMP22 alters the biophysical properties of GPMVs

(A) Percent phase separation of GPMVs containing N41Q PMP22 (green) or of GPMVs derived from cells transfected with an empty vector (MOCK; red) at various temperatures. Each point shows the average of three independent experiments and the error bars represent the standard error of the mean (SEM). >100 GPMVs were measured at each temperature in each experiment. Plots are fit to a sigmoidal curve. **(B)** Calculation of the phase miscibility temperature (T_{Misc}) for GPMVs from MOCK transfected cells, GPMVs containing N41Q PMP22, L16P/N41Q PMP22 or tgLAT. T_{Misc} is calculated from the fit of the sigmoidal curve for each independent experiment and the SEM is calculated from the three replicates. The reported value represents the mean T_{Misc} ± SEM. Significance was determined using a non-parametric Mann-Whitney U test comparing N41Q PMP22, L16P/N41Q PMP22, or tgLAT-containing GPMVs to MOCK GPMVs. **(C)** Ordered domain sizes (μm) from GPMVs obtained from cells transfected with either an empty vector (MOCK), GPMVs containing N41Q PMP22, or GPMVs containing L16P/N41Q PMP22. Data was obtained for three biological replicates for MOCK samples and L16P/N41Q and six biological replicates for PMP22. Total number of vesicles measured is reported in the graph. Significance was determined using a non-parametric Mann-Whitney U test. * p>0.05, ns=not significant.

2.5 PMP22 alters the biophysical properties of GPMVs and promotes formation of ordered phase domains.

Because it has been shown that PMP22 is critical for the formation of stable membrane domains in Schwann cells(*714*), we hypothesized that PMP22 may alter the stability of phase separation between ordered and disordered phase domains in GPMVs. To test this, we first determined the miscibility temperature (T_{Misc}) of PMP22-containing GPMVs compared to GPMVs derived from cells transfected with an empty vector ("MOCK" conditions; **Fig. 35A**). T_{Misc} is defined as the temperature at which 50% of the GPMVs exhibit phase separation.(*695, 697, 728*) A higher T_{Misc} suggests more stable phase-separated membrane domains. We collected images of >100 GPMVs at each temperature over temperatures ranging from 12.5˚C to 32.5˚C and calculated the fraction of phase-separated GPMVs at each temperature. Fitting this data to a sigmoidal curve allowed us to determine the T_{Misc} of the GPMVs. **Fig. 35B** shows the T_{Misc} seen for PMP22-containing GPMVs

and for GPMVs from MOCK transfected cells. PMP22-containing GPMVs exhibited a T_{Misc} of 20.2±0.6 °C whereas MOCK GPMVs showed a T_{Misc} of 18.8±0.4°C. The T_{Misc} seen for empty GPMVs was similar to what has previously been reported.(*695, 728*) To validate that the increase in T_{Misc} was not due to general overexpression of a TM protein at the plasma membrane, we measured the T_{Misc} of tgLAT containing GPMVs. GPMVs containing tgLAT exhibited a T_{Misc} of 18.4±0.4 °C, similar to MOCK conditions (**Fig. 35B**), suggesting that the T_{Misc} increase of PMP22-containing GPMVs was not due to generic membrane protein overexpression. Additionally, we measured the T_{Misc} of L16P PMP22-containing GPMVs to assess if this increased domain stability was associated with PMP22 ordered domain partitioning. We found that L16P containing GPMVs had a T_{Misc} of 19.2±0.4°C (**Fig. 35B**). This value was not statistically different than GPMVs obtained from MOCK transfected cells. These results indicate that wild type PMP22, but not an unstable disease variant of the protein, stabilizes phase separation in GPMVs.

We also examined whether the presence of PMP22 increased the size of ordered phase domains in GPMVs. To do this we imaged a large number of GPMVs derived from cells transfected with either an empty vector or one encoding WT or L16P PMP22 (three independent biological replicates with >30 GPMVs measured per replicate). For these images we measured the radii of individual GPMVs as well as the fraction of each GPMV that contained the disordered phase maker DiIC12. From this information we were able to calculate the relative size of ordered domains in GPMVs, as indicated in **Fig. 35C.** We found that GPMVs derived from cells transfected with an empty vector contained ordered domains with an average circumference of 11.8±0.9 μm. GPMVs with PMP22 contained ordered domains with a circumference of 16.6±0.1 μm, while GPMVs with L16P PMP22 contained ordered domains with a circumference of 11.9±2.5 μm. These results show that PMP22, but not unstable L16P PMP22 causes a significant increase in ordered domain size and suggests that PMP22 is able to stabilize the ordered membrane domains of GPMVs. Combined with the fact that PMP22 increases the T_{Misc} of GPMVs, we conclude that folded PMP22 is able to alter the biophysical properties of GPMVs to promote formation and stabilization of ordered phase domains.

3. Discussion

While there are a number of biochemical reports that identify multi-span membrane proteins found to co-localize with biochemically isolated “detergent-resistant” cell fractions (*729-731*), to the best of our knowledge this is the first work that *quantitively* demonstrates a preference to partition into ordered phase membrane domains by a multispan membrane protein in cell-derived GPMVs.

3.1 Factors contributing to the ordered phase domain preference of PMP22

Much effort has been devoted to understanding the driving forces of membrane phase preference for single-pass transmembrane proteins. In work conducted by the London lab, phase partitioning for the multispan beta barrel membrane protein PFO in synthetic lipid vesicles was found to be dependent on lipid composition, protein-associated sterols, pH, and hydrophobic matching between the protein TM segments and bilayer width.(*710, 711, 732*) In the Levental group, previous work culminated in an elegant paper that provided a quantitative model describing the biochemical and biophysical features promoting ordered phase domain partitioning for single-pass transmembrane proteins.(*704*) Ordered phase domain partitioning of single-pass proteins is promoted by increasing length for the transmembrane helix, by the presence of one or more palmitoyl chains, and by the presence of small amino acid side chains in the fully membrane-exposed TM segment which reduces the exposed surface area in the plane of the membrane, especially for the half that occupies the exoplasmic bilayer leaflet. Whether components of this model can be extrapolated to ordered phase-preferring multispan membrane proteins is not yet clear. However, this study of PMP22 represents an important step in exploring this question.

The results demonstrated that the tetraspan integral membrane protein PMP22 has a distinct preference to partition into ordered phase membrane domains of GPMVs derived from both HeLa and primary Schwann cells. Unlike ordered phase-preferring single-pass transmembrane proteins (*125, 704, 707*), partitioning of PMP22 is not driven by palmitoylation. Even though native PMP22 is palmitoylated, it retains its strong preference for the ordered phase even under conditions in which its palmitoylation site is mutated away. Our results demonstrate that this modification is not required for the ordered membrane phase preference of PMP22, as it seems to be for single-pass membrane proteins. Ordered phase partitioning of PMP22 was also found not to be associated with the putative CARC and CRAC cholesterol binding motifs present in PMP22.

This suggests that unlike PFO, sterol binding does not drive PMP22 phase partitioning although we cannot rule out the possibility that PMP22 associates with cholesterol through mechanisms independent of the CRAC/CARC motifs.

We observed that the conformational stability of the folded form of PMP22 plays a major role in mediating the phase preference of PMP22. Introduction of the destabilizing L16P mutation in the middle of TM1 reversed the phase preference of PMP22 so that it now favors the disordered phase. We have previously shown that the L16P mutant converts the straight and uninterrupted WT TM1 helical segment into a pair of helices linked by a flexible hinge.(*608, 665*) This causes TM1 to dissociate from the other TM helices to favor a destabilized form of the protein in which TM2, TM3, and TM4 remain in contact as a molten globular bundle while TM1 is dissociated in the membrane, tethered to the rest of the protein by the TM1-TM2 loop. While we do not have the same in-depth structural information on M69K, G93R and T118M PMP22, it has previously been shown that these mutations also destabilize the conformational stability of PMP22. Here, we find these mutations also decrease the affinity of PMP22 for ordered membrane domains, causing the disease variant forms of the protein to have either no preference for either phase (G93R) or to adopt a preference for disordered membrane phases (M69K and T118M). The A67T and I137V mutations, which either marginally destabilize or have no effect on the conformational stability of PMP22, retained a WT-like preference to partition into ordered phase membrane domains, further supporting our hypothesis about the role of conformational stability in the phase preference of PMP22.

In **Fig. 36A** we plot $P_{ordered}$ for the 7 forms of PMP22 examined in this work versus conformational stability, plasma membrane trafficking, and CMTD severity (as measured by nerve conduction velocity in patients with these single nucleotide polymorphisms).(*1*) We observed a strong positive correlation between stability, plasma membrane trafficking and nerve conduction velocity with ordered phase partitioning of PMP22. Protein stability reflects the equilibrium constant between the folded conformation of a protein and the unfolded form. As illustrated in **Fig. 36B**, stable forms of PMP22, such as wild type, preferentially partition into ordered membrane domains whereas unstable forms of PMP22, such as the L16P disease mutant, prefer the

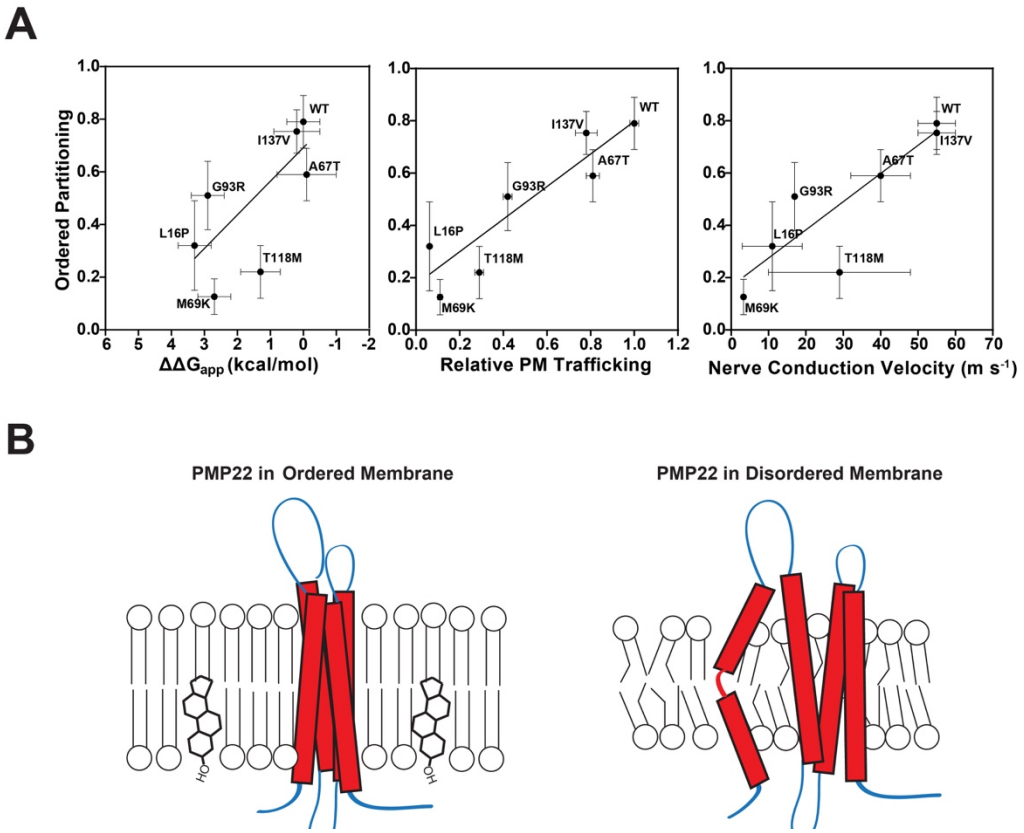

Figure 36. Ordered phase partitioning correlates with PMP22 stability, trafficking, and CMTD severity

(A) $P_{ordered}$ determined for the PMP22 mutants used in this study is plotted against tertiary stability (ΔΔG), relative plasma membrane trafficking efficiency compared to WT, and CMTD severity (as reported by the nerve conduction velocity measured in patients harboring these PMP22 variants). ΔΔG, plasma membrane trafficking efficiency, and nerve conduction velocities were obtained from (*1*). Linear regression analysis in GraphPad was used to show correlations. **(B)** Model for PMP22 preferential partitioning into ordered membrane domains. PMP22 that is able to adopt the proper tertiary packing within the membrane partitions into ordered domains and is able to traffic to the PM and assist in efficient nerve conduction velocities. PMP22 which is unable to adopt a stable tertiary fold does not traffic to the PM efficiently and therefore causes reduction in nerve conduction velocities.

disordered phase. It is now clear that the protein folding quality control system of the endoplasmic reticulum (ER) has mechanisms for recognizing and retaining unstable forms of PMP22, eventually leading to ERAD

pathway degradation of the protein. However, how quality control recognizes unstable PMP22 is not yet well understood.(*2*) It is noteworthy that while the ER is the site for cholesterol biosynthesis in the cell, its membrane has only modest quantities of cholesterol. Most cholesterol is exported on to the Golgi (which has roughly 2X higher cholesterol in its membranes) and from there on to the plasma membrane (roughly 6X higher).(*93*) Given that ordered membrane domains in cells are cholesterol-rich, the results of this work lead us to speculate that one of the mechanisms that promotes “escape” of stable (predominately folded) forms of PMP22 from ER quality control may be its partitioning into cholesterol-rich ordered domains that are then likely to traffic on to the Golgi and thence to the plasma membrane.

That folded PMP22 favors ordered phase domains makes sense in light of the Levental model for single span membrane proteins and with results from the London group on PFO. In the Levental model, one factor mediating membrane phase preference is the exposed protein surface area in the plane of the membrane. Minimizing this feature in a protein promotes ordered phase partitioning. Multispan helical membrane proteins that adopt a stable tertiary fold should have less exposed surface in the slab of the membrane compared to unfolded forms, which may promote ordered phase partitioning. Of course, not all folded multispan membrane proteins preferentially partition into ordered phase domains. This indicates that the folded structure of PMP22 has distinctive traits that favor ordered phase partitioning. For PFO, the London group discovered that hydrophobic matching of the length of its TM beta strands with bilayer width played a large role in phase partitioning.(*711*) Therefore, forms of PFO with longer hydrophobic beta-strands more strongly prefer ordered membrane phases, which are slightly thicker than the surrounding disordered membrane phase. Examination of a homology/Rosetta model for the structure of PMP22 (*608*) suggest that two of its transmembrane helices may be longer than average (at least 26 residues each) and that the transmembrane domain has a fairly featureless surface. While there does not seem to the general preponderance of residues with small side chains in the exoplasmic half of the PMP22 transmembrane domain as appears to be a feature of ordered phase-preferring single-pass membrane proteins (*39, 704*), the presence of a Ser-Ala-Ala-Ala segment at the exoplasmic end of TM3 is intriguing. The intracellular “domain” of PMP22 is another distinctive feature, being comprised only of the N-terminal amino group of Met1, a 4-residue loop connecting TM2 and TM3, and four charged residues that follow TM4. Testing whether any of these features

are contributing factors to PMP22's ordered phase preference will require many additional experiments, which we hope will be motivated by the results of this paper.

3.2 The preference of PMP22 for ordered phase membrane domains in cell-derived GPMVs does not extend to L_o phase domains in synthetic lipid vesicles

In previous work we showed that purified recombinant PMP22 can be reconstituted into giant unilamellar vesicles (GUVs) containing synthetic lipids.(*733*) Under GUV conditions in which the synthetic lipids separated into ideal liquid-disordered (L_D) and liquid-ordered (L_O) lipid phases, it was observed that PMP22 partitioned exclusively to the disordered L_D phase. Why are the results for PMP22 partitioning in GPMVs at odds with what was observed in GUVs? Our current results show that neither of the known post-translational modifications of PMP22, N-glycosylation at N41 or S-palmitoylation at C85, are required for the ordered phase preference of PMP22 in GPMVs. This allows us to rule out the possibility that the lack of post-translational modifications of the recombinant PMP22 used in the earlier GUV studies is the basis for its L_D phase preference. We suggest instead that the variance between the results from the GPMV and GUV studies point to the fact that the difference in order between phase-separated domains in cell-derived GPMVs is much reduced relative to GUVs comprised of a well-defined ternary mixture of synthetic lipids. This phenomenon has previously been documented for single span membrane proteins.(*115, 703, 734*) Given that the $P_{ordered}$ for PMP22 in GPMVs was seen in this work to be nearly 0.8 means that the energy by which PMP22 favors the ordered phase over the disordered phase in GPMVs is on the order of $-RT\ln(4) = -0.8$ kcal/mol. One can easily imagine that the highly-ordered packing that occurs in ideal L_O phases (but only to a much lesser degree in GPMVs) would need to be disrupted to accommodate partitioning of a membrane protein and that this unfavorable energy contribution could easily reverse the overall energetics of partitioning in GUVs to favor the L_D phase.

3.3 PMP22 stabilizes ordered phase domains and promotes their formation

While some proteins are thought to passively associate with raft-like ordered domains, others can actively promote their formation by clustering raft components and stabilizing ordered domains.(*708, 735*) Proteins that modulate membrane order or fluidity also are capable of regulating phase separation.(*736, 737*) Here, we identify PMP22 as a new example of a protein that can directly stabilize ordered phase membrane domains.

PMP22-containing GPMVs exhibited a higher T_{Misc} than GPMVs containing unstable L16P PMP22, tgLAT, or cells transfected with an empty vector (**Fig. 35A-B**). That phase separation persists at higher temperatures in GPMVs containing PMP22 suggests that this protein can directly stabilize ordered phase membrane domains.(*695*) This is consistent with previous results from studies of *pmp22 -/-* mice showing that the distribution of molecules typically associated with ordered phase membrane domains (such as cholesterol, and GM1 ganglioside) are decreased at the plasma membrane.(*714*) Moreover, Schwann cells isolated from these mice showed elongation and migration defects that could be corrected by external supplementation of the culture medium with cholesterol. Additionally, our results suggest that PMP22 is able to promote ordered domain formation. We showed that GPMVs containing PMP22 had ordered membrane domain circumferences on average ~5 μm larger than those in GPMVs without PMP22 or unstable L16P PMP22 (**Fig. 35C**). This may be due to an increased concentration in cholesterol in PMP22-containing GPMVs since it has recently been shown that PMP22 regulates cholesterol PM trafficking (*36*). It seems likely that the mechanisms underpinning this regulatory function of PMP22, as well as its ability to promote ordered phase formation, is closely related to its preference to partition into ordered membrane phase domains.

4. Conclusions

We have documented PMP22 as the first multispan helical membrane protein to exhibit a preference to partition into the ordered phase of cell-derived GPMVs. This phase preference appears to be closely linked to the formation of correct tertiary structure of the protein. Additional experiments will be required to determine exactly what features of its folded structure confer its preference for the ordered phase. Moreover, it remains unclear just how many other multispan helical membrane proteins will share the phase domain preference of PMP22 and whether they will resemble PMP22 in terms of driving traits. It is hoped that the results of this work will inspire future studies to address these issues.

Chapter V. Direct Relationship Between Increased Expression and Mistrafficking of the Charcot-Marie-Tooth-Associated Protein PMP22

Chapter V was adapted with permission from one of my previously published journal articles. (*738*)

1. Introduction

Charcot-Marie-Tooth disease (CMT) is an eponym for a large range of related neuropathies that occur with a prevalence of ~1:2500 in the human population.(*601, 635*) Patients with CMT suffer from a range of symptoms including impaired tendon reflexes, weakness of the distal musculature, abnormalities of the peripheral nerve axon and its adjacent myelin sheath and, in severe cases, confinement to a wheelchair.(*635, 739-741*) Over two-thirds of CMT cases result from mutations in the *PMP22* gene, including the most common form of the disease (CMT1A).(*742*) CMT1A is linked to a heterozygous duplication of chromosome fragment 17p11.2-12, resulting in the production of a third copy of the *PMP22* allele (trisomy). While 9 other proteins are also overexpressed in this process, it has been shown that CMT1A is caused by the additional copy of *PMP22*.(*601, 635, 743*) Whether the disease arises from an absolute increase in protein expression or resulting fluctuations in levels of PMP22 is up for debate; however, it is clear that increasing the copy number of *PMP22* in rodents results in pathological phenotypes similar to those observed in patients with CMT1A.(*530, 743, 744*) Deletion of a *PMP22* allele *(WT/null* conditions*)* and genetically dominant point mutations in PMP22 also result in forms of CMT.(*635, 742*)

PMP22 encodes a tetraspan integral membrane protein, PMP22, comprising 2-5% of the protein content in compact myelin of the PNS.(*712, 745*) The specific biological functions of PMP22 are still under investigation; however, substantial evidence suggests that it plays a structural role in the maintenance and development of compact myelin.(*635*) Indeed, when PMP22 is reconstituted into lipid bilayers, it is sufficient to induce wrapping of the membranes to produce myelin-like-assemblies.(*625*) However, PMP22 has also been implicated in a number of other processes within myelin-producing Schwann cells.(*601, 604, 635, 684, 714, 715*) *In vitro* studies revealed that PMP22 is only modestly stable in detergent micelles, with the native conformation favored over the denatured ensemble by only 1.5 ± 0.1 kcal mol^{-1}.(*1, 197*) That the folded form is

marginally stable appears to be directly related to why only ~20% of synthesized wild type (WT) protein is able to fully mature and traffic to the plasma membrane (PM).(*1, 639, 746*)

Why a third copy of *PMP22* results in neuropathy is not clearly established. Patients afflicted with CMT1A present slowed nerve conduction velocity and axonal loss, accompanied by a shortening of internodal length.(*635*) Beyond these morphological changes in compact myelin, overexpression of PMP22 has also been shown to cause Schwann cell apoptosis.(*747, 748*) Mouse models with multiple copies of WT *PMP22* or expressing disease mutant forms of PMP22, as well as CMT1A patient-derived dermal fibroblasts, display the presence of cytosolic PMP22 aggregates coinciding with a decrease in proteasomal activity.(*530, 604, 607, 635, 749*) Under normal conditions, PMP22 that is not able to mature beyond the endoplasmic reticulum (ER) is removed from the membrane by ER quality control and degraded in the cytosol via proteosomal and/or lysosomal pathways.(*607*) One hypothesis for CMT1A pathology is that under normal conditions expression of *PMP22* occurs at levels that approach saturation of the ER protein folding quality control system, such that introduction of a third copy of *PMP22* overwhelms the system leading to ER stress and accumulation of cytotoxic aggregates. This is supported by the fact that stimulation of autophagy leads to increased degradation of such aggregates and improved myelination in cultures and in mice.(*750, 751*) In this work, we quantitatively examine the question of whether increased expression of PMP22 in model cell lines results in increased formation of intracellularly-trapped protein and a decrease in PM trafficking efficiency.

2. Results

2.1 Measurement of PMP22 Trafficking Efficiency

For this study we used a previously described single-cell flow cytometry-based assay that quantitates the levels of both PM and intracellular PMP22.(*1*) Because the fusion of fluorescent reporter proteins to PMP22 has been shown to cause intracellular retention and aggregation, we inserted a c-myc epitope tag into the 2nd extracellular loop of the protein (**Fig. 37A**). This modification has been shown not to affect protein function or turnover.(*1, 722*) In our experimental workflow, PMP22-expressing cells are harvested and fixed followed by incubation with a myc antibody conjugated to phycoerythrin (PE), which labels surface-expressed PMP22 (properly trafficked, mature PMP22). Following a wash step, cells were permeabilized and internal PMP22 (misfolded PMP22 plus a likely small population of actively folding/trafficking protein) was labeled with the

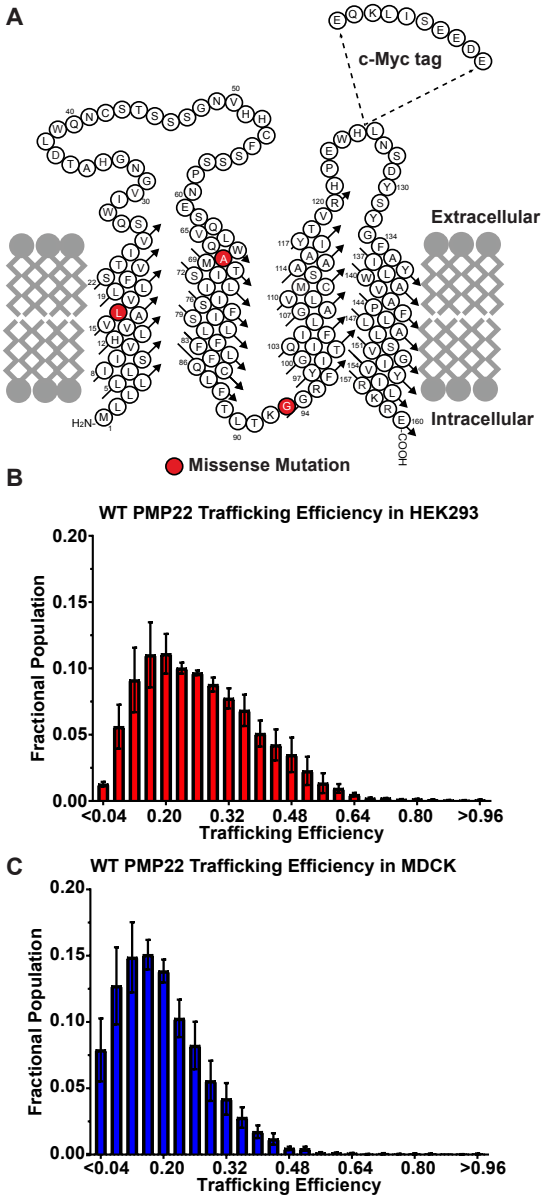

Figure 37. WT PMP22 Trafficking Efficiency

(A) Cartoon topology diagram of PMP22 in a membrane. The c-myc tag is shown where it was inserted into the sequence. Disease variant sites for mutants examined in this study are highlighted in red. **(B)** Population distribution of WT PMP22 trafficking efficiency measured in individual, transiently-transfected, HEK293 cells or (**C**) in Marine-Darby-Kidney (MDCK) cells, each from three independent biological experiments with 2500 cells measured per replicate. Fractional populations for each bin were calculated for each replicate and the mean ± SEM is shown. Data for (C) was obtained by re-analyzing a data set originally reported in (*17*).

same anti-myc antibody but this time conjugated to AlexaFluor647 (AF647). Surface and internal concentrations of PMP22 in single cells were then quantified using flow cytometry with fluorimetric detection. Fluorescent intensities of the two fluorophores were normalized by fixing and permeabilizing a population of PMP22 expressing cells, splitting the population in two, and labeling each half with only one antibody.

This experimental setup was used to measure WT PMP22 trafficking efficiency in transiently transfected HEK293 cells. We define trafficking efficiency as the fraction of PMP22 localized to the PM compared to the total PMP22 in the cell (= PM Intensity/(PM Intensity + Internal Intensity)). Efficiency can vary from 0.0 (all PMP22 is intracellular) to 1.0 (all PMP22 is found at the PM). In three biological replicates, interrogating 2500 individual HEK293 cells per experiment, we found that WT PMP22 traffics to the PM with a mean trafficking efficiency of 0.27 ± 0.01 (Mean ± 95% Confidence Interval; **Fig. 37B**).

We pooled the 7500 cells and binned them according to their trafficking efficiencies in bin sizes of 0.04 efficiency units (**Fig. 37B**). A population analysis of the cells revealed a left-skewed gaussian distribution centered around 0.2 corresponding with previously measured PMP22 trafficking efficiencies. We also reanalyzed previously reported data collected using the same experimental setup in Madin-Darby Canine Kidney (MDCK) cells(*17*). As shown in **Fig. 37C**, we observed a similar population distribution of trafficking efficiencies, but the curve is left-shifted relative to HEK293 and the mean trafficking efficiency (0.17 ± 0.03) is lower.

2.2 WT PMP22 Trafficking Efficiency as a Function of Total Expression

Normalized, background-corrected, total relative fluorescent intensity (RFU) of PMP22, corresponding to total cellular PMP22, ranged from roughly 50 to 125,000 RFU in individual HEK293 cells. In **Fig. 38A** we grouped measurements into 10 equal sized bins (750 cells per bin) based on total single-cell expression of PMP22 and plotted mean trafficking efficiency in each bin. We observed a concentration-dependence wherein increased

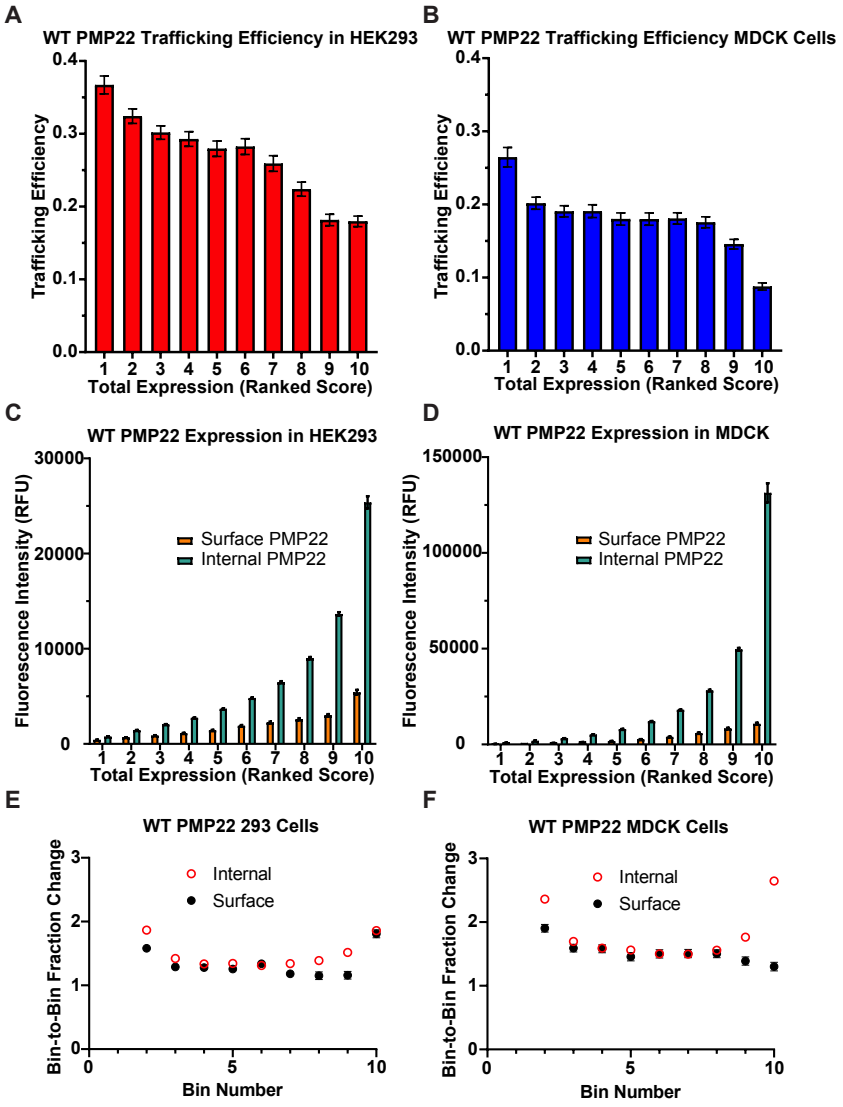

Figure 38. Relationship Between WT PMP22 Trafficking Efficiency and Expression

WT PMP22 trafficking efficiency in individual cells versus total PMP22 expression. PMP22 trafficking efficiency was measured for each of 7500 individual **(A)** transiently-transfected HEK293 cells or **(B)** transiently-transfected MDCK cells, each from three independent biological replicates. Cells were placed into 10 bins representing 750 cells each based on total PMP22 expression. The mean trafficking efficiency ± 95% confidence interval (CI) is plotted for each bin. Data for (B) was obtained from a data set originally reported in (*17*). **(C and D)** Trafficking efficiency values plotted in (A and B) were deconvoluted and the mean levels of cell surface PMP22 (orange) and of internal PMP22 (green) ± 95% confidence interval (CI) are plotted for each bin. **(E and F)** The fraction change of relative fluorescence between each bin (bin 2/bin1, bin 3/bin2…bin10/bin 9) was calculated for both cell surface (black circles) and internal (open red circles) PMP22 shown in C and D. Mean fraction change is reported ± 95% confidence interval (CI) (for values with no visible error bars the error was too small to be represented by bars).

expression leads to decreased trafficking efficiency. This data is interesting in light of the common CMT1A phenotype in which overexpression of PMP22 causes disease. To ensure that this observation was not cell line dependent, we performed the same analysis on data from MDCK cells.(*1*) MDCK cells also displayed decreased PMP22 trafficking efficiency at high total expression levels(**Fig. 38B**).

We next deconvoluted our data to examine the concentration-dependence of PM and intracellular populations of PMP22. For both cell lines, as the amount of total PMP22 increases, both internal and PM PMP22 increases (**Fig. 38C-D**). **Fig. 38E-F** quantitate the bin-to-bin changes in internal and surface PMP22. For both HEK293 and MDCK cells there is an initial (bin 1 to bin 2) jump in internal protein, followed by a plateau of steady increase where the bin to bin growth rate (measured as the fraction of mean protein expression in the two bins) is the same for both internal and surface PMP22 population. The growth of the internal PMP22 population increases at higher total expression levels, with the growth of the PM population remaining constant (MDCK cells) or increasing only between bins 9 and 10 (HEK293 cells). In total, **Fig. 38** shows that PMP22 trafficking efficiency decreases as total expression increases. The burden of trapped PMP22 in the cell increases disproportionately relative to the growth of the PM population of the protein.

2.3 Trafficking Efficiency for PMP22 Disease Mutants as a Function of Total Expression

Trafficking efficiency versus total expression was examined for three disease-causing PMP22 variants: L16P, A67T, and G93R. The L16P mutation, which results in the “Trembler-J” mouse phenotype, causes severe demyelination and consequent disease. G93R causes moderate demyelination and moderate CMT, while A67T causes a mild form of demyelination and a phenotype known as hereditary neuropathy with liability to pressure palsies (HNPP).(*635, 742*) The trafficking results for these three mutants are shown in **Figures 39A-**

C. **Fig. 40** breaks down surface versus internal levels of the three mutants as a function of total expression.

Fig. 39D shows that the average per-cell total expression levels for each mutant and for WT are comparable.

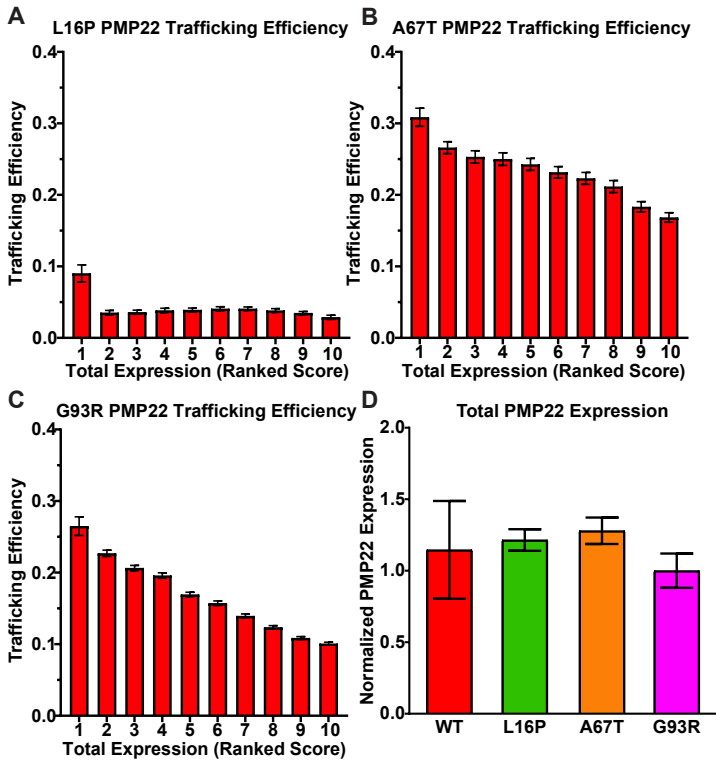

Figure 39. Relationship Between L16P PMP22 Trafficking Efficiency and Expression

Trafficking efficiencies for **(A)** L16P, **(B)** A67T, and **(C)** G93R, were calculated in each of 7500 individual HEK293 cells from three independent biological replicates and placed into 10 bins of 750 based on total PMP22 expression. The mean trafficking efficiency ± 95% confidence interval (CI) is plotted for each bin. **(D)** The mean total expression ± 95% confidence interval (CI) of transiently transfected cells expressing WT, L16P, A67T, and G93R PMP22 from three independent biological replicates is shown normalized to the expression of WT PMP22 in each replicate.

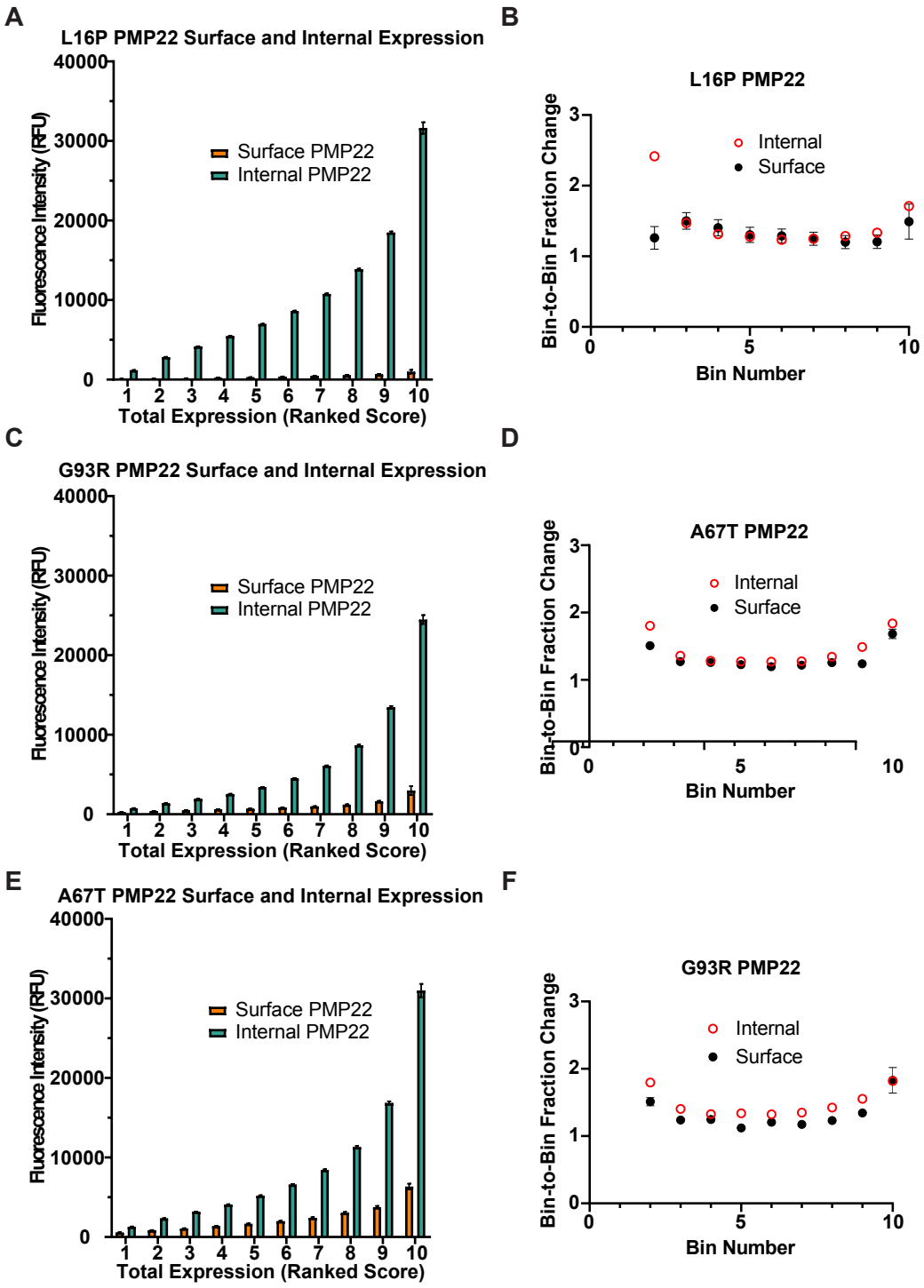

Figure 40. Deconvolution of CMTD PMP22 Trafficking Data

Trafficking efficiency values plotted in **Figure 39** were deconvoluted and the mean levels of cell surface PMP22 (orange) and of internal PMP22 (green) ± 95% confidence interval (CI) are plotted for each bin **(A)**, A67T **(C)** and G93R **(E)** PMP22. **(B, D, and F)** The fraction change of relative fluorescence between each bin (bin 2/bin1, bin 3/bin2…bin10/bin 9) was calculated for both cell surface (black circles) and internal (open red circles) PMP22 shown in A, C, and E. Mean fraction change is reported ± 95% confidence interval (CI) (for values with no visible error bars the error was too small to be represented by bars).

For L16P PMP22 the most precipitous decrease in trafficking efficiency was seen from bin 1 to bin 2 (**Fig. 39A** and **Fig. 40A-B**). This suggests that the pathway for productive folding and trafficking of L16P PMP22 is relatively efficient at very low total expression levels. After bin 1, the surface trafficking efficiency is reduced to roughly 3%, where it remains over a wide range of total expression levels. The data for A67T and G93R (**Fig. 39B-C** and **Fig. 40C-F**) is similar to that of WT PMP22 in that the highest trafficking efficiency for these mutants occurs at the lowest levels of total expression and trafficking efficiency gradually decreases as total expression increases. As for WT, the fractional growth of internal PMP22 population is usually higher than for the PM population at the initial bin 1-to-2 transition and also for the later bins (**Fig. 40B, 40D, 40F**).

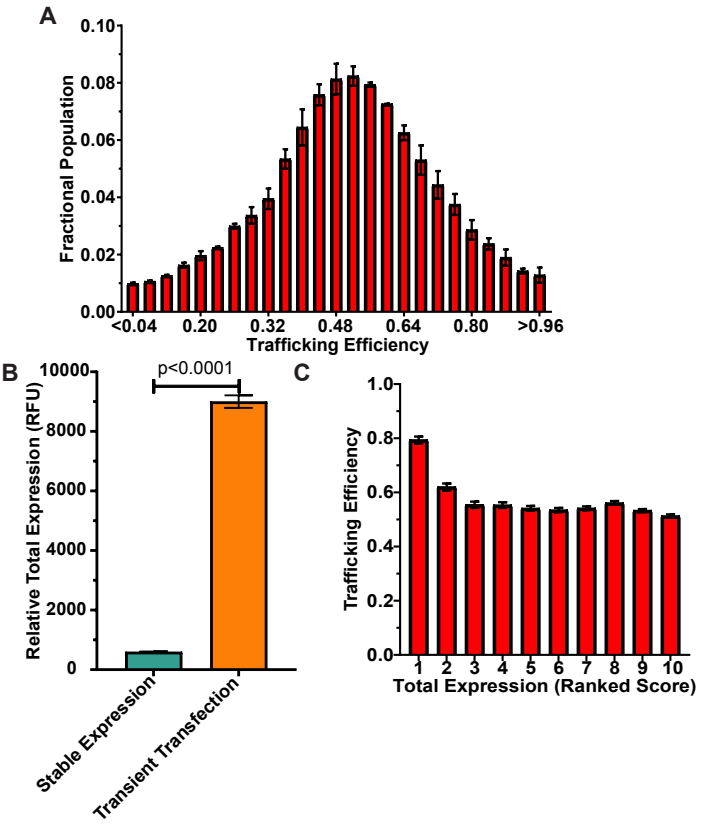

Figure 41. Trafficking efficiency for HEK293 cells stably expressing WT PMP22

(A) Population distribution of WT PMP22 trafficking efficiency measured in individual cells from two independent biological experiments with >11,000 cells measured per replicate. Fractional populations for each bin were calculated for each replicate and the mean ± SEM is shown. For comparison to transiently transfected HEK293 cells see **Fig. 1B**. **(B)** Average total expression (mean ± 95% CI) of WT PMP22 (calculated as RFU) in 22,960 individual HEK293 cells stably expressing WT PMP22 from two biological replicates (aqua) and 7500 individual HEK293 cells that were transiently transfected (three biological replicates, orange). Student's t-test was used for statistical analysis. Fractional populations for each bin were calculated for replicate and the mean ± SEM is shown. **(C)** PMP22 trafficking efficiencies for the 22,960 individual WT PMP22 stable expressor cells were placed into 10 bins of 2296 cells each based on total PMP22 expression levels. The mean trafficking efficiency ± 95% CI is plotted for each bin.

2.4 PMP22 Trafficking Efficiency Under Conditions of Stable Expression

In the above experiments, transient transfection was used to express PMP22 in HEK293 and MDCK cells. This process results in high levels of PMP22 expression. In contrast, stable expressor cell lines, which involve stable integration of plasmid DNA into the host cell genome, generally result in lower protein expression per cell.(*752*) To examine PMP22 trafficking under these conditions we generated HEK293 cells that stably expressed myc-tagged WT PMP22.

In **Fig. 41A**, we measured WT PMP22 PM and internal expression in single cells and plotted the population distribution of PMP22 trafficking efficiencies. The mean trafficking efficiency was higher (0.57 ±

0.01) and the population distribution was significantly different ($p<0.05$) than in transiently transfected cells (distribution compared using a pairwise Kolmogorov-Smirnov test).(*753*) **Fig. 41B** shows that the average per cell expression of PMP22 in our stable cell line was significantly lower than in transiently transfected cells. These results further support the idea that lower PMP22 expression leads to higher trafficking efficiency.

We binned WT PMP22 stable cell trafficking data as described above, splitting the data into 10 equal sized bins based on the total PMP22 expression in each cell (~2200 cells per bin). **Fig. 41C** shows that as total expression increases, there is an initial reduction in trafficking efficiency from about 80% at very low total PMP22 to about 55%, where it remains fairly constant over the remainder of the bins.

3. Discussion

WT PMP22 is overexpressed in the most common form of CMT disease, CMT1A. This has led to interest in the possibility that misfolded, non-degraded, PMP22 is a source of cytotoxicity contributing to disease etiology.(*604, 607, 611, 651*) Here, we examined expression of PMP22 in both transiently-transfected model cell lines and in stable cells. It should be considered that PMP22 expression in myelinating Schwann cells may be better modeled by the results from the higher expressing transiently-transfected cells (**Fig. 41B**). In myelinating Schwann cells, PMP22 is expressed at very high levels. *PMP22* is under the control of a powerful transcriptional system that utilizes two promotors, P1 and P2, and a super-enhancer upstream of P1.(*743*) Most cell types only express transcripts using P2 and consequently express only low levels of PMP22, whereas Schwann cells utilize both promotors to drive higher PMP22 expression. Transcription factor binding and open chromatin markers were found to be much more abundant at the PMP22 super-enhancer in myelinating Schwann cells compared to oligodendrocytes.(*754*) Furthermore, deletion of this super-enhancer in a Schwann cell line dramatically reduced PMP22 transcripts.(*755*) Under conditions of CMT1A trisomy, in which the super-enhancer and promotors are also duplicated, the level of expressed PMP22 may be even higher. We therefore argue that the results in transiently-transfected cells are more revealing than the results from stable cells.

Large populations of transiently transfected HEK293 and MDCK cells exhibited average WT PMP22 trafficking efficiencies in the vicinity of 0.20, which is what was previously documented for Schwann cells.(*639, 746*) It is notable, that the average trafficking efficiency in MDCK cells (0.17) is lower than in HEK293 cells (0.27). We

suggest that this is because the average expression level of PMP22 in MDCK cells is higher than in HEK293 cells, leading to increased misfolding (**Fig. 38C-D**). This is supported by the fact that the trafficking efficiency in stable cells, where average total expression level is significantly lower (**Fig. 41B**), jumps to 0.57. This same trend of lower trafficking efficiency at high expression levels is seen within each population of transiently-transfected cells (**Fig. 38A-B**) and to a modest degree in the stable cells (**Fig. 41C**). For both transiently-transfected cell lines, a jump is seen in the growth of the internal PMP22 population that is disproportionately higher than for the PM population both at low and high total expression levels (**Fig. 38E-F**). Between the two extremes, the growth of the internal fraction is roughly the same as the PM fraction. This suggests complexity in terms of the cellular PMP22 folding, misfolding, and trafficking processes, complexity that is not hard to imagine given the intricacies of the ER folding quality control system.(*2*) **Fig. 38C-D** show that high level expression of PMP22 results in a considerable burden of internal protein in cells, consistent with the hypothesis that misfolding of PMP22 and subsequent failure of the misfolded protein to be degraded contributes to CMT1A. Nevertheless, it is also seen that the population of PM PMP22 continues to grow as total expression increases, such that our data are consistent with the possibility that the added expression of WT PMP22 may also result in an aberrant gain of function effect.

Results for mutant forms of PMP22, A67T (mild CMT), G93R (moderate CMT), and L16P (severe CMT) show that the efficiency profile of A67T is similar to that of WT, the profile for G93R is similar to WT (except that the decline in efficiency with increased total expression is more steep), and L16P exhibits dramatically reduced efficiency even at the lowest expression levels, with a further reduction to a low level “basin” occurring as total expression increases (**Fig. 39**). It is interesting that the total amount of internal protein seen for all three of the disease mutants is similar at the highest total expression levels, while the amount of PM protein increases dramatically for L16P<G93R<A67T. This does not imply that the loss of PM protein alone explains the differences in disease severity. CMT disease caused by heterozygous L16P/WT *PMP22* expression (Dejerine-Sottas Syndrome, DSS) is much more severe than for WT/null patients who suffer from HNPP. The most likely explanation for this is that L16P undergoes misfolding and entrapment early in the secretory pathway of patients, and drags some of the WT protein down with it via WT/L16P heterodimerization.(*609, 651*) Consequently, the total loss in both L16P and WT forms of PMP22 is likely greater than occurs in WT/null

conditions. Thus, possible toxicity associated with the misfolded/mistrafficked protein may be compounded by the reduction in the surface-trafficked protein, leading to a more severe disease phenotype.

4. Conclusions

Previous studies have shown that PMP22 trafficking efficiency is related to the stability of its folded structure. Even WT PMP22 appears to have only marginal conformational stability(*197, 665*), which helps to explain its modest folding efficiency. Disease mutant forms of PMP22 are even less stable with mistrafficking and disease severity correlating with the degree of destabilization.(*1*) Aggregates and other misfolded forms of proteins in the ER can be recognized and removed from the ER for degradation via either proteasomal or lysosomal pathways.(*2, 607*) However, if these systems are saturated by an overabundance of misfolded protein, then that protein will accumulate—potentially becoming a source of cytotoxicity. Saturation of the membrane protein quality control machinery appears to occur when PMP22 is overexpressed.(*653*) Here, we explored the relationship between expression levels and surface trafficking efficiency of PMP22. It was found that there was a direct, negative, relationship between expression and trafficking efficiency. Moreover, reduced trafficking efficiency was due more to an increase in internal (likely misfolded) PMP22 at higher total expression levels than to reduced PM trafficking. While it has yet to be explored in tissue from CMT1A patients, the results of this work support the plausibility that the etiology of CMT1A is related to the accumulation of misfolded PMP22. Moreover, the long-term accumulation of misfolded PMP22 in Schwann cells and/or the weakened efficiency of protein degradation pathways with aging would help to explain why CMT1A is a progressive disorder.

Chapter VI. Glycosylation Limits Forward Trafficking of the Tetraspan Membrane Protein PMP22

1. Introduction

Secretary proteins and transmembrane proteins comprising over one third of the human proteome pass through the endoplasmic reticulum (ER) en route to their intracellular destination(*2, 756, 757*). For the majority of integral membrane proteins, integration into the ER membrane is intimately tied to translation. Translating ribosomes associate with the Sec61-translocon complex and thread transmembrane (TM) regions through a water exposed central pore(*329, 330, 336*). This pore contains a lateral gate allowing translocating polypeptides to sample both lipid and hydrophilic environments(*331*). Soluble secretary proteins translocate completely through the pore into the ER lumen, while TM proteins exit laterally into the ER membrane. Most membrane proteins adopt their secondary structure and attain correct membrane topology at this initial stage of assembly. Once fully synthesized, proteins are released from the translocon, diffuse away, and begin the second stage of membrane protein folding: acquiring tertiary and quaternary structure(*2, 7*). Once they are properly folded, proteins traffic beyond the ER via exit sites (ERES) to the Golgi complex and thence to their destination membrane(*756*). Proteins that fail to adopt proper structure are retained in the ER to allow additional time for folding or are targeted for degradation by the ER-associated degradation (ERAD) pathway or by ER-associated autophagy (ER-phagy)(*758*).

Protein folding in the ER is under constant surveillance by the resident ER-quality control network (ERQC)(*2, 759, 760*), which contains numerous folding sensors, chaperones, and other proteins, including those involved in ERAD and ER-phagy. Collectively, these proteins monitor, assist, and make logic decisions as to whether to retain, degrade, or authorize exit from the ER of nascent proteins. Much is known about the molecular details of this pathway for soluble proteins, but far less is understood about this process for TM proteins. In this chapter, we seek to expand our understanding of how ERQC manages quality control decision for human peripheral myelin protein 22 (PMP22).

PMP22 is a tetraspan integral membrane protein (**Figure 42A**) that is highly expressed (~2-5% by weight) in the plasma membrane (PM) of myelinating Schwann cells in the peripheral nervous system (PNS)(*712, 745*). The specific functions of PMP22 are not well-understood(*714, 719, 761*), but include a structural role for PMP22 in both the maintenance and development of compact myelin(*635*). PMP22 shares

~60% sequence similarity with claudin-15, one of the structural proteins involved in maintaining tight junctions(*608*). Moreover, when reconstituted in liposomes, PMP22 can induce flattening and wrapping of the vesicles to form myelin-like assemblies(*625*). Mutations in the *pmp22* gene, including gene duplication, gene deletion, or any one of more than 40 known single nucleotide polymorphisms, cause a range of peripheral neuropathies including Charcot-Marie-Tooth disease types 1A and E, hereditary neuropathy with liability to pressure palsies (HNPP), and Dejerine-Sottas syndrome (DSS)(*635, 742*). For the sake of simplicity, we collectively refer to these peripheral neuropathies as Charcot-Marie-Tooth disease (CMTD), which together afflict ~1:2500 individuals, with 70% of cases being due to due to *pmp22* mutations (*635*). The underlying cause of the disease is due to dysmyelination of PNS nerves, which reduces nerve conduction velocity along the peripheral axons. Depending on the causative mutation, CMTD ranges in severity, with symptoms including but not limited to abnormalities of peripheral axons, impaired tendon reflexes, progressive weakness of distal musculature, muscle cramping, and abnormal gait. Patients with a severe phenotype can be disabled, confined to a wheelchair, experience chronic pain, and possibly be afflicted with blindness and loss of hearing(*739-741*). There is presently no treatment for CMTD beyond symptom management(*740*).

The most common form of CMTD (type 1A) is caused by overproduction of PMP22, due to a heterozygous duplication of chromosome fragment 17p.11−2.12, resulting in trisomy (three copies) of the *pmp22* gene(*742*). One hypothesis for why WT PMP22 overexpression causes disease is that increased production of the protein results in oversaturation of ERQC, leading to accumulation of misfolded protein and resulting toxicity and/or cell stress (*530, 738*). This seems especially plausible in light of data indicating that even under healthy conditions, PMP22 is misfolding prone, with only 20% of newly expressed protein trafficking to the cell surface(*1, 639*). Mutant forms of PMP22 are known to traffic even less efficiently than WT PMP22, consistent with fact that these forms of peripheral neuropathy are also caused by defects in PMP22 trafficking.

We have previously carried out studies to elucidate the molecular defects in PMP22 that cause it to be particularly mistrafficking-prone. Biophysical studies of PMP22 in detergent micelles revealed that the protein was modestly stable, with the folded conformation favored over the partially folded or misfolded ensemble by only 1.5 ± 0.1 kcal mol^{-1}(*1, 197*). This marginal stability likely accounts for the limited amount of protein that manages to complete folding and traffic to the PM. Disease mutant forms of PMP22 were found to be even

less stable than WT. Indeed, accompanying quantitative cell trafficking measurements for this same panel of mutants revealed linear relationships between PMP22 surface trafficking efficiency and patient nerve conduction velocities, between PMP22 stability and surface trafficking efficiency, and between PMP22 stability and patient nerve conduction velocities(*1*). PMP22-linked CTMD appears to be disease that resembles cystic fibrosis, where the vast majority of disease cases are caused by folding defects and mistrafficking(*2*){Bridges, 2018 #26). ERQC is evidently attuned to be able to assess the conformational stability of PMP22.

Exactly how PMP22 folding is handled and monitored in the ER is not well understood. Common ER-resident chaperones involved in protein folding for many soluble proteins such as the heat shock protein (HSP) 70 binding immunoglobin factor (BiP), calreticulin, or the thiol-reductase ERp57, do not appear to be important for the maturation of PMP22{Dickson, 2002 #28;Shames, 2003 #27;Jung, 2011 #29}. The lectin chaperone calnexin (CNX) has been shown to engage WT and disease variants of PMP22 (*401, 647, 762-764*). Moreover, data indicates that RER1 can retrieve disease variants of PMP22 from the Golgi complex and return it to the ER(*763*). Beyond this, little is understood about the components of ER quality control that engage nascent PMP22 to determine the balance between its forward trafficking, retention in the ER, and targeting for degradation. In this paper, we determine that N-linked glycosylation of PMP22 significantly hinders the forward trafficking of both WT and disease variants of the protein. Furthermore, we used quantitative proteomics to identify, and CRISPR/Cas9 generated knockout cell lines to confirm the role of several ERQC proteins in mediating PMP22 trafficking.

2. Results

2.1 N-Glycosylation limits PMP22 forward trafficking

PMP22, like most proteins that are inserted into the ER, is post-translationally modified via the addition of a 14-sugar complex oligosaccharide (N-glycan) comprised of two N-acetyl glucosamines, nine mannose residues, and three glucose residues arranged in a tree-like structure(*765, 766*). This glycan is added to asparagine residues within the sequence motif N-X-S/T (where X is any amino acid not proline). PMP22 contains a lone glycosylation site, located in its extracellular loop 1 (ECL1) at asparagine-41 (N41; **Figure 1A** cyan). Within the lumen of the ER, changing the identity of the N-glycan through sugar addition or removal can trigger binding and modulate the affinity of folding client proteins for a subset of folding-assistive proteins known as lectin

chaperones(*766, 767*). Previous work has shown that for PMP22 the N-glycan may play a modest role in oligomer stability (*723*) and we have recently shown that it does not affect the membrane phase preference of this protein, which is known to prefer cholesterol-rich ordered phase domains(*691*). Here we tested the impact on PMP22 trafficking of mutating N41 to a glutamine (N41Q), thereby rendering PMP22 glycosylation deficient.

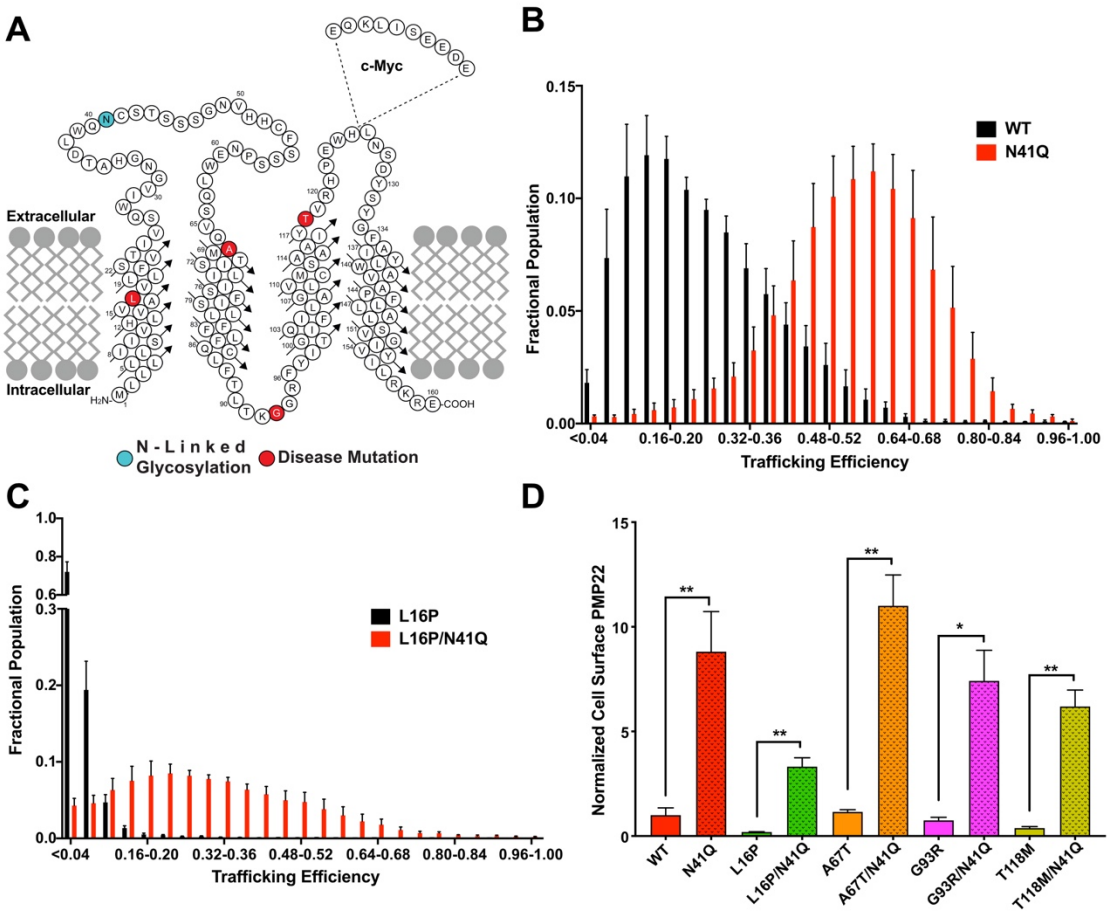

Figure 42. N-Glycosylation limits PMP22 forward trafficking

(A) Cartoon topology diagram of PMP22 in a membrane. The c-myc tag is shown where it was inserted into the sequence. Disease variant sites for mutants examined in this study are highlighted in red and the site of N-linked glycosylation is shown in cyan. (**B)** Population distribution of PMP22 trafficking efficiencies measured in individual HEK293 cells for WT (black) and N41Q (red) PMP22 and **(C)** L16P (black) and L16P/N41Q (red) PMP22. Measurements were obtained from 5 biological replicates with 2500 cells measured per replicate. Error bars represent standard deviations (SD) of the replicates. **(D)** Normalized cell surface expression of PMP22 variants and their glycosylation deficient partner. Values were obtained from 5 biological replicates with 2500 cells measured per replicate. All values were normalized to WT PMP22 cell surface expression in paired biological replicates. Error bars represent SD of the replicates. Student's t-test was used for statistical analysis. *=p<0.05, **=p<0.01.

Using a single-cell flow cytometry-based assay to directly quantitate both cell surface and internal (mistrafficked) levels of PMP22 in individual cells, we measured the trafficking efficiencies (the amount of cell surface PMP22 over total expressed PMP22) for the WT versus N41Q mutant forms PMP22 in HEK293 cells (**Figure 42B**). WT PMP22 displayed a mean trafficking efficiency of 18.6 ± 5.2% (mean ± standard deviation;

Figure 42B, black) which corroborates with previously obtained values using the same assay with Madin-Darby Canine Kidney cells and also in measurements using sciatic nerve lysates(*1, 639, 738*). Remarkably, we found that N41Q PMP22 trafficked to the cell surface with a nearly 3-fold greater efficiency, with a trafficking efficiency of 53.2 ± 6.9% (**Figure 43B**, red). We then measured the trafficking efficiency of a highly destabilized and disease-causing variant of PMP22, L16P, to see if glycosylation also affected its trafficking efficiency (**Figure 42C**). The severe CMTD L16P mutation in PMP22 causes a kink in TM1 which significantly destabilizes the protein and causes the majority of the protein to be retained intracellularly(*1, 530, 665, 768*). Our experiments reflect these previous observations as L16P PMP22 surface-trafficked with only 2.9 ± 0.9% efficiency (**Figure 42C**, black). However, if the glycosylation site is removed in this variant (L16P/N41Q) it was seen that the trafficking efficiency increased to 33.8 ± 9.0%, more than a 10-fold increase(**Figure 42C**, red).

In (*723*), the authors explored the role of N-linked glycosylation on WT PMP22 stability, oligomerization and localization. They observed no differences in PMP22 localization between the glycosylated and non-glycosylated form using cell surface biotinylation or confocal microscopy. However, the authors did note that they could have missed changes in PMP22 distribution due to the quantitative limitations of the techniques used. The trafficking assay employed in this study is highly quantitative, thus explaining why this change in PMP22 trafficking efficiency owing to N-linked glycoyslation was not previously observed.

Deconvolution of the data to look at total, internal, and cell-surface concentrations of PMP22 provides additional insight into the role of N-glycosylation in PMP22 trafficking (**Figure 42D** and **43**). For WT and all PMP22 disease variants, we noted a drastic and significant increase in cell surface expression for glycosylation-deficient variants compared to normally glycosylated isoforms (**Figure 42D**). Conversely, we noticed smaller changes in the amount of internally trapped PMP22 (**Figure 43A**) and total expression levels (**Figure 43B**) when we compared glycosylated versus non-glycosylated PMP22 variants. This data led us to hypothesize that N-linked glycosylation serves as a bottleneck in forward-trafficking of PMP22, limiting the amount of protein that reaches the cell surface.

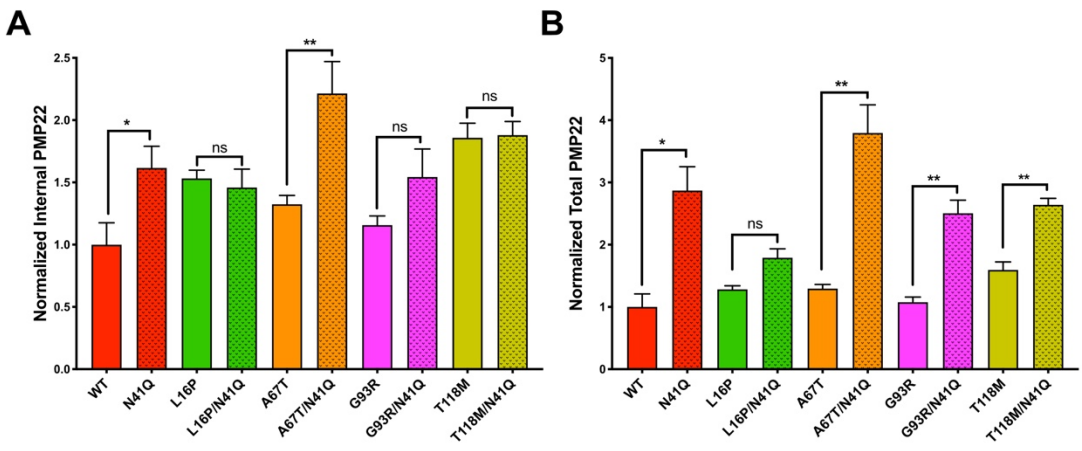

Figure 43. Normalized Internal and Total PMP22 Concentrations

Normalized **(A)** internal and **(B)** total expression of PMP22 variants and their glycosylation deficient partner. Values were obtained from 5 biological replicates with 2500 cells measured per replicate. All values were normalized to WT PMP22 cell surface expression in paired biological replicates. Error bars represent SD of the replicates. Student's t-test was used for statistical analysis. ns=not significant, *=p<0.05, **=p<0.01.

2.2 Mechanism of PMP22 Glycosylation

In light of the observation that N-linked glycosylation limits PMP22 forward trafficking, we sought to uncover the mechanism by which this modification occurs. In mammalian cells, the oligosaccharyltransferase (OST) complex catalyzes the transfer of a preassembled oligosaccharide from a dolichol pyrophosphate-linked oligosaccharide donor onto the target protein(*765, 766*). Mammalian cells express two OST complexes with different catalytic subunits (STT3A and STT3B), a shared set of non-catalytic subunits, plus some complex-specific subunits(*769*). Complexes containing STT3A (OST-A) are associated with the Sec61-translocon and catalyze canonical co-translational glycosylation as proteins are threaded into the ER from the ribosome(*770, 771*). Complexes containing STT3B (OST-B) are not associated with the translocon and catalyze glycosylation post-translationally(*771*). We sought to uncover which OST complex (OST-A or OST-B) was responsible for mediating PMP22 glycosylation.

We quantified PMP22 glycosylation via western blotting in cell lysates from HEK293 cells and from HEK293 cells in which STT3A or STT3B had been genetically knocked out using CRISPR/Cas9 (**Figure 44**)(*769*). WT PMP22 separates into three distinct bands on an SDS-PAGE gel (**Figure 44A**), where the identities of each can be confirmed via comparison with gel patterns following treatment of samples with different glycosidases. The lower band corresponds to non-glycosylated PMP22 (the band is

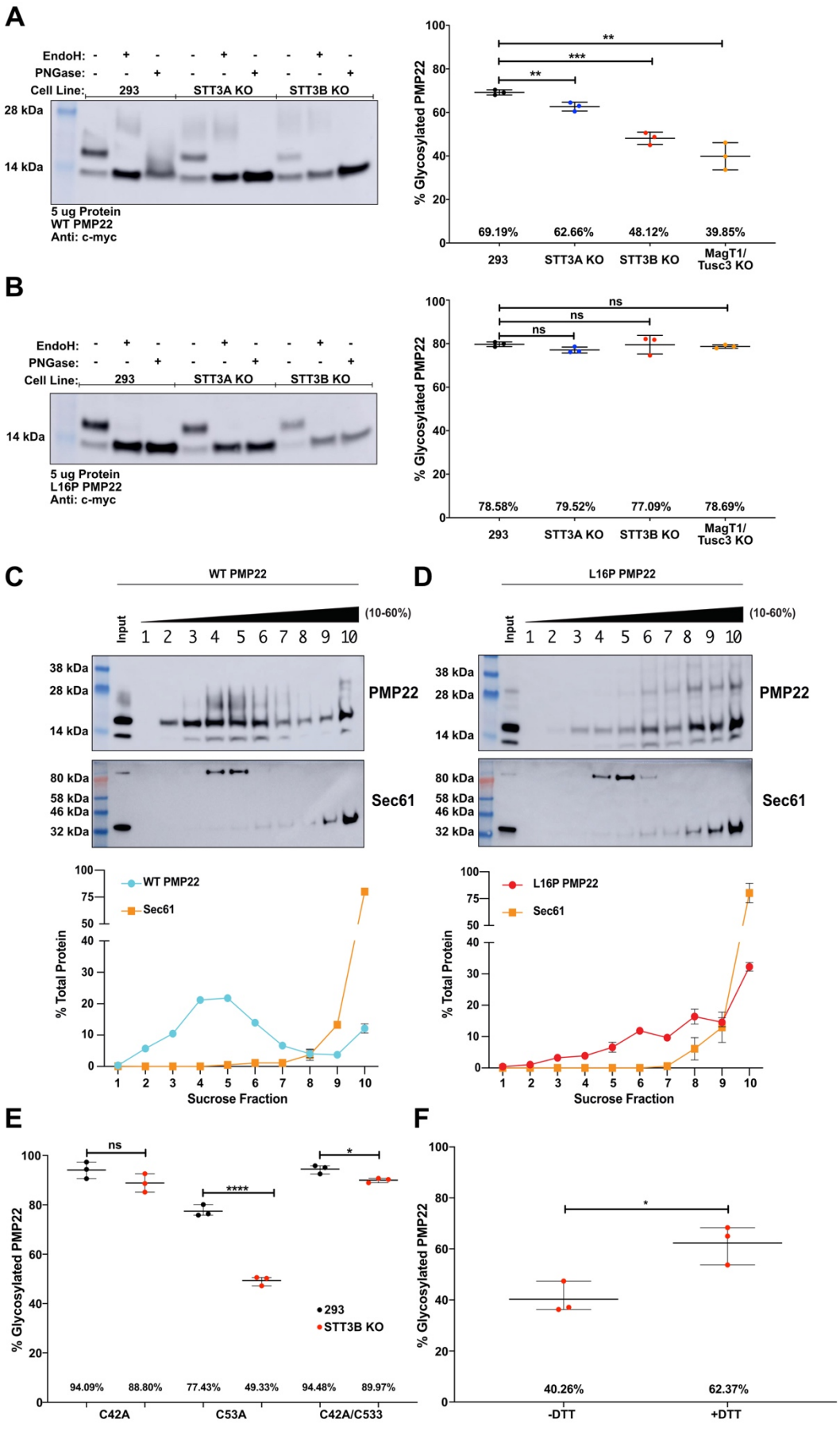
A
EndoH: - + - - + - - + -
PNGase: - - + - - + - - +
Cell Line: 293 STT3A KO STT3B KO
28 kDa
14 kDa
5 ug Protein
WT PMP22
Anti: c-myc
% Glycosylated PMP22
69.19%
62.66%
48.12%
39.85%
293
STT3A KO
STT3B KO
MagT1/ Tusc3 KO
B
EndoH: - + - - + - - + -
PNGase: - - + - - + - - +
Cell Line: 293 STT3A KO STT3B KO
14 kDa
5 ug Protein
L16P PMP22
Anti: c-myc
% Glycosylated PMP22
78.58%
79.52%
77.09%
78.69%
293
STT3A KO
STT3B KO
MagT1/ Tusc3 KO
C
WT PMP22
Input 1 2 3 4 5 6 7 8 9 10 (10-60%)
38 kDa
28 kDa
14 kDa
PMP22
80 kDa
58 kDa
46 kDa
32 kDa
Sec61
WT PMP22
Sec61
% Total Protein
Sucrose Fraction
D
L16P PMP22
Input 1 2 3 4 5 6 7 8 9 10 (10-60%)
38 kDa
28 kDa
14 kDa
PMP22
80 kDa
58 kDa
46 kDa
32 kDa
Sec61
L16P PMP22
Sec61
% Total Protein
Sucrose Fraction
E
% Glycosylated PMP22
293
STT3B KO
94.09%
88.80%
77.43%
49.33%
94.48%
89.97%
C42A
C53A
C42A/C533
F
% Glycosylated PMP22
40.26%
62.37%
-DTT
+DTT

Figure 44. Mechanism of PMP22 Glycosylation

(A, B) Western blots showing WT PMP22 **(A)** or L16P **(B)** PMP22 glycosylation in HEK293 cells, STT3A KO HEK293 cells, or STT3B HEK293 cells. Glycosidase treatments with EndoH or PNGase was used to confirm the identity of the bands. Quantified levels of glycosylated PMP22 from 3 independent biological replicates are shown on the right. Uncut western blots are shown in **Supplemental Figure 3**. **(C,D)** Sucrose density fractionation of cell lysates containing WT **(C)** or L16P (**D)**. Representative blots showing the distribution of PMP22 and Sec61 are shown with quantified levels of the two proteins from three independent biological replicates shown below. **(C)** Quantified levels of glycosylated C42A, C53A, or C42A/C53A PMP22 in HEK293 (black) or STT3B KO HEK293 (red) cells from three independent biological replicates. **(F**) Quantified levels of glycosylated WT PMP22 in STT3B KO HEK293 cells that were either not treated or treated with 2 mM dithiothreitol (DTT) for 2 hours prior to cell lysis. All error bars represent standard deivation and if not shown were too small to be visualized. Students t-test was used for all statistical analyses. ns=not significant, *p<0.05, **p<0.01, ***p<0.001, ****p<0.0001.

unchanged upon treatment with glycosidases), the middle band corresponds to ER-resident PMP22 (as identified by its disappearance upon treatment with EndoH), and the top smear corresponds to post-ER PMP22 (as identified by its resistance to EndoH and disappearance upon treatment with PNGase). Quantification of the fraction of PMP22 that is glycosylated in these cell lines from three independent biological replicates revealed that 69.2 ± 1.2% (mean ± standard deviation) of total WT PMP22 is glycosylated in HEK293 cells, 62.7 ± 2.0% is glycosylated in STT3A knock-out (KO) cells, and 48.1 ± 2.5% is glycosylated in STT3B KO cells (**Figure 44A**). These results suggest that while both OST complexes are able to glycosylate WT PMP22, post-translational glycosylation mediated by OST-B appears to be the predominant pathway as the STT3B KO cell line caused a significant loss in PMP22 glycosylation while the level of glycosylation in the STT3A KO cell line remained similar to normal HEK293 cells. To confirm this, we also quantified WT PMP22 glycosylation in MagT1/Tusc3 double KO cell lines. MagT1 and Tusc3 are accessory proteins found exclusively in the OST-B complex(*772*). In this cell line, 39.9 ± 6.2% of WT PMP22 was glycosylated, confirming OST-B as the predominate pathway of N-glycosylation for WT PMP22.

We next quantified the levels of L16P PMP22 glycosylation in these four cell lines (**Figure 44B**). In HEK293 cells 79.7 ± 1.1% of L16P PMP22 was glycosylated, 77.1 ± 1.4% was glycosylated in STT3A KO cells, 79.5 ± 4.3% was glycosylated in STT3B KO cells, and 78.7 ± 0.8% of was glycosylated in MagT1/Tusc3 double KO cells. Contrary to the results with WT PMP22, these results suggest that L16P PMP22 has no preference for glycosylation via either OST-A or OST-B. These results suggest that unlike with the WT protein, misfolding-prone CMTD variants of PMP22 can be glycosylated equally well co- or post-translationally. This suggests that for these variants of PMP22, co-translational glycosylation via OST-A plays the predominant role

in PMP22 glycosylation, since the protein will be exposed to OST-A as it is exposed in the ER lumen. OST-B may function to post-translationally glycosylate sequences that were missed via OST-A.

Why is glycosylation of WT PMP22, but not CMTD variants, sensitive to the loss of OST-B? One hypothesis is that the conformational instability of the CMTD mutants causes these proteins to remain associated with the translocation machinery, and thus in close proximity to OST-A, longer than for WT PMP22. As seen in **Figure 44A**, a significant portion of WT PMP22 is still glycosylated even in the absence of STT3B suggesting that WT PMP22 is still a substrate, albeit a suboptimal one, for OST-A glycosylation. If the CMTD variants are 'stuck' on the translocon they would be kept in close proximity to OST-A for a longer period of time than the WT protein allowing for more complete glycosylation. To test this hypothesis, we performed sucrose density fractionation of PMP22 containing-cell lysates(*773*). Western blotting was used to locate PMP22 as well as the Sec61 subunit of the translocon(*329, 330, 336, 770*) in the gradient. As seen in **Figure 44C**, WT PMP22 preferentially partitioned in fractions 3-6 with a second minor population partitioning in fraction 10. Sec61 predominantly partitioned in fractions 9 and 10 indicating that the majority of WT PMP22 is not associated with the translocon, as expected for this relatively well-folding form of the protein. **Figure 44D** shows the fractionation of L16P PMP22. Unlike WT PMP22, L16P PMP22 partitions into higher density fraction with a significant amount co-partitioning with Sec61. This suggests that more of the L16P PMP22 is 'stuck' at the translocon which could explain why its glycosylation is insensitive to STT3B KO. Thus, we propose that L16P PMP22 is insensitive to STT3B KO due to its increased association with the translocon and the accompanying OST-A complex.

The second question arising from **Figure 44A** is: why does a significant portion of WT PMP22 escape OST-A glycosylation as it is threaded into the ER lumen? It has been observed that glycosylation sequences with a cysteine residue at the N+1 position relative to the glycosylation site (-N-C-S/T sequences) tend to be skipped by OST-A(*772*). Human PMP22 contains a cysteine residue adjacent to the glycosylation site at amino acid residue 42 (C42). To test the importance of C42 in PMP22 glycosylation, we made an alanine mutation (C42A) and measured PMP22 glycosylation in HEK293 cells and STT3B KO cells. We also mutated the other solvent exposed cysteine in PMP22 to an alanine (C53A) or made double cysteine to alanine mutations (C42A/C53A). **Figure 44E** shows that like WT, the glycosylation of C53A PMP22 is sensitive to the loss of the OST-B complex leading to a reduction in glycosylation (77.4 $\pm$ 2.3% glycosylated in HEK293 cells and 49.3 $\pm$

1.9% glycosylated in STT3B KO cells). This suggests that C53A PMP22 is still predominately glycosylated post-translationally via OST-B. However, in the single C42A or double C42A/C53A PMP22 mutants, glycosylation was no longer sensitive to STT3B KO. C42A PMP22 was glycosylated 94.1 ± 3.4% in HEK293 cells and 88.8 ± 3.7% in STT3B KO cells while C42A/C53A PMP22 was glycosylated 94.5 ± 1.7% in HEK293 cells and 90.0 ±0.9 % in STT3B KO cells. This data suggests that these mutants can now be glycosylated via OST-A. Interestingly, C42A and C42A/C53A PMP22 had higher levels of glycosylation in HEK293 cells than WT PMP22 implying that the C42 makes PMP22 a suboptimal substrate for STT3A glycoyslation.

Structural studies comparing OST-A and OST-B complexes do not show significant differences in the active sites that could explain the differences in substrate specificity(*774*). We hypothesized that the redox state of C42 may be responsible for making PMP22 a suboptimal substrate for OST-A. To test this hypothesis, we measured PMP22 glycosylation in STT3B KO cells that had been treated with small amounts (2 mM) of the reducing agent dithiothreitol (DTT) for 2 hours prior to cell lysis (**Figure 44F**). This short treatment is not long enough to induce changes in the ER proteome due to activation of the unfolded protein response(*775*). We observed an increase in PMP22 glycosylation in STT3B KO cells from 40.3 ± 6.2% in untreated cells to 62.4 ± 7.7% in cells treated with DTT. While this short treatment did not restore the levels of WT PMP22 glycosylation to that observed in HEK293 cells (**Figure 44A**) it did cause a significant increase. This result combined with that observed in Figure 2E suggest that the efficiency of N-glycosylation of WT PMP22 by OST-A is dependent on the thiol redox potential of the lumen of the ER.

2.3 PMP22 Trafficking in Response to Loss of Glycosylation Machinery

We next tested what happens to PMP22 trafficking when specific mechanisms of glycosylation were inhibited. To explore this, we measured PMP22 trafficking in STT3A and STT3B KO cell lines. Additionally, we measured PMP22 trafficking under conditions in which one or both complexes were inhibited pharmacologically 24 hours prior to the experiment. NGI-1, a partial inhibitor of both STT3A and STT3B(*776*), reduced WT PMP22 glycosylation to 11.9 ± 0.5% (**Figure 45**). Whereas C19, a specific inhibitor of STT3B(*777*), reduced WT PMP22 glycosylation to 47.5 ± 2.1%, similar to what was observed in the STT3B KO cells (**Figure 45**).

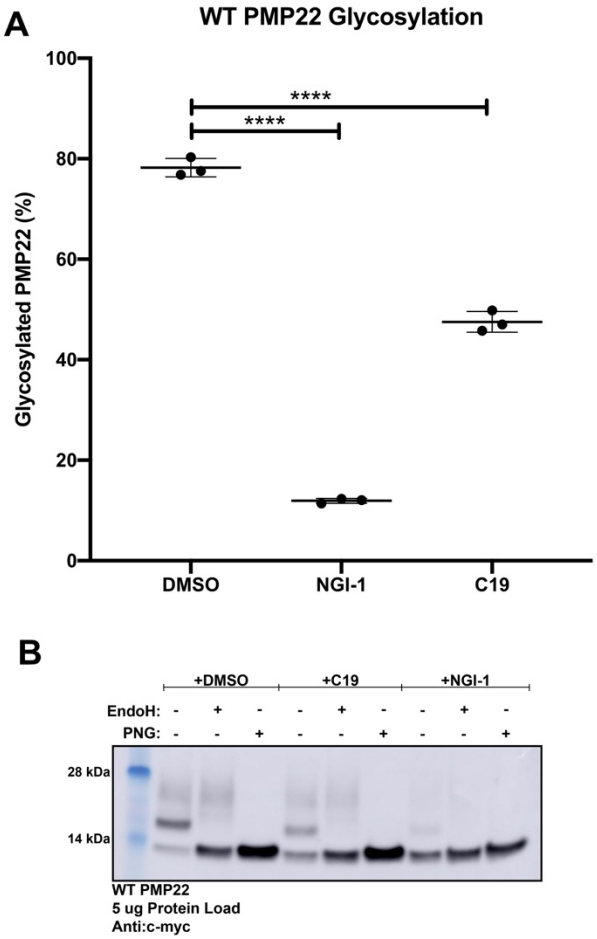

Figure 45. WT PMP22 Glycosylation with OST Inhibitors

(A) Quantification of the levels of WT PMP22 glycosylation from three biological replicates from lysates obtained from cells that had been treated for 24 hours with either DMSO, 10 μM NGI-1, or 10 μM C19. Error bars represent standard deviation. **(B)** Representative Western blot showing the levels of WT PMP22 glycosylation from lysates obtained from cells that had been treated for 24 hours with either DMSO, 10 μM NGI-1, or 10 μM C19. ****=p<0.0001 using student's t-test.

In **Figure 46** we measured PMP22 trafficking efficiencies under these various conditions. All efficiency values were normalized relative to WT PMP22 in either untreated HEK293 cells (experiments with STT3A or STT3B KO cells) or in HEK293 cells treated with DMSO (experiments with NGI-1 or C19) in paired experiments. As expected, STT3A KO had no effect on WT PMP22 trafficking efficiency, confirming its minor role in mediating WT PMP22 glycosylation. However, in STT3B KO cells WT PMP22 exhibit a 1.59 ± 0.34-fold increase (mean ± standard deviation) in trafficking efficiency. Treatment of HEK293 cells with NGI-1 further increased WT PMP22 trafficking efficiency 2.5 ± 0.2-fold over untreated cells, similar to the trafficking efficiency of N41Q PMP22.

Treating cells with the STT3B specific inhibitor, C19, caused a 1.66 ± 0.03-fold increase over untreated cells. WT PMP22 exhibited a significant increase in trafficking efficiency in cells treated with C19 or in STT3B KO cells, but not in STT3A KO cells, confirming that OST-B is the major facilitator of WT PMP22 glycosylation.

Since N41Q PMP22 is not glycosylated we expected no changes in trafficking efficiency under any of these conditions. As predicted, none of these experimental conditions significantly altered the trafficking efficiency of N41Q PMP22 (**Figure 46**). This result serves as an internal control for our experiments showing that neither OST KO cell line nor pharmacological inhibition of OST caused global changes in protein folding quality control and trafficking efficiency.

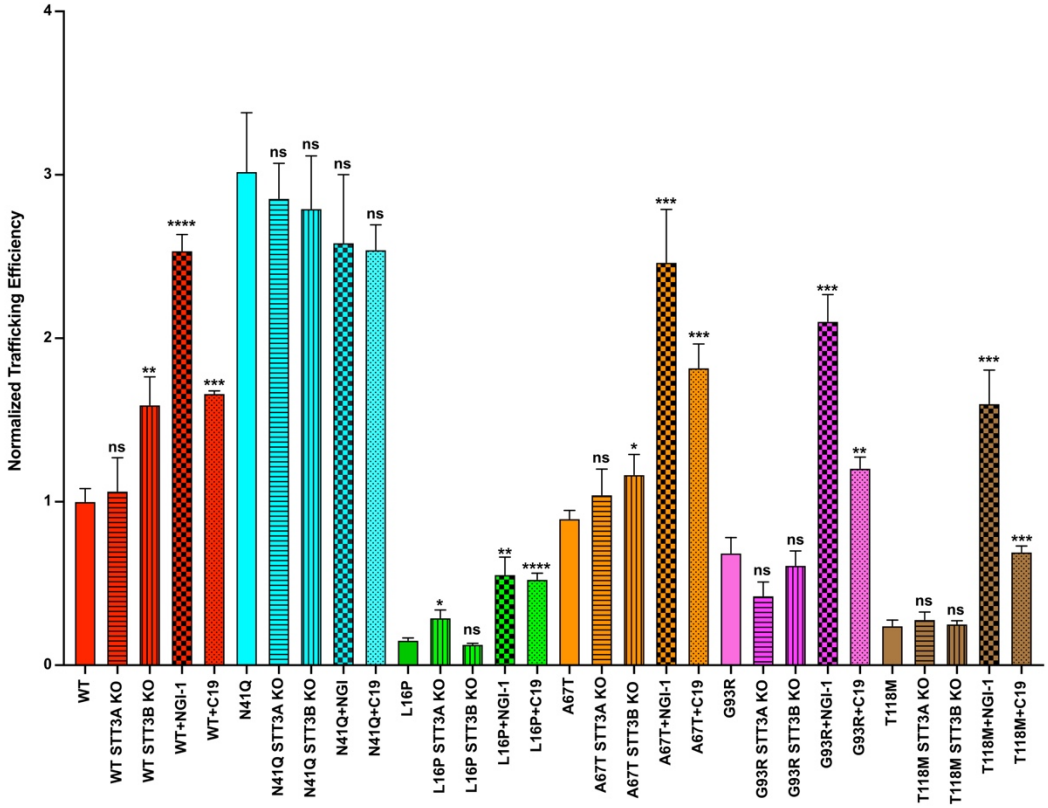

Figure 46. PMP22 Trafficking Efficiencies with Glycosylation Inhibition

Normalized trafficking efficiencies of PMP22 variants in HEK293 cells (solid color), STT3A KO HEK293 cells (horizontal stripes), STT3B KO HEK293 cells (vertical stripes), HEK293 cells treated for 24 hours with 10 μM NGI-1 (checkered) or HEK293 cells treated for 24 hours with 10 μM C19 (dots) from three independent biological replicates. All efficiency values were normalized to WT PMP22 trafficking in untreated HEK293 cells in paired biological replicates. Error bars represent SD. Student's t-test was used to compare the trafficking efficiencies in untreated cells to that in KO cell lines or in cell lines treated with the inhibitors. ns=not significant, *p<0.05, **p<0.01, ***p<0.001, ****p<0.0001.

Global inhibition of OST via NGI-1 caused increases in trafficking efficiency for all CMTD PMP22 variants studied (**Figure 46**). However, neither STT3A nor STT3B KO cell lines dramatically altered the trafficking efficiencies of these variants. This makes sense in light of the data in **Figure 44** which shows that KO of either STT3A or STT3B did not reduce the glycosylation levels of these CMTD variants to the same extent as WT PMP22. Interestingly, pharmacological inhibition of STT3B with C19 caused an increase in PMP22 trafficking efficiencies of all three CMTD mutants. This leaves open the possibility that all PMP22 variants are predominately glycosylated post-translationally via STT3B. The generation of clonal KO cell liens can cause selective pressure for cells to adapt to the loss of the KO gene and it is possible that the STT3B KO cell lines adapted by expressing more STT3A. Pharmacological inhibition does not apply the same selective pressure as generating CRISPR KO cells and may therefore be a better model. Our data suggests that a

significant fraction of PMP22 is glycosylated post-translationally by STT3B and inhibition of this process, either genetically or pharmacologically, increases PMP22 trafficking efficiency.

2.4 Identification of Novel PMP22 Interactors

We next set out to uncover proteins responsible for limiting or promoting PMP22 trafficking. Prior to this work, the only ERQC proteins that have been experimentally shown to interact with PMP22 have been CNX and RER1(*401, 762-764*). In order to discover novel PMP22 interactors, we turned to co-immunoprecipitation (co-IP) and liquid chromatography-mass spectrometry/mass spectrometry (LC-MS/MS) based proteomics. We expressed myc-tagged WT and selected mutant forms of PMP22 in HEK293 cells, immunopurified the protein using magnetic beads conjugated to myc antibodies under gentle lysis conditions and used shotgun proteomics to identify proteins that immunopurified with PMP22. We used tandem mass tag (TMT) labeling in order to quantitatively compare interactions across multiple samples. We compared interactions with WT PMP22 versus N41Q PMP22 to uncover glycosylation specific interactions, and WT versus L16P PMP22 to uncover interactions dependent on protein stability. Proteins co-purified with tagged PMP22 were compared to proteins that were co-purified from a 'MOCK' lysate (cells expressing untagged PMP22). **Figure 47** displays examples of the identified interactions that came out of our screen.

Overall, we identified 56 unique proteins that appear to interact with WT PMP22 (either directly or indirectly; **Figure 47A**). Additionally, 27 and 21 unique proteins appear to interact with N41Q and L16P PMP22 respectively. In all cases putative interactors were observed at levels with a $\log_2$ fold change >0.5 over MOCK conditions and were identified in multiple biological replicates and had a p-value<0.1. We then used the DAVID bioinformatic database to group these interactions based on GO_terms and composed the diagram shown **Figure 47B** to visualize interactions known to be involved either in protein biogenesis or quality control(*778, 779*). The table is organized temporally with respect to the start of biogenesis at the transcolon, with interactions predicted to occur earlier in PMP22 biogenesis shown at the top (Insertion and N-linked Glycosylation) and with interactions expected to occur later (Plasma Membrane Associated) shown at the

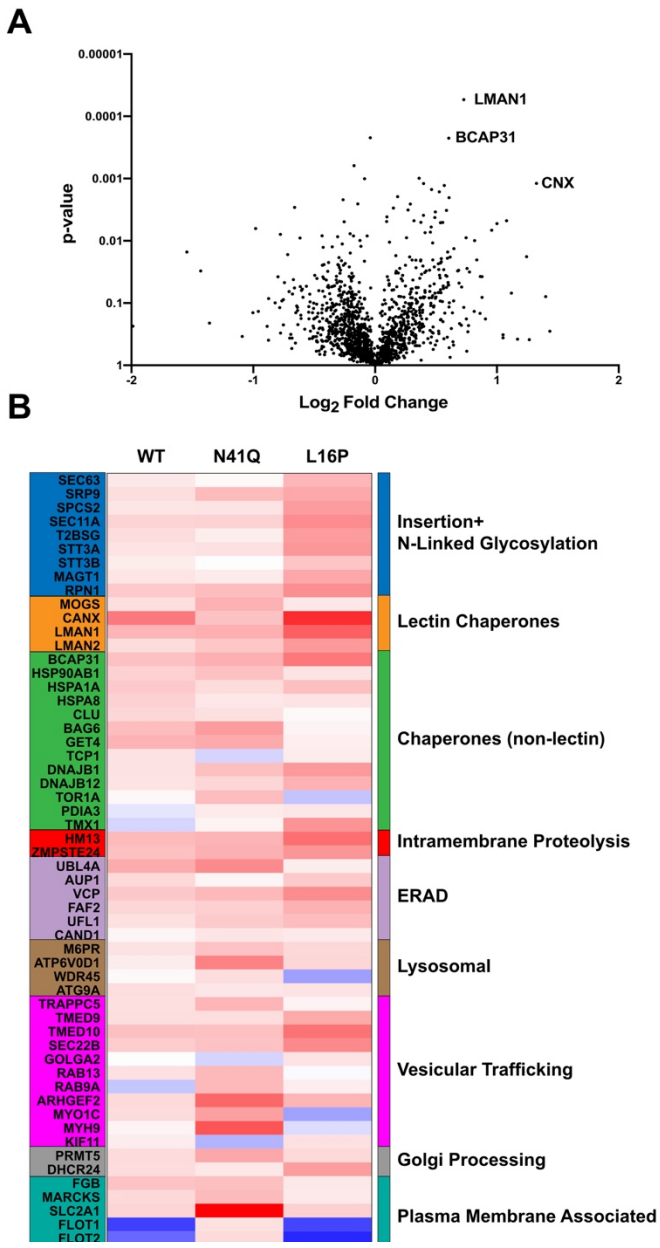

Figure 47. Proteomics to Uncover Novel PMP22 Interacting Partners

Co-immunoprecipitation and LC-MS/MS proteomics was used to uncover novel PMP22 interaction proteins. **(A)** is a volcano plot showing interacting proteins that were identified from 5 biological replicates. Log_2 fold change of the identified protein in the WT PMP22 sample compared to samples obtained from IPs with untagged PMP22 are shown on the x-axis and the p-value (student's t-test) for the interaction from the multiple replicates is shown on the y-axis. Selected interactions are identified. **(B)** Heat-map showing quantified interactions for WT, N41Q, or L16P PMP22 over background. The heat map is arranged temporally in regards to PMP22 biogenesis. The top of the map identifies interactions predicted to occur early in biogenesis and the bottom of the map shows interactions predicted to occur later in biogenesis. All interactions had a Log_2 fold change over background >0.5, p-value <0.1 and were identified in multiple biological replicates for at least one PMP22 variant.

bottom. The fact that we were able to identify CNX in our screen with ordered affinities of L16P>WT>N41Q, which is supported by previous literature results, served as a positive control for our screen(*401, 647, 762, 764*).

We noticed a couple key trends when the data was organized in the interaction network implied by **Figure 47B**. First, N41Q PMP22 had significantly higher interactions with proteins later in the pathway (Vesicular Trafficking, Golgi Processing, and Plasma Membrane Associated) than WT or L16P PMP22. This information makes sense in light of the results presented in **Figure 42**. Since N41Q PMP22 traffics to the cell surface much more efficiently than WT PMP22 it makes sense that its interactions with proteins at later stages in the trafficking pathway are more abundant. A second observation from the proteomic analysis is that the folding defect caused by the L16P mutation in PMP22 seems to be recognized very early in biogenesis. L16P PMP22 shows much higher interactions than WT or N41Q PMP22 with proteins associated with the 'Insertion and N-linked Glycosylation' and 'Lectin Chaperone' stages. This suggests that more and/or longer-lived binding events happen early on for this variant. This results also supports our hypothesis that misfolded variants of PMP22 tend to get 'stuck' on the translocon compared to WT PMP22, as L16P PMP22 interacted more strongly with Sec61 than WT or N41Q PMP22 (**Figure 47B**).

2.5 N-Glycan-Recognizing Chaperones involved in PMP22 Trafficking

Some of the putative interactors uncovered in our proteomic screen are known to bind ERQC client proteins in an N-glycan dependent manner (lectin chaperones). We set out to validate the role of these interactor in mediating PMP22 trafficking. We also were interested in the non-lectin chaperone RER1, in light of a previous report that it is involved in ERQC for PMP22(*763*). To validate whether these proteins do indeed function in PMP22 trafficking, we generated CRISPR/Cas9 clonal KO cell lines and quantitated PMP22 trafficking efficiency in these cell lines. We focused on four potential mediators of PMP22 trafficking: CNX, lectin mannose-binding protein 1 (LMAN1, also known as ERGIC53), UDP-glucose:glycoprotein glucosyltransferase 1 (UGGT1), and RER1. CNX and RER1, are the only previously-identified chaperones that engage PMP22(*401, 762-764*). CNX is believed to retain PMP22 in the ER to promote folding while RER1 is a sorting receptor in the Golgi and has been previously shown to function in retrograde trafficking of two variants of PMP22: L16P and G150D. LMAN1 was one of the strongest interactors to come out of our screen and is a mannose specific lectin that has been previously shown to promote maturation of glycoproteins from the ER to the Golgi complex(*780-782*). We hypothesized that LMAN1 might be responsible for promoting maturation of PMP22 in a glycan specific manner. UGGT1, which we didn't identify in our screen but is a main component of the CNX cycle and may not have been identified due to a transient interaction with PMP22, is thought to be the main folding sensor of the CNX cycle. UGGT1 either re-glucosylates folding-immature client proteins to allow reengagement with CNX or allows folded polypeptides to mature beyond the ER(*759, 783*). We hypothesized that a loss of UGGT1 would cause an increase in PMP22 maturation in a glycosylation dependent manner.

Figure 48 shows PMP22 trafficking efficiencies of WT, N41Q and L16P PMP22 in these four KO cell lines compared to HEK293 cells. The data is presented as violin plots, which show the population distribution of PMP22 trafficking efficiencies in individual cells from three independent biological replicates measuring >2000 cells per replicate. The dotted white lines separated the data into quartiles.

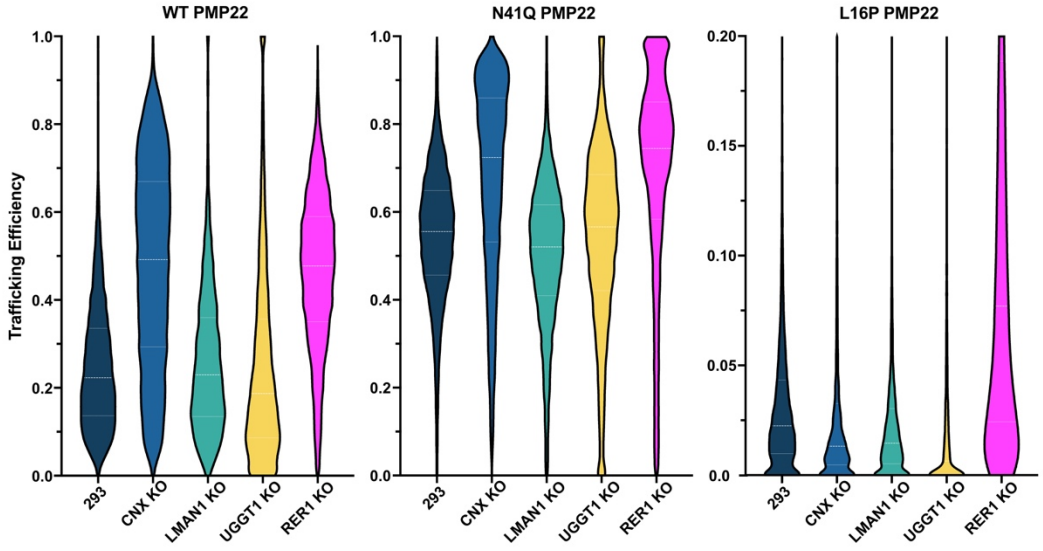

Figure 48. PMP22 Trafficking Efficiencies in CRISPR/Cas9 KO Cells of Potential ERQC Interactors

CRISPR/Cas9 was used to generated KO cells of potential proteins involved in mediating trafficking effects for PMP22. Violin plots showing population distributions of WT, N41Q and L16P PMP22 trafficking efficiencies from three biological replicates are shown. Data was collected in HEK293 cells (navy), CNX KO HEK293 cells (blue), LMAN1 KO HEK293 cells (green), UGGT1 KO HEK293 cells (yellow) and RER1 HEK293 KO cells (pink). White lines in the population distributions separate the data into quartiles.

KO of CNX caused a dramatic increase in PMP22 trafficking efficiency for both WT and N41Q PMP22 **Figure 48**). The fact that this increase was independent of glycosylation makes sense in light of previous experiments that showed that even though CNX is a “lectin chaperone”, it can engage PMP22 independent of its glycosylation state(*647*). L16P PMP22, on the other hand showed a no significant change in PMP22 trafficking efficiency when CNX was knocked out. Previous reports using confocal microscopy showed that CNX knockdown did not change the distribution of PMP22 in cells(*763*). Our results show that CNX KO can significantly increase the forward trafficking efficiency of WT PMP22 in a glycosylation independent manner, thus increasing the amount of protein at the PM. This discrepancy may be explained by previous studies use of GFP-tagged PMP22 which has been shown to promote intracellular retention(*784*). This result suggests that the modest (ca. 20%) trafficking efficiency by which WT PMP22 surface-traffics in may reflect a central role for CNX as a key protein responsible for intracellular retention.

Much to our surprise, KO of LMAN1 showed no effect on the trafficking efficiency of any of the PMP22 variants under study (**Figure 48**). This result could be explained via multiple different interpretations. First, it could mean means that any complex so-formed between PMP22 and LMAN1 does not play a major role in directing the traffic of PMP22. Additionally, it could mean that other ER sorting receptors (such as LMAN2,

which was also identified in the proteomic screen) have functional redundancy with LMAN1 thus allowing PMP22 PM trafficking in the LMAN1 KO cells.

UGGT1 KO cells showed a decrease in PMP22 trafficking in a glycosylation dependent manner (**Figure 48**). Initially this result was surprising. UGGT is thought to serve as the critical folding sensor in the CNX cycle that re-glucosylates the N-glycan on folding-immature client proteins and allowing them to reengage with calnexin or calreticulin. Bypassing reengagement with CNX, we hypothesized, would lead to an increase in overall PMP22 trafficking efficiency in a glycosylation dependent manner. As expected N41Q PMP22 showed no changes in trafficking efficiency in UGGT1 KO cells since this PMP22 variant does not contain an N-glycan moiety for UGGT1 to engage. However, WT and L16P PMP22 both showed lower trafficking efficiencies in the UGGT1 KO cells. A possible explanation for these results is that by re-glucosylating client proteins, UGGT1 both promotes PMP22 reassociation with calnexin but also protects PMP22 from premature degradation. This hypothesis is supported by examining total WT PMP22 levels in either HEK293 versus UGGT1 KO cells (**Figure 49**). In the UGGT1 KO cells there is a slight decrease in the total expression of PMP22 compared to normal HEK293 cells which could reflect increased degradation.

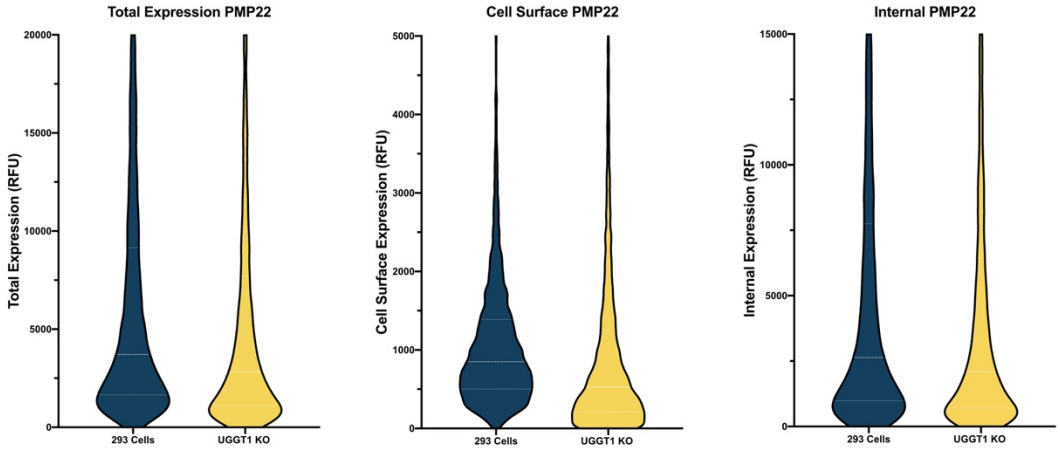

Figure 49. PMP22 Total, Cell Surface, and Internal Expression in HEK293 or UGGT KO Cells

PMP22 total, cell surface, and internal expression in HEK293 or UGGT1 KO Cells. Violin plots showing population distributions of WT PMP22 total, cell surface, or internal expression from three biological replicates are shown. Data was collected in HEK293 cells (navy), or UGGT1 KO HEK293 cells (yellow). White lines in the population distributions separate the data into quartiles.

RER1 KO cells showed increases in trafficking efficiencies for all PMP22 variants under study (**Figure 48**). This confirms both previous results suggesting that the role of RER1 in ERQC(*763*). This result suggests

that RER1 functions as a glycosylation-independent Golgi-to-ER retrograde transporter for both WT and disease mutant forms of PMP22 that may play a role in preventing folding-immature proteins escape from the ER. This result expands the role of RER1 to function not only in retrograde transport of disease variants of PMP22 but also functions in retrograde transport of the WT protein as well. Overall, these studies showed different roles for each of these ERQC proteins in mediating PMP22 trafficking and maturation.

3. Discussion

3.1 N-Glycosylation Limits Forward Trafficking of Human PMP22

Under healthy conditions, WT PMP22 traffics to the PM with a modest efficiency of ~ 20%(*1, 639, 738*). Disease mutant forms of the protein usually traffic with even lower efficiency, in some cases approaching 0%(*1, 530*). A key result of this work is that elimination of the single N-glycosylation site in PMP22 (N41) increases the surface trafficking efficiencies of both WT and disease mutant forms of the protein by several-fold (**Figure 42**). While N-glycosylation is often associated with promoting molecular recognition, protein stability, or protein solubility(*759, 765-767*), it clearly plays a limiting role in terms of its impact on PMP22 trafficking from the ER to the PM. This reflects the role of protein N-glycan moieties in ERQC. Here, the N-glycan serves as a “quality control barcode” to which monosaccharides are added or removed signaling to the ERQC machinery the folding status of the nascent protein, determining whether that protein needs to be retained in the ER for further attempts at folding or whether it should be targeted for degradation(*407, 408, 765, 766*). Mutations of N41 have yet to be discovered among the documented CMTD mutant forms of PMP22. Previous studies discovered that N-glycosylation is not important for the ability of PMP22 to partition into cholesterol-rich membrane domains (*691*), form specific trans-interactions with other myelin proteins (*661*), or modulate lipid ultrastructure *in vitro* (*625*). These reports suggest that N-glycosylation is not important for the function of PMP22.

Even unstable and very poorly trafficking disease mutant forms of PMP22 exhibit a dramatic enhancement in trafficking efficiency upon elimination or inhibition of N-glycosylation(**Figure 42C**). It is therefore interesting to wonder if inhibition of glycosylation for these CMTD mutant forms of PMP22 could lead to partial restoration of Schwann cell function that might alleviate some CMTD disease progression and symptoms. Inhibition of glycosylation could also be investigated as a possible therapeutic approach for the

HNPP form of CMTD (~20% of all CMTD cases(*635, 742*)), which is caused by loss of one WT PMP22 allele (WT/null conditions, “haploinsufficiency”). Mutations in STT3A and STT3B, the catalytic subunits to the OST-A and OST-B, respectively, are linked to a family of diseases known as congenital disorders of glycosylation(*785*). Nevertheless, partial inhibition, of either glycosylation pathway has emerged as a potential therapeutic approach for treating certain types of cancers(*776, 777*), implying that these treatments may also be useful for CMTD.

3.2 Different Pathways of Glycosylation for WT and CMTD Variants of PMP22

N-linked glycosylation is mediated by the OST complex in one of two ways: co-translationally via OST-A or post-translationally via OST-B(*769, 771*). Our results show that for WT PMP22, a significant fraction of the nascent protein is glycosylated post-translationally by OST-B. On the other hand, the severely folding defective L16P disease mutant form of PMP22 can be glycosylated equally well either co- or post-translationally (**Figure 44A and 44B**). This result, coupled with sucrose density fractionation experiments (**Figure 44C and 44D**), suggests that L16P PMP22 completes translation then diffuses beyond the translocon complex only very slowly compared to the WT protein. The prolonged residency of L16P PMP22 at the translocon would allow the OST-A glycosylation reaction to efficiently glycosylate this mutant before it reaches OST-B. The L16P mutation is located in the 1st transmembrane helix of the protein, induces a folding-destabilizing kink in this helix(*665*). The structural and folding defects induced by this mutation are evidently manifest even while the downstream protein sequence is still being translated, providing an example of misfolding that occurs at the stage of membrane integration(*1*).

Figures 44E and 44F show that oxidizing conditions impact the cysteine residue adjacent to the glycosylation site (C42), causing PMP22 to be a suboptimal substrate for STT3A. Because mutating cysteine residue 53 to an alanine did not cause PMP22 to become a better substrate for STT3A (**Figure 44E**) we could rule out the possibility that an intramolecular disulfide bond between cysteine 42 and cysteine 53 is related to this phenomenon. Sequence alignment of human PMP22 with homologs from multiple organisms shows that the cysteine at N+1 (relative to the glycosylation site) is highly conserved. The recently obtained cryo-EM structures for the OST-A and OST-B complex showed that the active sites for both catalytic subunits are very similar, ruling out the possibility that C42 is sterically hindering glycoyslation by STT3A(*774*). It is possible that

C42 engages in an intermolecular disulfide bond with an ER luminal protein as it emerges in the ER, leading to cessation of the OST-A reaction. This would explain why pretreatment of cells with DTT to lower the thiol oxidation potential reduced PMP22 sensitivity to STT3B KO. Indeed, several protein disulfide isomerases capable of such an interaction were identified in our proteomic screen. In contrast to OST-A, OST-B complexes contains MagT1 and Tusc3 subunits, which have oxidoreductase capabilities that could break this potential intramolecular disulfide bond allowing for OST-B mediated N-linked glycosylation(*772*). Future experiments are needed to explore this phenomenon and its physiological significance.

3.4 Proteomics Reveals that Key ERQC Decisions for WT PMP22 Occur Later in the Translocon-to-PM Trafficking Pathway than for the L16P Disease Mutant Form

Proteomics followed by pathway enrichment analysis was used to examine the interactome of three PMP22 variants: WT, N41Q and L16P in order to uncover interactions that were glycosylation dependent (WT vs N41Q) or dependent on the conformational stability of the protein (WT vs L16P). For the glycosylation deficient N41Q we found more interactions with proteins late in the biogenesis pathway and localized at the PM as compared to WT or L16P PMP22. Most interestingly, interactions with the severe disease mutant L16P PMP22 appeared to be enriched early on in the biogenesis pathway, at the level of translocon-mediated membrane integration and N-linked glycosylation. This data suggests that the folding defect in L16P PMP22 is detected very early on in the folding pathway, maybe even at the level of membrane integration. Further emphasizing this point, we found that L16P PMP22 in sucrose density fractionation experiments co-partitioned more strongly with the Sec61 component of the translocon than WT PMP22 (**Figure 44C and 44D**). Taken together this data implies that the folding defect in L16P PMP22 gets recognized very early in biogenesis. Additionally, we found that L16P PMP22 had stronger interactions with the lectin chaperones compared to non-lectin chaperones (**Figure 47B**). L16P PMP22 specifically had a stronger interaction with the lectin chaperone CNX than WT PMP22, confirming an important literature result(*401*). A possible interpretation of this data is that PMP22 is engaged by lectin chaperones prior to reaching key non-lectin chaperones in its biogenesis pathway. These results are consistent with prior results suggesting that proteins containing N-glycosylation sites within 50 residues of the N-terminus interact with lectin chaperones prior to non-lectin chaperones (*439*).

3.5 Clarification of the Roles of CNX, UGGT1, and RER1 in ERQC Management of PMP22 Folding and Trafficking

Four proteins were chosen for further study for involvement in PMP22 trafficking: two that had previously been shown to interact with PMP22 (CNX and RER1) and two novel potential interactors (LMAN1 and UGGT1). The roles of these proteins in PMP22 folding and trafficking were examined in cell lines in which the alleles encoding these proteins were genetically knocked-out using CRISPR/Cas9.

CNX has previously been reported to monitor the folding status of PMP22 in a manner that can be both glycosylation dependent and independent(*401, 647, 762-764*). Of particular note, Fontanini et al showed that CNX can bind both WT and L16P in their glycosylated forms, with the L16P complex being much longer lived than WT(*647*). That same study showed that N41Q PMP22 does not bind CNX, whereas the double L16P/N41Q mutant does. This suggests that calnexin has a dual recognition mechanism leading to binding of membrane proteins that are either N-glycosylated or conformationally defective, or both. Here, it was observed that the trafficking efficiencies of both WT and N41Q PMP22 increased in the CNX KO cell lines. However, the mean trafficking efficiency increased by 92% for WT PMP22 and 23% for N41Q PMP22 whereas N41Q PMP22 in CNX KO cells compared to HEK293 cells (**Figure 48**). This suggests that CNX recognizes and limits trafficking of both forms of the protein but elicits a much stronger effect on the glycosylated protein. This data complies with the previous suggested bipartite binding of CNX with client proteins. CNX can interact with PMP22 in both glycan dependent and independent manners with glycan dependent interactions being more effective. The fact that Fontanini et al. did not observe complex formation between N41Q PMP22 and calnexin likely reflects a modest interaction affinity.

A burgeoning idea in the field of ERQC is the role compartmentalization plays in managing protein biogenesis. Beyond the classical smooth and rough ER, the ER can be further sub-compartmentalized into regions where biogenesis, protein folding, ERAD, and ER-maturation are spatially separated (*786, 787*). CNX has been hypothesized to shuttle nascent proteins between these sub-compartments. In the absence of CNX, folded PMP22 may itself migrate towards sites of ER-maturation. Despite being the site of cholesterol biosynthesis the ER itself is inheritably cholesterol poor, as most cholesterol is exported to the Golgi complex and beyond(*93*). Folded PMP22 has an affinity for these cholesterol-rich membranes (*647, 691*)and it is plausible that association with CNX excludes a portion of folded PMP22 from these sites of ER-maturation.

Therefore, by removing CNX, more folded PMP22 is able to partition into sites of ER-maturation and thence to the Golgi complex and eventually the PM.

L16P PMP22 showed no change in trafficking efficiency in the CNX KO cells. To a degree, this result had been previously suggested, as transient knockdown of CNX did not change L16P PMP22 cell surface levels (*763*). On the other hand, this result is surprising in light of ours (**Figure 47**) and previous observations (*401, 647*) that CNX forms longer-lived interactions with L16P PMP22 than WT PMP22. Our results do not point to CNX being the major player in causing L16P PMP22 to have a 10-fold lower trafficking efficiency than L16P/N41Q PMP22 (**Figure 42C**). We suggest that the vast majority of L16P is retained early in the secretory pathway as a consequence of quality control decisions that are finalized before L16P PMP22 has had a chance to engage with CNX. The fact that L16P/N41Q traffics to the cell surface with 10-fold higher efficiency than L16P suggests that the decision to retain L16P intracellular happens *before* engagement with CNX. One potential mediator of this effect could be malectin, a lectin chaperone that binds to di-glucosylated glycoproteins(*2, 407, 408*). We did not generate malectin KO cells and test the effect on PMP22 trafficking because we only identified malectin in our proteomic experiments in one biological replicate. However, in this one experiment malectin did have a 2-fold greater interaction with L16P than WT PMP22 suggesting that it may target L16P PMP22 for ER retention prior to engagement with CNX. The fact that we only identified this protein once suggests that the interaction could be extremely transient. Further experiments will be needed to test this hypothesis. Additionally, the fact that CNX KO did not have a significant effect on L16P PMP22 trafficking, could reflect the fact that in. previous reports disruption of individual chaperones had only modest consequences due to their considerable redundancy(*742*).

UGGT1 is often described as being the key decision maker in the CNX cycle; it is thought to monitor the folding status of proteins after they have been released from CNX(*759, 760, 766*). UGGT1 either catalyzes the addition of a glucose residue onto the N-glycan of a folding-immature polypeptide in order to drive re-engagement with CNX or allows a fully folded protein to forward traffic beyond the ER(*783*). KO of UGGT1 in HEK293 cells caused a decrease in the trafficking efficiency for both WT and L16P PMP22 but did not change the trafficking efficiency of N41Q PMP22 (**Figure 48**). The fact that N41Q PMP22 trafficking efficiency is unchanged is as expected since this protein is not glycosylated, such that it should not be engaged by UGGT1. However, the *decrease* in trafficking efficiencies for WT and L16P PMP22 were surprising. We had supposed

that, as in the CNX KO cells, stripping away this level of quality control would result in an increase in PMP22 trafficking efficiency. One hypothesis to explain this data is that glucosylation by UGGT1 protects PMP22 from premature degradation via ERAD. In **Figure 49**, we observed a decrease in total PMP22 levels in UGGT1 KO cells compared to 293 cells. Folding glycoproteins can be targeted for ERAD through trimming of mannose residues on the N-glycan by mannosidases (*2, 407, 408, 759*). This 'mannose-timer' hypothesis is thought to be inherently slow yet, once it occurs, irreversibly marks proteins for degradation. UGGT1 functions to protect proteins from this process both by binding the client protein and by glucosylating them to drive calnexin binding, in both cases preventing mannose trimming. In the absence of this protection, more PMP22 is likely targeted for ERAD thus decreasing the total amount of protein that is able to make it to the cell surface.

Finally, we explored the effect of RER1 KO on PMP22 trafficking efficiency. RER1 had previously been characterized to play a role in retrieving misfolded L16P and G150D PMP22 mutants from the Golgi and returning these proteins to the ER(*763*). It thereby appears to play a role in recognizing any misfolded PMP22 that escapes the quality control network. We took these experiments a step further and looked at the trafficking efficiency of multiple PMP22 variants in the RER1 KO cell line. As expected, RER1 KO caused an increase in the surface trafficking efficiency of L16P PMP22. Surprisingly, we found that both WT and N41Q PMP22 exhibited increased trafficking efficiency in the RER1 KO cell line. This result suggests that not only can RER1 recognize misfolded PMP22 in post-ER compartments, but it may also recognize folded variants and return them as well. As seen for CNX, this would be an example of overzealous quality control. While under homozygous WT conditions this may be beneficial, when the total amount of a client protein is reduced, as occurs in HNPP where one *pmp22* allele is deleted, this phenomenon can become problematic. Therefore, approaches that could reduce the affinity of RER1 for PMP22 might, in some cases, be therapeutically beneficial.

In addition to the four proteins tested in this study, our proteomic screen identified numerous additional apparent PMP22-interacting proteins that may play a role in mediating PMP22 folding and trafficking *in vivo*. It is hoped that this initial work will set the stage for future study to explore the roles of these proteins in PMP22 folding and trafficking. Some proteins that seem particularly interesting are: CCDC47, BCAP31, DNAJ proteins, myosin motor proteins, CAND1 and VCP. These proteins may play specific roles in PMP22 folding (CCDC47, BCAP31, DNAJ proteins), transport (myosin motor proteins), or degradation (CAND1 and VCP). The screen

also uncovered two intermembrane proteases HM13 (also known as signal peptide protease or SPP) and ZMPSTE24. These proteases may be involved in non-canonical pathways of membrane protein degradation. Traditionally, ERAD targets are retrotranslocated from the ER via a dislocon (or retrotranslocon) channel for degradation in the cytosol via the proteasome(*788*). However, this pathway is associated with a large energetic barrier for removal of misfolded integral membrane proteins from the ER membrane(*2*). Thus, a hypothesis has been forwarded that intermembrane proteases function to clip integral membrane proteins marked for proteasomal degradation in their transmembrane domains, thus chopping them up into easier-to-handle fragments and lowering the energy expenditure required for their removal from the membrane(*758, 789-791*). Our results suggest the possibility that PMP22 might be pre-degraded in this fashion, a matter that will require experimental testing.

4. Conclusions

In this work it was seen that elimination of N-glycosylation of PMP22 dramatically enhances the surface trafficking efficiency of both WT PMP22 and also of very unstable mutant forms of the protein such as the L16P CMTD mutant. We showed that the mechanisms of glycosylation differ for WT and disease mutant forms of PMP22 most likely due to increased association of disease forms of PMP22 at Sec61 translocon. As expected, the lectin chaperones seen to be an important contributor to this limiting role for N-glycosylation. The results of this work also confirmed a direct but complicated role for UGGT1 and CNX in ERQC of PMP22 and also clarified an important N-glycan-independent role for RER1 in stringent Golgi-to-ER retrieval of proteins that have passed all other stages of ERQC. Finally, this work contributed a proteomic census of PMP22 interactive-proteins that includes the differential levels of binding for the interactors to WT versus L16P and WT versus non-glycosylated PMP22. We hope that will be useful in guiding future efforts to further map out the complex ERQC landscape for PMP22, a landscape that varies between WT and mutant forms.

Chapter VII. Conclusions and Future Directions

In this thesis dissertation I explored the potential *in vivo* function of PMP22 as well as uncovered factors, such as membrane phase partitioning, expression levels, protein-protein interactions, and post-translational modifications, that mediate PMP22 trafficking.

In **Chapter III,** I showed that PMP22 by itself, *in vitro,* is able to induce wrapping of lipid vesicles. This observation suggests a role for PMP22 in initiating and/or maintaining the tight, regular, wrapping of myelin around a central axon. This biological function had been previously hypothesized(*632, 635, 659, 674, 740, 792*); however, this thesis work definitively shows that PMP22 is able to perform this process. While these myelin-like assemblies (MLAs) did form in vesicles of specific lipid compositions and concentrations of PMP22, they did not form with high efficiency. Even in our most optimal sample preparations, the primary lipid morphology we observed was multilamellar lipid vesicles. It will be interesting to test if the inclusion of additional purified PNS proteins such as P_0 and/or myelin basic protein can improve the efficiency of MLA formation. Performing reconstitution experiments with strictly defined protein compositions, in addition to defined lipid compositions, may help define the mechanism of myelin compaction in the PNS.

Another question that arises from the results in **Chapter III** is: where exactly PMP22 is localized in these MLAs? Our collaborator on the project, Dr. Mel Ohi, is currently addressing this question using gold-particle labeling of PMP22 and electron microscopy imaging. Localizing PMP22 in these assemblies will help define how the protein is forming these structures. If PMP22 is localized diffusely throughout the MLAs, the protein is most likely forming trans-homophilic interactions with PMP22 localized to adjacent bilayers which can 'zipper' the two bilayers together. However, if PMP22 is localized to discreet regions in the MLAs, such as areas of high degrees of curvature, then a different hypothesis may emerge. Localizing PMP22 in these lipid vesicles is the nest step in defining the biological function of PMP22 in PNS myelin assembly.

In **Chapter IV** I showed that PMP22 preferentially partitions into cholesterol-rich, liquid-ordered like membrane domains. Disruption of this phase partitioning limits protein trafficking to the PM. This link between membrane phase partitioning and trafficking may not be a feature unique to PMP22 but could extend to other membrane proteins. It has been observed that, for single pass transmembrane proteins, longer TM spanning regions, which prefer thicker liquid-ordered like membranes, are enriched at the PM(*117, 705, 711*). Therefore,

a feature that is important for PM trafficking of integral membrane proteins may be ordered phase preference. My work on PMP22 membrane phase preference lends credence to this hypothesis about the role of membrane phase preference in the trafficking of integral membrane proteins.

The obvious extension of this work will be to test phase partitioning of other integral membrane proteins and see if it correlates with trafficking efficiency. Because GPMVs are generated from the PM, this work will be limited to PM localized proteins. A good candidate protein to start with would be rhodopsin, which is PM localized and numerous mutations have been characterized that effect its trafficking (*2*). Another future direction for this work would be to test if the expression of PMP22 alters PM lipid composition of cultured cells. It has been hypothesized that PMP22 is involved in cholesterol trafficking(*714, 715, 719*), and our work shows that PMP22 can stabilize liquid ordered membrane domains in GPMVs(*691*). One potential explanation of this increased stability is an increased cholesterol concentration in GPMVs derived from cells expressing PMP22. We attempted to characterize the lipid profile of GPMVs derived from cells with and without PMP22 however due to the COVID-19 lab shutdowns we were unable to complete these studies. Future experiments completing these preliminary experiments could be used to definitively show that PMP22 can alter the lipid profile of the PM.

In **Chapter V,** I showed that there is an inverse relationship between PMP22 expression and trafficking efficiency. Cells that express more PMP22 show lower trafficking efficiency than those that express less PMP22. This may be due to the relative instability of the protein. As concentrations of PMP22 increase, so does the possibility that the protein will form misfolded aggregates that decrease the overall trafficking efficiency. Much like with the results from **Chapter IV**, it will be extremely interesting to see if this observation holds true for other integral membrane proteins. By looking at this relationship in stable versus unstable proteins, one could potentially find out whether this relationship is due to an increased intracellular aggregation or through overwhelming the ER export machinery. Another way to address this question, in regard to PMP22 specifically, would be to sort cells based on PMP22 total expression and quantify intracellular aggregation via confocal microscopy in the lowest and highest expressing cells.

In **Chapter VI**, I explored the role of N-linked glycosylation and specific protein-protein interactions in mediating PMP22 trafficking. I found that N-linked glycosylation, mediated via a non-traditional pathway involving OST-B, significantly limited PMP22 forward trafficking. Genetic or pharmacological inhibition of this

process significantly increased trafficking efficiencies. Because this process is mediated via a non-traditional pathway, this could be a target for treating CMTD in patients who express too little PMP22 at the PM. This possibility remains to be explored and will hopefully be addressed once there is an OST-B inhibitor with better pharmacological properties. I have been in contact with the researcher at Yale who identified the OST-B specific inhibitor, C19, used in these studies(*777*). Dr. Contessa is very interested in testing a pharmacological OST-B inhibitor in a mouse model of HNPP that contains only one genomic copy of PMP22. These studies could show that increasing PMP22 expression at the PM is sufficient to offset some of the disease phenotypes of CMTD.

Mass spectrometry-based proteomics was used to uncover >50 unique proteins that interact with different variants of PMP22. I explored the role of a select few of these interactors in mediating PMP22 trafficking efficiencies and both confirmed previous results and uncovered new roles for lectin chaperones in PMP22 folding and trafficking. However, a broad spectrum of proteins were identified in this study apart from the lectin chaperones. Further experiments aimed at elucidating the role these other proteins play in PMP22 function or biogenesis remain to be explored. Of particular personal interest, we uncovered two intramembrane proteases, HM13 (or SPP) and ZMPSTE24, that interacted strongly with all three PMP22 variants in our proteomics experiments. These proteins may be involved in PMP22 degradation via a mechanism that involves intramembrane proteolysis. In the classical mechanism of ERAD, proteins are dislocated from the membrane via a hypothesized retrotranslocation channel and the ATPase activity of p97(*2*). For integral membrane proteins this membrane extraction would be energetically costly. Therefore, it has been proposed that intramembrane proteolysis may be involved to lower this energetic cost(*790*). This hypothesis is supported by studies that have uncovered numerous active (or inactive) proteases found in ERAD machinery(*500*). The results from my proteomic experiments leave open the possibility that PMP22 is degraded via a mechanism that requires intramembrane proteolysis.

In this chapter, I briefly discussed a few potential future directions that can come out of my work. However, this discussion is not meant to be comprehensive. Many different future directions are possible based on the results from this work. I hope that my dissertation, the culmination of almost five years and countless hours of work both in and out of the lab, will contribute to our understanding and inspire potential treatment of CMTD. When choosing a lab to join as a first-year graduate student, I wanted to work on a project

that had a direct relationship to human health and disease. I hope that my work on PMP22 can eventually lead to alleviating the pain and suffering of patients afflicted with CMTD.

References

1. J. P. Schlebach *et al.*, Conformational Stability and Pathogenic Misfolding of the Integral Membrane Protein PMP22. *Journal of the American Chemical Society* **137**, 8758-8768 (2015).
2. J. T. Marinko *et al.*, Folding and Misfolding of Human Membrane Proteins in Health and Disease: From Single Molecules to Cellular Proteostasis. *Chem Rev* **119**, 5537-5606 (2019).
3. J. Deisenhofer, O. Epp, K. Miki, R. Huber, H. Michel, Structure of the protein subunits in the photosynthetic reaction centre of Rhodopseudomonas viridis at 3A resolution. *Nature* **318**, 618-624 (1985).
4. J. C. Kendrew *et al.*, A three-dimensional model of the myoglobin molecule obtained by x-ray analysis. *Nature* **181**, 662-666 (1958).
5. K. S. Huang, H. Bayley, M. J. Liao, E. London, H. G. Khorana, Refolding of an integral membrane protein. Denaturation, renaturation, and reconstitution of intact bacteriorhodopsin and two proteolytic fragments. *J Biol Chem* **256**, 3802-3809 (1981).
6. E. London, H. G. Khorana, Denaturation and renaturation of bacteriorhodopsin in detergents and lipid-detergent mixtures. *J Biol Chem* **257**, 7003-7011 (1982).
7. J. L. Popot, S. E. Gerchman, D. M. Engelman, Refolding of bacteriorhodopsin in lipid bilayers. A thermodynamically controlled two-stage process. *J Mol Biol* **198**, 655-676 (1987).
8. J. L. Popot, J. Trewhella, D. M. Engelman, Reformation of crystalline purple membrane from purified bacteriorhodopsin fragments. *EMBO J* **5**, 3039-3044 (1986).
9. P. J. Booth *et al.*, Intermediates in the folding of the membrane protein bacteriorhodopsin. *Nat Struct Biol* **2**, 139-143 (1995).
10. F. Lau, J. Bowie, A method for assessing the stability of a membrane protein. *Biochemistry* **36**, 5884-5892 (1997).
11. E. Haber, C. B. Anfinsen, Side-chain interactions governing the pairing of half-cystine residues in ribonuclease. *J Biol Chem* **237**, 1839-1844 (1962).
12. C. B. Anfinsen, Principles that govern the folding of protein chains. *Science* **181**, 223-230 (1973).
13. M. A. Lemmon *et al.*, Glycophorin A dimerization is driven by specific interactions between transmembrane alpha-helices. *J Biol Chem* **267**, 7683-7689 (1992).
14. M. A. Lemmon, J. M. Flanagan, H. R. Treutlein, J. Zhang, D. M. Engelman, Sequence specificity in the dimerization of transmembrane alpha-helices. *Biochemistry* **31**, 12719-12725 (1992).
15. H. R. Treutlein, M. A. Lemmon, D. M. Engelman, A. T. Brunger, The glycophorin A transmembrane domain dimer: sequence-specific propensity for a right-handed supercoil of helices. *Biochemistry* **31**, 12726-12732 (1992).
16. J. L. Popot, D. M. Engelman, Membrane protein folding and oligomerization: the two-stage model. *Biochemistry* **29**, 4031-4037 (1990).
17. J. L. Popot, D. M. Engelman, Helical membrane protein folding, stability, and evolution. *Annual review of biochemistry* **69**, 881-922 (2000).
18. F. Cymer, G. von Heijne, S. H. White, Mechanisms of Integral Membrane Protein Insertion and Folding. *Journal of Molecular Biology* **427**, 999-1022 (2014).
19. S. H. White, W. C. Wimley, Membrane protein folding and stability: physical principles. *Annu Rev Biophys Biomol Struct* **28**, 319-365 (1999).
20. A. K. Chamberlain, S. Faham, S. Yohannan, J. U. Bowie, Construction of helix-bundle membrane proteins. *Adv Protein Chem* **63**, 19-46 (2003).
21. J. Neumann, N. Klein, D. E. Otzen, D. Schneider, Folding energetics and oligomerization of polytopic alpha-helical transmembrane proteins. *Arch Biochem Biophys* **564**, 281-296 (2014).
22. D. E. Otzen, K. K. Andersen, Folding of outer membrane proteins. *Arch Biochem Biophys* **531**, 34-43 (2013).
23. H. Hong, Toward understanding driving forces in membrane protein folding. *Arch Biochem Biophys* **564**, 297-313 (2014).
24. E. London, K. Shahidullah, Transmembrane vs. non-transmembrane hydrophobic helix topography in model and natural membranes. *Current opinion in structural biology* **19**, 464-472 (2009).
25. K. G. Fleming, Energetics of membrane protein folding. *Annu Rev Biophys* **43**, 233-255 (2014).
26. D. Chaturvedi, R. Mahalakshmi, Transmembrane beta-barrels: Evolution, folding and energetics. *Biochim Biophys Acta* **1859**, 2467-2482 (2017).

27. L. K. Tamm, H. Hong, B. Liang, Folding and assembly of beta-barrel membrane proteins. *Biochim Biophys Acta* **1666**, 250-263 (2004).
28. P. J. Booth, The trials and tribulations of membrane protein folding in vitro. *Biochim Biophys Acta* **1610**, 51-56 (2003).
29. P. J. Booth *et al.*, In vitro studies of membrane protein folding. *Crit Rev Biochem Mol Biol* **36**, 501-603 (2001).
30. B. Schiffrin, D. J. Brockwell, S. E. Radford, Outer membrane protein folding from an energy landscape perspective. *BMC Biol* **15**, 123 (2017).
31. A. Senes, D. E. Engel, W. F. DeGrado, Folding of helical membrane proteins: the role of polar, GxxxG-like and proline motifs. *Current opinion in structural biology* **14**, 465-479 (2004).
32. K. R. Mackenzie, Folding and stability of alpha-helical integral membrane proteins. *Chem Rev* **106**, 1931-1977 (2006).
33. J. L. Popot, Membrane Proteins in Aqueous Solutions: From Detergents to Amphipols. *Biol Med Phys Biomed*, 1-708 (2018).
34. M. H. Bracey, B. F. Cravatt, R. C. Stevens, Structural commonalities among integral membrane enzymes. *FEBS letters* **567**, 159-165 (2004).
35. R. M. Garavito, A. M. Mulichak, The structure of mammalian cyclooxygenases. *Annu Rev Biophys Biomol Struct* **32**, 183-206 (2003).
36. K. T. Root, S. M. Plucinsky, K. J. Glover, Recent progress in the topology, structure, and oligomerization of caveolin: a building block of caveolae. *Curr Top Membr* **75**, 305-336 (2015).
37. D. M. Engelman, T. A. Steitz, A. Goldman, Identifying nonpolar transbilayer helices in amino acid sequences of membrane proteins. *Annu Rev Biophys Biophys Chem* **15**, 321-353 (1986).
38. J. Kyte, R. F. Doolittle, A simple method for displaying the hydropathic character of a protein. *J Mol Biol* **157**, 105-132 (1982).
39. H. J. Sharpe, T. J. Stevens, S. Munro, A comprehensive comparison of transmembrane domains reveals organelle-specific properties. *Cell* **142**, 158-169 (2010).
40. G. von Heijne, Membrane protein structure prediction. Hydrophobicity analysis and the positive-inside rule. *J Mol Biol* **225**, 487-494 (1992).
41. G. von Heijne, Membrane-protein topology. *Nat Rev Mol Cell Biol* **7**, 909-918 (2006).
42. D. M. Engelman, T. A. Steitz, The spontaneous insertion of proteins into and across membranes: the helical hairpin hypothesis. *Cell* **23**, 411-422 (1981).
43. N. Fluman, V. Tobiasson, G. von Heijne, Stable membrane orientations of small dual-topology membrane proteins. *Proc Natl Acad Sci U S A* **114**, 7987-7992 (2017).
44. S. U. Heinrich, W. Mothes, J. Brunner, T. A. Rapoport, The Sec61p complex mediates the integration of a membrane protein by allowing lipid partitioning of the transmembrane domain. *Cell* **102**, 233-244 (2000).
45. M. B. Ulmschneider, M. S. Sansom, Amino acid distributions in integral membrane protein structures. *Biochim Biophys Acta* **1512**, 1-14 (2001).
46. M. B. Ulmschneider, M. S. Sansom, A. Di Nola, Properties of integral membrane protein structures: derivation of an implicit membrane potential. *Proteins* **59**, 252-265 (2005).
47. J. U. Bowie, Membrane protein folding: how important are hydrogen bonds? *Current opinion in structural biology* **21**, 42-49 (2011).
48. Z. Cao, J. U. Bowie, Shifting hydrogen bonds may produce flexible transmembrane helices. *Proc Natl Acad Sci U S A* **109**, 8121-8126 (2012).
49. M. C. Wiener, S. H. White, Structure of a fluid dioleoylphosphatidylcholine bilayer determined by joint refinement of x-ray and neutron diffraction data. III. Complete structure. *Biophys J* **61**, 434-447 (1992).
50. D. W. Deamer, J. Bramhall, Permeability of lipid bilayers to water and ionic solutes. *Chem Phys Lipids* **40**, 167-188 (1986).
51. M. Miyano, H. Ago, H. Saino, T. Hori, K. Ida, Internally bridging water molecule in transmembrane alpha-helical kink. *Current opinion in structural biology* **20**, 456-463 (2010).
52. T. Orban, S. Gupta, K. Palczewski, M. R. Chance, Visualizing water molecules in transmembrane proteins using radiolytic labeling methods. *Biochemistry* **49**, 827-834 (2010).
53. N. Klein, J. Neumann, J. D. O'Neil, D. Schneider, Folding and stability of the aquaglyceroporin GlpF: Implications for human aqua(glycero)porin diseases. *Biochim Biophys Acta* **1848**, 622-633 (2015).

54. A. Kauko, K. Illergard, A. Elofsson, Coils in the membrane core are conserved and functionally important. *J Mol Biol* **380**, 170-180 (2008).
55. H. Viklund, E. Granseth, A. Elofsson, Structural classification and prediction of reentrant regions in alpha-helical transmembrane proteins: application to complete genomes. *J Mol Biol* **361**, 591-603 (2006).
56. M. T. De Marothy, A. Elofsson, Marginally hydrophobic transmembrane alpha-helices shaping membrane protein folding. *Protein Sci* **24**, 1057-1074 (2015).
57. J. F. Hunt, P. Rath, K. J. Rothschild, D. M. Engelman, Spontaneous, pH-dependent membrane insertion of a transbilayer alpha-helix. *Biochemistry* **36**, 15177-15192 (1997).
58. A. D. Meruelo, I. Samish, J. U. Bowie, TMKink: a method to predict transmembrane helix kinks. *Protein Sci* **20**, 1256-1264 (2011).
59. S. Yohannan, S. Faham, D. Yang, J. P. Whitelegge, J. U. Bowie, The evolution of transmembrane helix kinks and the structural diversity of G protein-coupled receptors. *Proc Natl Acad Sci U S A* **101**, 959-963 (2004).
60. H. Luecke, B. Schobert, H. T. Richter, J. P. Cartailler, J. K. Lanyi, Structure of bacteriorhodopsin at 1.55 A resolution. *J Mol Biol* **291**, 899-911 (1999).
61. C. Jorgensen *et al.*, Lateral Fenestrations in K(+)-Channels Explored Using Molecular Dynamics Simulations. *Mol Pharm* **13**, 2263-2273 (2016).
62. M. Lichtenegger *et al.*, An optically controlled probe identifies lipid-gating fenestrations within the TRPC3 channel. *Nat Chem Biol* **14**, 396-404 (2018).
63. Q. Zhao *et al.*, Structure and mechanogating mechanism of the Piezo1 channel. *Nature* **554**, 487-492 (2018).
64. H. De Loof, S. C. Harvey, J. P. Segrest, R. W. Pastor, Mean field stochastic boundary molecular dynamics simulation of a phospholipid in a membrane. *Biochemistry* **30**, 2099-2113 (1991).
65. N. J. Harris, K. Charalambous, H. E. Findlay, P. J. Booth, Lipids modulate the insertion and folding of the nascent chains of alpha helical membrane proteins. *Biochemical Society transactions* **46**, 1355-1366 (2018).
66. P. Curnow, M. Lorch, K. Charalambous, P. J. Booth, The reconstitution and activity of the small multidrug transporter EmrE is modulated by non-bilayer lipid composition. *J Mol Biol* **343**, 213-222 (2004).
67. E. van den Brink-van der Laan, V. Chupin, J. A. Killian, B. de Kruijff, Stability of KcsA tetramer depends on membrane lateral pressure. *Biochemistry* **43**, 4240-4250 (2004).
68. P. J. Booth, P. Curnow, Folding scene investigation: membrane proteins. *Current opinion in structural biology* **19**, 8-13 (2009).
69. P. A. Janmey, P. K. Kinnunen, Biophysical properties of lipids and dynamic membranes. *Trends Cell Biol* **16**, 538-546 (2006).
70. A. G. Karabadzhak *et al.*, Bilayer Thickness and Curvature Influence Binding and Insertion of a pHLIP Peptide. *Biophys J* **114**, 2107-2115 (2018).
71. T. Surrey, F. Jahnig, Refolding and oriented insertion of a membrane protein into a lipid bilayer. *Proc Natl Acad Sci U S A* **89**, 7457-7461 (1992).
72. I. K. Jarsch, F. Daste, J. L. Gallop, Membrane curvature in cell biology: An integration of molecular mechanisms. *J Cell Biol* **214**, 375-387 (2016).
73. H. T. McMahon, J. L. Gallop, Membrane curvature and mechanisms of dynamic cell membrane remodelling. *Nature* **438**, 590-596 (2005).
74. T. Itoh, P. De Camilli, BAR, F-BAR (EFC) and ENTH/ANTH domains in the regulation of membrane-cytosol interfaces and membrane curvature. *Biochim Biophys Acta* **1761**, 897-912 (2006).
75. C. Mim, V. M. Unger, Membrane curvature and its generation by BAR proteins. *Trends in biochemical sciences* **37**, 526-533 (2012).
76. M. Simunovic, G. A. Voth, A. Callan-Jones, P. Bassereau, When Physics Takes Over: BAR Proteins and Membrane Curvature. *Trends Cell Biol* **25**, 780-792 (2015).
77. A. Holt, J. A. Killian, Orientation and dynamics of transmembrane peptides: the power of simple models. *Eur Biophys J* **39**, 609-621 (2010).
78. T. K. Nyholm, S. Ozdirekcan, J. A. Killian, How protein transmembrane segments sense the lipid environment. *Biochemistry* **46**, 1457-1465 (2007).

79. Y. Song, K. F. Mittendorf, Z. Lu, C. R. Sanders, Impact of bilayer lipid composition on the structure and topology of the transmembrane amyloid precursor C99 protein. *J Am Chem Soc* **136**, 4093-4096 (2014).
80. R. B. Gennis, *Biomembranes : molecular structure and function*. Springer advanced texts in chemistry (Springer-Verlag, New York, 1989), pp. xvii, 533 pages.
81. A. D. Dupuy, D. M. Engelman, Protein area occupancy at the center of the red blood cell membrane. *Proc Natl Acad Sci U S A* **105**, 2848-2852 (2008).
82. N. Kucerka, M. P. Nieh, J. Pencer, J. N. Sachs, J. Katsaras, What determines the thickness of a biological membrane. *Gen Physiol Biophys* **28**, 117-125 (2009).
83. K. Mitra, I. Ubarretxena-Belandia, T. Taguchi, G. Warren, D. M. Engelman, Modulation of the bilayer thickness of exocytic pathway membranes by membrane proteins rather than cholesterol. *Proc Natl Acad Sci U S A* **101**, 4083-4088 (2004).
84. L. E. Cybulski, D. de Mendoza, Bilayer hydrophobic thickness and integral membrane protein function. *Curr Protein Pept Sci* **12**, 760-766 (2011).
85. O. Soubias, W. E. Teague, Jr., K. G. Hines, K. Gawrisch, Rhodopsin/lipid hydrophobic matching-rhodopsin oligomerization and function. *Biophys J* **108**, 1125-1132 (2015).
86. A. V. Botelho, T. Huber, T. P. Sakmar, M. F. Brown, Curvature and hydrophobic forces drive oligomerization and modulate activity of rhodopsin in membranes. *Biophys J* **91**, 4464-4477 (2006).
87. B. W. Berger *et al.*, Consensus motif for integrin transmembrane helix association. *Proc Natl Acad Sci U S A* **107**, 703-708 (2010).
88. S. M. Anderson, B. K. Mueller, E. J. Lange, A. Senes, Combination of Calpha-H Hydrogen Bonds and van der Waals Packing Modulates the Stability of GxxxG-Mediated Dimers in Membranes. *J Am Chem Soc* **139**, 15774-15783 (2017).
89. S. D. Goldberg, G. D. Clinthorne, M. Goulian, W. F. DeGrado, Transmembrane polar interactions are required for signaling in the Escherichia coli sensor kinase PhoQ. *Proc Natl Acad Sci U S A* **107**, 8141-8146 (2010).
90. I. D. Pogozheva, A. L. Lomize, Evolution and adaptation of single-pass transmembrane proteins. *Biochim Biophys Acta Biomembr* **1860**, 364-377 (2018).
91. A. Oberai, Y. Ihm, S. Kim, J. U. Bowie, A limited universe of membrane protein families and folds. *Protein Sci* **15**, 1723-1734 (2006).
92. A. Y. Andreyev *et al.*, Subcellular organelle lipidomics in TLR-4-activated macrophages. *J Lipid Res* **51**, 2785-2797 (2010).
93. G. van Meer, D. R. Voelker, G. W. Feigenson, Membrane lipids: where they are and how they behave. *Nat Rev Mol Cell Biol* **9**, 112-124 (2008).
94. J. E. Vance, Phospholipid synthesis and transport in mammalian cells. *Traffic* **16**, 1-18 (2015).
95. M. Bloom, E. Evans, O. G. Mouritsen, Physical properties of the fluid lipid-bilayer component of cell membranes: a perspective. *Q Rev Biophys* **24**, 293-397 (1991).
96. T. Rog, M. Pasenkiewicz-Gierula, I. Vattulainen, M. Karttunen, Ordering effects of cholesterol and its analogues. *Biochim Biophys Acta* **1788**, 97-121 (2009).
97. J. M. Boggs, Lipid intermolecular hydrogen bonding: influence on structural organization and membrane function. *Biochim Biophys Acta* **906**, 353-404 (1987).
98. J. P. Slotte, The importance of hydrogen bonding in sphingomyelin's membrane interactions with co-lipids. *Biochim Biophys Acta* **1858**, 304-310 (2016).
99. H. J. Kaiser *et al.*, Lateral sorting in model membranes by cholesterol-mediated hydrophobic matching. *Proc Natl Acad Sci U S A* **108**, 16628-16633 (2011).
100. S. J. Singer, G. L. Nicolson, The fluid mosaic model of the structure of cell membranes. *Science* **175**, 720-731 (1972).
101. F. M. Goni, The basic structure and dynamics of cell membranes: an update of the Singer-Nicolson model. *Biochim Biophys Acta* **1838**, 1467-1476 (2014).
102. A. Kusumi *et al.*, Dynamic organizing principles of the plasma membrane that regulate signal transduction: commemorating the fortieth anniversary of Singer and Nicolson's fluid-mosaic model. *Annu Rev Cell Dev Biol* **28**, 215-250 (2012).
103. G. L. Nicolson, The Fluid-Mosaic Model of Membrane Structure: still relevant to understanding the structure, function and dynamics of biological membranes after more than 40 years. *Biochim Biophys Acta* **1838**, 1451-1466 (2014).

104. D. A. Brown, E. London, Functions of lipid rafts in biological membranes. *Annu. Rev. Cell. Dev. Biol.* **14**, 111-136 (1998).
105. A. Rietveld, K. Simons, The differential miscibility of lipids as the basis for the formation of functional membrane rafts. *Biochim Biophys Acta* **1376**, 467-479 (1998).
106. P. J. Quinn, C. Wolf, The liquid-ordered phase in membranes. *Biochim Biophys Acta* **1788**, 33-46 (2009).
107. L. S. Debruin, G. Harauz, White matter rafting--membrane microdomains in myelin. *Neurochem Res* **32**, 213-228 (2007).
108. G. Saher, S. Quintes, K. A. Nave, Cholesterol: a novel regulatory role in myelin formation. *Neuroscientist* **17**, 79-93 (2011).
109. X. Cao, M. A. Surma, K. Simons, Polarized sorting and trafficking in epithelial cells. *Cell Res* **22**, 793-805 (2012).
110. R. G. Parton, Caveolae: Structure, Function, and Relationship to Disease. *Annu Rev Cell Dev Biol* **34**, 111-136 (2018).
111. D. A. Brown, E. London, Structure of detergent-resistant membrane domains: does phase separation occur in biological membranes? *Biochem Biophys Res Commun* **240**, 1-7 (1997).
112. D. Delacour, R. Jacob, Apical protein transport. *Cell Mol Life Sci* **63**, 2491-2505 (2006).
113. R. J. Morris, A. Jen, A. Warley, Isolation of nano-meso scale detergent resistant membrane that has properties expected of lipid 'rafts'. *J Neurochem* **116**, 671-677 (2011).
114. K. Simons, E. Ikonen, Functional rafts in cell membranes. *Nature* **387**, 569-572 (1997).
115. I. Levental, S. Veatch, The Continuing Mystery of Lipid Rafts. *J. Mol. Biol.* **428**, 4749-4764 (2016).
116. D. Lingwood, K. Simons, Lipid rafts as a membrane-organizing principle. *Science* **327**, 46-50 (2010).
117. E. Sezgin, I. Levental, S. Mayor, C. Eggeling, The mystery of membrane organization: composition, regulation and roles of lipid rafts. *Nat Rev Mol Cell Biol* **18**, 361-374 (2017).
118. K. R. Levental, I. Levental, Giant plasma membrane vesicles: models for understanding membrane organization. *Curr Top Membr* **75**, 25-57 (2015).
119. K. Morigaki, Y. Tanimoto, Evolution and development of model membranes for physicochemical and functional studies of the membrane lateral heterogeneity. *Biochim Biophys Acta Biomembr*, (2018).
120. S. P. Rayermann, G. E. Rayermann, C. E. Cornell, A. J. Merz, S. L. Keller, Hallmarks of Reversible Separation of Living, Unperturbed Cell Membranes into Two Liquid Phases. *Biophys J* **113**, 2425-2432 (2017).
121. M. L. Kraft, Plasma membrane organization and function: moving past lipid rafts. *Mol Biol Cell* **24**, 2765-2768 (2013).
122. P. F. Almeida, A. Pokorny, A. Hinderliter, Thermodynamics of membrane domains. *Biochim Biophys Acta* **1720**, 1-13 (2005).
123. J. H. Lorent, I. Levental, Structural determinants of protein partitioning into ordered membrane domains and lipid rafts. *Chem Phys Lipids* **192**, 23-32 (2015).
124. A. Shah *et al.*, RaftProt: mammalian lipid raft proteome database. *Nucleic Acids Res* **43**, D335-338 (2015).
125. I. Levental, D. Lingwood, M. Grzybek, U. Coskun, K. Simons, Palmitoylation regulates raft affinity for the majority of integral raft proteins. *Proc Natl Acad Sci U S A* **107**, 22050-22054 (2010).
126. J. H. Lorent *et al.*, Structural determinants and functional consequences of protein affinity for membrane rafts. *Nat Commun* **8**, 1219 (2017).
127. L. D. Nelson, S. Chiantia, E. London, Perfringolysin O association with ordered lipid domains: implications for transmembrane protein raft affinity. *Biophys J* **99**, 3255-3263 (2010).
128. S. T. Yang, V. Kiessling, J. A. Simmons, J. M. White, L. K. Tamm, HIV gp41-mediated membrane fusion occurs at edges of cholesterol-rich lipid domains. *Nat Chem Biol* **11**, 424-431 (2015).
129. C. Nicolini *et al.*, Visualizing association of N-ras in lipid microdomains: influence of domain structure and interfacial adsorption. *J Am Chem Soc* **128**, 192-201 (2006).
130. K. Weise, G. Triola, L. Brunsveld, H. Waldmann, R. Winter, Influence of the lipidation motif on the partitioning and association of N-Ras in model membrane subdomains. *J Am Chem Soc* **131**, 1557-1564 (2009).
131. M. Burns, K. Wisser, J. Wu, I. Levental, S. L. Veatch, Miscibility Transition Temperature Scales with Growth Temperature in a Zebrafish Cell Line. *Biophys J* **113**, 1212-1222 (2017).

132. A. R. Honerkamp-Smith *et al.*, Line tensions, correlation lengths, and critical exponents in lipid membranes near critical points. *Biophys J* **95**, 236-246 (2008).
133. A. R. Honerkamp-Smith, S. L. Veatch, S. L. Keller, An introduction to critical points for biophysicists; observations of compositional heterogeneity in lipid membranes. *Biochim. Biophys. Acta* **1788**, 53-63 (2009).
134. S. L. Veatch *et al.*, Critical fluctuations in plasma membrane vesicles. *ACS Chem Biol* **3**, 287-293 (2008).
135. D. Marsh, Liquid-ordered phases induced by cholesterol: a compendium of binary phase diagrams. *Biochim Biophys Acta* **1798**, 688-699 (2010).
136. M. B. Stone, S. A. Shelby, M. F. Nunez, K. Wisser, S. L. Veatch, Protein sorting by lipid phase-like domains supports emergent signaling function in B lymphocyte plasma membranes. *Elife* **6**, (2017).
137. S. L. Veatch, S. L. Keller, Seeing spots: complex phase behavior in simple membranes. *Biochim Biophys Acta* **1746**, 172-185 (2005).
138. J. F. Frisz *et al.*, Sphingolipid domains in the plasma membranes of fibroblasts are not enriched with cholesterol. *J Biol Chem* **288**, 16855-16861 (2013).
139. D. Wustner, M. Modzel, F. W. Lund, M. A. Lomholt, Imaging approaches for analysis of cholesterol distribution and dynamics in the plasma membrane. *Chem Phys Lipids* **199**, 106-135 (2016).
140. J. F. Frisz *et al.*, Direct chemical evidence for sphingolipid domains in the plasma membranes of fibroblasts. *Proc Natl Acad Sci U S A* **110**, E613-622 (2013).
141. M. L. Kraft, Sphingolipid Organization in the Plasma Membrane and the Mechanisms That Influence It. *Front Cell Dev Biol* **4**, 154 (2016).
142. X. Cong, Y. Liu, W. Liu, X. Liang, A. Laganowsky, Allosteric modulation of protein-protein interactions by individual lipid binding events. *Nat Commun* **8**, 2203 (2017).
143. K. Gupta *et al.*, Identifying key membrane protein lipid interactions using mass spectrometry. *Nat Protoc* **13**, 1106-1120 (2018).
144. A. G. Lee, How lipids affect the activities of integral membrane proteins. *Biochim Biophys Acta* **1666**, 62-87 (2004).
145. G. Jaipuria *et al.*, Cholesterol-mediated allosteric regulation of the mitochondrial translocator protein structure. *Nat Commun* **8**, 14893 (2017).
146. M. Manna *et al.*, Mechanism of allosteric regulation of beta2-adrenergic receptor by cholesterol. *Elife* **5**, (2016).
147. I. Liko *et al.*, Lipid binding attenuates channel closure of the outer membrane protein OmpF. *Proc Natl Acad Sci U S A* **115**, 6691-6696 (2018).
148. F. J. Taberner, G. Fernandez-Ballester, A. Fernandez-Carvajal, A. Ferrer-Montiel, TRP channels interaction with lipids and its implications in disease. *Biochim Biophys Acta* **1848**, 1818-1827 (2015).
149. S. B. Hansen, Lipid agonism: The PIP2 paradigm of ligand-gated ion channels. *Biochim Biophys Acta* **1851**, 620-628 (2015).
150. K. C. Taylor, C. R. Sanders, Regulation of KCNQ/Kv7 family voltage-gated K(+) channels by lipids. *Biochim Biophys Acta* **1859**, 586-597 (2017).
151. A. G. Lee, Lipid-protein interactions. *Biochemical Society transactions* **39**, 761-766 (2011).
152. C. R. Sanders, J. M. Hutchison, Membrane properties that shape the evolution of membrane enzymes. *Current opinion in structural biology* **51**, 80-91 (2018).
153. K. Gupta *et al.*, The role of interfacial lipids in stabilizing membrane protein oligomers. *Nature* **541**, 421-424 (2017).
154. C. Hunte, Specific protein-lipid interactions in membrane proteins. *Biochemical Society transactions* **33**, 938-942 (2005).
155. M. Landreh, M. T. Marty, J. Gault, C. V. Robinson, A sliding selectivity scale for lipid binding to membrane proteins. *Current opinion in structural biology* **39**, 54-60 (2016).
156. L. Qin, M. A. Sharpe, R. M. Garavito, S. Ferguson-Miller, Conserved lipid-binding sites in membrane proteins: a focus on cytochrome c oxidase. *Current opinion in structural biology* **17**, 444-450 (2007).
157. P. L. Yeagle, Non-covalent binding of membrane lipids to membrane proteins. *Biochim Biophys Acta* **1838**, 1548-1559 (2014).
158. M. Bogdanov, W. Dowhan, Lipid-assisted protein folding. *J Biol Chem* **274**, 36827-36830 (1999).
159. M. Bogdanov, W. Dowhan, H. Vitrac, Lipids and topological rules governing membrane protein assembly. *Biochim Biophys Acta* **1843**, 1475-1488 (2014).

160. A. M. Seddon *et al.*, Phosphatidylglycerol lipids enhance folding of an alpha helical membrane protein. *J Mol Biol* **380**, 548-556 (2008).
161. J. Skorko-Glonek *et al.*, HtrA heat shock protease interacts with phospholipid membranes and undergoes conformational changes. *J Biol Chem* **272**, 8974-8982 (1997).
162. D. K. Debnath, R. V. Basaiawmoit, K. L. Nielsen, D. E. Otzen, The role of membrane properties in Mistic folding and dimerisation. *Protein engineering, design & selection : PEDS* **24**, 89-97 (2011).
163. A. H. Dewald, J. C. Hodges, L. Columbus, Physical determinants of beta-barrel membrane protein folding in lipid vesicles. *Biophys J* **100**, 2131-2140 (2011).
164. F. Cymer, A. Veerappan, D. Schneider, Transmembrane helix-helix interactions are modulated by the sequence context and by lipid bilayer properties. *Biochim Biophys Acta* **1818**, 963-973 (2012).
165. S. J. Allen, A. R. Curran, R. H. Templer, W. Meijberg, P. J. Booth, Controlling the folding efficiency of an integral membrane protein. *J Mol Biol* **342**, 1293-1304 (2004).
166. M. R. Sanders, H. E. Findlay, P. J. Booth, Lipid bilayer composition modulates the unfolding free energy of a knotted alpha-helical membrane protein. *Proc Natl Acad Sci U S A* **115**, E1799-E1808 (2018).
167. M. Bogdanov, E. Mileykovskaya, W. Dowhan, Lipids in the assembly of membrane proteins and organization of protein supercomplexes: implications for lipid-linked disorders. *Subcell Biochem* **49**, 197-239 (2008).
168. K. F. Mittendorf *et al.*, Peripheral myelin protein 22 alters membrane architecture. *Science Advances* **3**, (2017).
169. J. L. Popot, D. M. Engelman, Membranes Do Not Tell Proteins How To Fold. *Biochemistry* **55**, 5-18 (2016).
170. N. P. Ulrih, D. Gmajner, P. Raspor, Structural and physicochemical properties of polar lipids from thermophilic archaea. *Appl Microbiol Biotechnol* **84**, 249-260 (2009).
171. P. J. Stansfeld, E. E. Jefferys, M. S. Sansom, Multiscale simulations reveal conserved patterns of lipid interactions with aquaporins. *Structure* **21**, 810-819 (2013).
172. K. Matsumoto, Dispensable nature of phosphatidylglycerol in Escherichia coli: dual roles of anionic phospholipids. *Mol Microbiol* **39**, 1427-1433 (2001).
173. I. Shibuya, Metabolic regulations and biological functions of phospholipids in Escherichia coli. *Prog Lipid Res* **31**, 245-299 (1992).
174. C. R. Sanders, K. F. Mittendorf, Tolerance to changes in membrane lipid composition as a selected trait of membrane proteins. *Biochemistry* **50**, 7858-7867 (2011).
175. T. Dahmane, F. Rappaport, J. L. Popot, Amphipol-assisted folding of bacteriorhodopsin in the presence or absence of lipids: functional consequences. *Eur Biophys J* **42**, 85-101 (2013).
176. B. M. Gorzelle *et al.*, Amphipols can support the activity of a membrane enzyme. *J Am Chem Soc* **124**, 11594-11595 (2002).
177. K. A. Dill, H. S. Chan, From Levinthal to pathways to funnels. *Nat Struct Biol* **4**, 10-19 (1997).
178. S. W. Englander, L. Mayne, The nature of protein folding pathways. *Proc Natl Acad Sci U S A* **111**, 15873-15880 (2014).
179. C. Park, S. Zhou, J. Gilmore, S. Marqusee, Energetics-based protein profiling on a proteomic scale: identification of proteins resistant to proteolysis. *J Mol Biol* **368**, 1426-1437 (2007).
180. S. Bibow, S. Hiller, A guide to quantifying membrane protein dynamics in lipids and other native-like environments by solution-state NMR spectroscopy. *The FEBS journal*, (2018).
181. A. Dutta *et al.*, Differential dynamics of extracellular and cytoplasmic domains in denatured States of rhodopsin. *Biochemistry* **53**, 7160-7169 (2014).
182. A. Dutta, K. C. Tirupula, U. Alexiev, J. Klein-Seetharaman, Characterization of membrane protein non-native states. 1. Extent of unfolding and aggregation of rhodopsin in the presence of chemical denaturants. *Biochemistry* **49**, 6317-6328 (2010).
183. H. Tafer, S. Hiller, C. Hilty, C. Fernandez, K. Wuthrich, Nonrandom structure in the urea-unfolded Escherichia coli outer membrane protein X (OmpX). *Biochemistry* **43**, 860-869 (2004).
184. M. Sakakura, A. Hadziselimovic, Z. Wang, K. L. Schey, C. R. Sanders, Structural Basis for the Trembler-J Phenotype of Charcot-Marie-Tooth Disease. *Structure* **19**, 1160-1169 (2011).
185. H. Huang *et al.*, Mechanisms of KCNQ1 channel dysfunction in long QT syndrome involving voltage sensor domain mutations. *Sci Adv* **4**, eaar2631 (2018).

186. C. Redfield, NMR studies of partially folded molten-globule states. *Methods Mol Biol* **278**, 233-254 (2004).
187. J. H. Kleinschmidt, J. L. Popot, Folding and stability of integral membrane proteins in amphipols. *Arch Biochem Biophys* **564**, 327-343 (2014).
188. J. H. Kleinschmidt, Folding of beta-barrel membrane proteins in lipid bilayers - Unassisted and assisted folding and insertion. *Biochim Biophys Acta* **1848**, 1927-1943 (2015).
189. F. Barrera *et al.*, Unfolding and refolding in vitro of a tetrameric, alpha-helical membrane protein: the prokaryotic potassium channel KcsA. *Biochemistry* **44**, 14344-14352 (2005).
190. H. Hong, L. Tamm, Elastic coupling of integral membrane protein stability to lipid bilayer forces. *Proc Natl Acad Sci U S A* **101**, 4065-4070 (2004).
191. C. P. Moon, K. G. Fleming, Side-chain hydrophobicity scale derived from transmembrane protein folding into lipid bilayers. *Proc Natl Acad Sci U S A* **108**, 10174-10177 (2011).
192. H. E. Findlay, N. G. Rutherford, P. J. Henderson, P. J. Booth, Unfolding free energy of a two-domain transmembrane sugar transport protein. *Proc Natl Acad Sci U S A* **107**, 18451-18456 (2010).
193. N. J. Harris, H. E. Findlay, J. Simms, X. Liu, P. J. Booth, Relative domain folding and stability of a membrane transport protein. *J Mol Biol* **426**, 1812-1825 (2014).
194. J. K. Nagy, W. L. Lonzer, C. R. Sanders, Kinetic study of folding and misfolding of diacylglycerol kinase in model membranes. *Biochemistry* **40**, 8971-8980 (2001).
195. D. Otzen, Folding of DsbB in mixed micelles: a kinetic analysis of the stability of a bacterial membrane protein. *J Mol Biol* **330**, 641-649 (2003).
196. W. Paslawski *et al.*, Cooperative folding of a polytopic alpha-helical membrane protein involves a compact N-terminal nucleus and nonnative loops. *Proc Natl Acad Sci U S A* **112**, 7978-7983 (2015).
197. J. P. Schlebach *et al.*, Reversible folding of human peripheral myelin protein 22, a tetraspan membrane protein. *Biochemistry* **52**, 3229-3241 (2013).
198. Y. C. Chang, J. U. Bowie, Measuring membrane protein stability under native conditions. *Proc Natl Acad Sci U S A* **111**, 219-224 (2014).
199. R. Guo *et al.*, Steric trapping reveals a cooperativity network in the intramembrane protease GlpG. *Nat Chem Biol* **12**, 353-360 (2016).
200. R. E. Jefferson, D. Min, K. Corin, J. Y. Wang, J. U. Bowie, Applications of Single-Molecule Methods to Membrane Protein Folding Studies. *J Mol Biol* **430**, 424-437 (2018).
201. D. Min *et al.*, Unfolding of a ClC chloride transporter retains memory of its evolutionary history. *Nat Chem Biol*, (2018).
202. D. J. Muller *et al.*, Stability of bacteriorhodopsin alpha-helices and loops analyzed by single-molecule force spectroscopy. *Biophys J* **83**, 3578-3588 (2002).
203. D. Shortle, The denatured state (the other half of the folding equation) and its role in protein stability. *FASEB J* **10**, 27-34 (1996).
204. G. Chen, E. Gouaux, Probing the folding and unfolding of wild-type and mutant forms of bacteriorhodopsin in micellar solutions: evaluation of reversible unfolding conditions. *Biochemistry* **38**, 15380-15387 (1999).
205. N. Burgess, T. Dao, A. Stanley, K. Fleming, Beta-barrel proteins that reside in the Escherichia coli outer membrane in vivo demonstrate varied folding behavior in vitro. *J Biol Chem* **283**, 26748-26758 (2008).
206. C. P. Moon, N. R. Zaccai, P. J. Fleming, D. Gessmann, K. G. Fleming, Membrane protein thermodynamic stability may serve as the energy sink for sorting in the periplasm. *Proc Natl Acad Sci U S A* **110**, 4285-4290 (2013).
207. J. Bakelar, S. K. Buchanan, N. Noinaj, The structure of the beta-barrel assembly machinery complex. *Science* **351**, 180-186 (2016).
208. D. A. Holdbrook *et al.*, A Spring-Loaded Mechanism Governs the Clamp-like Dynamics of the Skp Chaperone. *Structure* **25**, 1079-1088 e1073 (2017).
209. S. K. McDonald, K. G. Fleming, Aromatic Side Chain Water-to-Lipid Transfer Free Energies Show a Depth Dependence across the Membrane Normal. *J Am Chem Soc* **138**, 7946-7950 (2016).
210. D. C. Marx, K. G. Fleming, Influence of Protein Scaffold on Side-Chain Transfer Free Energies. *Biophys J* **113**, 597-604 (2017).
211. H. Hong, D. Rinehart, L. K. Tamm, Membrane depth-dependent energetic contribution of the tryptophan side chain to the stability of integral membrane proteins. *Biochemistry* **52**, 4413-4421 (2013).

212. Y. Yang *et al.*, Folding-Degradation Relationship of a Membrane Protein Mediated by the Universally Conserved ATP-Dependent Protease FtsH. *J Am Chem Soc* **140**, 4656-4665 (2018).
213. R. R. Kopito, Aggresomes, inclusion bodies and protein aggregation. *Trends Cell Biol* **10**, 524-530 (2000).
214. V. Krishnamani, B. G. Hegde, R. Langen, J. K. Lanyi, Secondary and Tertiary Structure of Bacteriorhodopsin in the SDS Denatured State. *Biochemistry*, (2012).
215. P. Curnow, P. Booth, Combined kinetic and thermodynamic analysis of alpha-helical membrane protein unfolding. *Proc Natl Acad Sci U S A* **104**, 18970-18975 (2007).
216. S. Faham *et al.*, Side-chain contributions to membrane protein structure and stability. *J Mol Biol* **335**, 297-305 (2004).
217. Z. Cao, J. Schlebach, C. Park, J. U. Bowie, Thermodynamic stability of bacteriorhodopsin mutants measured relative to the bacterioopsin unfolded state. *Biochim Biophys Acta*, (2011).
218. R. P. Baker, S. Urban, Architectural and thermodynamic principles underlying intramembrane protease function. *Nat Chem Biol* **8**, 759-768 (2012).
219. M. Faerch *et al.*, Diverse vasopressin V2 receptor functionality underlying partial congenital nephrogenic diabetes insipidus. *Am J Physiol Renal Physiol* **297**, F1518-1525 (2009).
220. R. L. Wiseman, E. T. Powers, J. N. Buxbaum, J. W. Kelly, W. E. Balch, An adaptable standard for protein export from the endoplasmic reticulum. *Cell* **131**, 809-821 (2007).
221. E. T. Powers, D. L. Powers, L. M. Gierasch, FoldEco: a model for proteostasis in E. coli. *Cell Rep* **1**, 265-276 (2012).
222. S. M. Costello, A. M. Plummer, P. J. Fleming, K. G. Fleming, Dynamic periplasmic chaperone reservoir facilitates biogenesis of outer membrane proteins. *Proc Natl Acad Sci U S A* **113**, E4794-4800 (2016).
223. M. Santra, D. W. Farrell, K. A. Dill, Bacterial proteostasis balances energy and chaperone utilization efficiently. *Proc Natl Acad Sci U S A* **114**, E2654-E2661 (2017).
224. R. E. Jefferson, T. M. Blois, J. U. Bowie, Membrane proteins can have high kinetic stability. *J. Am. Chem. Soc.* **135**, 15183-15190 (2013).
225. R. Benyair, N. Ogen-Shtern, G. Z. Lederkremer, Glycan regulation of ER-associated degradation through compartmentalization. *Seminars in cell & developmental biology* **41**, 99-109 (2015).
226. D. E. Otzen, Folding of DsbB in mixed micelles: a kinetic analysis of the stability of a bacterial membrane protein. *J Mol Biol* **330**, 641-649 (2003).
227. P. Sehgal, D. E. Otzen, Thermodynamics of unfolding of an integral membrane protein in mixed micelles. *Protein Sci* **15**, 890-899 (2006).
228. P. Curnow, P. J. Booth, The contribution of a covalently bound cofactor to the folding and thermodynamic stability of an integral membrane protein. *J Mol Biol* **403**, 630-642 (2010).
229. N. J. Leidenheimer, Pharmacological chaperones: beyond conformational disorders. *Handb Exp Pharmacol* **245**, 135-153 (2018).
230. A. G. Shearer, R. Y. Hampton, Lipid-mediated, reversible misfolding of a sterol-sensing domain protein. *EMBO J* **24**, 149-159 (2005).
231. Y. X. Tao, P. M. Conn, Chaperoning G protein-coupled receptors: from cell biology to therapeutics. *Endocr Rev* **35**, 602-647 (2014).
232. M. B. Gill, P. Vivithanaporn, G. T. Swanson, Glutamate binding and conformational flexibility of ligand-binding domains are critical early determinants of efficient kainate receptor biogenesis. *J Biol Chem* **284**, 14503-14512 (2009).
233. A. Prodohl, T. Volkmer, C. Finger, D. Schneider, Defining the structural basis for assembly of a transmembrane cytochrome. *J Mol Biol* **350**, 744-756 (2005).
234. D. M. Engelman *et al.*, Membrane protein folding: beyond the two stage model. *FEBS letters* **555**, 122-125 (2003).
235. T. Zhang, Y. Xu, Y. Liu, Y. Ye, gp78 functions downstream of Hrd1 to promote degradation of misfolded proteins of the endoplasmic reticulum. *Molecular Biology of the Cell* **26**, 4438-4450 (2015).
236. H. Tian, T. P. Sakmar, T. Huber, The Energetics of Chromophore Binding in the Visual Photoreceptor Rhodopsin. *Biophys J* **113**, 60-72 (2017).
237. M. A. Wangeline, N. Vashistha, R. Y. Hampton, Proteostatic Tactics in the Strategy of Sterol Regulation. *Annu Rev Cell Dev Biol* **33**, 467-489 (2017).
238. R. G. Gardner, R. Y. Hampton, A 'distributed degron' allows regulated entry into the ER degradation pathway. *EMBO J* **18**, 5994-6004 (1999).

239. C. Levinthal. (Journal de chimie physique et de physico-chimie biologique, 1968), vol. 65, pp. 44-45.
240. Y. Bai, T. R. Sosnick, L. Mayne, S. W. Englander, Protein folding intermediates: native-state hydrogen exchange. *Science* **269**, 192-197 (1995).
241. R. Bravo *et al.*, Endoplasmic reticulum and the unfolded protein response: dynamics and metabolic integration. *Int Rev Cell Mol Biol* **301**, 215-290 (2013).
242. R. B. Best, G. Hummer, Microscopic interpretation of folding varphi-values using the transition path ensemble. *Proc Natl Acad Sci U S A* **113**, 3263-3268 (2016).
243. J. Bowie, Solving the membrane protein folding problem. *Nature* **438**, 581-589 (2005).
244. M. Riley, B. Wallace, S. Flitsch, P. Booth, Slow alpha helix formation during folding of a membrane protein. *Biochemistry* **36**, 192-196 (1997).
245. P. Beguin, U. Hasler, O. Staub, K. Geering, Endoplasmic reticulum quality control of oligomeric membrane proteins: Topogenic determinants involved in the degradation of the unassembled Na,K-ATPase alpha subunit and in its stabilization by beta subunit assembly. *Molecular Biology of the Cell* **11**, 1657-1672 (2000).
246. P. Curnow *et al.*, Stable folding core in the folding transition state of an alpha-helical integral membrane protein. *Proc Natl Acad Sci U S A* **108**, 14133-14138 (2011).
247. A. R. Fersht, A. Matouschek, L. Serrano, The folding of an enzyme. I. Theory of protein engineering analysis of stability and pathway of protein folding. *J Mol Biol* **224**, 771-782 (1992).
248. J. P. Schlebach, Z. Cao, J. U. Bowie, C. Park, Revisiting the folding kinetics of bacteriorhodopsin. *Protein Sci* **21**, 97-106 (2012).
249. J. P. Schlebach, N. B. Woodall, J. U. Bowie, C. Park, Bacteriorhodopsin folds through a poorly organized transition state. *J Am Chem Soc* **136**, 16574-16581 (2014).
250. K. W. Plaxco, K. T. Simons, D. Baker, Contact order, transition state placement and the refolding rates of single domain proteins. *J Mol Biol* **277**, 985-994 (1998).
251. T. C. Gruenhagen, J. J. Ziarek, J. P. Schlebach, Bicelle size modulates the rate of bacteriorhodopsin folding. *Protein Sci*, (2018).
252. D. E. Otzen, Mapping the folding pathway of the transmembrane protein DsbB by protein engineering. *Protein engineering, design & selection : PEDS* **24**, 139-149 (2011).
253. H. J. Nam, S. K. Han, J. U. Bowie, S. Kim, Rampant exchange of the structure and function of extramembrane domains between membrane and water soluble proteins. *PLoS Comput Biol* **9**, e1002997 (2013).
254. T. Surrey, F. Jahnig, Kinetics of folding and membrane insertion of a beta-barrel membrane protein. *J Biol Chem* **270**, 28199-28203 (1995).
255. T. Surrey, A. Schmid, F. Jahnig, Folding and membrane insertion of the trimeric beta-barrel protein OmpF. *Biochemistry* **35**, 2283-2288 (1996).
256. K. Du, G. L. Lukacs, Cooperative assembly and misfolding of CFTR domains in vivo. *Mol Biol Cell* **20**, 1903-1915 (2009).
257. J. H. Kleinschmidt, T. den Blaauwen, A. J. Driessen, L. K. Tamm, Outer membrane protein A of Escherichia coli inserts and folds into lipid bilayers by a concerted mechanism. *Biochemistry* **38**, 5006-5016 (1999).
258. J. H. Kleinschmidt, L. K. Tamm, Secondary and tertiary structure formation of the beta-barrel membrane protein OmpA is synchronized and depends on membrane thickness. *J Mol Biol* **324**, 319-330 (2002).
259. L. K. Tamm, A. Arora, J. H. Kleinschmidt, Structure and assembly of beta-barrel membrane proteins. *J Biol Chem* **276**, 32399-32402 (2001).
260. G. H. Huysmans, S. E. Radford, S. A. Baldwin, D. J. Brockwell, Malleability of the folding mechanism of the outer membrane protein PagP: parallel pathways and the effect of membrane elasticity. *J Mol Biol* **416**, 453-464 (2012).
261. G. H. Huysmans, S. A. Baldwin, D. J. Brockwell, S. E. Radford, The transition state for folding of an outer membrane protein. *Proc Natl Acad Sci U S A* **107**, 4099-4104 (2010).
262. E. J. Danoff, K. G. Fleming, Membrane defects accelerate outer membrane beta-barrel protein folding. *Biochemistry* **54**, 97-99 (2015).
263. E. J. Danoff, K. G. Fleming, Novel Kinetic Intermediates Populated along the Folding Pathway of the Transmembrane beta-Barrel OmpA. *Biochemistry* **56**, 47-60 (2017).

264. R. Voulhoux, M. P. Bos, J. Geurtsen, M. Mols, J. Tommassen, Role of a highly conserved bacterial protein in outer membrane protein assembly. *Science* **299**, 262-265 (2003).
265. A. M. Plummer, K. G. Fleming, BamA Alone Accelerates Outer Membrane Protein Folding In Vitro through a Catalytic Mechanism. *Biochemistry* **54**, 6009-6011 (2015).
266. T. A. Walton, C. M. Sandoval, C. A. Fowler, A. Pardi, M. C. Sousa, The cavity-chaperone Skp protects its substrate from aggregation but allows independent folding of substrate domains. *Proc Natl Acad Sci U S A* **106**, 1772-1777 (2009).
267. T. M. Blois, H. Hong, T. H. Kim, J. U. Bowie, Protein unfolding with a steric trap. *J Am Chem Soc* **131**, 13914-13915 (2009).
268. J. P. Schlebach, C. R. Sanders, The safety dance: biophysics of membrane protein folding and misfolding in a cellular context. *Quarterly Reviews of Biophysics* **48**, 1-34 (2015).
269. H. Hong, T. M. Blois, Z. Cao, J. U. Bowie, Method to measure strong protein-protein interactions in lipid bilayers using a steric trap. *Proc Natl Acad Sci U S A* **107**, 19802-19807 (2010).
270. H. Hong, J. U. Bowie, Dramatic destabilization of transmembrane helix interactions by features of natural membrane environments. *J. Am. Chem. Soc.* **133**, 11389-11398 (2011).
271. D. Min, R. E. Jefferson, J. U. Bowie, T. Y. Yoon, Mapping the energy landscape for second-stage folding of a single membrane protein. *Nat Chem Biol* **11**, 981-987 (2015).
272. J. L. Popot, Integral Membrane-Protein Structure - Transmembrane Alpha-Helices as Autonomous Folding Domains. *Current opinion in structural biology* **3**, 532-540 (1993).
273. C. King, V. Raicu, K. Hristova, Understanding the FRET Signatures of Interacting Membrane Proteins. *J Biol Chem* **292**, 5291-5310 (2017).
274. C. King, M. Stoneman, V. Raicu, K. Hristova, Fully quantified spectral imaging reveals in vivo membrane protein interactions. *Integr Biol (Camb)* **8**, 216-229 (2016).
275. S. Sarabipour, K. Ballmer-Hofer, K. Hristova, VEGFR-2 conformational switch in response to ligand binding. *Elife* **5**, e13876 (2016).
276. W. D. Comar, S. M. Schubert, B. Jastrzebska, K. Palczewski, A. W. Smith, Time-resolved fluorescence spectroscopy measures clustering and mobility of a G protein-coupled receptor opsin in live cell membranes. *J Am Chem Soc* **136**, 8342-8349 (2014).
277. Y. Huang *et al.*, Molecular basis for multimerization in the activation of the epidermal growth factor receptor. *Elife* **5**, (2016).
278. W. D. Van Horn, C. R. Sanders, Prokaryotic diacylglycerol kinase and undecaprenol kinase. *Annual review of biophysics* **41**, 81-101 (2012).
279. D. Li *et al.*, Crystal structure of the integral membrane diacylglycerol kinase. *Nature* **497**, 521-524 (2013).
280. D. Li *et al.*, Ternary structure reveals mechanism of a membrane diacylglycerol kinase. *Nat Commun* **6**, 10140 (2015).
281. J. Wen, X. Chen, J. U. Bowie, Exploring the allowed sequence space of a membrane protein. *Nat Struct Biol* **3**, 141-148 (1996).
282. Y. Zhou, J. Wen, J. U. Bowie, A passive transmembrane helix. *Nat Struct Biol* **4**, 986-990 (1997).
283. B. M. Gorzelle *et al.*, Reconstitutive refolding of diacylglycerol kinase, an integral membrane protein. *Biochemistry* **38**, 16373-16382 (1999).
284. M. Lorch, P. J. Booth, Insertion kinetics of a denatured alpha helical membrane protein into phospholipid bilayer vesicles. *J Mol Biol* **344**, 1109-1121 (2004).
285. D. Mi, H. J. Kim, A. Hadziselimovic, C. R. Sanders, Irreversible misfolding of diacylglycerol kinase is independent of aggregation and occurs prior to trimerization and membrane association. *Biochemistry* **45**, 10072-10084 (2006).
286. J. K. Nagy, C. R. Sanders, Destabilizing mutations promote membrane protein misfolding. *Biochemistry* **43**, 19-25 (2004).
287. J. K. Nagy, C. R. Sanders, A critical residue in the folding pathway of an integral membrane protein. *Biochemistry* **41**, 9021-9025 (2002).
288. C. R. Sanders, J. K. Myers, Disease-related misassembly of membrane proteins. *Annu Rev Biophys Biomol Struct* **33**, 25-51 (2004).
289. J. P. Schlebach *et al.*, Conformational Stability and Pathogenic Misfolding of the Integral Membrane Protein PMP22. *Journal of the American Chemical Society* **137**, 8758-8768 (2015).

290. K. Stroobants *et al.*, Amyloid-like Fibrils from an alpha-Helical Transmembrane Protein. *Biochemistry* **56**, 3225-3233 (2017).
291. F. Chiti *et al.*, Designing conditions for in vitro formation of amyloid protofilaments and fibrils. *Proc Natl Acad Sci U S A* **96**, 3590-3594 (1999).
292. A. Saenz *et al.*, Folding and Intramembraneous BRICHOS Binding of the Prosurfactant Protein C Transmembrane Segment. *J Biol Chem* **290**, 17628-17641 (2015).
293. J. Lee *et al.*, Amyloid beta Ion Channels in a Membrane Comprising Brain Total Lipid Extracts. *ACS Chem Neurosci* **8**, 1348-1357 (2017).
294. M. Serra-Batiste *et al.*, Abeta42 assembles into specific beta-barrel pore-forming oligomers in membrane-mimicking environments. *Proc Natl Acad Sci U S A* **113**, 10866-10871 (2016).
295. M. Serra-Batiste, J. Tolchard, F. Giusti, M. Zoonens, N. Carulla, Stabilization of a Membrane-Associated Amyloid-beta Oligomer for Its Validation in Alzheimer's Disease. *Front Mol Biosci* **5**, 38 (2018).
296. B. L. Kagan, Membrane pores in the pathogenesis of neurodegenerative disease. *Prog Mol Biol Transl Sci* **107**, 295-325 (2012).
297. H. Jang *et al.*, Disordered amyloidogenic peptides may insert into the membrane and assemble into common cyclic structural motifs. *Chem Soc Rev* **43**, 6750-6764 (2014).
298. R. Bystrom *et al.*, Disordered proteins: biological membranes as two-dimensional aggregation matrices. *Cell biochemistry and biophysics* **52**, 175-189 (2008).
299. I. Dikiy, D. Eliezer, Folding and misfolding of alpha-synuclein on membranes. *Biochim Biophys Acta* **1818**, 1013-1018 (2012).
300. G. P. Gorbenko, P. K. Kinnunen, The role of lipid-protein interactions in amyloid-type protein fibril formation. *Chem Phys Lipids* **141**, 72-82 (2006).
301. J. Habchi *et al.*, Cholesterol catalyses Abeta42 aggregation through a heterogeneous nucleation pathway in the presence of lipid membranes. *Nature chemistry* **10**, 673-683 (2018).
302. J. Kazlauskaite, T. J. Pinheiro, Aggregation and fibrillization of prions in lipid membranes. *Biochemical Society symposium*, 211-222 (2005).
303. M. Stefani, Biochemical and biophysical features of both oligomer/fibril and cell membrane in amyloid cytotoxicity. *The FEBS journal* **277**, 4602-4613 (2010).
304. J. E. Straub, D. Thirumalai, Membrane-Protein Interactions Are Key to Understanding Amyloid Formation. *The journal of physical chemistry letters* **5**, 633-635 (2014).
305. M. S. Terakawa *et al.*, Impact of membrane curvature on amyloid aggregation. *Biochim Biophys Acta*, (2018).
306. K. Matsuzaki, K. Kato, K. Yanagisawa, Abeta polymerization through interaction with membrane gangliosides. *Biochim Biophys Acta* **1801**, 868-877 (2010).
307. V. Rangachari, D. N. Dean, P. Rana, A. Vaidya, P. Ghosh, Cause and consequence of Abeta - Lipid interactions in Alzheimer disease pathogenesis. *Biochim Biophys Acta*, (2018).
308. M. Decock *et al.*, Glycines from the APP GXXXG/GXXXA Transmembrane Motifs Promote Formation of Pathogenic Abeta Oligomers in Cells. *Frontiers in aging neuroscience* **8**, 107 (2016).
309. C. Galvagnion, The Role of Lipids Interacting with alpha-Synuclein in the Pathogenesis of Parkinson's Disease. *J Parkinsons Dis* **7**, 433-450 (2017).
310. A. West, B. E. Brummel, A. R. Braun, E. Rhoades, J. N. Sachs, Membrane remodeling and mechanics: Experiments and simulations of alpha-Synuclein. *Biochim Biophys Acta* **1858**, 1594-1609 (2016).
311. M. Gao, R. Winter, The Effects of Lipid Membranes, Crowding and Osmolytes on the Aggregation, and Fibrillation Propensity of Human IAPP. *J Diabetes Res* **2015**, 849017 (2015).
312. A. Rawat, R. Langen, J. Varkey, Membranes as modulators of amyloid protein misfolding and target of toxicity. *Biochim Biophys Acta*, (2018).
313. K. Sasahara, Membrane-mediated amyloid deposition of human islet amyloid polypeptide. *Biophys Rev* **10**, 453-462 (2018).
314. D. Sarnataro, A. Pepe, C. Zurzolo, Cell Biology of Prion Protein. *Prog Mol Biol Transl Sci* **150**, 57-82 (2017).
315. R. Goold *et al.*, Rapid cell-surface prion protein conversion revealed using a novel cell system. *Nat Commun* **2**, 281 (2011).
316. S. Ambadi Thody, M. K. Mathew, J. B. Udgaonkar, Mechanism of aggregation and membrane interactions of mammalian prion protein. *Biochim Biophys Acta*, (2018).

317. J. C. Samuelson *et al.*, YidC mediates membrane protein insertion in bacteria. *Nature* **406**, 637-641 (2000).
318. R. J. Cabelli, L. Chen, P. C. Tai, D. B. Oliver, SecA protein is required for secretory protein translocation into E. coli membrane vesicles. *Cell* **55**, 683-692 (1988).
319. U. S. Chio, H. Cho, S. O. Shan, Mechanisms of Tail-Anchored Membrane Protein Targeting and Insertion. *Annu Rev Cell Dev Biol* **33**, 417-438 (2017).
320. R. S. Hegde, R. J. Keenan, Tail-anchored membrane protein insertion into the endoplasmic reticulum. *Nat Rev Mol Cell Biol* **12**, 787-798 (2011).
321. A. Mateja, R. J. Keenan, A structural perspective on tail-anchored protein biogenesis by the GET pathway. *Current opinion in structural biology* **51**, 195-202 (2018).
322. A. Guna, N. Volkmar, J. C. Christianson, R. S. Hegde, The ER membrane protein complex is a transmembrane domain insertase. *Science* **359**, 470-473 (2018).
323. M. J. Shurtleff *et al.*, The ER membrane protein complex interacts cotranslationally to enable biogenesis of multipass membrane proteins. *Elife* **7**, (2018).
324. P. J. Chitwood, S. Juszkiewicz, A. Guna, S. Shao, R. S. Hegde, EMC Is Required to Initiate Accurate Membrane Protein Topogenesis. *Cell*, (2018).
325. T. Becker *et al.*, Structure of monomeric yeast and mammalian Sec61 complexes interacting with the translating ribosome. *Science* **326**, 1369-1373 (2009).
326. S. Pfeffer *et al.*, Structure and 3D arrangement of endoplasmic reticulum membrane-associated ribosomes. *Structure* **20**, 1508-1518 (2012).
327. J. Frauenfeld *et al.*, Cryo-EM structure of the ribosome-SecYE complex in the membrane environment. *Nat Struct Mol Biol* **18**, 614-621 (2011).
328. Y. Freudenberg-Hua *et al.*, Disease variants in genomes of 44 centenarians. *Mol Genet Genomic Med* **2**, 438-450 (2014).
329. M. Gogala *et al.*, Structures of the Sec61 complex engaged in nascent peptide translocation or membrane insertion. *Nature* **506**, 107-110 (2014).
330. R. M. Voorhees, I. S. Fernandez, S. H. Scheres, R. S. Hegde, Structure of the mammalian ribosome-Sec61 complex to 3.4 A resolution. *Cell* **157**, 1632-1643 (2014).
331. P. F. Egea, R. M. Stroud, Lateral opening of a translocon upon entry of protein suggests the mechanism of insertion into membranes. *Proc Natl Acad Sci U S A* **107**, 17182-17187 (2010).
332. B. Van den Berg *et al.*, X-ray structure of a protein-conducting channel. *Nature* **427**, 36-44 (2004).
333. R. D. Baldridge, T. A. Rapoport, Autoubiquitination of the Hrd1 Ligase Triggers Protein Retrotranslocation in ERAD. *Cell* **166**, 394-407 (2016).
334. R. C. Boucher, Airway surface dehydration in cystic fibrosis: pathogenesis and therapy. *Annu Rev Med* **58**, 157-170 (2007).
335. S. M. Saparov *et al.*, Determining the conductance of the SecY protein translocation channel for small molecules. *Mol Cell* **26**, 501-509 (2007).
336. S. Pfeffer *et al.*, Structure of the native Sec61 protein-conducting channel. *Nat Commun* **6**, 8403 (2015).
337. R. M. Voorhees, R. S. Hegde, Structure of the Sec61 channel opened by a signal sequence. *Science* **351**, 88-91 (2016).
338. F. Cymer, G. von Heijne, S. H. White, Mechanisms of integral membrane protein insertion and folding. *J Mol Biol* **427**, 999-1022 (2015).
339. J. W. Chartron, K. C. Hunt, J. Frydman, Cotranslational signal-independent SRP preloading during membrane targeting. *Nature* **536**, 224-228 (2016).
340. W. Lu *et al.*, Assembling of AcrB trimer in cell membrane. *J Mol Biol* **423**, 123-134 (2012).
341. L. Brundage, J. P. Hendrick, E. Schiebel, A. J. Driessen, W. Wickner, The purified E. coli integral membrane protein SecY/E is sufficient for reconstitution of SecA-dependent precursor protein translocation. *Cell* **62**, 649-657 (1990).
342. K. Braunger *et al.*, Structural basis for coupling protein transport and N-glycosylation at the mammalian endoplasmic reticulum. *Science* **360**, 215-219 (2018).
343. S. Pfeffer *et al.*, Structure of the mammalian oligosaccharyl-transferase complex in the native ER protein translocon. *Nat Commun* **5**, 3072 (2014).
344. Y. Harada, H. Li, H. Li, W. J. Lennarz, Oligosaccharyltransferase directly binds to ribosome at a location near the translocon-binding site. *Proc Natl Acad Sci U S A* **106**, 6945-6949 (2009).

345. R. Glozman *et al.*, N-glycans are direct determinants of CFTR folding and stability in secretory and endocytic membrane traffic. *J Cell Biol* **184**, 847-862 (2009).
346. S. Shrimal, N. A. Cherepanova, R. Gilmore, Cotranslational and posttranslocational N-glycosylation of proteins in the endoplasmic reticulum. *Semin. Cell Dev. Biol.* **41**, 71-78 (2015).
347. G. von Heijne, A new method for predicting signal sequence cleavage sites. *Nucleic Acids Res* **14**, 4683-4690 (1986).
348. D. Gorlich, E. Hartmann, S. Prehn, T. A. Rapoport, A protein of the endoplasmic reticulum involved early in polypeptide translocation. *Nature* **357**, 47-52 (1992).
349. A. Sauri, P. J. McCormick, A. E. Johnson, I. Mingarro, Sec61alpha and TRAM are sequentially adjacent to a nascent viral membrane protein during its ER integration. *J Mol Biol* **366**, 366-374 (2007).
350. E. Hartmann *et al.*, A tetrameric complex of membrane proteins in the endoplasmic reticulum. *Eur J Biochem* **214**, 375-381 (1993).
351. R. D. Fons, B. A. Bogert, R. S. Hegde, Substrate-specific function of the translocon-associated protein complex during translocation across the ER membrane. *J Cell Biol* **160**, 529-539 (2003).
352. N. Sommer, T. Junne, K. U. Kalies, M. Spiess, E. Hartmann, TRAP assists membrane protein topogenesis at the mammalian ER membrane. *Biochim Biophys Acta* **1833**, 3104-3111 (2013).
353. J. Tyedmers *et al.*, Homologs of the yeast Sec complex subunits Sec62p and Sec63p are abundant proteins in dog pancreas microsomes. *Proc Natl Acad Sci U S A* **97**, 7214-7219 (2000).
354. J. H. Reithinger, J. E. Kim, H. Kim, Sec62 protein mediates membrane insertion and orientation of moderately hydrophobic signal anchor proteins in the endoplasmic reticulum (ER). *J Biol Chem* **288**, 18058-18067 (2013).
355. K. E. Matlack, B. Misselwitz, K. Plath, T. A. Rapoport, BiP acts as a molecular ratchet during posttranslational transport of prepro-alpha factor across the ER membrane. *Cell* **97**, 553-564 (1999).
356. R. P. Zahedi *et al.*, Analysis of the membrane proteome of canine pancreatic rough microsomes identifies a novel Hsp40, termed ERj7. *Proteomics* **9**, 3463-3473 (2009).
357. S. Pfeffer, J. Dudek, R. Zimmermann, F. Forster, Organization of the native ribosome-translocon complex at the mammalian endoplasmic reticulum membrane. *Biochim Biophys Acta* **1860**, 2122-2129 (2016).
358. S. Pfeffer *et al.*, Dissecting the molecular organization of the translocon-associated protein complex. *Nat Commun* **8**, 14516 (2017).
359. T. Hessa *et al.*, Recognition of transmembrane helices by the endoplasmic reticulum translocon. *Nature* **433**, 377-381 (2005).
360. W. C. Wimley, T. P. Creamer, S. H. White, Solvation energies of amino acid side chains and backbone in a family of host-guest pentapeptides. *Biochemistry* **35**, 5109-5124 (1996).
361. J. C. Gumbart, I. Teo, B. Roux, K. Schulten, Reconciling the roles of kinetic and thermodynamic factors in membrane-protein insertion. *J Am Chem Soc* **135**, 2291-2297 (2013).
362. K. Ojemalm, K. K. Halling, I. Nilsson, G. von Heijne, Orientational preferences of neighboring helices can drive ER insertion of a marginally hydrophobic transmembrane helix. *Mol Cell* **45**, 529-540 (2012).
363. S. H. White, W. C. Wimley, Hydrophobic interactions of peptides with membrane interfaces. *Biochim Biophys Acta* **1376**, 339-352 (1998).
364. N. Joh *et al.*, Modest stabilization by most hydrogen-bonded side-chain interactions in membrane proteins. *Nature* **453**, 1266-1270 (2008).
365. L. Zhang *et al.*, Contribution of hydrophobic and electrostatic interactions to the membrane integration of the Shaker K+ channel voltage sensor domain. *Proc Natl Acad Sci U S A* **104**, 8263-8268 (2007).
366. A. Elazar *et al.*, Mutational scanning reveals the determinants of protein insertion and association energetics in the plasma membrane. *Elife* **5**, (2016).
367. K. Ojemalm *et al.*, Energetics of side-chain snorkeling in transmembrane helices probed by nonproteinogenic amino acids. *Proc Natl Acad Sci U S A* **113**, 10559-10564 (2016).
368. N. M. Meindl-Beinker, C. Lundin, I. Nilsson, S. H. White, G. von Heijne, Asn- and Asp-mediated interactions between transmembrane helices during translocon-mediated membrane protein assembly. *EMBO Rep* **7**, 1111-1116 (2006).
369. A. Bernsel *et al.*, Prediction of membrane-protein topology from first principles. *Proc Natl Acad Sci U S A* **105**, 7177-7181 (2008).
370. K. Illergard, A. Kauko, A. Elofsson, Why are polar residues within the membrane core evolutionary conserved? *Proteins* **79**, 79-91 (2011).

371. T. Hessa *et al.*, Molecular code for transmembrane-helix recognition by the Sec61 translocon. *Nature* **450**, 1026-1030 (2007).
372. G. Gafvelin, G. von Heijne, Topological "frustration" in multispanning E. coli inner membrane proteins. *Cell* **77**, 401-412 (1994).
373. K. Moss, A. Helm, Y. Lu, A. Bragin, W. R. Skach, Coupled translocation events generate topological heterogeneity at the endoplasmic reticulum membrane. *Mol Biol Cell* **9**, 2681-2697 (1998).
374. M. Hermansson, G. von Heijne, Inter-helical hydrogen bond formation during membrane protein integration into the ER membrane. *J Mol Biol* **334**, 803-809 (2003).
375. M. T. Virkki *et al.*, Folding of Aquaporin 1: Multiple evidence that helix 3 can shift out of the membrane core. *Protein Sci*, (2014).
376. M. Bogdanov, P. N. Heacock, W. Dowhan, A polytopic membrane protein displays a reversible topology dependent on membrane lipid composition. *EMBO J* **21**, 2107-2116 (2002).
377. A. Kauko *et al.*, Repositioning of transmembrane alpha-helices during membrane protein folding. *J Mol Biol* **397**, 190-201 (2010).
378. R. C. Van Lehn, B. Zhang, T. F. Miller, 3rd, Regulation of multispanning membrane protein topology via post-translational annealing. *Elife* **4**, (2015).
379. N. B. Woodall, S. Hadley, Y. Yin, J. U. Bowie, Complete topology inversion can be part of normal membrane protein biogenesis. *Protein Sci* **26**, 824-833 (2017).
380. T. M. Buck, W. R. Skach, Differential stability of biogenesis intermediates reveals a common pathway for aquaporin-1 topological maturation. *J Biol Chem* **280**, 261-269 (2005).
381. J. P. Schlebach, C. R. Sanders, Influence of Pathogenic Mutations on the Energetics of Translocon-Mediated Bilayer Integration of Transmembrane Helices. *Journal of Membrane Biology* **248**, 371-381 (2015).
382. P. G. Needham, J. L. Brodsky, How early studies on secreted and membrane protein quality control gave rise to the ER associated degradation (ERAD) pathway: the early history of ERAD. *Biochim Biophys Acta* **1833**, 2447-2457 (2013).
383. O. Brandman, R. S. Hegde, Ribosome-associated protein quality control. *Nat Struct Mol Biol* **23**, 7-15 (2016).
384. S. Hurtley, A. Helenius, Protein Oligomerization in the Endoplasmic Reticulum. *Annual Reviews Cell Biology* **5**, 277-307 (1989).
385. L. Ellgaard, A. Helenius, ER Quality Control: Towards an Understranding at the Molecular Level. *Current Opinion in Cell Biology* **13**, 431-437 (2001).
386. T. Anelli, R. Sitia, Protein Quality Control in the Early Secratory Pathway. *The EMBO JOurnal* **27**, 315-327 (2008).
387. K. Araki, K. Nagata, Protein Folding and quality Control in the ER. *Cold Spring Harbor Perspectives in Biology* **3**, 1-25 (2011).
388. K. McCaffrey, I. Braakman, Protein Quality Control at the Endoplasmic Reticulum. *Essays in Biochemistry* **60**, 227-235 (2016).
389. C. J. Guerriero, J. L. Brodsky, The delicate balance between secreted protein folding and endoplasmic reticulum-associated degradation in human physiology. *Physiol Rev* **92**, 537-576 (2012).
390. S. S. Vembar, J. L. Brodsky, One step at a time: endoplasmic reticulum-associated degradation. *Nature reviews. Molecular cell biology* **9**, 944-957 (2008).
391. J. L. Brodsky, Cleaning up: ER-associated degradation to the rescue. *Cell* **151**, 1163-1167 (2012).
392. A. Buchberger, B. Bukau, T. Sommer, Protein quality control in the cytosol and the endoplasmic reticulum: brothers in arms. *Mol Cell* **40**, 238-252 (2010).
393. L. Vincenz-Donnelly, M. S. Hipp, The endoplasmic reticulum: A hub of protein quality control in health and disease. *Free Radic Biol Med* **108**, 383-393 (2017).
394. C. Hetz, E. Chevet, S. A. Oakes, Proteostasis control by the unfolded protein response. *Nat Cell Biol* **17**, 829-838 (2015).
395. H. Wu, P. Carvalho, G. K. Voeltz, Here, there, and everywhere: The importance of ER membrane contact sites. *Science* **361**, (2018).
396. C. M. Farinha, M. D. Amaral, Most F508del-CFTR is targeted to degradation at an early folding checkpoint and independently of calnexin. *Mol Cell Biol* **25**, 5242-5252 (2005).
397. S. J. Kim, W. R. Skach, Mechanisms of CFTR Folding at the Endoplasmic Reticulum. *Front Pharmacol* **3**, 201 (2012).

398. S. Pankow *et al.*, F508 CFTR interactome remodelling promotes rescue of cystic fibrosis. *Nature* **528**, 510-516 (2015).
399. O. Staub *et al.*, Regulation of stability and function of the epithelial Na+ channel (ENaC) by ubiquitination. *EMBO J* **16**, 6325-6336 (1997).
400. T. M. Buck *et al.*, Interactions between intersubunit transmembrane domains regulate the chaperone-dependent degradation of an oligomeric membrane protein. *Biochemical Journal* **474**, 357-376 (2017).
401. K. M. Dickson *et al.*, Association of calnexin with mutant peripheral myelin protein-22 ex vivo: a basis for "gain-of-function" ER diseases. *Proceedings of the National Academy of Sciences of the United States of America* **99**, 9852-9857 (2002).
402. R. Apweiler, H. Hermjakob, N. Sharon, On the Frequency of Protein Glycosylation, as deduced from analysis of the SWISS-PROT database. *Biochimica et Biophysica Acta* **1473**, 4-8 (1999).
403. D. F. Zielinska, F. Gnad, J. R. Wisniewski, M. Mann, Precision Mapping of an In Vivo N-Glycoproteome Reveals Rigid Topological and Sequnce Constraints. *Cell* **141**, 897-907 (2010).
404. J. Breitling, M. Aebi, N-Linked Protein Glycosylation in the Endoplasmic Reticulum. *Cold Spring Harbor Perspectives in Biology* **5**, 1-14 (2013).
405. J. J. Caramelo, A. J. Parodi, A Sweet Code for Glycoprotein Folding. *FEBS letters* **589**, 3379-3387 (2015).
406. L. Lehle, W. Tanner, The Specific Site of Tunicamycin Inhibition in the Formation of Dolichol-bound N-acetylglucosamine derivatives. *FEBS letters* **72**, 167-170 (1976).
407. L. Lamriben, J. B. Graham, B. M. Adams, D. N. Hebert, N-Glycan-based ER Molecular Chaperone and Protein Quality Control System: The Calnexin Binding Cycle. *Traffic* **17**, 308-326 (2016).
408. A. Tannous, G. B. Pisoni, D. N. Hebert, M. Molinari, N-linked Sugar-regulated Protein Folding and Quality Control in the ER. *Seminars in Cell and Developmental Biology* **41**, 79-89 (2015).
409. C. Galli, R. Bernasconi, T. Solda, V. Calanca, M. Molinari, Malectin Participates in a Backup Glycoprotein Quality Control Pathway in the Mammalian ER. *PLOS One* **6**, 1-10 (2011).
410. Y. Chen *et al.*, Role of malectin in Glc(2)Man(9)GlcNAc(2)-dependent quality control of alpha1-antitrypsin. *Molecular Biology of the Cell* **22**, 3559-3570 (2011).
411. I. Wada, S.-i. Imai, M. Kai, F. Sakane, H. Kanoh, Chaperone Function of Calreticulin When Expressed in the Endoplasmic Reticulum as the Membrane-anchored and Soluble Forms. *Journal of Biological Chemistry* **270**, 20298-20304 (1995).
412. J. Schrag, D. *et al.*, The Structure of Calnexin, an ER Chaperone Involved in Quality Control of Protein Folding. *Molecular Cell* **8**, 633-644 (2001).
413. A. Vassilakos, M. Michalak, M. A. Lehrman, D. B. Williams, Oligosacharide Binding Characteristics of the Molecular Chaperones Calnexin and Calreticulin. *Biochemistry* **37**, 3480-3490 (1998).
414. A. Fontanini *et al.*, Glycan-independent Role of Calnexin in the Intracellular Retention of Charcot-Marie Tooth 1A Gas3/PMP22 Mutants. *Journal of Biological Chemistry* **280**, 2378-2387 (2005).
415. U. G. Danilczyk, D. B. Williams, The Lectin Chaperone Calnexin Utilizes Polypeptide-based Interactions to Associate with Many of Its Substrates in Vivo. *Journal of Biological Chemistry* **276**, 25532-25540 (2001).
416. E. Swanton, S. High, P. Woodman, Role of Calnexin in the glycan-independent Quality Control of Proteolipid Protein. *The EMBO JOurnal* **22**, 2948-2958 (2003).
417. D. B. Williams, Beyond Lectins: the Calnexin/Calreticulin Chaperone System of the Endoplasmic Reticulum. *Journal of Cell Science* **119**, 615-623 (2006).
418. V. M. Korkhov *et al.*, Peptide-Based Interactions with Calnexin Target Misassembled Membrane Proteins into Endoplasmic Reticulum-Derived Multilamellar Bodies. *Journal of Molecular Biology* **378**, 337-352 (2008).
419. T. Hara *et al.*, Rer1 and calnexin regulate endoplasmic reticulum retention of a peripheral myelin protein 22 mutant that causes type 1A Charcot-Marie-Tooth disease. *Scientific reports* **4**, 6992 (2014).
420. C. P. Wanamaker, W. N. Green, N-linked Glycosylation is Required for Nicotinic Receptor Assemby but Not for Subunit Associations with Calnexin. *Journal of Biological Chemistry* **280**, 33800-33810 (2005).
421. C. D'Alessio, J. J. Caramelo, A. J. Parodi, UDP-GlC:glycoprotein glucosyltransferase-glucosidase II, the ying-yang of the ER quality control. *Semin Cell Dev Biol* **21**, 491-499 (2010).
422. E. S. Trombetta, A. Helenius, Conformational Requirements for Glycoprotein Reglucosylation in the Endoplasmic Reticulum. *Journal of Cell Biology* **148**, 1123-1129 (2000).

423. J. J. Caramelo, O. A. Castro, d. Prat-Gay, A. J. Parodi, The Endoplasmic Reticulum Glucosyltransferase Recognizes Nearly Native Glycoprotein Folding Intermediates *Journal of Biological Chemistry* **279**, 46280-46285 (2004).
424. Y. Ito, Y. Takeda, A. Seko, M. Izumi, Y. Kajihara, Functional analysis of endoplasmic reticulum glucosyltransferase (UGGT): Synthetic chemistry's initiative in glycobiology. *Semin Cell Dev Biol* **41**, 90-98 (2015).
425. T. Solda, C. Galli, R. J. Kaufman, M. Molinari, Substrate-Specific Requirements for UGT1-Dependent Release from Calnexin. *Molecular Cell* **27**, 238-249 (2007).
426. Y. Takeda *et al.*, Effects of Domain Composition of Catalytic Activity of Human Glucose:Glycoprotein Glucosyltransferases. *Glycobiology* **26**, 999-1006 (2016).
427. D. Calles-Garcia *et al.*, Single-particle electron microscopy structure of UDP-glucose:glycoprotein glucosyltransferase suggests a selectivity mechanism for misfolded proteins. *J Biol Chem* **292**, 11499-11507 (2017).
428. T. Satoh *et al.*, Visualisation of a flexible modular structure of the ER folding-sensor enzyme UGGT. *Sci Rep* **7**, 12142 (2017).
429. P. Roversi *et al.*, Interdomain Conformational Flexibility Underpins the Activity of UGGT, the Eukaryotic Glycoprotein Secretion Checkpoint. *PNAS* **114**, 8544-8549 (2017).
430. J. Merulla, T. Solda, M. Molinari, A novel UGGT1 and p97-dependent checkpoint for native ectodomains with ionizable intramembrane residue. *Mol Biol Cell* **26**, 1532-1542 (2015).
431. C. Fagiolo, R. Sitia, Mannose Trimming by Endoplasmic Reticulum Mannosidase I Times the Proteasomal Degradation of Unassembled Immunoglobulin Subunits. *Journal of Biological Chemistry* **276**, 12885-12892 (2001).
432. R. M. Vabilas, F. U. Hartl, Protein Synthesis upon Acute Nutrient Restriction Relies on Proteasome Function. *Science* **310**, 1960-1963 (2005).
433. J. Roth, C. Zuber, Quality control of glycoprotein folding and ERAD: the role of N-glycan handling, EDEM1 and OS-9. *Histochem Cell Biol* **147**, 269-284 (2017).
434. M. Shenkman *et al.*, A shared Endoplasmic Reticulum-associated Degradation Pathway Involving the EDEM Protein for Glycosylated and Nonglycosylated Proteins. *Journal of Biological Chemistry* **288**, 2167-2178 (2013).
435. L. Ellgaard, N. McCaul, A. Chatsisvilli, I. Braakman, Co- and Post-Translational Protein Folding in the ER. *Traffic* **17**, 615-638 (2016).
436. L. M. Hendershot, The ER function BiP is a Master Regulator of ER Function. *Mount Sinai Journal of Medicine A Journal of Translational and Personalized Medicine* **71**, 289-297 (2004).
437. J. Behnke, M. J. Feige, L. M. Hendershot, BiP and Its Nucleotide Exchange Factors Grp170 and Sil1: Mechanisms of Action and Biological Functions. *Journal of Molecular Biology* **427**, 1589-1608 (2015).
438. A. Melnyk, H. Rieger, R. Zimmermann, in *The Networking of Chaperones by Co-Chaperones*. (2014), pp. 179-200.
439. M. Molinari, A. Helenius, Chaperone selection during glycoprotein translocation into the endoplasmic reticulum. *Science* **288**, 331-333 (2000).
440. O. Vanoni, P. Paganetti, M. Molinari, Consequences of individual N-glycan deletions and of proteasomal inhibition on secretion of active BACE. *Molecular Biology of the Cell* **19**, 4086-4098 (2008).
441. E. Tokhtaeva, G. Sachs, O. Vagin, Diverse pathways for maturation of the Na,K-ATPase beta1 and beta2 subunits in the endoplasmic reticulum of Madin-Darby canine kidney cells. *The Journal of biological chemistry* **285**, 39289-39302 (2010).
442. D. Eletto, D. Dersh, Y. Argon, GRP94 in ER quality control and stress responses. *Semin Cell Dev Biol* **21**, 479-485 (2010).
443. O. Ostrovsky, C. A. Makarewich, E. L. Snapp, Y. Argon, An essential role for ATP binding and hydrolysis in the chaperone activity of GRP94 in cells. *Proc Natl Acad Sci U S A* **106**, 11600-11605 (2009).
444. J. Melnick, J. L. Dul, Y. Argon, Sequential interaction of the chaperones BiP and GRP94 with immunoglobulin chains in the endoplasmic reticulum. *Nature* **370**, 373-375 (1994).
445. M. P. Weekes *et al.*, Proteomic plasma membrane profiling reveals an essential role for gp96 in the cell surface expression of LDLR family members, including the LDL receptor and LRP6. *J Proteome Res* **11**, 1475-1484 (2012).

446. S. Wu *et al.*, The molecular chaperone gp96/GRP94 interacts with Toll-like receptors and integrins via its C-terminal hydrophobic domain. *J Biol Chem* **287**, 6735-6742 (2012).
447. J. C. Christianson, T. A. Shaler, R. E. Tyler, R. R. Kopito, OS-9 and GRP94 deliver mutant alpha1-antitrypsin to the Hrd1-SEL1L ubiquitin ligase complex for ERAD. *Nature cell biology* **10**, 272-282 (2008).
448. P. Maattanen, K. Gehring, J. J. Bergeron, D. Y. Thomas, Protein quality control in the ER: the recognition of misfolded proteins. *Seminars in cell & developmental biology* **21**, 500-511 (2010).
449. M. Okumura, H. Kadokura, K. Inaba, Structures and functions of protein disulfide isomerase family members involved in proteostasis in the endoplasmic reticulum. *Free Radic Biol Med* **83**, 314-322 (2015).
450. M. Hagiwara, K. Nagata, Redox-dependent protein quality control in the endoplasmic reticulum: folding to degradation. *Antioxid Redox Signal* **16**, 1119-1128 (2012).
451. A. Y. Denisov *et al.*, Solution structure of the bb' domains of human protein disulfide isomerase. *Febs Journal* **276**, 1440-1449 (2009).
452. R. Benyair *et al.*, Mammalian ER mannosidase I resides in quality control vesicles, where it encounters its glycoprotein substrates. *Mol Biol Cell* **26**, 172-184 (2015).
453. J. Leitman *et al.*, Herp coordinates compartmentalization and recruitment of HRD1 and misfolded proteins for ERAD. *Mol Biol Cell* **25**, 1050-1060 (2014).
454. A. Pagano *et al.*, Sec24 proteins and sorting at the endoplasmic reticulum. *J Biol Chem* **274**, 7833-7840 (1999).
455. G. Huyer *et al.*, A striking quality control subcompartment in Saccharomyces cerevisiae: The endoplasmic reticulum-associated compartment. *Molecular Biology of the Cell* **15**, 908-921 (2004).
456. E. M. Sontag, W. I. M. Vonk, J. Frydman, Sorting out the trash: the spatial nature of eukaryotic protein quality control. *Current Opinion in Cell Biology* **26**, 139-146 (2014).
457. J. C. Young, The role of the cytosolic HSP70 chaperone system in diseases caused by misfolding and aberrant trafficking of ion channels. *Disease models & mechanisms* **7**, 319-329 (2014).
458. S. Shao, R. S. Hegde, Target Selection during Protein Quality Control. *Trends in biochemical sciences* **41**, 124-137 (2016).
459. J. J. Caramelo, O. A. Castro, L. G. Alonso, G. De Prat-Gay, A. J. Parodi, UDP-Glc:glycoprotein glucosyltransferase recognizes structured and solvent accessible hydrophobic patches in molten globule-like folding intermediates. *Proc Natl Acad Sci U S A* **100**, 86-91 (2003).
460. A. Guna, R. S. Hegde, Transmembrane Domain Recognition during Membrane Protein Biogenesis and Quality Control. *Curr Biol* **28**, R498-R511 (2018).
461. M. H. Smith, H. L. Ploegh, J. S. Weissman, Road to ruin: targeting proteins for degradation in the endoplasmic reticulum. *Science* **334**, 1086-1090 (2011).
462. M. J. Feigel, L. M. Hendershot, Quality Control of Integral Membrane Proteins by Assembly-Dependent Membrane Integration. *Molecular Cell* **51**, 297-309 (2013).
463. M. Heyden, J. A. Freites, M. B. Ulmschneider, S. H. White, D. J. Tobias, Assembly and stability of alpha-helical membrane proteins. *Soft Matter* **8**, 7742-7752 (2012).
464. P. Beguin, U. Hasler, A. Beggah, J. D. Horisberger, K. Geering, Membrane integration of Na,K-ATPase alpha-subunits and beta-subunit assembly. *The Journal of biological chemistry* **273**, 24921-24931 (1998).
465. A. T. Beggah, P. Beguin, K. Bamberg, G. Sachs, K. Geering, beta-subunit assembly is essential for the correct packing and the stable membrane insertion of the H,K-ATPase alpha-subunit. *Journal of Biological Chemistry* **274**, 8217-8223 (1999).
466. R. M. Garza, B. K. Sato, R. Y. Hampton, In vitro analysis of Hrd1p-mediated retrotranslocation of its multispanning membrane substrate 3-hydroxy-3-methylglutaryl (HMG)-CoA reductase. *The Journal of biological chemistry* **284**, 14710-14722 (2009).
467. B. K. Sato, D. Schulz, P. H. Do, R. Y. Hampton, Misfolded membrane proteins are specifically recognized by the transmembrane domain of the Hrd1p ubiquitin ligase. *Molecular Cell* **34**, 212-222 (2009).
468. J. Jung, H. Coe, M. Michalak, Specialization of endoplasmic reticulum chaperones for the folding and function of myelin glycoproteins P0 and PMP22. *Faseb Journal* **25**, 3929-3937 (2011).

469. G. M. Preston, C. J. Guerriero, M. B. Metzger, S. Michaelis, J. L. Brodsky, Substrate Insolubility Dictates Hsp104-Dependent Endoplasmic-Reticulum-Associated Degradation. *Mol Cell* **70**, 242-253 e246 (2018).
470. Z. Sun, J. L. Brodsky, The degradation pathway of a model misfolded protein is determined by aggregation propensity. *Mol Biol Cell* **29**, 1422-1434 (2018).
471. T. Ravid, M. Hochstrasser, Diversity of degradation signals in the ubiquitin-proteasome system. *Nat Rev Mol Cell Biol* **9**, 679-690 (2008).
472. A. Ray-Sinha, B. C. Cross, A. Mironov, E. Wiertz, S. High, Endoplasmic reticulum-associated degradation of a degron-containing polytopic membrane protein. *Mol Membr Biol* **26**, 448-464 (2009).
473. G. Habeck, F. A. Ebner, H. Shimada-Kreft, S. G. Kreft, The yeast ERAD-C ubiquitin ligase Doa10 recognizes an intramembrane degron. *J Cell Biol* **209**, 621 (2015).
474. I. Shapira, D. Charuvi, Y. Elkabetz, K. Hirschberg, S. Bar-Nun, Distinguishing between retention signals and degrons acting in ERAD. *J Cell Sci* **120**, 4377-4387 (2007).
475. C. Barlowe, A. Helenius, Cargo Capture and Bulk Flow in the Early Secretory Pathway. *Annu Rev Cell Dev Bi* **32**, 197-222 (2016).
476. A. Budnik, D. J. Stephens, ER exit sites--localization and control of COPII vesicle formation. *FEBS letters* **583**, 3796-3803 (2009).
477. C. Lord, S. Ferro-Novick, E. A. Miller, The highly conserved COPII coat complex sorts cargo from the endoplasmic reticulum and targets it to the golgi. *Cold Spring Harbor Perspectives in Biology* **5**, (2013).
478. M. W. Wendeler, J. P. Paccaud, H. P. Hauri, Role of Sec24 isoforms in selective export of membrane proteins from the endoplasmic reticulum. *EMBO Rep* **8**, 258-264 (2007).
479. Y. Kamiya *et al.*, Molecular basis of sugar recognition by the human L-type lectins ERGIC-53, VIPL, and VIP36. *The Journal of biological chemistry* **283**, 1857-1861 (2008).
480. S. Pagant, A. Wu, S. Edwards, F. Diehl, E. A. Miller, Sec24 is a coincidence detector that simultaneously binds two signals to drive ER export. *Curr Biol* **25**, 403-412 (2015).
481. C. A. Bue, C. Barlowe, Molecular dissection of Erv26p identifies separable cargo binding and coat protein sorting activities. *The Journal of biological chemistry* **284**, 24049-24060 (2009).
482. C. Adrain, M. Zettl, Y. Christova, N. Taylor, M. Freeman, Tumor necrosis factor signaling requires iRhom2 to promote trafficking and activation of TACE. *Science* **335**, 225-228 (2012).
483. N. Y. Marcus, D. H. Perlmutter, Glucosidase and mannosidase inhibitors mediate increased secretion of mutant alpha1 antitrypsin Z. *The Journal of biological chemistry* **275**, 1987-1992 (2000).
484. N. Borgese, Getting membrane proteins on and off the shuttle bus between the endoplasmic reticulum and the Golgi complex. *Journal of Cell Science* **129**, 1537-1545 (2016).
485. A. Dukhovny, Y. Yaffe, J. Shepshelovitch, K. Hirschberg, The length of cargo-protein transmembrane segments drives secretory transport by facilitating cargo concentration in export domains. *Journal of Cell Science* **122**, 1759-1767 (2009).
486. P. Ronchi, S. Colombo, M. Francolini, N. Borgese, Transmembrane domain-dependent partitioning of membrane proteins within the endoplasmic reticulum. *The Journal of cell biology* **181**, 105-118 (2008).
487. A. H. Futerman, H. Riezman, The ins and outs of sphingolipid synthesis. *Trends Cell Biol* **15**, 312-318 (2005).
488. A. Ridsdale *et al.*, Cholesterol is required for efficient endoplasmic reticulum-to-Golgi transport of secretory membrane proteins. *Mol Biol Cell* **17**, 1593-1605 (2006).
489. H. Runz, K. Miura, M. Weiss, R. Pepperkok, Sterols regulate ER-export dynamics of secretory cargo protein ts-O45-G. *EMBO J* **25**, 2953-2965 (2006).
490. K. Briant, N. Johnson, E. Swanton, Transmembrane domain quality control systems operate at the endoplasmic reticulum and Golgi apparatus. *PLOS One* **12**, e0173924 (2017).
491. S. Vavassori *et al.*, A pH-regulated quality control cycle for surveillance of secretory protein assembly. *Molecular Cell* **50**, 783-792 (2013).
492. S. Sannino *et al.*, Progressive quality control of secretory proteins in the early secretory compartment by ERp44. *Journal of Cell Science* **127**, 4260-4269 (2014).
493. C. Hammond, A. Helenius, Quality control in the secretory pathway: retention of a misfolded viral membrane glycoprotein involves cycling between the ER, intermediate compartment, and Golgi apparatus. *J Cell Biol* **126**, 41-52 (1994).
494. K. Yamamoto *et al.*, The KDEL receptor mediates a retrieval mechanism that contributes to quality control at the endoplasmic reticulum. *EMBO J* **20**, 3082-3091 (2001).

495. M. Babst, Quality control: quality control at the plasma membrane: one mechanism does not fit all. *J Cell Biol* **205**, 11-20 (2014).
496. T. Okiyoneda *et al.*, Chaperone-Independent Peripheral Quality Control of CFTR by RFFL E3 Ligase. *Dev Cell* **44**, 694-708 e697 (2018).
497. J. A. Olzmann, R. R. Kopito, J. C. Christianson, The mammalian endoplasmic reticulum-associated degradation system. *Cold Spring Harbor Perspectives in Biology* **5**, (2013).
498. X. Hou *et al.*, Dissection of the Role of VIMP in Endoplasmic Reticulum-Associated Degradation of CFTRDeltaF508. *Scientific reports* **8**, 4764 (2018).
499. I. Printsev, D. Curiel, K. L. Carraway, 3rd, Membrane Protein Quantity Control at the Endoplasmic Reticulum. *J Membr Biol* **250**, 379-392 (2017).
500. J. C. Christianson *et al.*, Defining human ERAD networks through an integrative mapping strategy. *Nature cell biology* **14**, 93-105 (2011).
501. J. Hwang *et al.*, Characterization of protein complexes of the endoplasmic reticulum-associated degradation E3 ubiquitin ligase Hrd1. *The Journal of biological chemistry* **292**, 9104-9116 (2017).
502. J. Hwang, L. Qi, Quality Control in the Endoplasmic Reticulum: Crosstalk between ERAD and UPR pathways. *Trends in biochemical sciences* **43**, 593-605 (2018).
503. M. D. Shoulders *et al.*, Stress-independent activation of XBP1s and/or ATF6 reveals three functionally diverse ER proteostasis environments. *Cell Rep* **3**, 1279-1292 (2013).
504. H. Meyer, C. C. Weihl, The VCP/p97 system at a glance: connecting cellular function to disease pathogenesis. *Journal of Cell Science* **127**, 3877-3883 (2014).
505. M. Aridor, Visiting the ER: the endoplasmic reticulum as a target for therapeutics in traffic related diseases. *Adv Drug Deliv Rev* **59**, 759-781 (2007).
506. K. Kanehara, W. Xie, D. T. Ng, Modularity of the Hrd1 ERAD complex underlies its diverse client range. *The Journal of cell biology* **188**, 707-716 (2010).
507. M. Mehnert, T. Sommer, E. Jarosch, ERAD ubiquitin ligases: multifunctional tools for protein quality control and waste disposal in the endoplasmic reticulum. *Bioessays* **32**, 905-913 (2010).
508. A. Neutzner *et al.*, A systematic search for endoplasmic reticulum (ER) membrane-associated RING finger proteins identifies Nixin/ZNRF4 as a regulator of calnexin stability and ER homeostasis. *The Journal of biological chemistry* **286**, 8633-8643 (2011).
509. J. L. Brodsky, R. J. Wojcikiewicz, Substrate-specific mediators of ER associated degradation (ERAD). *Curr Opin Cell Biol* **21**, 516-521 (2009).
510. R. Bernasconi, T. Pertel, J. Luban, M. Molinari, A dual task for the Xbp1-responsive OS-9 variants in the mammalian endoplasmic reticulum: inhibiting secretion of misfolded protein conformers and enhancing their disposal. *The Journal of biological chemistry* **283**, 16446-16454 (2008).
511. N. Hosokawa *et al.*, Human XTP3-B forms an endoplasmic reticulum quality control scaffold with the HRD1-SEL1L ubiquitin ligase complex and BiP. *The Journal of biological chemistry* **283**, 20914-20924 (2008).
512. J. Leitman *et al.*, Herp coordinates compartmentalization and recruitment of HRD1 and misfolded proteins for ERAD. *Molecular Biology of the Cell* **25**, 1050-1060 (2014).
513. G. Morreale, L. Conforti, J. Coadwell, A. L. Wilbrey, M. P. Coleman, Evolutionary divergence of valosin-containing protein/cell division cycle protein 48 binding interactions among endoplasmic reticulum-associated degradation proteins. *The FEBS journal* **276**, 1208-1220 (2009).
514. A. Stolz, R. S. Schweizer, A. Schafer, D. H. Wolf, Dfm1 forms distinct complexes with Cdc48 and the ER ubiquitin ligases and is required for ERAD. *Traffic* **11**, 1363-1369 (2010).
515. S. Neal *et al.*, The Dfm1 Derlin Is Required for ERAD Retrotranslocation of Integral Membrane Proteins. *Molecular Cell* **69**, 306-320 e304 (2018).
516. S. Schoebel *et al.*, Cryo-EM structure of the protein-conducting ERAD channel Hrd1 in complex with Hrd3. *Nature* **548**, 352-355 (2017).
517. A. Stolz, W. Hilt, A. Buchberger, D. H. Wolf, Cdc48: a power machine in protein degradation. *Trends in biochemical sciences* **36**, 515-523 (2011).
518. I. Rouiller *et al.*, Conformational changes of the multifunction p97 AAA ATPase during its ATPase cycle. *Nat Struct Biol* **9**, 950-957 (2002).
519. K. Nakatsukasa, J. L. Brodsky, T. Kamura, A stalled retrotranslocation complex reveals physical linkage between substrate recognition and proteasomal degradation during ER-associated degradation. *Mol Biol Cell* **24**, 1765-1775, S1761-1768 (2013).

520. V. E. Pye *et al.*, Going through the motions: the ATPase cycle of p97. *J Struct Biol* **156**, 12-28 (2006).
521. D. Xia, W. K. Tang, Y. Ye, Structure and function of the AAA+ ATPase p97/Cdc48p. *Gene* **583**, 64-77 (2016).
522. J. M. Davies, A. T. Brunger, W. I. Weis, Improved structures of full-length p97, an AAA ATPase: implications for mechanisms of nucleotide-dependent conformational change. *Structure* **16**, 715-726 (2008).
523. Z. Cao, J. M. Hutchison, C. R. Sanders, J. U. Bowie, Backbone Hydrogen Bond Strengths Can Vary Widely in Transmembrane Helices. *J Am Chem Soc* **139**, 10742-10749 (2017).
524. L. Fleig *et al.*, Ubiquitin-dependent intramembrane rhomboid protease promotes ERAD of membrane proteins. *Molecular Cell* **47**, 558-569 (2012).
525. D. Avci, M. K. Lemberg, Clipping or Extracting: Two Ways to Membrane Protein Degradation. *Trends in cell biology* **25**, 611-622 (2015).
526. R. Garcia-Mata, Y. S. Gao, E. Sztul, Hassles with taking out the garbage: aggravating aggresomes. *Traffic* **3**, 388-396 (2002).
527. J. A. Johnston, C. L. Ward, R. R. Kopito, Aggresomes: a cellular response to misfolded proteins. *J Cell Biol* **143**, 1883-1898 (1998).
528. J. Fortun, W. A. Dunn, Jr., S. Joy, J. Li, L. Notterpek, Emerging role for autophagy in the removal of aggresomes in Schwann cells. *J Neurosci* **23**, 10672-10680 (2003).
529. J. Fortun *et al.*, The formation of peripheral myelin protein 22 aggregates is hindered by the enhancement of autophagy and expression of cytoplasmic chaperones. *Neurobiology of Disease* **25**, 252-265 (2007).
530. L. Notterpek, M. C. Ryan, A. R. Tobler, E. M. Shooter, PMP22 accumulation in aggresomes: implications for CMT1A pathology. *Neurobiology of disease* **6**, 450-460 (1999).
531. M. C. Ryan, E. M. Shooter, L. Notterpek, Aggresome formation in neuropathy models based on peripheral myelin protein 22 mutations. *Neurobiol Dis* **10**, 109-118 (2002).
532. Y. F. Chen, I. J. Wang, L. L. Lin, M. S. Chen, Examining rhodopsin retention in endoplasmic reticulum and intracellular localization in vitro and in vivo by using truncated rhodopsin fragments. *J Cell Biochem* **112**, 520-530 (2011).
533. R. S. Saliba, P. M. Munro, P. J. Luthert, M. E. Cheetham, The cellular fate of mutant rhodopsin: quality control, degradation and aggresome formation. *J Cell Sci* **115**, 2907-2918 (2002).
534. A. Tiwari *et al.*, Caveolin-1 is an aggresome-inducing protein. *Sci Rep* **6**, 38681 (2016).
535. S. M. Lee, J. A. Olzmann, L. S. Chin, L. Li, Mutations associated with Charcot-Marie-Tooth disease cause SIMPLE protein mislocalization and degradation by the proteasome and aggresome-autophagy pathways. *J Cell Sci* **124**, 3319-3331 (2011).
536. M. C. Cleophas *et al.*, ABCG2 polymorphisms in gout: insights into disease susceptibility and treatment approaches. *Pharmgenomics Pers Med* **10**, 129-142 (2017).
537. I. Kovacs, K. M. Lentini, L. M. Ingano, D. M. Kovacs, Presenilin 1 forms aggresomal deposits in response to heat shock. *J Mol Neurosci* **29**, 9-19 (2006).
538. J. M. Hyttinen *et al.*, Clearance of misfolded and aggregated proteins by aggrephagy and implications for aggregation diseases. *Ageing Res Rev* **18**, 16-28 (2014).
539. J. J. Driscoll, R. D. Chowdhury, Molecular crosstalk between the proteasome, aggresomes and autophagy: translational potential and clinical implications. *Cancer Lett* **325**, 147-154 (2012).
540. S. Wojcik, Crosstalk between autophagy and proteasome protein degradation systems: possible implications for cancer therapy. *Folia Histochem Cytobiol* **51**, 249-264 (2013).
541. N. Zaarur, A. B. Meriin, V. L. Gabai, M. Y. Sherman, Triggering aggresome formation. Dissecting aggresome-targeting and aggregation signals in synphilin 1. *J Biol Chem* **283**, 27575-27584 (2008).
542. C. M. Pickart, D. Fushman, Polyubiquitin chains: polymeric protein signals. *Curr Opin Chem Biol* **8**, 610-616 (2004).
543. K. L. Lim, V. L. Dawson, T. M. Dawson, Parkin-mediated lysine 63-linked polyubiquitination: a link to protein inclusions formation in Parkinson's and other conformational diseases? *Neurobiol Aging* **27**, 524-529 (2006).
544. J. Moscat, M. T. Diaz-Meco, M. W. Wooten, Signal integration and diversification through the p62 scaffold protein. *Trends in biochemical sciences* **32**, 95-100 (2007).
545. B. G. Burnett, R. N. Pittman, The polyglutamine neurodegenerative protein ataxin 3 regulates aggresome formation. *Proc Natl Acad Sci U S A* **102**, 4330-4335 (2005).

546. H. Wang, Z. Ying, G. Wang, Ataxin-3 regulates aggresome formation of copper-zinc superoxide dismutase (SOD1) by editing K63-linked polyubiquitin chains. *J Biol Chem* **287**, 28576-28585 (2012).
547. R. Heir *et al.*, The UBL domain of PLIC-1 regulates aggresome formation. *EMBO Rep* **7**, 1252-1258 (2006).
548. Y. Kawaguchi *et al.*, The deacetylase HDAC6 regulates aggresome formation and cell viability in response to misfolded protein stress. *Cell* **115**, 727-738 (2003).
549. S. Tan, E. Wong, Kinetics of Protein Aggregates Disposal by Aggrephagy. *Methods Enzymol* **588**, 245-281 (2017).
550. M. Gamerdinger, A. M. Kaya, U. Wolfrum, A. M. Clement, C. Behl, BAG3 mediates chaperone-based aggresome-targeting and selective autophagy of misfolded proteins. *EMBO Rep* **12**, 149-156 (2011).
551. Z. Xu *et al.*, 14-3-3 protein targets misfolded chaperone-associated proteins to aggresomes. *J Cell Sci* **126**, 4173-4186 (2013).
552. D. J. Klionsky, S. D. Emr, Autophagy as a regulated pathway of cellular degradation. *Science* **290**, 1717-1721 (2000).
553. D. G. McEwan, I. Dikic, The Three Musketeers of Autophagy: phosphorylation, ubiquitylation and acetylation. *Trends Cell Biol* **21**, 195-201 (2011).
554. L. Ruan, X. Zhang, R. Li, Recent insights into the cellular and molecular determinants of aging. *J Cell Sci* **131**, (2018).
555. M. Loi, I. Fregno, C. Guerra, M. Molinari, Eat it right: ER-phagy and recovER-phagy. *Biochemical Society transactions* **46**, 699-706 (2018).
556. H. Nakatogawa, K. Mochida, Reticulophagy and nucleophagy: New findings and unsolved issues. *Autophagy* **11**, 2377-2378 (2015).
557. M. Smith, S. Wilkinson, ER homeostasis and autophagy. *Essays Biochem* **61**, 625-635 (2017).
558. S. Song, J. Tan, Y. Miao, Q. Zhang, Crosstalk of ER stress-mediated autophagy and ER-phagy: Involvement of UPR and the core autophagy machinery. *J Cell Physiol* **233**, 3867-3874 (2018).
559. S. Bershtein, M. Segal, R. Bekerman, N. Tokuriki, D. S. Tawfik, Robustness-epistasis link shapes the fitness landscape of a randomly drifting protein. *Nature* **444**, 929-932 (2006).
560. D. M. Taverna, R. A. Goldstein, Why are proteins so robust to site mutations? *J Mol Biol* **315**, 479-484 (2002).
561. C. R. Sanders, J. K. Myers, Disease-Related Misassembly of Membrane Proteins. *Annu. Rev. Biophys. Biomol. Struct.* **33**, 25-51 (2004).
562. C. R. Sanders, J. K. Nagy, Misfolding of membrane proteins in health and disease: the lady or the tiger? *Current opinion in structural biology* **10**, 438-442 (2000).
563. S. B. Qian, M. F. Princiotta, J. R. Bennink, J. W. Yewdell, Characterization of rapidly degraded polypeptides in mammalian cells reveals a novel layer of nascent protein quality control. *J Biol Chem* **281**, 392-400 (2006).
564. K. Van Craenenbroeck *et al.*, Folding efficiency is rate-limiting in dopamine D4 receptor biogenesis. *J Biol Chem* **280**, 19350-19357 (2005).
565. B. Medicherla, A. L. Goldberg, Heat shock and oxygen radicals stimulate ubiquitin-dependent degradation mainly of newly synthesized proteins. *J Cell Biol* **182**, 663-673 (2008).
566. U. Schubert *et al.*, Rapid degradation of a large fraction of newly synthesized proteins by proteasomes. *Nature* **404**, 770-774 (2000).
567. H. C. Yen, Q. Xu, D. M. Chou, Z. Zhao, S. J. Elledge, Global protein stability profiling in mammalian cells. *Science* **322**, 918-923 (2008).
568. J. W. Yewdell, J. R. Lacsina, M. C. Rechsteiner, C. V. Nicchitta, Out with the old, in with the new? Comparing methods for measuring protein degradation. *Cell Biol Int* **35**, 457-462 (2011).
569. S. Pareek *et al.*, Neurone promote the translocation of peripheral myelin protein 22 into myelin. *Journal of Neuroscience* **17**, 7754-7762 (1997).
570. S. Pareek *et al.*, Detection and Processing of Peripheral Myelin Protein Pmp22 in Cultured Schwann-Cells. *Journal of Biological Chemistry* **268**, 10372-10379 (1993).
571. B. Terragni, P. Scalmani, S. Franceschetti, S. Cestele, M. Mantegazza, Post-translational dysfunctions in channelopathies of the nervous system. *Neuropharmacology* **132**, 31-42 (2018).
572. K. M. Doyle *et al.*, Unfolded proteins and endoplasmic reticulum stress in neurodegenerative disorders. *J Cell Mol Med* **15**, 2025-2039 (2011).

573. K. Niforou, C. Cheimonidou, I. P. Trougakos, Molecular chaperones and proteostasis regulation during redox imbalance. *Redox Biol* **2**, 323-332 (2014).
574. Y. Zhang, S. K. Calderwood, Autophagy, protein aggregation and hyperthermia: a mini-review. *Int J Hyperthermia* **27**, 409-414 (2011).
575. T. Gidalevitz, A. Ben-Zvi, K. H. Ho, H. R. Brignull, R. I. Morimoto, Progressive disruption of cellular protein folding in models of polyglutamine diseases. *Science* **311**, 1471-1474 (2006).
576. J. Vijg, Somatic mutations, genome mosaicism, cancer and aging. *Curr. Opin. Genet. Dev.* **26**, 141-149 (2014).
577. I. Martincorena, P. J. Campbell, Somatic mutation in cancer and normal cells. *Science* **349**, 1483-1489 (2015).
578. S. B. Prusiner, Molecular biology and transgenetics of prion diseases. *Crit Rev Biochem Mol Biol* **26**, 397-438 (1991).
579. B. M. Verheijen, M. Vermulst, F. W. van Leeuwen, Somatic mutations in neurons during aging and neurodegeneration. *Acta Neuropathol* **135**, 811-826 (2018).
580. R. Morales, K. Callegari, C. Soto, Prion-like features of misfolded Abeta and tau aggregates. *Virus Res* **207**, 106-112 (2015).
581. S. Ramchandren, Charcot-Marie-Tooth Disease and Other Genetic Polyneuropathies. *Continuum (Minneap Minn)* **23**, 1360-1377 (2017).
582. C. The UniProt, UniProt: the universal protein knowledgebase. *Nucleic Acids Res* **45**, D158-D169 (2017).
583. Z. Zhang, Q. Ren, Why are essential genes essential? - The essentiality of Saccharomyces genes. *Microb Cell* **2**, 280-287 (2015).
584. M. Aridor, L. A. Hannan, Traffic jam: a compendium of human diseases that affect intracellular transport processes. *Traffic* **1**, 836-851 (2000).
585. M. Aridor, L. A. Hannan, Traffic jams II: an update of diseases of intracellular transport. *Traffic* **3**, 781-790 (2002).
586. P. D. Stenson *et al.*, The Human Gene Mutation Database: towards a comprehensive repository of inherited mutation data for medical research, genetic diagnosis and next-generation sequencing studies. *Human genetics* **136**, 665-677 (2017).
587. V. Bernier *et al.*, Pharmacologic chaperones as a potential treatment for X-linked nephrogenic diabetes insipidus. *J Am Soc Nephrol* **17**, 232-243 (2006).
588. H. I. Cheong, H. Y. Cho, H. W. PARK, I. S. Ha, Y. Choi, Molecular genetic study of congenital nephrogenic diabetes insipidus and rescue of mutant vasopressin V2 receptor by chemical chaperones. *Nephrology* **12**, 113-117 (2007).
589. H. B. Moeller, S. Rittig, R. A. Fenton, Nephrogenic diabetes insipidus: essential insights into the molecular background and potential therapies for treatment. *Endocr Rev* **34**, 278-301 (2013).
590. B. Mouillac, C. Mendre, in *Targeting Trafficking in Drug Development,* A. Ulloa-Aguirre, Y.-X. Tao, Eds. (Springer International Publishing, Cham, 2018), pp. 63-83.
591. J. H. Robben, N. V. A. M. Knoers, P. M. T. Deen, Characterization of vasopressin V2 receptor mutants in nephrogenic diabetes insipidus in a polarized cell model. *American Journal of Physiology-Renal Physiology* **289**, F265-F272 (2005).
592. D. G. Bichet, V2R mutations and nephrogenic diabetes insipidus. *Prog Mol Biol Transl Sci* **89**, 15-29 (2009).
593. A. W. Partridge, A. G. Therien, C. M. Deber, Polar mutations in membrane proteins as a biophysical basis for disease. *Biopolymers* **66**, 350-358 (2002).
594. R. Casadio, M. Vassura, S. Tiwari, P. Fariselli, P. Luigi Martelli, Correlating disease-related mutations to their effect on protein stability: a large-scale analysis of the human proteome. *Hum. Mutat.* **32**, 1161-1170 (2011).
595. Z. Shi, J. Moult, Structural and functional impact of cancer-related missense somatic mutations. *J. Mol. Biol.* **413**, 495-512 (2011).
596. S. Stefl, H. Nishi, M. Petukh, A. R. Panchenko, E. Alexov, Molecular mechanisms of disease-causing missense mutations. *J. Mol. Biol.* **425**, 3919-3936 (2013).
597. P. Yue, Z. Li, J. Moult, Loss of protein structure stability as a major causative factor in monogenic disease. *J. Mol. Biol.* **353**, 459-473 (2005).

598. Y. Sekijima *et al.*, The biological and chemical basis for tissue-selective amyloid disease. *Cell* **121**, 73-85 (2005).
599. D. P. Ng, B. E. Poulsen, C. M. Deber, Membrane protein misassembly in disease. *Biochim Biophys Acta* **1818**, 1115-1122 (2012).
600. J. Li, B. Parker, C. Martyn, C. Natarajan, J. S. Guo, The PMP22 Gene and Its Related Diseases. *Molecular Neurobiology* **47**, 673-698 (2013).
601. A. M. Jetten, U. Suter, The peripheral myelin protein 22 and epithelial membrane protein family. *Prog. Nucleic Acid Res. Mol. Biol.* **64**, 97-129 (2000).
602. R. El-Abassi, J. D. England, G. T. Carter, Charcot-Marie-Tooth Disease: An Overview of Genotypes, Phenotypes, and Clinical Management Strategies. *Pm&R* **6**, 342-355 (2014).
603. J. M. Vallat, S. Mathis, B. Funalot, The various Charcot-Marie-Tooth diseases. *Current Opinion in Neurology* **26**, 473-480 (2013).
604. S. Lee *et al.*, Elevated Peripheral Myelin Protein 22, Reduced Mitotic Potential, and Proteasome Impairment in Dermal Fibroblasts from Charcot-Marie-Tooth Disease Type 1A Patients. *Am J Pathol* **188**, 728-738 (2018).
605. J. P. Schlebach *et al.*, Reversible Folding of Human Peripheral Myelin Protein 22, a Tetraspan Membrane Protein. *Biochemistry* **52**, 3229-3241 (2013).
606. K. Cuanalo-Contreras, A. Mukherjee, C. Soto, Role of protein misfolding and proteostasis deficiency in protein misfolding diseases and aging. *Int J Cell Biol* **2013**, 638083 (2013).
607. J. Fortun *et al.*, Alterations in degradative pathways and protein aggregation in a neuropathy model based on PMP22 overexpression. *Neurobiol Dis* **22**, 153-164 (2006).
608. K. F. Mittendorf, B. M. Kroncke, J. Meiler, C. R. Sanders, The homology model of PMP22 suggests mutations resulting in peripheral neuropathy disrupt transmembrane helix packing. *Biochemistry* **53**, 6139-6141 (2014).
609. C. R. Sanders, F. Ismail-Beigi, M. W. McEnery, Mutations of peripheral myelin protein 22 result in defective trafficking through mechanisms which may be common to diseases involving tetraspan membrane proteins. *Biochemistry* **40**, 9453-9459 (2001).
610. A. Kraus *et al.*, Calnexin Deficiency Leads to Dysmyelination. *Journal of Biological Chemistry* **285**, 18928-18938 (2010).
611. V. G. Chittoor-Vinod, S. Lee, S. M. Judge, L. Notterpek, Inducible HSP70 is critical in preventing the aggregation and enhancing the processing of PMP22. *ASN Neuro* **7**, (2015).
612. N. H. Joh *et al.*, De novo design of a transmembrane Zn(2)(+)-transporting four-helix bundle. *Science* **346**, 1520-1524 (2014).
613. P. Lu *et al.*, Accurate computational design of multipass transmembrane proteins. *Science* **359**, 1042-1046 (2018).
614. L. C. Wyatt, J. S. Lewis, O. A. Andreev, Y. K. Reshetnyak, D. M. Engelman, Applications of pHLIP Technology for Cancer Imaging and Therapy. *Trends Biotechnol* **35**, 653-664 (2017).
615. H. Yin *et al.*, Computational design of peptides that target transmembrane helices. *Science* **315**, 1817-1822 (2007).
616. J. S. Slusky, Outer membrane protein design. *Current opinion in structural biology* **45**, 45-52 (2017).
617. W. B. Kauffman, S. Guha, W. C. Wimley, Synthetic molecular evolution of hybrid cell penetrating peptides. *Nat Commun* **9**, 2568 (2018).
618. S. Li *et al.*, Potent Macromolecule-Sized Poration of Lipid Bilayers by the Macrolittins, A Synthetically Evolved Family of Pore-Forming Peptides. *J Am Chem Soc* **140**, 6441-6447 (2018).
619. N. Vaidehi, R. Grisshammer, C. G. Tate, How Can Mutations Thermostabilize G-Protein-Coupled Receptors? *Trends Pharmacol Sci* **37**, 37-46 (2016).
620. Y. Zhou, J. U. Bowie, Building a thermostable membrane protein. *J Biol Chem* **275**, 6975-6979 (2000).
621. B. M. Kroncke *et al.*, Documentation of an Imperative To Improve Methods for Predicting Membrane Protein Stability. *Biochemistry* **55**, 5002-5009 (2016).
622. B. M. Kroncke, C. G. Vanoye, J. Meiler, A. L. George, Jr., C. R. Sanders, Personalized biochemistry and biophysics. *Biochemistry* **54**, 2551-2559 (2015).
623. B. R. Fonslow *et al.*, Single-step inline hydroxyapatite enrichment facilitates identification and quantitation of phosphopeptides from mass-limited proteomes with MudPIT. *J Proteome Res* **11**, 2697-2709 (2012).

624. F. A. Ran *et al.*, Genome engineering using the CRISPR-Cas9 system. *Nat Protoc* **8**, 2281-2308 (2013).
625. K. F. Mittendorf *et al.*, Peripheral myelin protein 22 alters membrane architecture. *Sci Adv* **3**, e1700220 (2017).
626. K. A. Nave, H. B. Werner, Myelination of the nervous system: mechanisms and functions. *Annual review of cell and developmental biology* **30**, 503-533 (2014).
627. S. S. Scherer, E. J. Arroyo, Recent progress on the molecular organization of myelinated axons. *Journal of the peripheral nervous system : JPNS* **7**, 1-12 (2002).
628. S. Ramon y Cajal, *Degeneration and regeneration of the nervous system.* . Ed., (Oxford University Press, Oxford, 1928).
629. J. P. Revel, D. W. Hamilton, The double nature of the intermediate dense line in peripheral nerve myelin. *The Anatomical record* **163**, 7-15 (1969).
630. C. J. Hollingshead, D. L. Caspar, V. Melchior, D. A. Kirschner, Compaction and particle segregation in myelin membrane arrays. *The Journal of cell biology* **89**, 631-644 (1981).
631. H. Inouye, D. A. Kirschner, Evolution of myelin ultrastructure and the major structural myelin proteins. *Brain research*, (2015).
632. K. Adlkofer *et al.*, Hypermyelination and demyelinating peripheral neuropathy in Pmp22-deficient mice. *Nature genetics* **11**, 274-280 (1995).
633. S. Carenini, D. Neuberg, M. Schachner, U. Suter, R. Martini, Localization and functional roles of PMP22 in peripheral nerves of P0-deficient mice. *Glia* **28**, 256-264 (1999).
634. J. R. Lupski, An inherited DNA rearrangement and gene dosage effect are responsible for the most common autosomal dominant peripheral neuropathy: Charcot-Marie-Tooth disease type 1A. *Clinical research* **40**, 645-652 (1992).
635. J. Li, B. Parker, C. Martyn, C. Natarajan, J. Guo, The PMP22 gene and its related diseases. *Molecular neurobiology* **47**, 673-698 (2013).
636. P. Berger, A. Niemann, U. Suter, Schwann cells and the pathogenesis of inherited motor and sensory neuropathies (Charcot-Marie-Tooth disease). *Glia* **54**, 243-257 (2006).
637. T. Bertorini, P. Narayanaswami, H. Rashed, Charcot-Marie-Tooth disease (hereditary motor sensory neuropathies) and hereditary sensory and autonomic neuropathies. *The neurologist* **10**, 327-337 (2004).
638. G. A. Nicholson, The dominantly inherited motor and sensory neuropathies: clinical and molecular advances. *Muscle & nerve* **33**, 589-597 (2006).
639. S. Pareek *et al.*, Neurons promote the translocation of peripheral myelin protein 22 into myelin. *J Neurosci* **17**, 7754-7762 (1997).
640. U. Suter, S. S. Scherer, Disease mechanisms in inherited neuropathies. *Nat Rev Neurosci* **4**, 714-726 (2003).
641. P. Young, U. Suter, Disease mechanisms and potential therapeutic strategies in Charcot-Marie-Tooth disease. *Brain research. Brain research reviews* **36**, 213-221 (2001).
642. E. Nelis, N. Haites, C. Van Broeckhoven, Mutations in the peripheral myelin genes and associated genes in inherited peripheral neuropathies. *Human mutation* **13**, 11-28 (1999).
643. A. A. Gabreels-Festen *et al.*, Charcot-Marie-Tooth disease type 1A: morphological phenotype of the 17p duplication versus PMP22 point mutations. *Acta neuropathologica* **90**, 645-649 (1995).
644. R. Madrid, G. Bradley, he pathology of neuropathies with focal thickening of the myelin sheath (tomaculous neuropathy): studies on the formation of the abnormal myelin sheath. *Journal of the neurological sciences* **25**, 415–448 (1975).
645. F. Behse, F. Buchthal, F. Carlsen, G. G. Knappeis, Hereditary neuropathy with liability to pressure palsies. Electrophysiological and histopathological aspects. *Brain : a journal of neurology* **95**, 777-794 (1972).
646. A. M. Robertson, R. H. King, J. R. Muddle, P. K. Thomas, Abnormal Schwann cell/axon interactions in the Trembler-J mouse. *Journal of anatomy* **190 (Pt 3)**, 423-432 (1997).
647. A. Fontanini *et al.*, Glycan-independent role of calnexin in the intracellular retention of Charcot-Marie-tooth 1A Gas3/PMP22 mutants. *J Biol Chem* **280**, 2378-2387 (2005).
648. R. Naef, K. Adlkofer, B. Lescher, U. Suter, Aberrant protein trafficking in Trembler suggests a disease mechanism for hereditary human peripheral neuropathies. *Molecular and cellular neurosciences* **9**, 13-25 (1997).

649. J. Colby *et al.*, PMP22 carrying the trembler or trembler-J mutation is intracellularly retained in myelinating Schwann cells. *Neurobiology of disease* **7**, 561-573 (2000).
650. R. Naef, U. Suter, Impaired intracellular trafficking is a common disease mechanism of PMP22 point mutations in peripheral neuropathies. *Neurobiology of disease* **6**, 1-14 (1999).
651. A. R. Tobler, N. Liu, L. Mueller, E. M. Shooter, Differential aggregation of the Trembler and Trembler J mutants of peripheral myelin protein 22. *Proc Natl Acad Sci U S A* **99**, 483-488 (2002).
652. D. D'Urso, R. Prior, R. Greiner-Petter, A. A. Gabreels-Festen, H. W. Muller, Overloaded endoplasmic reticulum-Golgi compartments, a possible pathomechanism of peripheral neuropathies caused by mutations of the peripheral myelin protein PMP22. *J Neurosci* **18**, 731-740 (1998).
653. J. Fortun *et al.*, Impaired proteasome activity and accumulation of ubiquitinated substrates in a hereditary neuropathy model. *J Neurochem* **92**, 1531-1541 (2005).
654. C. H. Wilson, D. K. Hartline, Novel organization and development of copepod myelin. ii. nonglial origin. *The Journal of comparative neurology* **519**, 3281-3305 (2011).
655. G. Hoglund, H. Ringertz, X-ray diffraction studies on peripheral nerve myelin. *Acta physiologica Scandinavica* **51**, 290-295 (1961).
656. D. F. Parsons, C. K. Akers, Neutron diffraction of cell membranes (myelin). *Science (New York, N.Y* **165**, 1016-1018 (1969).
657. R. J. Chandross, R. S. Bear, R. L. Montgomery, An X-ray diffraction comparison of myelins from the human nervous system. *The Journal of comparative neurology* **177**, 1-9 (1978).
658. L. Shapiro, J. P. Doyle, P. Hensley, D. R. Colman, W. A. Hendrickson, Crystal structure of the extracellular domain from P0, the major structural protein of peripheral nerve myelin. *Neuron* **17**, 435-449 (1996).
659. C. Huxley *et al.*, Correlation between varying levels of PMP22 expression and the degree of demyelination and reduction in nerve conduction velocity in transgenic mice. *Hum Mol Genet* **7**, 449-458 (1998).
660. C. Huxley *et al.*, Construction of a mouse model of Charcot-Marie-Tooth disease type 1A by pronuclear injection of human YAC DNA. *Human molecular genetics* **5**, 563-569 (1996).
661. B. Hasse, F. Bosse, H. Hanenberg, H. W. Muller, Peripheral myelin protein 22 kDa and protein zero: domain specific trans-interactions. *Mol Cell Neurosci* **27**, 370-378 (2004).
662. K. Kitamura *et al.*, Structure of a major oligosaccharide of PASII/PMP22 glycoprotein in bovine peripheral nerve myelin. *Journal of neurochemistry* **75**, 853-860 (2000).
663. U. Suter *et al.*, Trembler mouse carries a point mutation in a myelin gene. *Nature* **356**, 241-244 (1992).
664. L. J. Valentijn *et al.*, Identical point mutations of PMP-22 in Trembler-J mouse and Charcot-Marie-Tooth disease type 1A. *Nature genetics* **2**, 288-291 (1992).
665. M. Sakakura, A. Hadziselimovic, Z. Wang, K. L. Schey, C. R. Sanders, Structural basis for the Trembler-J phenotype of Charcot-Marie-Tooth disease. *Structure* **19**, 1160-1169 (2011).
666. G. L. Mendz *et al.*, Characterization of dodecylphosphocholine/myelin basic protein complexes. *Biochemistry* **27**, 379-386 (1988).
667. R. M. Gould *et al.*, Myelin sheaths are formed with proteins that originated in vertebrate lineages. *Neuron Glia Biol* **4**, 137-152 (2008).
668. W. Mobius, J. Patzig, K. A. Nave, H. B. Werner, Phylogeny of proteolipid proteins: divergence, constraints, and the evolution of novel functions in myelination and neuroprotection. *Neuron Glia Biol* **4**, 111-127 (2008).
669. J. S. Simske *et al.*, The cell junction protein VAB-9 regulates adhesion and epidermal morphology in C. elegans. *Nature cell biology* **5**, 619-625 (2003).
670. S. Niemann, M. W. Sereda, U. Suter, I. R. Griffiths, K. A. Nave, Uncoupling of myelin assembly and schwann cell differentiation by transgenic overexpression of peripheral myelin protein 22. *J Neurosci* **20**, 4120-4128 (2000).
671. Y. Ohsawa, T. Murakami, Y. Miyazaki, T. Shirabe, Y. Sunada, Peripheral myelin protein 22 is expressed in human central nervous system. *Journal of the neurological sciences* **247**, 11-15 (2006).
672. K. J. Roux, S. A. Amici, L. Notterpek, The temporospatial expression of peripheral myelin protein 22 at the developing blood-nerve and blood-brain barriers. *The Journal of comparative neurology* **474**, 578-588 (2004).

673. K. J. Roux, S. A. Amici, B. S. Fletcher, L. Notterpek, Modulation of epithelial morphology, monolayer permeability, and cell migration by growth arrest specific 3/peripheral myelin protein 22. *Molecular biology of the cell* **16**, 1142-1151 (2005).
674. J. Guo *et al.*, Abnormal junctions and permeability of myelin in PMP22-deficient nerves. *Annals of neurology* **75**, 255-265 (2014).
675. N. Palaniyar, J. L. Semotok, D. D. Wood, M. A. Moscarello, G. Harauz, Human proteolipid protein (PLP) mediates winding and adhesion of phospholipid membranes but prevents their fusion. *Biochimica et biophysica acta* **1415**, 85-100 (1998).
676. M. Bakhti, S. Aggarwal, M. Simons, Myelin architecture: zippering membranes tightly together. *Cellular and molecular life sciences : CMLS* **71**, 1265-1277 (2014).
677. D. A. Yool, J. M. Edgar, P. Montague, S. Malcolm, The proteolipid protein gene and myelin disorders in man and animal models. *Human molecular genetics* **9**, 987-992 (2000).
678. M. E. Shy, Peripheral neuropathies caused by mutations in the myelin protein zero. *Journal of the neurological sciences* **242**, 55-66 (2006).
679. E. J. Arroyo, S. S. Scherer, On the molecular architecture of myelinated fibers. *Histochemistry and cell biology* **113**, 1-18 (2000).
680. M. Furuse, K. Fujita, T. Hiiragi, K. Fujimoto, S. Tsukita, Claudin-1 and -2: novel integral membrane proteins localizing at tight junctions with no sequence similarity to occludin. *The Journal of cell biology* **141**, 1539-1550 (1998).
681. M. Furuse, H. Sasaki, K. Fujimoto, S. Tsukita, A single gene product, claudin-1 or -2, reconstitutes tight junction strands and recruits occludin in fibroblasts. *The Journal of cell biology* **143**, 391-401 (1998).
682. M. Furuse, S. Tsukita, Claudins in occluding junctions of humans and flies. *Trends in cell biology* **16**, 181-188 (2006).
683. S. Angelow, R. Ahlstrom, A. S. Yu, Biology of claudins. *American journal of physiology. Renal physiology* **295**, F867-876 (2008).
684. L. Notterpek *et al.*, Peripheral myelin protein 22 is a constituent of intercellular junctions in epithelia. *Proc Natl Acad Sci U S A* **98**, 14404-14409 (2001).
685. E. Jo, J. M. Boggs, Aggregation of acidic lipid vesicles by myelin basic protein: dependence on potassium concentration. *Biochemistry* **34**, 13705-13716 (1995).
686. M. B. ter Beest, D. Hoekstra, Interaction of myelin basic protein with artificial membranes. Parameters governing binding, aggregation and dissociation. *European journal of biochemistry / FEBS* **211**, 689-696 (1993).
687. J. Hu, W. A. Prinz, T. A. Rapoport, Weaving the web of ER tubules. *Cell* **147**, 1226-1231 (2011).
688. J. C. Stachowiak *et al.*, Membrane bending by protein-protein crowding. *Nature cell biology* **14**, 944-949 (2012).
689. J. Patzig *et al.*, Proteolipid protein modulates preservation of peripheral axons and premature death when myelin protein zero is lacking. *Glia* **64**, 155-174 (2016).
690. D. D'Urso, P. Ehrhardt, H. W. Muller, Peripheral myelin protein 22 and protein zero: a novel association in peripheral nervous system myelin. *J Neurosci* **19**, 3396-3403 (1999).
691. J. T. Marinko, A. K. Kenworthy, C. R. Sanders, Peripheral myelin protein 22 preferentially partitions into ordered phase membrane domains. *Proc Natl Acad Sci U S A* **117**, 14168-14177 (2020).
692. S. L. Veatch, S. L. Keller, Separation of liquid phases in giant vesicles of ternary mixtures of phospholipids and cholesterol. *Biophys J* **85**, 3074-3083 (2003).
693. M. J. Ackerman, Genetic purgatory and the cardiac channelopathies: Exposing the variants of uncertain/unknown significance issue. *Heart Rhythm* **12**, 2325-2331 (2015).
694. X. Cheng, J. C. Smith, Biological Membrane Organization and Cellular Signaling. *Chem Rev*, (2019).
695. S. L. Veatch *et al.*, Critical fluctuations in plasma membrane vesicles. *ACS Chem Biol* **3**, 287-293 (2008).
696. E. Gielen *et al.*, Rafts in oligodendrocytes: evidence and structure-function relationship. *Glia* **54**, 499-512 (2006).
697. T. Baumgart *et al.*, Large-scale fluid/fluid phase separation of proteins and lipids in giant plasma membrane vesicles. *Proc Natl Acad Sci U S A* **104**, 3165-3170 (2007).
698. M. Aureli, S. Grassi, S. Prioni, S. Sonnino, A. Prinetti, Lipid membrane domains in the brain. *Biochim Biophys Acta* **1851**, 1006-1016 (2015).

699. D. A. Brown, Preparation of detergent-resistant membranes (DRMs) from cultured mammalian cells. *Methods Mol Biol* **1232**, 55-64 (2015).
700. D. A. Brown, Lipid rafts, detergent-resistant membranes, and raft targeting signals. *Physiology (Bethesda)* **21**, 430-439 (2006).
701. H. Heerklotz, Triton promotes domain formation in lipid raft mixtures. *Biophys J* **83**, 2693-2701 (2002).
702. S. Schuck, M. Honsho, K. Ekroos, A. Shevchenko, K. Simons, Resistance of cell membranes to different detergents. *Proc Natl Acad Sci U S A* **100**, 5795-5800 (2003).
703. K. R. Levental, I. Levental, Giant plasma membrane vesicles: models for understanding membrane organization. *Curr Top Membr* **75**, 25-57 (2015).
704. J. H. Lorent *et al.*, Structural determinants and functional consequences of protein affinity for membrane rafts. *Nature communications* **8**, 1219 (2017).
705. E. Sezgin *et al.*, Elucidating membrane structure and protein behavior using giant plasma membrane vesicles. *Nat Protoc* **7**, 1042-1051 (2012).
706. A. S. Klymchenko, R. Kreder, Fluorescent probes for lipid rafts: from model membranes to living cells. *Chem Biol* **21**, 97-113 (2014).
707. B. B. Diaz-Rohrer, K. R. Levental, K. Simons, I. Levental, Membrane raft association is a determinant of plasma membrane localization. *Proceedings of the National Academy of Sciences of the United States of America* **111**, 8500-8505 (2014).
708. K. Raghunathan *et al.*, Glycolipid Crosslinking Is Required for Cholera Toxin to Partition Into and Stabilize Ordered Domains. *Biophys J* **111**, 2547-2550 (2016).
709. P. Sengupta, A. Hammond, D. Holowka, B. Baird, Structural determinants for partitioning of lipids and proteins between coexisting fluid phases in giant plasma membrane vesicles. *Biochim Biophys Acta* **1778**, 20-32 (2008).
710. Q. Lin, E. London, Transmembrane protein (perfringolysin o) association with ordered membrane domains (rafts) depends upon the raft-associating properties of protein-bound sterol. *Biophys J* **105**, 2733-2742 (2013).
711. Q. Lin, E. London, Altering hydrophobic sequence lengths shows that hydrophobic mismatch controls affinity for ordered lipid domains (rafts) in the multitransmembrane strand protein perfringolysin O. *J Biol Chem* **288**, 1340-1352 (2013).
712. G. J. Snipes, U. Suter, A. A. Welcher, E. M. Shooter, Characterization of a novel peripheral nervous system myelin protein (PMP-22/SR13). *J Cell Biol* **117**, 225-238 (1992).
713. B. W. van Paassen *et al.*, PMP22 related neuropathies: Charcot-Marie-Tooth disease type 1A and Hereditary Neuropathy with liability to Pressure Palsies. *Orphanet J Rare Dis* **9**, 38 (2014).
714. S. Lee *et al.*, PMP22 is critical for actin-mediated cellular functions and for establishing lipid rafts. *J Neurosci* **34**, 16140-16152 (2014).
715. Y. Zhou *et al.*, PMP22 Regulates Cholesterol Trafficking and ABCA1-Mediated Cholesterol Efflux. *J Neurosci* **39**, 5404-5418 (2019).
716. G. Saher *et al.*, High cholesterol level is essential for myelin membrane growth. *Nat Neurosci* **8**, 468-475 (2005).
717. G. Gopalakrishnan *et al.*, Lipidome and proteome map of myelin membranes. *J Neurosci Res* **91**, 321-334 (2013).
718. S. Larrouquere-Regnier, F. Boiron, D. Darriet, C. Cassagne, J. M. Bourre, Lipid composition of sciatic nerve from dysmyelinating trembler mouse. *Neurosci Lett* **15**, 135-139 (1979).
719. Y. Zhou *et al.*, A neutral lipid-enriched diet improves myelination and alleviates peripheral nerve pathology in neuropathic mice. *Exp Neurol* **321**, 113031 (2019).
720. R. Fledrich *et al.*, Targeting myelin lipid metabolism as a potential therapeutic strategy in a model of CMT1A neuropathy. *Nat Commun* **9**, 3025 (2018).
721. B. Hasse, F. Bosse, H. W. Muller, Proteins of peripheral myelin are associated with glycosphingolipid/cholesterol-enriched membranes. *J Neurosci Res* **69**, 227-232 (2002).
722. N. Liu, J. Yamauchi, E. M. Shooter, Recessive, but not dominant, mutations in peripheral myelin protein 22 gene show unique patterns of aggregation and intracellular trafficking. *Neurobiol Dis* **17**, 300-309 (2004).
723. M. C. Ryan, L. Notterpek, A. R. Tobler, N. Liu, E. M. Shooter, Role of the peripheral myelin protein 22 N-linked glycan in oligomer stability. *J Neurochem* **75**, 1465-1474 (2000).

724. S. J. Zoltewicz *et al.*, The palmitoylation state of PMP22 modulates epithelial cell morphology and migration. *ASN Neuro* **4**, 409-421 (2012).
725. Y. Song, A. K. Kenworthy, C. R. Sanders, Cholesterol as a co-solvent and a ligand for membrane proteins. *Protein Sci* **23**, 1-22 (2014).
726. J. Fantini, C. Di Scala, C. J. Baier, F. J. Barrantes, Molecular mechanisms of protein-cholesterol interactions in plasma membranes: Functional distinction between topological (tilted) and consensus (CARC/CRAC) domains. *Chem Phys Lipids* **199**, 52-60 (2016).
727. C. Di Scala *et al.*, Relevance of CARC and CRAC Cholesterol-Recognition Motifs in the Nicotinic Acetylcholine Receptor and Other Membrane-Bound Receptors. *Curr Top Membr* **80**, 3-23 (2017).
728. I. Levental, M. Grzybek, K. Simons, Raft domains of variable properties and compositions in plasma membrane vesicles. *Proc Natl Acad Sci U S A* **108**, 11411-11416 (2011).
729. A. Mohamed, H. Robinson, P. J. Erramouspe, M. M. Hill, Advances and challenges in understanding the role of the lipid raft proteome in human health. *Expert Rev Proteomics* **15**, 1053-1063 (2018).
730. S. Minogue, M. G. Waugh, Lipid rafts, microdomain heterogeneity and inter-organelle contacts: impacts on membrane preparation for proteomic studies. *Biol Cell* **104**, 618-627 (2012).
731. Y. Z. Zheng, L. J. Foster, Contributions of quantitative proteomics to understanding membrane microdomains. *J Lipid Res* **50**, 1976-1985 (2009).
732. L. D. Nelson, A. E. Johnson, E. London, How interaction of perfringolysin O with membranes is controlled by sterol structure, lipid structure, and physiological low pH: insights into the origin of perfringolysin O-lipid raft interaction. *J Biol Chem* **283**, 4632-4642 (2008).
733. J. P. Schlebach *et al.*, Topologically Diverse Human Membrane Proteins Partition to Liquid-Disordered Domains in Phase-Separated Lipid Vesicles. *Biochemistry* **55**, 985-988 (2016).
734. H. Shogomori *et al.*, Palmitoylation and intracellular domain interactions both contribute to raft targeting of linker for activation of T cells. *J Biol Chem* **280**, 18931-18942 (2005).
735. S. A. Johnson *et al.*, Temperature-dependent phase behavior and protein partitioning in giant plasma membrane vesicles. *Biochim Biophys Acta* **1798**, 1427-1435 (2010).
736. J. Podkalicka, A. Biernatowska, M. Majkowski, M. Grzybek, A. F. Sikorski, MPP1 as a Factor Regulating Phase Separation in Giant Plasma Membrane-Derived Vesicles. *Biophys J* **108**, 2201-2211 (2015).
737. C. Raggi *et al.*, Caveolin-1 Endows Order in Cholesterol-Rich Detergent Resistant Membranes. *Biomolecules* **9**, (2019).
738. J. T. Marinko, B. D. Carter, C. R. Sanders, Direct relationship between increased expression and mistrafficking of the Charcot-Marie-Tooth-associated protein PMP22. *J Biol Chem* **295**, 11963-11970 (2020).
739. R. El-Abassi, J. D. England, G. T. Carter, Charcot-Marie-Tooth disease: an overview of genotypes, phenotypes, and clinical management strategies. *PM R* **6**, 342-355 (2014).
740. J. Morena, A. Gupta, J. C. Hoyle, Charcot-Marie-Tooth: From Molecules to Therapy. *Int J Mol Sci* **20**, (2019).
741. D. Pareyson, P. Saveri, C. Pisciotta, New developments in Charcot-Marie-Tooth neuropathy and related diseases. *Curr Opin Neurol* **30**, 471-480 (2017).
742. C. DiVincenzo *et al.*, The allelic spectrum of Charcot-Marie-Tooth disease in over 17,000 individuals with neuropathy. *Mol Genet Genomic Med* **2**, 522-529 (2014).
743. H. Pantera, M. E. Shy, J. Svaren, Regulating PMP22 expression as a dosage sensitive neuropathy gene. *Brain Res* **1726**, 146491 (2020).
744. J. Li, Caveats in the Established Understanding of CMT1A. *Ann Clin Transl Neurol* **4**, 601-607 (2017).
745. A. A. Welcher *et al.*, Isolation of transcriptionally regulated sequences associated with neuronal and non-neuronal cell interactions. *Prog Brain Res* **94**, 163-176 (1992).
746. S. Pareek *et al.*, Detection and processing of peripheral myelin protein PMP22 in cultured Schwann cells. *J Biol Chem* **268**, 10372-10379 (1993).
747. E. Fabbretti, P. Edomi, C. Brancolini, C. Schneider, Apoptotic phenotype induced by overexpression of wild-type gas3/PMP22: its relation to the demyelinating peripheral neuropathy CMT1A. *Genes Dev* **9**, 1846-1856 (1995).
748. L. Nobbio *et al.*, Impairment of PMP22 transgenic Schwann cells differentiation in culture: implications for Charcot-Marie-Tooth type 1A disease. *Neurobiol Dis* **16**, 263-273 (2004).

749. J. Fortun *et al.*, The formation of peripheral myelin protein 22 aggregates is hindered by the enhancement of autophagy and expression of cytoplasmic chaperones. *Neurobiol Dis* **25**, 252-265 (2007).
750. S. Rangaraju *et al.*, Rapamycin activates autophagy and improves myelination in explant cultures from neuropathic mice. *J Neurosci* **30**, 11388-11397 (2010).
751. J. Nicks *et al.*, Rapamycin improves peripheral nerve myelination while it fails to benefit neuromuscular performance in neuropathic mice. *Neurobiol Dis* **70**, 224-236 (2014).
752. M. R. Dyson, Fundamentals of Expression in Mammalian Cells. *Adv Exp Med Biol* **896**, 217-224 (2016).
753. F. Lampariello, On the use of the Kolmogorov-Smirnov statistical test for immunofluorescence histogram comparison. *Cytometry* **39**, 179-188 (2000).
754. C. Lopez-Anido *et al.*, Differential Sox10 genomic occupancy in myelinating glia. *Glia* **63**, 1897-1914 (2015).
755. H. Pantera *et al.*, Regulation of the neuropathy-associated Pmp22 gene by a distal super-enhancer. *Hum Mol Genet* **27**, 2830-2839 (2018).
756. C. Barlowe, A. Helenius, Cargo Capture and Bulk Flow in the Early Secretory Pathway. *Annu Rev Cell Dev Biol* **32**, 197-222 (2016).
757. C. K. Barlowe, E. A. Miller, Secretory protein biogenesis and traffic in the early secretory pathway. *Genetics* **193**, 383-410 (2013).
758. I. Fregno, M. Molinari, Proteasomal and lysosomal clearance of faulty secretory proteins: ER-associated degradation (ERAD) and ER-to-lysosome-associated degradation (ERLAD) pathways. *Crit Rev Biochem Mol Biol* **54**, 153-163 (2019).
759. K. McCaffrey, I. Braakman, Protein quality control at the endoplasmic reticulum. *Essays Biochem* **60**, 227-235 (2016).
760. Z. Sun, J. L. Brodsky, Protein quality control in the secretory pathway. *J Cell Biol* **218**, 3171-3187 (2019).
761. C. G. Vanoye *et al.*, Peripheral myelin protein 22 modulates store-operated calcium channel activity, providing insights into Charcot-Marie-Tooth disease etiology. *J Biol Chem* **294**, 12054-12065 (2019).
762. I. Shames, A. Fraser, J. Colby, W. Orfali, G. J. Snipes, Phenotypic differences between peripheral myelin protein-22 (PMP22) and myelin protein zero (P0) mutations associated with Charcot-Marie-Tooth-related diseases. *J Neuropathol Exp Neurol* **62**, 751-764 (2003).
763. T. Hara *et al.*, Rer1 and calnexin regulate endoplasmic reticulum retention of a peripheral myelin protein 22 mutant that causes type 1A Charcot-Marie-Tooth disease. *Sci Rep* **4**, 6992 (2014).
764. J. Jung, H. Coe, M. Michalak, Specialization of endoplasmic reticulum chaperones for the folding and function of myelin glycoproteins P0 and PMP22. *FASEB J* **25**, 3929-3937 (2011).
765. M. Aebi, N-linked protein glycosylation in the ER. *Biochim Biophys Acta* **1833**, 2430-2437 (2013).
766. N. Cherepanova, S. Shrimal, R. Gilmore, N-linked glycosylation and homeostasis of the endoplasmic reticulum. *Curr Opin Cell Biol* **41**, 57-65 (2016).
767. B. R. Pearse, D. N. Hebert, Lectin chaperones help direct the maturation of glycoproteins in the endoplasmic reticulum. *Biochim Biophys Acta* **1803**, 684-693 (2010).
768. J. K. Myers, C. K. Mobley, C. R. Sanders, The peripheral neuropathy-linked Trembler and Trembler-J mutant forms of peripheral myelin protein 22 are folding-destabilized. *Biochemistry* **47**, 10620-10629 (2008).
769. N. A. Cherepanova, R. Gilmore, Mammalian cells lacking either the cotranslational or posttranslocational oligosaccharyltransferase complex display substrate-dependent defects in asparagine linked glycosylation. *Sci Rep* **6**, 20946 (2016).
770. B. J. Conti, P. K. Devaraneni, Z. Yang, L. L. David, W. R. Skach, Cotranslational stabilization of Sec62/63 within the ER Sec61 translocon is controlled by distinct substrate-driven translocation events. *Mol Cell* **58**, 269-283 (2015).
771. C. Ruiz-Canada, D. J. Kelleher, R. Gilmore, Cotranslational and posttranslational N-glycosylation of polypeptides by distinct mammalian OST isoforms. *Cell* **136**, 272-283 (2009).
772. N. A. Cherepanova, S. Shrimal, R. Gilmore, Oxidoreductase activity is necessary for N-glycosylation of cysteine-proximal acceptor sites in glycoproteins. *J Cell Biol* **206**, 525-539 (2014).
773. N. Tanese, Small-scale density gradient sedimentation to separate and analyze multiprotein complexes. *Methods* **12**, 224-234 (1997).

774. A. S. Ramirez, J. Kowal, K. P. Locher, Cryo-electron microscopy structures of human oligosaccharyltransferase complexes OST-A and OST-B. *Science* **366**, 1372-1375 (2019).
775. L. Plate *et al.*, Small molecule proteostasis regulators that reprogram the ER to reduce extracellular protein aggregation. *Elife* **5**, (2016).
776. C. Lopez-Sambrooks *et al.*, Oligosaccharyltransferase inhibition induces senescence in RTK-driven tumor cells. *Nat Chem Biol* **12**, 1023-1030 (2016).
777. N. Rinis *et al.*, Editing N-Glycan Site Occupancy with Small-Molecule Oligosaccharyltransferase Inhibitors. *Cell Chem Biol* **25**, 1231-1241 e1234 (2018).
778. W. Huang da, B. T. Sherman, R. A. Lempicki, Bioinformatics enrichment tools: paths toward the comprehensive functional analysis of large gene lists. *Nucleic Acids Res* **37**, 1-13 (2009).
779. W. Huang da, B. T. Sherman, R. A. Lempicki, Systematic and integrative analysis of large gene lists using DAVID bioinformatics resources. *Nat Protoc* **4**, 44-57 (2009).
780. C. Appenzeller, H. Andersson, F. Kappeler, H. P. Hauri, The lectin ERGIC-53 is a cargo transport receptor for glycoproteins. *Nat Cell Biol* **1**, 330-334 (1999).
781. B. Nyfeler *et al.*, Identification of ERGIC-53 as an intracellular transport receptor of alpha1-antitrypsin. *J Cell Biol* **180**, 705-712 (2008).
782. Y. L. Fu, B. Zhang, T. W. Mu, LMAN1 (ERGIC-53) promotes trafficking of neuroreceptors. *Biochem Biophys Res Commun* **511**, 356-362 (2019).
783. S. P. Ferris, N. S. Jaber, M. Molinari, P. Arvan, R. J. Kaufman, UDP-glucose:glycoprotein glucosyltransferase (UGGT1) promotes substrate solubility in the endoplasmic reticulum. *Mol Biol Cell* **24**, 2597-2608 (2013).
784. Y. Chen *et al.*, A novel small molecule chaperone of rod opsin and its potential therapy for retinal degeneration. *Nat Commun* **9**, 1976 (2018).
785. S. Shrimal, B. G. Ng, M. E. Losfeld, R. Gilmore, H. H. Freeze, Mutations in STT3A and STT3B cause two congenital disorders of glycosylation. *Hum Mol Genet* **22**, 4638-4645 (2013).
786. M. Shenkman, G. Z. Lederkremer, Compartmentalization and Selective Tagging for Disposal of Misfolded Glycoproteins. *Trends in biochemical sciences* **44**, 827-836 (2019).
787. J. Leitman, E. Ron, N. Ogen-Shtern, G. Z. Lederkremer, Compartmentalization of endoplasmic reticulum quality control and ER-associated degradation factors. *DNA Cell Biol* **32**, 2-7 (2013).
788. P. G. Needham, C. J. Guerriero, J. L. Brodsky, Chaperoning Endoplasmic Reticulum-Associated Degradation (ERAD) and Protein Conformational Diseases. *Cold Spring Harb Perspect Biol* **11**, (2019).
789. C. Y. Chen *et al.*, Signal peptide peptidase functions in ERAD to cleave the unfolded protein response regulator XBP1u. *EMBO J* **33**, 2492-2506 (2014).
790. D. Avci, M. K. Lemberg, Clipping or Extracting: Two Ways to Membrane Protein Degradation. *Trends Cell Biol* **25**, 611-622 (2015).
791. N. Kuhnle, V. Dederer, M. K. Lemberg, Intramembrane proteolysis at a glance: from signalling to protein degradation. *J Cell Sci* **132**, (2019).
792. R. Naef, U. Suter, Many facets of the peripheral myelin protein PMP22 in myelination and disease. *Microsc Res Tech* **41**, 359-371 (1998).